Host immunity against acute viral respiratory infection: investigation of IFITM3 & discovery of SARS-CoV-2-specific T cell responses

Zixi Yin
University College

Supervisor: Professor Tao Dong
Co-supervisor: Dr Dannielle Wellington

Thesis Submitted for the Degree of
Doctor of Philosophy
in
Clinical Medicine

Trinity Term 2022

Host immunity against acute viral respiratory infection: investigation of IFITM3 & discovery of SARS-CoV-2-specific T cell responses

Zixi Yin, University College, Oxford
D. Phil Thesis, Trinity Term 2022

Abstract

Appropriate host immune responses to acute viral respiratory infections are necessary for viral clearance and can determine clinical disease severity. Two such respiratory infections are coronavirus disease-19 (COVID-19) and influenza, the causative agents of which are severe acute respiratory syndrome coronavirus 2 (SARS-CoV-2) and influenza A virus (IAV), respectively. Interferon (IFN)-induced transmembrane protein 3 (IFITM3), an innate immune effector, has been shown to restrict replication of IAVs and several other enveloped RNA viruses. While, both anti- and pro-viral activities of IFITM3 have been reported for SARS-CoV-2. Understanding the role of IFITM3 during virus infection is vital as it presents an opportunity to increase viral restriction, but it has yet to be fully elucidated and appears to change subject to the virus. At later stages of an infection, T cells are essential in viral immunity. While T cell responses to IAVs are well characterised, responses against SARS-CoV-2 were poorly defined when the COVID-19 started to spread worldwide in early 2020.

The first part of this study (Chapter 3) investigates the impact of IFITM3 during IAV and SARS-CoV-2 infection using induced pluripotent stem cell (iPSC)-derived macrophages (iPSDMs). Our data demonstrated IFITM3 as a restrictor for H1N1 infection, a subtype of IAV, while a facilitator for SARS-CoV-2 in iPSDMs. By analysing RNA-Seq data from IFITM3$^{+/+}$ and IFITM3$^{-/-}$ iPSDMs following virus infection, we uncovered potential associations of IFITM3 with antigen processing and presentation, and cytokine signalling pathways. Chapter 4 characterises SARS-CoV-2-specific T cell responses in 42 COVID-19 convalescent patients. We observed broad and strong memory T cell responses against SARS-CoV-2 and identified seven dominant CD8^{+} epitopes. Finally, I show work evaluating T cell responses to SARS-CoV-2 variants of concern (VoCs) in a small cohort of COVID-19 convalescent patients and uninfected donors vaccinated with ChAdOx1. We established two systems to evaluate T cell responses to naturally processed and presented SARS-CoV-2 spike antigens using recombinant vaccinia virus and live SARS-CoV-2 virus. We found that both natural infection and vaccination could induce multi-functional T cell responses with overall T cell responses remaining despite the identification of escape mutations in VoCs.

Declaration

I declare that the work presented in this DPhil thesis entitled “Host immunity against acute viral respiratory infection: investigation of IFITM3 & discovery of SARS-CoV-2-specific T cell responses” is my own, except for where the contributions of collaborators have been clearly acknowledged. No part of this thesis has been submitted for any other degree or other qualification at the University of Oxford or elsewhere.

Zixi Yin
Trinity Term 2022

Acknowledgements

Over the past four years, I have met so many people who have given me great support through my DPhil study. I would like to thank all of you who have made me here.

Firstly, I would like to thank all the patients and donors who have generously donated blood for our COVID-19 studies. I truly appreciate your support for our study and your contribution in this scientific field.

I would like to express my sincere gratitude to my supervisors Professor Tao Dong and Dr Dannielle Wellington. Particular thanks to Tao for giving me the opportunity to study in Oxford University, and for all your insightful advice and suggestions on my projects. I always feel fortunate to have such an understanding and supportive supervisor. Great and deepest thanks to Dannielle, my daily supervisor, who has influenced me most in my DPhil life. You have taught me so many things, experimental techniques, presentation skills, writing skills, critical thinking, time management… I just can't list them all. Thank you for always being supportive, patient and encouraging, which helped me get through the hard times in my DPhil journey. I would not have made it to this stage if it wasn't for you. I would also like to thank Professor Alain Townsend and Professor Jan Rehwinkel for all your great advice and excellent ideas, especially as members of my Thesis Committee. I would further like to acknowledge the Chinese Government for providing me the CSC scholarship to cover my living cost in Oxford and making my life much easier.

Huge thanks go to our COVID-19 research team, a group of very hard-working and passionate researchers. It was a hard time due to COVID-19 but working with you has made it the most valuable experience in my DPhil life. Thanks to Peng for all the guidance on T cell study design and experiments. Thanks to Xuan and Guihai for spending countless hours with me in CL3 for SARS-CoV-2 infection work. Thanks to Jili for all the vaccinia virus infection work and to Beibei for growing all those valuable T cell lines. I would further like to thank all current and past members in Tao's lab for the advice and support throughout the study process, and for making our lab a warm and friendly place. Special thanks to Jessica Forbester for kindly and patiently teaching me iPS technology, which constituted an important part of my thesis. I would also like to thank our fantastic collaborators. Thanks to Jack Tiong Tan for kindly sharing S-Flu with us, to Peter Wing and Chang Liu for SARS-CoV-2 strains, and to Yongxu Lu for recombinant vaccinia strains. Thanks to Leila Godfrey for invaluable T cell lines from vaccinated donors. I also want to extend my thanks to the brilliant WIMM facilities staff, especially to Philip Hublitz and Ryan Beveridge for making all those ACE2 lentiviruses, and to Tim Rostron for huge number of sequencing performed.

My heartfelt thanks go to my lovely friends here, especially Ziqi for being my best DPhil buddy. A massive thanks also goes to Shengpan, Dingxi, Wenbo, Yuqi, Siyu,

Zhu, Fei, Yu and Sixian for being the constant and reliable source of friendship, and everyone else for making these years such a fantastic time. Particular thanks to Zinan for helping in RNA-Seq data analysis.

Finally, I would like to thank my parents for the unconditional love and support, and for being the most understanding listeners for all my happy and sad moments. Warmest thanks to my father for your passion in science which makes me keep moving forward. Although we did not get to meet in the past three year, I know you are always there caring for me.

Authored Publications

- Y. Peng[#], S. Felce[#], D. Dong[#], F. Penkava[#], A. Mentzer[#], X. Yao[#], G. Liu[#], **Z. Yin**[#], J. Chen[#]... T. Dong. An immunodominant NP105–113-B*07:02 cytotoxic T cell response controls viral replication and is associated with less severe COVID-19 disease. *Nature Immunology,* 23, 50-61 (2021, co-first author[#]).
- Y. Peng[#], A. Mentzer[#], G. Liu[#], X. Yao[#], **Z. Yin**[#], D. Dong[#], W. Dejnirattisai[#]... T. Dong. Broad and strong memory $CD4^+$ and $CD8^+$ T cells induced by SARS-CoV-2 in UK convalescent individuals following COVID-19. *Nature Immunology*, 21, 1336-1345 (2020, co-first author[#]).
- D. Wellington, **Z. Yin**, B. Kessler, T. Dong. Immunodominance complexity: lessons yet to be learned from dominant T cell responses to SARS- COV-2. *Current Opinion in Virology*, 50, 183-191 (2021).
- D. Wellington, **Z. Yin**, A. Abdel-Haq, L. Zhang, J. Forbester, K. Kite… T. Dong. IFITM3-specific antibody reveals interferon preferences and slow interferon induction of the anti-viral factor IFITM3 in humans. *European Journal of Immunology*, 51, 742-745 (2020).
- T. Silva, G. Liu, B. Lindsey, D. Dong, S. Moore, N. Hsu… **Z. Yin**… T. Dong. The impact of viral mutations on recognition by SARS-CoV-2 specific T cells. *iScience*, 24, 103353 (2021).
- D. Wellington[#], **Z. Yin**[#], Z. Yu[#], R. Heilig, S. Davis, R. Fischer… T. Dong. SARS-CoV-2 mutations affect proteasome processing to alter $CD8^+$ T cell responses. *BioRxiv* (2022, co-first author[#]).
- **Z. Yin**[#], J. Chen[#], Y. Lu[#], B. Wang[#], L. Godfrey[#], X. Yao… T. Dong. Recombinant vaccinia virus allows efficient evaluation of T cell responses to naturally processed SARS-CoV-2 spike antigens. *Manuscript in preparation* (2022, co-first author[#]).
- COvid-19 Multi-omics Blood ATlas (COMBAT) Consortium. A blood atlas of COVID-19 defines hallmarks of disease severity and specificity. *Cell,* 185, 916-938 (2021, member of COMBAT Consortium)

Awards

- China Scholarship Council - University of Oxford Scholarship, 2018-2022.
- WIMM Student Travel Fund, 2019.
- Best oral presentation, Viral Immunology Away Day, Nuffield Department of Medicine, 2019.

Table of Contents

Chapter 1 Introduction *1*

1.1 Acute viral respiratory infection. **1**

1.1.1 Acute viral respiratory infection and pandemics. 1

1.1.2 Influenza A viruses and health burden. 4

1.1.3 SARS-CoV-2 and health burden. 6

1.2 Innate immunity against RNA viruses. **9**

1.2.1 Recognition of RNA viruses by pattern-recognition receptors (PRRs). 9

1.2.2 Activation of innate immune signalling by type I IFNs. 10

1.2.3 ISG restriction of RNA viruses. 12

1.2.4 Antiviral activities of IFITM3. 13

1.2.5 Mechanisms of IFITM3-mediated IAV restriction. 16

1.2.6 Actions of IFITM3 during SARS-CoV-2 infection. 19

1.3 Adaptive immunity against RNA viruses. **20**

1.3.1 Actions of professional antigen-presenting cells (APCs). 20

1.3.2 Antigen processing and presentation through MHC class I pathway 22

1.3.3 $CD8^+$ T cell responses during virus infection. 25

1.3.4 Antigen processing and presentation through MHC class II pathway 25

1.3.5 $CD4^+$ T cell responses during virus infection. 27

1.4 Overall aims. **29**

Chapter 2 Methods and Materials *31*

2.1 Study participants. 31

2.2 Extraction of gDNA from cells. 31

2.3 Extraction of RNA using RNeasy Plus Mini kit. 32

2.4 Preparation of cDNA from RNA using High-Capacity RNA-to-cDNA kit... 32

2.5 Quantification of mRNA transcripts via qPCR. 32

2.6 Western blotting. 33

2.7 Infection of adherent cells with S-Flu. 34

2.8 Preparation of RNA-Seq samples. 34

2.9 Culture of iPSCs. 34

2.10 Differentiation of iPSCs to macrophages. 35

2.11 Isolation of mononuclear cells from peripheral blood. 35

2.12 Generation of antigen-specific T cells *in vitro*. 36

2.13 Generation of ACE2-transduced EBV-transformed BCLs. 36

2.14 Intracellular cytokine staining. 37

2.15 IFNγ-based ELISpot assay. 37

2.16 Live virus suppression assay. 37

2.17 Peptide-MHC class I tetramer staining. 38

2.18 Evaluation of T cell responses to live virus infection. 38

2.19 S-Flu virus. 38

2.20 Propagation and titration of SARS-CoV-2 live virus. 39

2.21 Antibody information. **40**

2.22 Synthetic peptides. **40**

2.23 Statistical analysis. **40**

Chapter 3 Understanding the impact of IFITM3 on influenza virus and SARS-CoV-2 infection ***42***

3.1 Introduction. **42**

3.2 Aims. **45**

3.3 Hypothesis. **46**

3.4 Results. **46**

3.4.1 IFITM3 is inducible by type I, II and III interferons in HEK293 cells. 46

3.4.2 IFITM3 reduces H1N1 infection rate in HEK293 cells. 47

3.4.4 IFITM3 is not correlated with antigen processing and presentation genes in iPSDMs. 52

3.4.5 IFITM3 promotes SARS-CoV-2 infection. 55

3.4.6 RNA sequencing was performed to study IFITM3-dependent gene expression. 56

3.4.7 Differentially expressed genes were observed due to IFITM3 depletion. 60

3.4.8 IFITM3 is correlated with antigen processing and presentation in iPSDMs during IFN-β stimulation. 70

3.4.9 IFITM3 is correlated with response to virus in iPSDMs during H1N1 infection. 73

3.4.10 IFITM3 is correlated with receptor signalling pathways in iPSDMs during H5N1 infection. 77

3.4.11 Differentially regulated genes were observed during SARS-CoV-2 infection due to IFITM3 depletion. 81

3.5 Discussion 84

3.6 Future directions 87

Chapter 4 Mapping and characterizing dominant T cell responses against SARS-CoV-2 in COVID-19 convalescent patients 89

4.1 Introduction. 89

4.2 Aims. 92

4.3 Study participants. 92

4.4 Results. 94

4.4.1 Broad and strong memory T cell responses specific to SARS-CoV-2 were observed by ex vivo assessment. 94

4.4.2 SARS-CoV-2-specific $CD8^+$ T cell responses were associated with disease severity. 97

4.4.3 Identification of one $CD8^+$ epitope from SARS-CoV-2 Spike. 98

4.4.4 Defining HLA restriction of the S-98 peptide. 100

4.4.5 Defining epitope sequence within the S-98 peptide. 103

4.4.6 Identification of SARS-CoV-2 $CD8^+$ epitopes from patient memory responses. 106

4.5 Discussion 108

4.6 Future directions 113

Chapter 5 Evaluating T cell responses against naturally processed spike antigens of SARS-CoV-2 and variants of concern *115*

5.1 Introduction. **115**

5.2 Aims. **118**

5.3 Hypotheses. **118**

5.4 Study participants. **119**

5.5 Results. **120**

5.5.1 ACE2 lentivirus transduction of B cell lines. 120

5.5.2 Live SARS-CoV-2 infection system was established to evaluate antiviral T cell immune responses. 123

5.5.3 Non-autologous BCLs were screened for target cells. 126

5.5.4 Robust T cell responses was observed against original SARS-CoV-2 virus in both vaccinated and convalescent cohorts. 129

5.5.5 Recombinant vaccinia virus system was established to evaluate antiviral T cell immune responses. 131

5.5.6 Evaluation of cross-reactivity of spike-specific T cells against SARS-CoV-2 variants using both systems. 134

5.5.7 T cell escape mutants were identified by vaccinia virus system and confirmed by live virus system. 137

5.6 Discussion **140**

5.7 Future directions **145**

Chapter 6 Summary and Final Discussion *147*

References..... *147*

List of Figures and Tables

Figure 1.1 The structure of influenza A virus. 6

Figure 1.2 The structure of SARS-CoV-2. 8

Figure 1.3 Genomic and proteomic organization of SARS-CoV-2. 8

Figure 1.4 Canonical and uncanonical type I IFN signalling pathways. 12

Figure 1.5 A schematic model of IFITM3 in the membrane. 16

Figure 1.6 Models for IFITM3-mediated restriction of IAV infection. 18

Figure 1.7 Antigen processing pathway via MHC class I. 24

Figure 1.8 Antigen processing pathway via MHC class II. 27

Figure 3.1 Correlation between TAP1 and IFITM3. 45

Figure 3.2 Stimulation of IFITM3 by IFNs in HEK293. 47

Figure 3.3 S-Flu PR8 (H1N1) infection rate in IFITM3$^{+/+}$ (WT) and IFITM3$^{-/-}$ (KO) HEK293. 48

Figure 3.4 S-Flu PR8 (H1N1) infection rate in IFITM3$^{+/+}$ (WT) and IFITM3$^{-/-}$ (KO) iPSDMs. 51

Figure 3.5 H5N1 S-Flu PR8 infection in IFITM3$^{+/+}$ and IFITM3$^{-/-}$ iPSDMs. 52

Figure 3.6 Expression of several antigen processing and presentation related proteins in IFITM3$^{+/+}$ (WT) and IFITM3$^{-/-}$ (KO) iPSDMs. 54

Figure 3.7 SARS-CoV-2 infection in IFITM3$^{+/+}$ and IFITM3$^{-/-}$ iPSDMs and SARS-CoV-2-specific T cell responses against infected iPSDMs. 56

Figure 3.8 The impact of IFITM3 depletion in iPSCs. 62

Figure 3.9 The impact of IFITM3 depletion in iPSDMs. 66

Figure 3.10 The impact of IFITM3 depletion in A549. 69

Figure 3.11 The impact of IFITM3 depletion in iPSDMs during IFN-β stimulation. 72

Figure 3.12 The impact of IFITM3 depletion in iPSDMs during H1N1 infection..76

Figure 3.13 The impact of IFITM3 depletion in iPSDMs during H5N1 infection..80

Figure 3.14 The impact of IFITM3 depletion in iPSDMs during SARS-CoV-2 infection.. 83

Figure 4.1 Participant characteristics...... 93

Figure 4.2 Comparison of the magnitude of T cell responses specific to each viral protein between mild (n=28) and severe cases (n=14)...... 95

Figure 4.3 Comparison of the relative proportion of SARS-CoV-2 peptide-pool-reactive $CD8^+$ T cells between mild and severe cases...... 98

Figure 4.4 Mapping of peptides containing SARS-CoV-2 T cell epitopes in the patient C-COV19-064...... 100

Figure 4.5 Identification of HLA restriction for S-98 CD8 epitope from C-COV19-064. 102

Figure 4.6 Identification of the optimal epitope sequence recognized by S98 CD8-064. 105

Figure 5.1 Transduction of ACE2 into BCLs. 123

Figure 5.2 Establishment of live SARS-CoV-2 infection system...... 125

Figure 5.3 Identification of non-autologous BCLs as target cells.. 127

Figure 5.4 Functional evaluation of T cell responses against original SARS-CoV-2 virus in vaccinated and convalescent cohorts.. 130

Figure 5.5 Evaluation of spike-specific $CD4^+$ and $CD8^+$ T cell responses to BCLs infected with VV_SARS2 or VV_Zika. 133

Figure 5.6 Evaluation of spike-specific $CD4^+$ and $CD8^+$ T cell responses to SARS-CoV-2 VoCs using recombinant vaccinia virus system and live SARS-CoV-2 infection system. 136

Figure 5.7 Confirmation of single escape mutation in Omicron. 139

Table 1 Timeline of the pandemics in human history. 3

Table 2 Viruses restricted by IFITMs. 15

Table 3.1 Antigen processing and presentation related genes that correlate with IFITM3. 45

Table 3.2 RNA-Seq plan. 59

Table 3.3 Differentially expressed genes in $IFITM3^{-/-}$ iPSCs compared to $IFITM3^{+/+}$ iPSCs 63

Table 4.1 Two-dimensional peptide pools spanning SARS-CoV-2 Spike, NP, M, Env and ORFs 96

Table 4.2 Peptides containing SARS-CoV-2 T cell epitopes. 107

Table 4.3 SARS-CoV-2 CD8 optimal epitopes. 108

Table 5.1 HLA-typing of BCL-ACE2 123

Table 5.2 HLA-typing of donors that don't have autologous BCL-ACE2. 127

Table 5.3 Plan of target cell screening for $CD8^+$ T cell lines 128

Table 5.4 Plan of target cell screening for $CD4^+$ T cell lines 128

Table 5.5 Summary of target cells for each T cell line 128

Table 5.6 Potential T cell immune escape observed by vaccinia virus system. 140

Table 5.7 T cell epitopes that contain immune escape mutations. 140

Table 5.8 Comparison of current methods for T cell functional evaluation. 144

List of Abbreviations

ACE2	angiotensin-converting enzyme 2
AMs	alveolar macrophages
ARIs	acute respiratory infections
APCs	antigen-presenting cells
BCLs	B cell lymphoblastoids
CD	cluster of differentiation
cDCs	conventional dendritic cells
CMV	cytomegalovirus
CoVs	coronaviruses
COVID-19	coronavirus disease-2019
CTLs	cytotoxic T lymphocytes
DNA	deoxyribonucleic acid
DCs	dendritic cells
dsDNA	double-stranded DNA
dsRNA	Double-stranded RNA
EBV	Epstein-Barr virus
ER	endoplasmic reticulum
ERK1/2	extracellular signal-regulated protein kinase 1/2
FACS	fluorescence-activated cell sorting
Fas-L	Fas ligand
GFP	green fluorescent protein
HLA	human leukocyte antigen
HIV-1	human immunodeficiency virus-1

IAV	influenza virus A
IFNγ	interferon gamma
IFITM3	interferon-induced transmembrane protein 3
IL-2	interleukin 2
ISRE	interferon-sensitive response element
IRF9	interferon regulatory factor 9
ISG	interferon stimulated genes
JAK	janus tyronsine kinase
LNs	lymph nodes
MHC	major histocompatibility complex
NLR	NOD-like receptor
NK cells	natural killer cells
ORFs	open reading frames
mRNA	messenger ribonucleic acid
PBMC	peripheral blood mononuclear cells
PCR	polymerase chain reaction
PAMP	pathogen-associated molecular patterns
PRRs	pattern recognition receptors
RLR	RIG-I-like receptors
SARS-CoV	severe acute respiratory syndrome coronavirus
SARS-CoV-2	severe acute respiratory syndrome coronavirus 2
MERS-CoV	Middle East respiratory syndrome coronavirus
SNP	single nucleotide polymorphism
ssRNA	single-stranded RNA

STAT	signal transducer and activator of transcription
TAP	transporter-associated protein
TCR	T cell receptor
TLRs	Toll-like receptors
TNFα	tumor necrosis factor alpha
vRNP	viral ribonucleoprotein

Chapter 1

Introduction

1.1 Acute viral respiratory infection.

1.1.1 Acute viral respiratory infection and pandemics.

Acute respiratory infections (ARIs) are classified as upper respiratory tract infections (URIs) or lower respiratory tract infections (LRIs). ARIs are mostly limited to the upper airways and are self-limiting, but a small percentage can progress to LRIs as bronchiolitis and pneumonia[1]. Most URIs have a viral aetiology. Rhinoviruses account for 25 to 30 percent of URIs; respiratory syncytial viruses (RSVs), parainfluenza and influenza viruses, human metapneumoviruses, and adenoviruses for 25 to 35 percent; coronaviruses (CoVs) for 10 percent; and for the remaining percentage the cause is unknown[2]. As for LRIs, the most common causes are RSV, parainfluenza and influenza viruses. Human respiratory virus infection leads to a spectrum of respiratory symptoms and disease severity, contributing to substantial morbidity, mortality, and economic losses worldwide.

The most worrying respiratory viruses are those that cause epidemics and pandemics. Since the 20th century, influenza A viruses (IAVs) and CoVs, including severe acute respiratory syndrome coronavirus (SARS-CoV), Middle East respiratory syndrome coronavirus (MERS-CoV) and the newly emerged SARS-CoV-2, have become the main pathogens that cause pandemics (**Table 1**)[3]. This is not surprising as one of the main characteristics of respiratory viruses is their relatively easy mode of transmission: direct (physical) contact, indirect contact (fomite), droplets and aerosols[4]. Another characteristic of IAVs and CoVs that contributes to their high transmissibility is that they

are all zoonotic pathogens. Due to increased contact with animals through breeding, hunting and global trade activities, those zoonotic pathogens are easily transmitted to humans.

IAV and SARS-CoV-2 infection represent major diseases and have a huge economic burden worldwide. Understanding both virus-dependent and host-dependent factors in viral clearance and resolution of infection is critical for both prevention and treatment of these respiratory diseases.

Table 1 Timeline of the pandemics in human history. *Adapted from Piret et al. Front. Microbiol. 2021*

Years	Pandemics	Pathogens	Vectors
541–543	Plague of Justinian	*Yersinia pestis*	Fleas associated to wild rodents
1347–1351	Black Death	*Yersinia pestis*	Fleas associated to wild rodents
1817–1824	First cholera pandemic	*Vibrio cholerae*	Contaminated water
1827–1835	Second cholera pandemic	*Vibrio cholerae*	Contaminated water
1839–1856	Third cholera pandemic	*Vibrio cholerae*	Contaminated water
1863–1875	Fourth cholera pandemic	*Vibrio cholerae*	Contaminated water
1881–1886	Fifth cholera pandemic	*Vibrio cholerae*	Contaminated water
1885–ongoing	Third plague	*Yersinia pestis*	Fleas associated to wild rodents
1889–1893	Russian flu	Influenza A/H3N8?	Avian?
1899–1923	Sixth cholera pandemic	*Vibrio cholerae*	Contaminated water
1918–1919	Spanish flu	Influenza A/H1N1	Avian
1957–1959	Asian flu	Influenza A/H2N2	Avian
1961-ongoing	Seventh cholera pandemic	*Vibrio cholerae*	Contaminated water
1968–1970	Hong Kong flu	Influenza A/H3N2	Avian
2002–2003	Severe acute respiratory syndrome (SARS)	SARS-CoV	Bats, palm civets
2009–2010	Swine flu	Influenza A/H1N1	Pigs
2015-ongoing	Middle East respiratory syndrome (MERS)	MERS-CoV	Bats, dromedary camels
2019-ongoing	COVID-19	SARS-CoV-2	Bats, pangolins?

1.1.2 Influenza A viruses and health burden.

Influenza viruses are enveloped viruses characterized by a segmented, negative sense and single-stranded RNA genome[5]. They are classified as 4 genera: type A, B, C and D, of which only type A and B (IAVs and IBVs) are clinically relevant to humans. IAVs and IBVs share similar structures; both have 8 viral RNA (vRNA) gene segments encoding 10 viral proteins. A representative structure of IAV is shown in **Figure 1.1**. The viral genome is encapsulated by the nucleoprotein (NP) which stabilises the polymerase complexes, consisting of the three RNA polymerase proteins PB1, PB2 and PA. The whole viral ribonucleoprotein (vRNP) complexes are encircled by the matrix protein M1 and lipid bilayer envelope in which glycoproteins haemagglutinin (HA) and neuraminidase (NA) as well as the matrix protein M2 are embedded[5].

The detailed classification of IAVs is based on the genetic and antigenic properties of the HA (H1-H18) and NA (N1-N11). These two transmembrane proteins mediate the viral entry and release, respectively[6]. IBVs are not divided into subtypes, but instead are further classified into only two lineages: B/Yamagata and B/Victoria[1] due to the slower mutation rate than is seen in IAVs [1].

Although both IAVs and IBVs can cause seasonal epidemics, influenza A is the only type that has been reported to cause pandemics so far. Seasonal influenza is estimated by World Health Organization (WHO) to cause 290,000-650,000 deaths globally each year due to respiratory disease only. New lineages of IAV emerge every few decades, and those that lack immunity in the human population result in pandemics[5]. New IAVs emerge through antigenic drift in avian viruses (1918 Spanish flu: H1N1, 40-100 million deaths; 2009 North American flu: H1N1, 300,000 deaths) or through antigenic shift, which is the reassortment of gene segments in animal hosts infected with

two different viruses (1957 Asian flu: H2N2, 2 million deaths; 1968 Hong Kong flu: H3N2, 500,000 deaths).

Annual influenza vaccination is the current strategy to prevent infection. Most influenza vaccines in use are manufactured influenza virus propagated in eggs and formalin inactivated, with antigens presented as split or subunit[7]. Most available vaccines worldwide are quadrivalent, consisting of an A(H3N2), an A(H1N1)pdm09, and a representative of each of the Victoria and Yamagata lineages of IBVs. In some countries, influenza vaccines are trivalent, containing the two IAV strains and only one IBV lineage. The viral antigens in the vaccines are updated regularly to cope with the antigenic drift among circulating influenza viruses. The effectiveness of influenza vaccines varies depending on many factors, such as antigenic match between circulating influenza virus strains and vaccine components, time post vaccination, and host factors such as age, immune function, earlier exposure to influenza viruses and vaccination history[8]. During 2004-2020, influenza vaccine effectiveness against medically attended influenza among outpatients in the USA ranged from 10% to 60%[9].

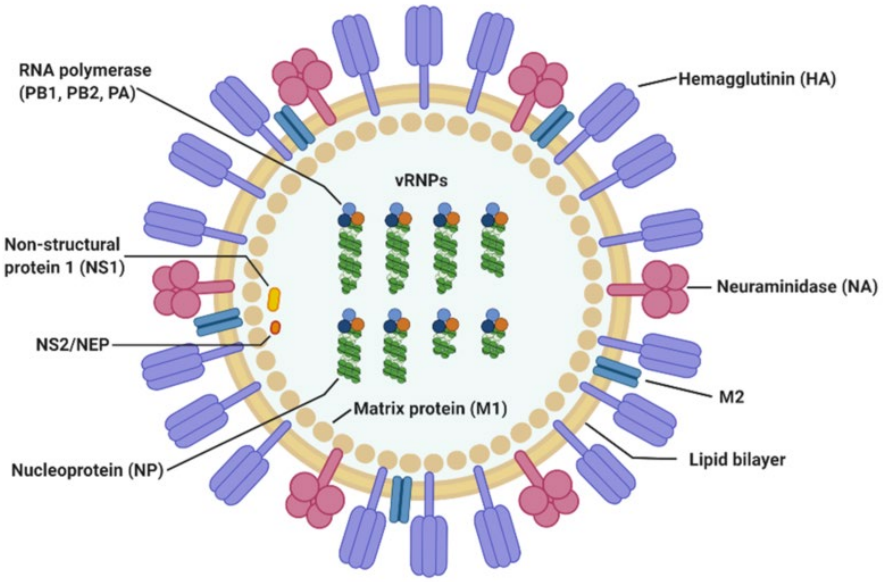


Figure 1.1 The structure of influenza A virus. *The IAV genome is divided into eight segments that encode 10 viral proteins: HA, NA, M1, M2, NP, NS1, NS2, PA, PB1 and PB2. The viral envelope of IAV contains the transmembrane protein HA, NA and M2. Adapted from Jung et al. Viruses. 2020.*

1.1.3 SARS-CoV-2 and health burden.

SARS-CoV-2, which emerged in late 2019, causes a pandemic of coronavirus disease 2019 (COVID-19). The virus rapidly spread all over the world within a few months and is still circulating now. As of August 2022, more than 600 million infections and more than 6.4 million deaths were caused by COVID-19 worldwide, posing an extraordinary threat to global public health.

Like IAV, SARS-CoV-2 is an enveloped positive-sense single-stranded RNA virus and belongs to the family *Coronaviridae*[10]. *Coronaviridae* includes the subfamilies, *Letovirinae* and *Orthocoronavirinae*; the members of this family are known as CoVs. CoVs are specified into four genera: alpha, beta, gamma and delta. Alphacoronaviruses (α-CoVs) and betacoronaviruses (β-CoVs) exclusively infect mammalian species, while the other two have a wider range of hosts, including avian species[11]. To date, seven human coronaviruses (HCoVs) have been identified that cause seasonal respiratory diseases. HCoV-229E and -OC43, which belong to the α-CoVs, are the causative agents of

common cold[12]. HCoV-NL63 and -HKU1, which belong to the β-CoVs, cause more severe but rarely fatal respiratory illnesses[12]. SARS-CoV, MERS-CoV and SARS-CoV-2, which also belong to β-CoVs, are highly pathogenic and even life-threatening[13].

The genome of SARS-CoV-2 encodes four structural proteins: spike protein (S), envelope protein (E), membrane protein (M), nucleocapsid protein (N)[14]. The structure of SARS-CoV-2 is shown in **Figure 1.2**. A varying number of open reading frames encoding non-structural proteins are scattered among the structural genes[15] (**Figure 1.3**). The non-structural proteins participate in virus replication but are not incorporated into the virion.

Vaccination is again proved to be an important tool in stopping the pandemic in case of COVID-19. Currently, more than six advanced technology platforms are used to develop COVID-19 vaccines, including nucleic acid technologies (genetically modified DNA and mRNA), non-replicating or replicating viral vectors, inactivated viruses, attenuated viruses, virus-like particles, and protein subunits[16]. COVID-19 vaccine performance is affected by SARS-CoV-2 viral mutations due to highly variable receptor-binding motif in the Spike[17]. A significant reduction of neutralization activity was observed against B.1.351 (Beta) variant in vaccinees[18]. The effectiveness of different types of COVID-19 vaccines varies but mRNA vaccines, BNT162b2 and mRNA-1273, generally show the best overall efficacy. A study on the effectiveness of mRNA vaccines in American healthcare workers showed that the overall efficacy of BNT162b and mRNA-1273 were 88.8% and 88.9%, respectively[19].

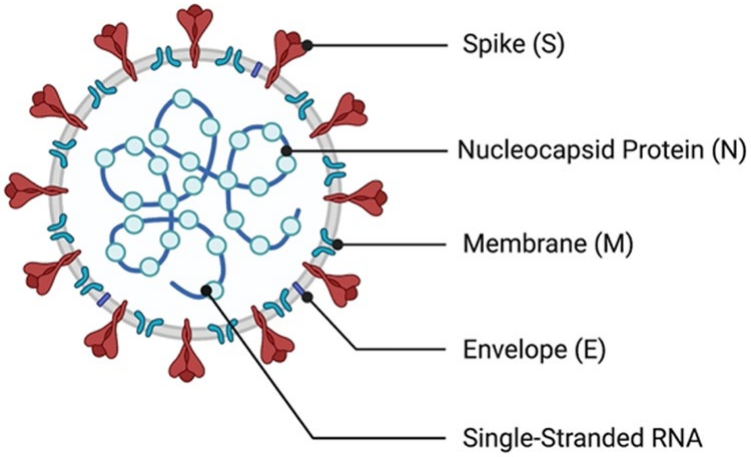


Figure 1.2 The structure of SARS-CoV-2. *The envelope of SARS-CoV-2 contains spike glycoprotein (S), membrane glycoprotein (M), envelope glycoprotein (E). Nucleocapsid phosphoprotein (N) holds viral RNA. Adapted from Jamison et al. Eur. J. Hum. Genet. 2022.*

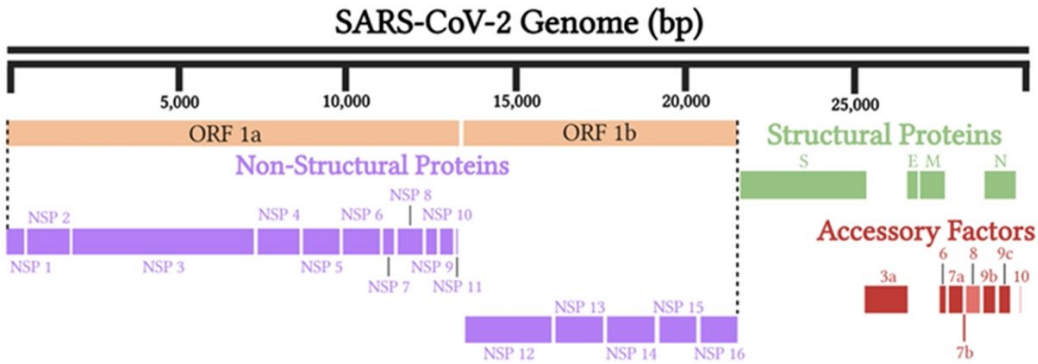


Figure 1.3 Genomic and proteomic organization of SARS-CoV-2. *ORF1a and ORF1b encode non-structural proteins, while the other genes encode structural proteins (S, E, M and N) and accessory proteins (ORF3a, ORF6, ORF7a, ORF7b, ORF8, ORF9b, ORF9c and ORF10). Adapted from Jamison et al. Eur. J. Hum. Genet. 2022.*

Respiratory viruses have the potential to cause major epidemics, even pandemics, due to their relatively easy modes of transmission and high mutation rates. Vaccination plays a critical role in preventing the spread of virus and ultimately quelling the epidemics or pandemics. Understanding viral immunity against respiratory viruses is pivotal in vaccine development, including evaluating the safety and protective efficacy, determining the injection schedule, and establishing the effective dosage. As both influenza virus and CoVs are RNA viruses, we are particularly interested in the viral immunity against RNA viruses.

1.2 Innate immunity against RNA viruses.

1.2.1 Recognition of RNA viruses by pattern-recognition receptors (PRRs).

The first line of defence against invading RNA viruses is the innate immune system, which is comprised of physical barriers (mucus and collectins) and phagocytic cells. Recognition of pathogen-associated molecular patterns (PAMPs) is the first and essential step in innate immune responses[20]. These PAMPs are molecular structures such as glycoproteins, lipopolysaccharides, proteoglycans and nucleic acids that are unique to invading pathogens[21]. Sense of PAMPs by pattern recognition receptors (PRRs), which are expressed by a variety of immune cells, initiates innate immune responses.

Toll-like receptors (TLRs) are the most extensively studied family of PRRs so far. TLRs are transmembrane glycoprotein receptors with a N-terminal extracellular PAMP-binding region and a C-terminal intracellular signalling region. The N-terminal region contains multiple leucine-rich repeats (LRRs) which form a horseshoe structure. The C-terminal region, which is referred to as the Toll/IL-1R homology (TIR) domain, mediates downstream signalling pathways upon activation of the receptor[22]. Once the extracellular ligands bind to the N-terminus of TLRs, TLRs will be induced to dimerize, bringing together the cytoplasmic TIR domains and subsequently recruiting adaptor molecules to initiate the signalling process[23]. The human TLR multigene family comprises 10 members, of which TLR2, -3, -4, -7 and -8 are thought to be important in the recognition of structural components of RNA viruses, including single-stranded RNA (ssRNA), double-stranded RNA (dsRNA) and surface glycoproteins. Among these receptors, TLR3, -7 and -8 recognize nucleic acid motifs and are preferentially confined to intracellular compartments, such as the endoplasmic reticulum (ER), endosomes, lysosomes, and

endolysosomes, rather than being expressed at the cell surface, which is the case for most of the TLR family members[21].

Following early reports of TLR-independent mechanism of viral sensing, the retinoic acid-inducible gene I (RIG-I)-like receptors (RLRs) were discovered as cytosolic sensors of RNA viruses[24]. The recognition by RLRs is essential in early antiviral responses to several viruses. RLRs are expressed at low concentrations in most cells of the human organism, and these concentrations are greatly increased upon stimulation[24-26].

Besides the TLRs and the RLRs, nucleotide-binding oligomerization domain-containing (NOD)-like receptors (NLRs) were also described to sense RNA virus invasion. NLRs are cytosolic sensors of ssRNA viruses such as Sendai virus and IAVs, as well as double-stranded DNA (dsDNA) viruses such as adenoviruses. NLRs are known to regulate interleukin-1β (IL-1β) maturation through activation of caspase-1[27,28].

1.2.2 Activation of innate immune signalling by type I IFNs.

Sensing of PAMPs by PRRs markedly activates the transcription of genes involved in inflammatory responses, leading to the production of proinflammatory cytokines/chemokines, type I interferons (IFNs, primarily IFN-α and IFN-β) and antimicrobial proteins. Type I IFNs are produced by a wide range of cells, including professional innate immune cells such as dendritic cells (DCs) and macrophages, and non-professional cells such as fibroblasts[29]. Type I IFNs play a central role in the antiviral process as they trigger the transcription of many IFN-stimulated genes (ISGs) which are involved in eliminating viral components from infected cells, inducing apoptosis of infected cells and conferring resistance to viral infection on uninfected cells. Type I IFNs

also enhance maturation of DCs, cytotoxicity of natural killer (NK) cells, and the differentiation of $CD8^+$ T cells, thus providing an important link between innate and adaptive immune responses[30].

Type I IFNs activate intracellular signalling pathways via type I IFN receptors, the mechanisms of which are shown in **Figure 1.4**. Canonically, after binding to type I IFNs, IFNAR, which consists of IFNAR1 and IFNAR2, phosphorylates and activates the associated tyrosine kinases JAK1 and non-receptor tyrosine kinase 2 (TYK2)[31], which subsequently induces phosphorylation of signal transducer and activator of transcription 1 (STAT1) and STAT2. Phosphorylated STAT1 and STAT2 dimerize and in turn recruit IFN-regulatory factor 9 (IRF9). The whole complex then translocates into the nucleus and binds to IFN-stimulated response elements (ISREs) to activate the transcription of antiviral genes[32]. In addition, phosphorylated STAT1 can also homodimerize. The homodimer translocates into the nucleus and binds to gamma-activated sequence (GAS) in the promoters of pro-inflammatory genes[33]. Besides the JAK-STAT dependent pathway, type I IFNs can also activate downstream signalling independent of STAT. Activation of mitogen activated protein kinases (MAPKs) pathways induces an extracellular signal regulated kinase 1/2 (ERK1/2) signalling[34], which can further induce transcription of ISGs. Additionally, the phosphatidylinositol 3-kinase (PI3K) pathway can also mediate type I IFNs-stimulated gene transcription[31]. Another downstream signalling component of PI3K-AKT pathway is mammalian target of rapamycin (mTOR), a key protein regulating mRNA translation[35].

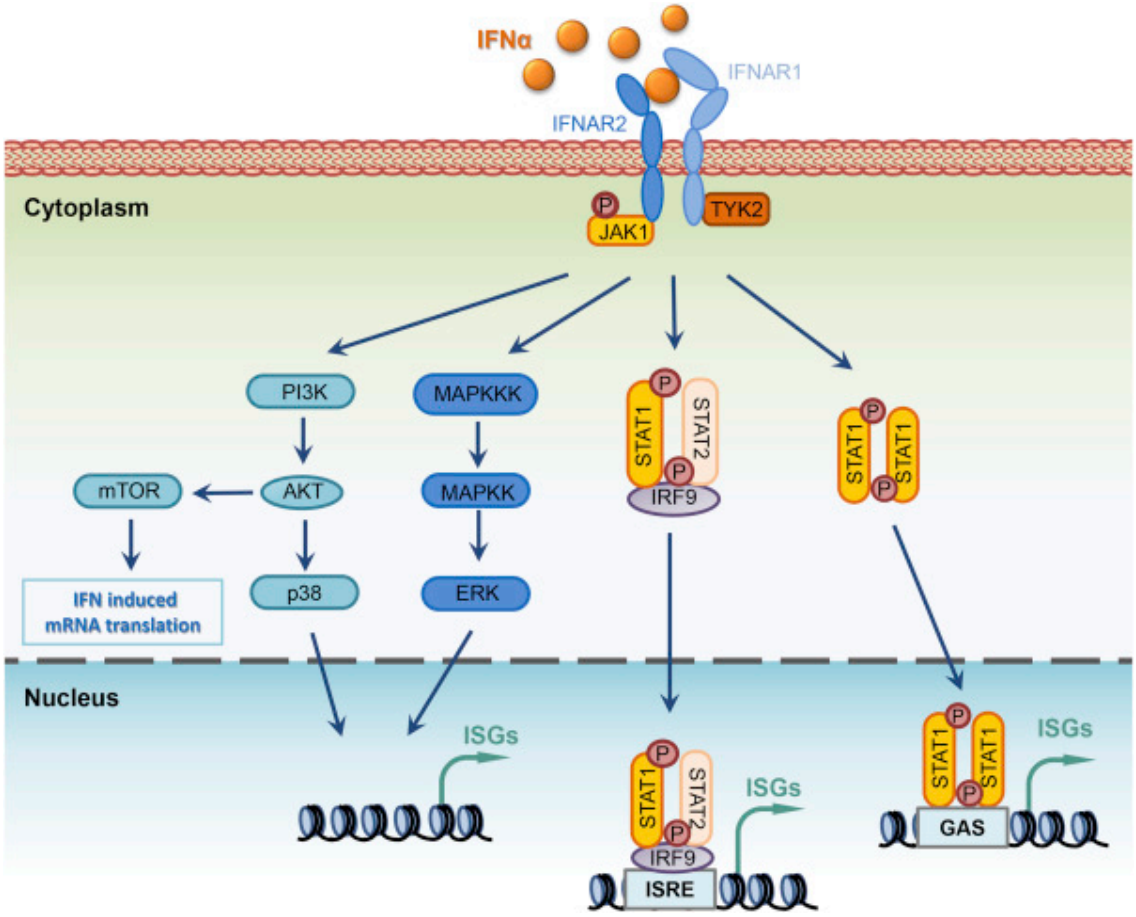


Figure 1.4 Canonical and uncanonical type I IFN signalling pathways. *Adapted from Chen et al. J. Autoimmun. 2017.*

1.2.3 ISG restriction of RNA viruses.

The primary function of type I IFN signalling pathway is to trigger transcriptional changes of ISGs, which have antiviral, antiproliferative, or proinflammatory effects, in affected cells and neighbouring cells. The concentration of environmental type I IFNs is highly related to the transcription that occurs in the cells. It has been reported that low concentration of type I IFNs is enough to stimulate antiviral gene expression, however, more immunopathogenic genes, such as those involved in cell antiproliferation, are induced under higher IFN concentration[36]. A large portion of antiviral ISGs was discovered by discovery-based screens for antiviral effects on virus replication[37-40]. Typically, virus replication was assessed using infectious viruses that can undergo a full

life cycle, including entry, uncoating, genome replication, particle assembly and egress. Alternatively, replication can be assessed with replicons, which are viral genomes that are genetically engineered to be competent for replication but unable to produce infectious viruses. Some ISGs show broad activities against a wide range of viruses, while others are more restricted in specificity.

ISGs work in combination to achieve a fully functional antiviral state and they can potentially inhibit all steps of viral life cycle. Targeting early, post-entry life cycle events is a common mode of ISG action. For example, interferon-induced transmembrane (IFITM) proteins have been found to inhibit viral entry and viral particle trafficking. Virus assembly and egress have also been reported to be viable ISG targets. For example, bone marrow stromal cell antigen 2 (BST2), an ISG encoding tetherin, prevents release of HIV-1 virions from the cell surface[41]. Viperin inhibits the release of IAVs through interactions with the cellular enzyme farnesyl diphosphate synthase to perturb lipid rafts[42].

A large number of ISGs are involved in PRR recognition, IFN induction and IFN signalling, such as RLRs, STAT1 and IRFs[43,44]. The antiviral activities of those downstream IFN effectors partly serve to reinforce upstream signalling pathways, which highlights the ability of IFN to self-regulate.

1.2.4 Antiviral activities of IFITM3.

Interferon-induced transmembrane protein 3 (IFITM3) is an important downstream effector of type I IFN signalling pathway. IFITM3 belongs to the IFITM family, which are a group of homologous proteins localized in the plasma and endolysosomal membranes[45-47]. There are five functional members of IFITM family: IFITM1, 2, and 3 are IFN-inducible and have antiviral properties, while IFITM5 and 10 are not IFN-

inducible or antiviral. Although there is overlap among viruses restricted by IFITM proteins, IFITM1 better prevents early endosome-entering viruses, and IFITM2 and IFITM3 exert more resistance to viruses that enter in the late endosomes or lysosomes, such as IAV[48,49]. The specificity of IFITM-mediated restriction is consistent with their location. IFITM1 is localised to the plasma membrane and early endosomal membranes, whereas IFITM2 and IFITM3 are found in late endosomal and lysosomal membranes[50]. IFITM2 behaves similarly to IFITM3 in terms of viral specificity, albeit with weaker effect[38].

As of 2017, IFITM3 has been reported to restrict at least 16 viruses, most of which are RNA viruses, including IAV and SARS-CoV (**Table 2**). IFITM3 has been identified as a restriction factor for IAV by a genome-wide small interfering RNA (siRNA) screening[51]. Using *ifitm3* KO mice, the lack of IFITM3 has been shown to be associated with higher virus replication and higher death rates in IAV-infected mice[52]. A variant of IFITM3, the single nucleotide polymorphism (SNP) rs12252-C, is associated with more severe IAV infections, suggesting that IFITM3 genotype within a population may influence the course of seasonal influenza epidemics and pandemics[53]. The restriction of SARS-CoV by IFITM3 was demonstrated in A549 overexpressing angiotensin-converting enzyme 2 (ACE2) and Vero E6 cells[54].

Table 2 Viruses restricted by IFITMs. *(Summarized by Dannielle Wellington)*

Virus	Type	Restricted by	Reference
African Swine Fever	dsDNA	IFITM 1/2/3	Munoz-Moreno *et al*, 2016;
Dengue	ssRNA	IFITM 2/3	Brass *et al* , 2009; Jiang *et al*, 2010;
Ebola	ssRNA	IFITM 1/2/3	Huang *et al* , 2011; Wrensch *et al* , 2013;
Hantaan	ssRNA	IFITM 3	Xu-Yang *et al* , 2016;
Hepatitis C	ssRNA	IFITM 3	Yao *et al* , 2011; Narayana *et al* , 2015;
HIV-1	ssRNA	IFITM 1/2/3	Lu *et al* , 2011; Compton *et al*, 2014; Jia *et al* , 2015; Zhang *et al*, 2015; Foster *et al*, 2016; Raposo *et al*, 2017; Calonge *et al* , 2017;
Influenza A	ssRNA	IFITM 1/2/3	Brass *et al* , 2009; Feeley *et al* , 2011; Huang *et al* , 2011; Bailey *et al* , 2012; Everitt *et al* , 2012; Zhang *et al*, 2013; Desai *et al* , 2014; Williams *et al* , 2014; Sun *et al* , 2016; Allen *et al* , 2017; Gerlach *et al* , 2017; Randolph *et al* , 2017;
Influenza B	ssRNA	IFITM 3	Everitt *et al*, 2012;
Marburg	ssRNA	IFITM 1/2/3	Huang *et al*, 2011;
Rift Valley Fever	ssRNA	IFITM 2/3	Mudhasani *et al* , 2013;
SARS	ssRNA	IFITM 1/2/3	Huang *et al*, 2011;
Semliki Forest	ssRNA	IFITM 2/3	Weston *et al* , 2016;
Sindbis	ssRNA	IFITM 2/3	Weston *et al* , 2016;
Vesicular Stomatitis	ssRNA	IFITM 3	Weidner *et al* , 2010;
West Nile	ssRNA	IFITM 1/2/3	Brass *et al* , 2009; Jiang *et al* 2010;
Zika	ssRNA	IFITM 1/3	Savidis *et al* , 2016;

The IFITM3 protein is a small, membrane bound, 133 amino acids and 15 kilodaltons (kDa) protein. The crystal structure of IFITM3 is not currently available as its highly hydrophobic nature is a barrier to crystallisation. A combination of Electron Paramagnetic Resonance (EPR) and Nuclear Magnetic Resonance (NMR) identified a transmembrane α-helix at C-terminal and two short intramembrane α-helices at N-terminal which is now the current accepted structure for IFITM3 (**Figure 1.5**)[55].

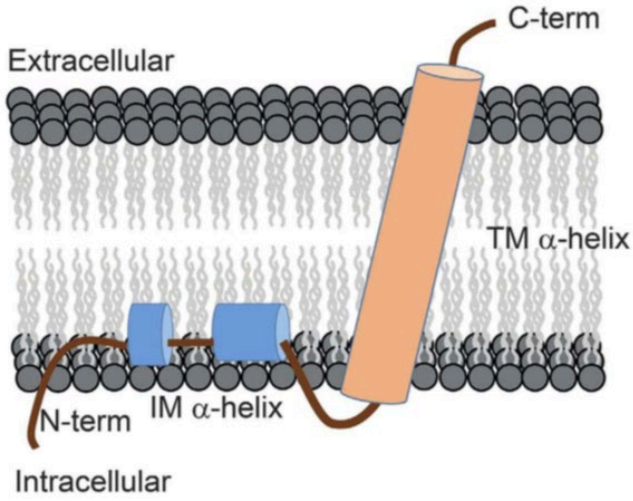


Figure 1.5 A schematic model of IFITM3 in the membrane. *IFITM3 contains a C-terminal transmembrane α-helix and two short intramembrane α-helices. Adapted from Ling et al. Sci. Rep. 2016.*

1.2.5 Mechanisms of IFITM3-mediated IAV restriction.

The mechanisms by which IFITM3 restricts IAV infection have been intensively investigated. Currently, it is understood that IFITM3 restricts the entry of the viral genome from the endosomal compartment into the cytosol for replication, and their localisation at late endosome is critical. The entry of IAV, shown in **Figure 1.6**, is initiated by the binding of HA on the viral envelope with the glycoconjugates, which contain terminal sialic acid (SA) residues, on host cell surfaces. Once inside the cell, the virus is trafficked to the endosome where the low pH facilitates a conformational change in HA, promoting the hemifusion of the viral envelope with the endosomal membrane.

The low pH also opens M2 ion channels on the viral envelope to release viral ribonucleoproteins (vRNPs) by acidifying the viral interior. HA further collapses into a trimer of hairpins to promote the formation of fusion pores, which releases vRNPs into the host cell cytoplasm. vRNA then enters the nucleus for replication, led by the exposed nuclear localization signals (NLS) on vRNPs[56].

IFITM3 localizes predominantly within the late endosomal membrane and plays an important role in endosomal pathway. Early studies investigating the mechanisms of IFITM3-mediated viral restriction suggested that IFITM3 inhibits virus-host hemifusion[57]. In contrast to those studies, Desai *et al* showed that IFITM3 prevents the release of viral genomes into the cytosol by inhibiting viral entry after hemifusion but prior to fusion pore formation[58] (**Figure 1.6**). The function of IFITM3 was described as stabilizing the cytoplasmic leaflet of the endosomal membranes without affecting the luminal leaflet. Thus, the virus-endosome hemifusion still happens but the formation of fusion pores on the endosomal membrane is blocked by IFITM3. Therefore, the viral RNA is retained within the late endosome and later degraded in the lysosome. In their study, they proposed three hypotheses on how IFITM3 interferes with pore formation: 1) IFITM3 directly partitions into the cytoplasmic leaflet of a hemifusion intermediate; 2) IFITM3 indirectly modulates the lipid/protein composition of this leaflet; 3) IFITM3 may redirect IAV fusion to a non-productive pathway, perhaps by promoting fusion with intralumenal vesicles within multivesicular bodies/late endosomes.

Besides the role of IFITM3 in blocking fusion pore formation, another study also demonstrated that IFITM3 on endosomal membranes enhanced the trafficking of IAV-containing endosomes to lysosomes, which facilitated the degradation of IAVs[59]. In addition, loss of clathrin at the cell surface and decreased rates of clathrin-mediated

endocytosis were observed in *ifitm3*$^{-/-}$ mice[60]. In the same study, they also observed direct interaction between Ifitm3 and v-ATPase, which was crucial for nominal acidification.

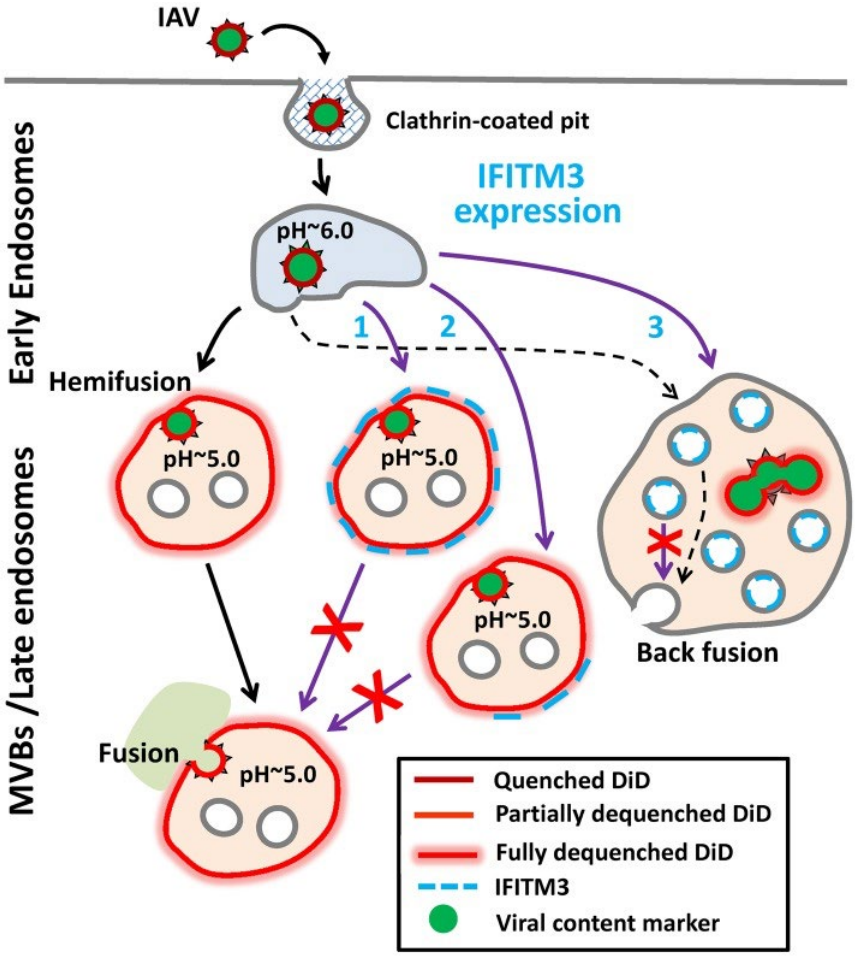


Figure 1.6 Models for IFITM3-mediated restriction of IAV infection. *IAV particles are co-labelled with AF488 (green) and vDiD (red). IAV hemifusion with an endosomal membrane (gray) leads to vDiD dequenching. Black arrows illustrate IAV fusion pathway. Purple arrows illustrate possible mechanisms on how IFITM3 blocks fusion pore formation. Dashed black arrows illustrate possible IAV fusion pathway in cells expressing low, endogenous levels of IFITM3. Adapted from Desai et al. PLoS Pathog. 2014.*

Beyond IFITM3's role in the endosomal pathway, more and more studies have suggested that IFITM3 functions as part of a multiprotein complex. Fu *et al* reported that the interaction between IFITM3 and Zinc Metallopeptidase STE24 (ZMPSTE24), a transmembrane metalloprotease, was required for IFITM3-mediated IAV restriction[61]. Jiang *et al* showed that the interaction between excess IFITM3 and IRF3 facilitated the autophagosomal degradation of IRF3 and suppressed the further induction of IFN-β,

presenting a role of IFITM3 in negative feedback regulation[62]. Clement *et al* demonstrated that IFITM3 bound to the reticulon 4 isoform Nogo-B, the mediator of TLR-dependent pro-inflammatory cytokine production, and promoted its proteasomal degradation, leading to the reduced IL-6 production in response to human cytomegalovirus (HCMV)[63].

1.2.6 Actions of IFITM3 during SARS-CoV-2 infection.

Following the outbreak of COVID-19, researchers started to look into the role of IFITM3 during SARS-CoV-2 infection. Regino-Zamarripa *et al* observed upregulated IFITM3 mRNA expression in peripheral leukocytes from severe COVID-19 patients, compared to healthy controls[64]. However, no association was observed between IFITM3 expression and COVID-19 mortality in their study. IFITM3 mRNA expression in nasopharyngeal swabs was also higher in SARS-CoV-2-positive individuals compared to negative ones[65].

Both pro- and anti-viral activities mediated by IFITM3 have been reported for SARS-CoV-2. Overexpression of IFITM3 was shown to be capable of inhibiting SARS-CoV-2 RNA production in HEK293 cells overexpressing ACE2[66,67]. Shi *et al* showed that amphipathic helix of IFITM3 restricts SARS-CoV-2 entry by inhibiting Spike-mediated fusion with the plasma membrane[67]. Another study reported that IFITM3 reduced the spread of SARS-CoV-2 virus by inhibiting the Spike-mediated fusion of SARS-CoV-2-infected cells, which expressed Spike at the cell surface, with ACE2-postive neighbouring cells[68].

On the other hand, it is also reported that silencing of endogenous IFITM3 expression in human epithelial lung cancer cell line Calu-3 strongly impairs SARS-CoV-2 RNA production, indicating that SARS-CoV-2 Spike protein may exploit any

interaction with IFITM3[66]. Another study showed that IFITM3 was required for efficient replication of SARS-CoV-2 in cardiomyocytes and gut organoids. They further investigated the impact of IFITM3 on the propagation of SARS-CoV-2 VoCs and found that depletion of IFITM3 reduced viral RNA production by all VoCs in the Calu-3[69].

1.3 Adaptive immunity against RNA viruses.

While the innate immune system senses viral invasion and initiates antiviral responses, complete viral clearance relies on the adaptive immune responses. Different from innate immune responses, which recognize certain molecular patterns and are nonspecific defences, adaptive immune responses specifically recognize a great variety of different viral antigens. Efficient processing and presentation of viral antigens in antigen-presenting cells is vital for adaptive immune responses. The adaptive immunity, including cellular immunity and humoral immunity, is mediated by T cells and B cells. The cellular immune response functions through regulatory $CD4^+$ T cells and cytotoxic $CD8^+$ T cells, while the humoral immune response through antibodies produced by B cells.

1.3.1 Actions of professional antigen-presenting cells (APCs).

Professional antigen-presenting cells (APCs) are a heterogeneous group of immune cells that mediate cellular immune response by processing and presenting antigens for recognition by certain lymphocytes such as T cells. Classical APCs include dendritic cells (DCs), macrophages, Langerhans cells and B cells.

Professional APCs in the lung, including alveolar macrophages (AMs) and DCs, play an important role in initiating adaptive immune responses during respiratory infections. Under steady-state conditions, AMs in the lung phagocytose inhaled

particulates or pathogens and degrade them without triggering inflammation or adaptive immunity[70]. In the context of viral infection, AMs facilitate viral clearance by complement activation, phagocytosis, the production of inflammatory mediators, and the recruitment of neutrophils[71]. In addition to their antiviral functions, AMs are also able to reduce the severity of immune-mediated lung damage by suppressing inflammation and promoting airway repair[72].

Lung conventional DCs (cDCs) are divided into three subsets: $CD103^+$ cDCs, $CD11b^+$ cDCs and plasmacytoid DCs (pDCs). In addition, monocyte-derived DCs (moDCs) have been described to populate the lungs upon inflammation[73]. Specific DC subsets are differentially susceptible to virus infection, which is related to the level of major histocompatibility complex class II (MHC II) expression. $CD103^+$ cDCs and $CD11b^+$ cDCs that express high level of MHC II were reported to be efficiently infected by IAV, whereas pDCs with low MHC II expression were not susceptible to IAV infection[74]. Upon lung IAV infection, DCs carrying IAV antigens will migrate from lungs to the T-cell zone of the draining lymph nodes (LNs) where they will prime the virus-specific naïve T cell with their cognate antigens[75]. Studies have shown that $CD103^+$ cDCs are the most efficient DC subset that can induce adaptive immune responses. One of the reasons is that they are the only subset that is able to capture and cross-present apoptotic cells died from viral infection. Desch *et al* concluded that $CD103^+$ cDCs expressed receptors for apoptotic cells along with the machinery to cross-present phagocytosed dead cells[76].

1.3.2 Antigen processing and presentation through MHC class I pathway.

Within the adaptive immune responses, virus-infected cells are eliminated by cytotoxic $CD8^+$ T cells, which recognize viral antigens displayed on MHC class I molecules of the target cells. MHC class I are expressed by all nucleated cells. Thus, antigen processing and presentation by MHC class I happens in almost all kinds of human cells (the only exemptions are red blood cells and platelets). However, only professional APCs are able to prime naïve $CD8^+$ T cells. In the MHC class I antigen-processing pathway, as shown in **Figure 1.7**, antigenic peptides are generated mainly within the ubiquitin-proteasome pathway[77,78], translocated into the lumen of the endoplasmic reticulum (ER) by the transporter associated with antigen processing (TAP)[79,80], loaded onto MHC class I molecules, and delivered to the cell surface.

The proteasome plays an eminent role in the cytosolic degradation and turnover of proteins marked for degradation via ubiquitinylation. One of the numerous functions of this multi-catalytic protease complex is to generate peptide epitopes derived from endogenous proteins. The proteasome consists of a catalytic core particle (20s) and one or two terminal 19s regulatory particles. The 20s catalytic core cleaves at the C-terminal side of basic, acidic and hydrophobic amino acid residues[81]. In an infection setting, a highly related structure termed the immunoproteasome can be induced by IFN-γ or TNF-α. The immunoproteasome is able to generate more antigenic peptides at a faster rate, compared to the constitutive proteasomes[82]. Following first degradation by proteasome, peptides are released into the cytosol, where they can undergo further trimming by cytosolic peptidases, such as tripeptidyl peptidase II (TPPII)[83], leucine aminopeptidase (LAP)[84], thimet oligopeptidase (TOP)[85] and puromycin-sensitive aminopeptidase (PSA)[86]. After being transported into the ER, peptides can be further trimmed at N-

terminus by endoplasmic reticulum aminopeptidase 1 (ERAP1) and ERAP 2[87]. ERAP1 is more important for the generation of MHC class I peptides as it doesn't bind to peptides smaller than 8 or 9 amino acids, while ERAP2 can continue trimming smaller peptides, which cannot bind to MHC class I[87]. ERAP1 is essential for the generation of many major epitopes in infection settings and loss of ERAP1 leads to reduced peptide-MHC complexes at the cell surface[88].

The transport complex TAP is required for the compartmentalization of antigens transferring the ''inside'' to the ''outside''. TAP belongs to the large family of ATP-binding cassette (ABC) transporters, which translocate a vast variety of solutes across membranes. The TAP complex is a half transporter composed of TAP1 (ABCB2) and TAP2 (ABCB3), each consisting of an N-terminal transmembrane domain and a C-terminal, cytosolic nucleotide-binding domain. TAP-dependent transport across the ER membrane is catalysed by ATP hydrolysis[79,89]. Subsequent peptide binding to MHC class I is accomplished by a multi-component peptide-loading complex (PLC) comprising the two TAP subunits, tapasin[90], MHC heavy chain, b2-microglobulin and various chaperones, such as calreticulin and the oxidoreductase ERp57, associated in sub-stoichiometric ratios[91]. After productive loading, peptide-MHC complexes dissociate from the PLC and are transported to the cell surface for inspection of their antigen cargo through cytotoxic $CD8^+$ T cells[92].

Cross-presentation is another way of MHC class I presentation that happens in professional APCs, mostly DCs, and is critical for initiating $CD8^+$ T cell immunity against pathogens. In general, there are two main cross-presentation pathways: the vacuolar pathway and the endosome-to-cytosol pathway. In the vacuolar pathway, antigens are degraded in endosomal or lysosomal compartments by lysosomal proteases and loaded

onto MHC class I there[93]. In the endosome-to-cytosol pathway, antigens are transported into the cytosol for proteasomal degradation. Afterward, antigen-derived peptides are transported back into the endosomes and trimmed by insulin responsive aminopeptidase (IRAP), or into the ER and trimmed by ERAP, and loaded onto MHC class I[94]. It has been reported that cross-presentation by uninfected DCs of minute amounts of endocytosed exogenous IAV was ~300-fold more efficient than presentation of IAV antigens processed by infected cells and resulted in a statistically significant increase in expansion of IAV-specific $CD8^+$ T cells[95].

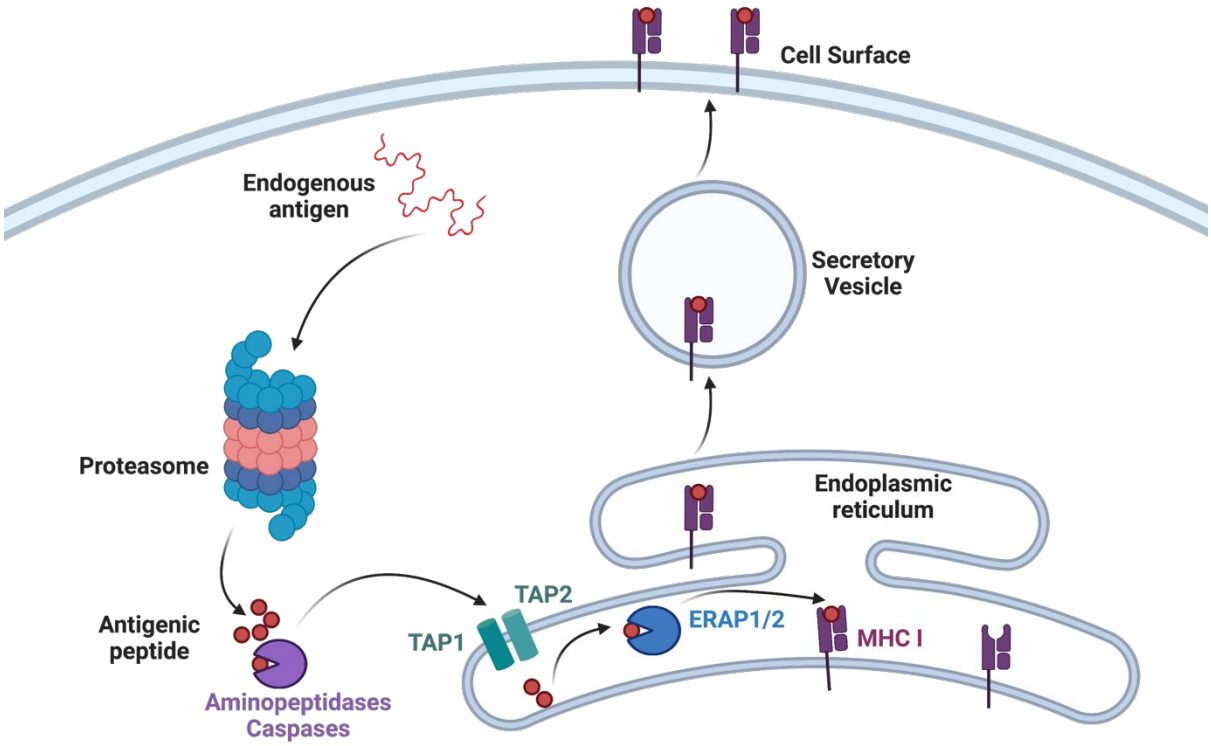


Figure 1.7 Antigen processing pathway via MHC class I. *When vRNPs enter the cytoplasm, they are broken down into peptides by the proteasome. TAP1 transports the "chopped" peptides into the lumen of the rough ER and helps uploading peptides onto MHC class I molecules. MHC class I-peptide complexes are transported to the cell surface. Figure generated with BioRender.*

1.3.3 $CD8^+$ T cell responses during virus infection.

In the lymph nodes, following the contact of viral antigens, usually consisting of 8-10 amino acids, presented by DCs, naïve $CD8^+$ T cells differentiate into cytotoxic T cells (CTLs) that produce cytokines and effector molecules that impair viral replication and kill virus-infected cells, which are essential for the clearance of most pulmonary viruses such as IAVs[96].

Following activation and differentiation in LNs, CTLs downregulate CCR7 and upregulate receptors like CXCR3 and CCR4, which promote their translocation to the lung, where they encounter and kill virus-infected cells[97]. The primary function of $CD8^+$ T cells during respiratory viral infections is the elimination of virus-infected cells by inducing apoptosis through a variety of mechanisms. Upon identification of virus-infected cells, CTLs produce cytotoxic granules such as perforin and granzymes. Perforin binds to target cells and induces pore formation on the cell membrane, which promotes passive diffusion of granzymes to induce apoptosis[98]. In addition, CTLs have the ability to induce apoptosis by expressing cytokines such as TNF, FASL and TRAIL, which recruit death receptors in virus-infected cells[99]. CTLs are also potent producers of the antiviral cytokine, IFN-γ, which activates inflammatory cells like macrophages and promotes antiviral gene expression in surrounding cells[100].

1.3.4 Antigen processing and presentation through MHC class II pathway.

While antigens bound to MHC Class I molecules activate $CD8^+$ T cells, $CD4^+$ T cells respond to antigens presented by MHC Class II molecules. The antigens presented by MHC class I are cytosolic (synthesized by the cells performing the presentation or other

cells, but processed in the cytosol) and those presented by MHC class II are endosomal (synthesized by other cells and processed in the endosomal compartments)[101].

MHC class II molecules bind to peptides derived from proteins degraded in the endocytic pathway, as shown in **Figure 1.8**. MHC class II complexes consists of α- and β-chains that are assembled in the ER and are stabilised by invariant chain (Ii)[102]. The complex of MHC class II and Ii is transported through the Golgi into a compartment termed the MHC class II compartment (MIIC). Due to acidic pH, proteases cathepsin S and cathepsin L are activated and digest Ii, leaving a residual class II-associated Ii peptide (CLIP) in the peptide-binding groove of the MHC class II[103]. Later, the CLIP is exchanged for an antigenic peptide derived from a protein degraded in the endosomal pathway. This process requires the chaperone HLA-DM, and, in the case of B cells, the HLA-DO molecule[104]. MHC class II molecules loaded with foreign peptide are then transported to the cell membrane to present their cargo to $CD4^+$ T cells. As opposed to MHC class I, MHC class II molecules do not dissociate at the plasma membrane. The mechanisms that control MHC class II degradation have not been established yet, but MHC class II molecules can be ubiquitinised and then internalised in an endocytic pathway.

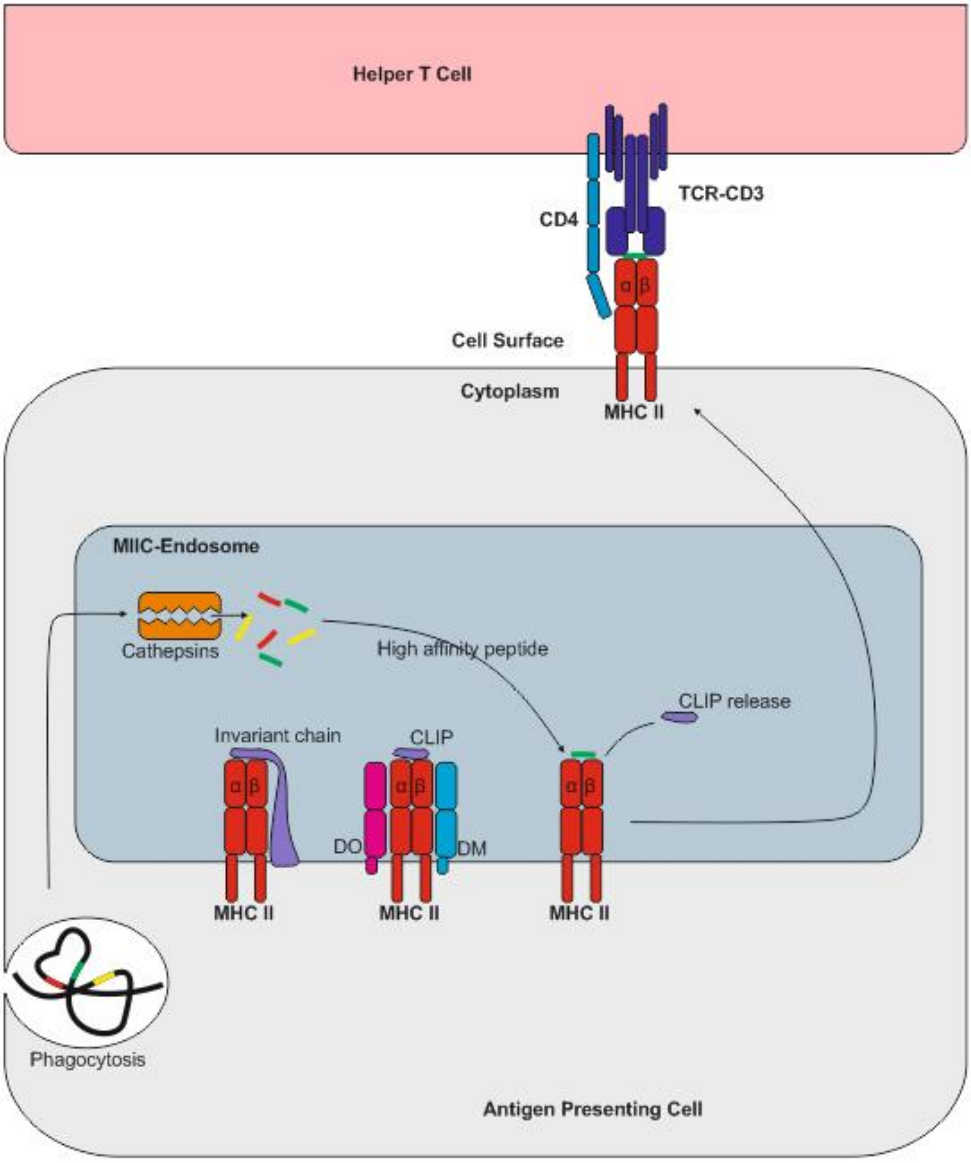


Figure 1.8 Antigen processing pathway via MHC class II. *Adapted from https://www.immunology.org/public-information/bitesized-immunology/systems-and-processes/antigen-processing-and-presentation.*

1.3.5 $CD4^+$ T cell responses during virus infection.

Similar to $CD8^+$ T cells, $CD4^+$ T cells are activated by DCs that migrate from the lung to the LNs during virus infection. Once activated, naïve $CD4^+$ T cells will differentiate into Th1 cells, which are characterized by the production of antiviral cytokines such as IFN-γ, TNF-α and IL-2. $CD4^+$ T cells are also able to differentiate into Th2, Th17, regulatory T cells (Treg cells), follicular helper T cells (Tfh), and sometimes as killer cells.

$CD4^+$ T cells are essential for the differentiation of antibody-producing B cells[105], the activation of virus-specific $CD8^+$ T cells[106], the local activation of AMs[107], and the recruitment of inflammatory cells into the lung[108]. Resistance to a variety of viruses, including IAVs, is compromised in the absence of $CD4^+$ T cells, even though the activities of $CD8^+$ T cells and T cell-independent antibodies can mediate delayed viral clearance in many cases[109]. Nevertheless, long-term antibody responses are completely dependent on help from $CD4^+$ T cells, meaning that successful vaccination requires a functional $CD4^+$ T cell compartment[110].

Th1 cells regulate $CD8^+$ T cell differentiation and $CD8^+$ T cell responses to IAV infection. This help can be indirect, in which Th1 cells activate DCs by providing costimulation in the form of CD40 ligand (CD40L)[111]. CD40 signalling on DCs and monocytes potently up-regulates IL-12, which facilitates $CD8^+$ T-cell differentiation. $CD4^+$ T cells may also help $CD8^+$ T cell directly via CD40L: CD40 signalling, similar to how they help B cells. Additionally, $CD4^+$ T cells provide help to $CD8^+$ T cells in the form of cytokines like IL-2 and IFNγ[112]. Thus, $CD4^+$ T cell helps to enhance most $CD8^+$ T-cell responses to respiratory viruses.

Tfh cells play a critical role in facilitating an effective B cell response during infection. Tfh cells are phenotypically identified by their expression of the chemokine receptor, CXCR5, the inhibitory receptor, programmed death-1 (PD-1), the costimulatory molecule, inducible T-cell costimulator (ICOS), CD40L and the cytokine, IL-21. As in B cell help, CD40L–CD40 interactions between $CD4^+$ T cells and APCs are crucial[113]. Th2 cells also play an important role in promoting B cell responses by producing IL-4, -5, -10 and -13 but are mainly involved in type 2 immune responses, which are important for eradication of extracellular parasites and bacterial infection[114].

Th17 cells are characterized by production of IL-17, and are essential for host protection against extracellular bacteria and some fungi. Th17 responses are also observed in viral infections and the effect of Th17 response is virus-dependent[115]. It has been reported that the responses from Th17 cells cause chronic inflammation during persistent viral infections through the production of IL-17[115].

Treg cells function as a suppressor of immune response, thereby maintaining homeostasis and self-tolerance. It has been shown that Treg cells are able to inhibit activation, proliferation and cytokine production of both $CD4^+$ and $CD8^+$ T cells, as well as B cells and DCs. Treg cells have been reported to reduce the accumulation and alter the distribution of monocytes/macrophages in the lungs of IAV-infected mice, thereby limiting pathology induced by IAV infection[116].

1.4 Overall aims.

In this study, we aimed to understand host immune responses against acute respiratory virus infections, in particular to IAV and SARS-CoV-2, with a focus on the processing and presentation of viral antigens. In the first year of my DPhil study, I focused on the IFITM3 protein and its interaction partners in order to understand its functions in the innate immune responses to IAV. Following the outbreak of COVID-19, there was an urgency to understand host immune responses to this novel virus. Therefore, I started characterizing the overall T cell immune responses against SARS-CoV-2. Following on from this, with the increased circulation of SARS-CoV-2 variants, an urgent need arose to understand the effect of mutations on T cell recognition as well as to compare vaccine- and infection-induced T cell responses. Additionally, the role of IFITM3 in SARS-CoV-2 infection, compared to IAV, also need further investigation.

With all these in mind, our research aims were to:

- Understand the impact of IFITM3 during IAV and SARS-CoV-2 infection (Chapter 3).
- Understand the role of memory T cell responses in COVID-19 pathogenesis and long-term protection (Chapter 4).
- Assess the cross-reactivity of infection- or vaccination-induced T cell responses against SARS-CoV-2 variants (Chapter 5).

Chapter 2

Methods and Materials

2.1 Study participants.

Chapter 4: A total of 42 individuals were recruited following recovery from COVID-19, including 28 mild cases and 14 severe cases.

Chapter 5: 9 individuals were recruited following recovery from COVID-19, and 9 were recruited following the first dose of ChAdOx1.

For the COVID-19 convalescent cohort used in both Chapter 4 and 5, patients were recruited from the John Radcliffe Hospital in Oxford, UK, between March 2020 and September 2021 by identification of patients hospitalized during the COVID-19 pandemic and recruited into the Sepsis Immunomics study. Patients were sampled at least 28 days after symptom onset. Written informed consent was obtained from all patients. Ethical approval was given by the South Central-Oxford C Research Ethics Committee in England (ref. 19/SC/0296).

2.2 Extraction of gDNA from cells.

Cells were washed with Dulbecco's phosphate-buffered saline (DPBS) and then centrifuged at 1500 rotations per minute (rpm), 5 min. Cell pellets were frozen at -20 °C or immediately used for genomic DNA (gDNA) extraction. Cells were resuspended in 600 µl of cell lysis solution (QIAGEN). Cells were vortexed and incubated at room temperature (RT) for 30 min. 200 µl of protein precipitation solution (QIAGEN) was added to lysis solution. Cell lysate was vortexed and centrifuged at 13,000 rpm, 25 min. Supernatant was transferred to a new microcentrifuge tube. 600 µl isopropanol was added

and mixed well before 10 min centrifugation at 13,000 rpm. Supernatant was discarded and 70% ethanol was added before 5 min centrifugation at 13,000 rpm. Supernatant was discarded before another 3 min centrifugation at 13,000 rpm. Remaining liquid was removed via pipette. DNA pellets were air dried for 10 min before addition of 30 µl nuclease-free water. gDNA concentration was measured via nanodrop. gDNA samples were stored at -20 °C.

2.3 Extraction of RNA using RNeasy Plus Mini kit.

β-mercaptoethanol (2-ME) was added to RLT plus buffer with a ratio of 10 µl per ml. Cells were washed with DPBS before addition of 350 µl RLT plus buffer with 2-ME. Cell lysate was added directly onto QIAshredder columns (QIAGEN). QIAshredder columns were centrifuged at 13,000 rpm, 2 min. Flow-through was frozen at -80 °C, or used immediately for RNA extraction. RNeasy Plus Mini Kit (QIAGEN) was used following manufacturer's instructions. RNA was eluted into 30 µL nuclease-free water. RNA concentration was measured via nanodrop. RNA samples were stored at -80 °C.

2.4 Preparation of cDNA from RNA using High-Capacity RNA-to-cDNA kit.

Conversion of RNA to cDNA was performed with the High-Capacity RNA-to-cDNA kit (Thermo Fisher Scientific) according to manufacturer's instructions. A consistent quantity of RNA was used across samples to ensure reverse-transcriptase efficiency was consistent across samples. cDNA was diluted with nuclease-free water in a ratio of 1:4.

2.5 Quantification of mRNA transcripts via qPCR.

qPCR mix was prepared with TaqMan Gene Expression Master Mix (Thermo Fisher Scientific) and TaqMan probes (Thermo Fisher Scientific). In each reaction, 5 µl of Master Mix was mixed with 0.5 µl of probe, and 4.5 µl of cDNA dilution. Volumes were halved in cases where a 384-well qPCR plate was used, as opposed to 96-well plates.

Glyceraldehyde 3-phosphate dehydrogenase (GAPDH) was used as an internal control gene. Plates were run on a QuantStudio 7 Flex Real-Time PCR System (Thermo Fisher Scientific) according to standard protocols.

2.6 Western blotting.

Cells were harvested and centrifuged at 3,000 rpm, 2 min. Cells were resuspended in RIPA lysis buffer (Thermo Fisher Scientific) with addition of 10 µl per ml protease inhibitor cocktail (Sigma-Aldrich). Cells were vortexed for 1 min, and incubated on ice for 30 min. Lysate was centrifuged at 13,000 rpm, 10 min. Supernatant was collected and combined with 4x Laemmli Sample Buffer (Bio-Rad) at a ratio of 3:1 before incubation at 90 °C for 5 min. Samples were loaded onto a 16% Novex Tris-Glycine Protein Gel (Thermo Fisher Scientific) in a XCell SureLock Mini-Cell Gel Tank (Thermo Fisher Scientific). Samples were run in 1x Novex Tris-Glycine SDS Running Buffer (Thermo Fisher Scientific) alongside a Precision Plus Protein duo ladder (Bio-Rad). Gel was stacked at 60 volts (V) for 15 min, before running for 90 min at 120 V. Transfer sandwich was prepared with sponges, gel, Western Blotting Filter Paper (Thermo Fisher Scientific) and methanol-activated Immobilon-FL Membranes (Merck). Transfer sandwich was placed in gel tank with 1x Novex Tris-Glycine Transfer Buffer (Thermo Fisher Scientific). Samples were run at 26 V for 75 min. 5% skim milk in Tris-Buffered Saline with Tween-20 (TBST) (Thermo Fisher Scientific) was prepared. After transfer, membrane was removed, and blocked in skim milk for 1 hour (h) on shaker. Membrane was incubated with primary antibodies against target proteins and GAPDH (Merck) overnight on shaker at 4 °C. Membrane was washed three times in TBST, and incubated with secondary antibodies against mouse or rabbit (Li-Cor) for 1 h on shaker. Membrane was washed in TBST three times, and visualised using the Li-Cor Odyssey Imaging System (Li-Cor).

2.7 Infection of adherent cells with S-Flu.

Cells were seeded in a 24-well cell culture plate at $1x10^5$ cells per well and left overnight. Media was aspirated and cells were washed once with DPBS. Virus was diluted from stock solution to the appropriate multiplicity of infection (MOI)/dilution factor in DMEM. 100 µl of virus solution was added to cells and left for 1.5 h. 1 ml of fresh cell culture medium was added to cells. Cells were incubated for 16-24 h at 37 °C.

2.8 Preparation of RNA-Seq samples.

RNA was extracted from cells using RNeasy 96 kit (QIAGEN). gDNA was removed using RNase-Free DNase Set (QIAGEN). RNA concentration was measured using Qubit RNA Broad-Range Assay (Thermo Fisher Scientific). Quality of RNA was checked using tapestation (Agilent) and RNA integrity number (RIN) values of all samples were above 8. OD ratios of RNA were measured using nanodrop and A260/A280 ratios of all samples were ~2. RNA samples were provided in 30 µl of ultrapure water at the concentration of 3.3-33 ng/µl. RNA samples were sent to Oxford Genomics Centre for sequencing and polyA library was made.

2.9 Culture of iPSCs.

The healthy control human iPSC line Kolf2 was acquired through the Human Induced Pluripotent Stem Cells Initiative Consortium (HipSci; www.hipsci.org). Consent was obtained for the use of cell lines for the HipSci project from healthy volunteers. IFITM3$^{-/-}$ iPSC lines were generated using CRISPR/Cas9 technology by Wellcome Trust Sanger Institute core gene-editing pipeline. Wild type and two homozygous IFITM3$^{-/-}$ clones were given as a gift from Ian Humphrey's group and used in downstream differentiation assays.

Prior to differentiation, iPSCs were grown feeder-free using the Essential 8 Flex Medium kit (Thermo Fisher Scientific) on Vitronectin (VTN-N, Thermo Fisher Scientific) coated plates as per manufacturer's instructions to 70–80% confluency. iPSCs were harvested for differentiation using Versene solution (Thermo Fisher Scientific).

2.10 Differentiation of iPSCs to macrophages.

iPSC colonies were detached with Versene and transferred into ultra-low attachment plates (CORNING) and cultured for 4-5 days in iPSC base media with Rock inhibitor (Sigma-Aldrich), 50 ng/ml BMP-4 (Bio-Techne), 50 ng/ml VEGF (Peprotech) and 20 ng/ml SCF (Bio-Techne) to form a three-germ layer containing embryoid bodies (EBs). For long-term production of myeloid precursors, EBs were transferred into gelatin-coated plates in X-VIVO 15 medium (Lonza) supplemented with 25 ng/ml IL-3 and 50 ng/ml M-CSF (both R&D). Terminal differentiation of myeloid precursors into mature macrophages was achieved by culturing myeloid precursors in 100 ng/ml M-CSF in R10, which is Roswell Park Memorial Institute Medium (RPMI)-1640 supplemented with 10% fetal calf serum (SIGMA), 2 mM L-Glutamine (Sigma-Aldrich) and 1% v/v (500U/ml) penicillin streptomycin (Sigma-Aldrich), for 4-5 days.

2.11 Isolation of mononuclear cells from peripheral blood.

Peripheral blood mononuclear cells (PBMC) were isolated from fresh blood using density gradient centrifugation. 30-50 ml of blood was drawn from donors. 16 ml of Lymphoprep (STEMCELL Technologies) was added to 50 ml Falcon tubes (Greiner Bio-One). A maximum of 30 ml of blood was added to each tube, and centrifuged at 2,000 rpm, 20 min, without brake. Lymphocytes were pipetted out, and added to a 50 ml Falcon tube before topped up to 50 ml RPMI. Cells were washed with RPMI twice, and resuspended in R10.

2.12 Generation of antigen-specific T cells *in vitro.*

PBMCs isolated from donors were stimulated with SARS-CoV-2 spike peptide pools, and cultured in R10 at 37 °C. After 14 days, antigen-specific T cells were FACS sorted using Cell Enrichment and Detection kit (Miltenyi Biotec) after stimulation with SARS-CoV-2 spike peptide library. T cells were tested for mycoplasma monthly.

2.13 Generation of ACE2-transduced EBV-transformed BCLs.

$1x10^6$ PBMCs were pulsed with 100 µl neat Epstein-Barr virus (EBV, made by Xuan Yao) at 37°C for 3 h, and topped with 100 µl R20, which is RPMI-1640 supplemented with 20% fetal calf serum (SIGMA), 2 mM L-Glutamine (Sigma-Aldrich) and 1% v/v (500U/ml) penicillin streptomycin (Sigma-Aldrich), supplemented with 2 µg/ml cyclosporine A (CSA). Cells were cultured in R10 with 1 µg/ml CSA for ~14 days until B cell colonies appeared in the wells. BCLs were cultured in R10 thereafter and tested for mycoplasma monthly.

The complementary DNA for the human ACE2 gene (ENSG00000130234) was cloned into a lentiviral vector that allows co-expression of enhanced green fluorescent protein (eGFP) and a puromycin resistance marker (Addgene, plasmid no. 17488). The plasmids were co-transfected with packaging plasmids pMD2.G and psPAX2 into HEK293-TLA using PEIpro (Polyplus). Lentiviral supernatant was collected 48 h and 72 h post-transfection and concentrated by ultracentrifugation. EBV-transformed BCLs were infected by ACE2 lentivirus at a MOI of 0.1 with 8 µg/ml of polybrene (Sigma-Aldrich) overnight, then washed and cultured for 3–5 days. ACE2-expressing B cells were stained using primary goat anti-human ACE2 antibody (R&D, 1:20) and donkey anti-goat AF647 secondary antibody (Abcam, 1:1,000), followed by cell sorting via flow cytometry. B

cells with stable expression of ACE2 (BCLs-ACE2) were maintained in R10 with 0.5 μg/ml of puromycin (Thermo Fisher Scientific).

2.14 Intracellular cytokine staining.

T cells were cocultured with live SARS-CoV-2-infected BCLs-ACE2 at an E:T ratio of 1:2 for 6 h with GolgiPlug and GolgiStop (both BD Biosciences), and surface stained with PE-anti-CD107a (BD Biosciences, 1:20). Dead cells were labelled using Live/Dead Fixable Aqua dye (Invitrogen, 1:1000). After fixated with Cytofix/Cytoperm (BD Biosciences), $CD8^+$ T cells were stained with BV421-anti-CD8 (Biolegend, 1:33), PE-Cy7-anti-IFNγ (BD Biosciences, 1:33), APC-anti-TNFα (eBioscience, 1:500) and APC-H7-anti-MIP1β (BD Biosciences, 1:33); $CD4^+$ T cells were stained with APC-anti-CD4 (eBioscience, 1:33), PE-Cy7-anti-IFNγ (BD Biosciences, 1:33), APC-Cy7-anti-TNFα (Biolegend, 1:33) and BV421-anti-IL2 (Biolegend, 1:33). Negative controls without virus infection were run for each sample. All samples were acquired on Attune NxT Flow Cytometer (software v.3.2.1) and analysed using FlowJo v.10 software (FlowJo LLC).

2.15 IFNγ-based ELISpot assay.

$2x10^5$ PBMCs were pulsed with peptides at a final concentration of 2 μg/ml, or 400-2,000 T cells were cocultured with peptide-pulsed BCLs on IFNγ ELISpot plates, for 16–18 h. IFNγ-based ELISpot assay was performed using IFNγ ELISpot kit (R&D) as per manufacturer's instructions.

2.16 Live virus suppression assay.

EBV-transformed BCLs expressing ACE2 were infected with SARS-CoV-2 viruses at an MOI of 0.1 for 120 min at 37 °C. Cells were washed and cocultured with T cells at an E:T ratio of 4:1. Control wells containing virus-infected targets with T cells unspecific to SARS-CoV-2 were also included. After 48 h incubation, cells were washed with DPBS

and lysed with RLT Plus Buffer (QIAGEN). RNA was extracted using RNeasy 96 kit (QIAGEN). Virus copies were quantified with Takyon Dry one-step RT-qPCR (Eurogentec) using SARS-CoV-2 (2019-nCoV) CDC qPCR Probe Assay (IDT, ISO 13485:2016) and human β2-microglobulin as an endogenous control (Applied Biosystems). The suppression rate was calculated by the percentage reduction of virus replication by T cells.

2.17 Peptide-MHC class I tetramer staining.

T cell lines were incubated with peptide-MHC class I tetramer for 15 min at 37°C. Cells were then incubated with BV421-anti-CD8 (BD Biosciences, 1:40) and Propidium Iodide (eBioscience). All samples were acquired on Attune NxT Flow Cytometer (software v.3.2.1) and analysed using FlowJo v.10 software (FlowJo LLC).

2.18 Evaluation of T cell responses to live virus infection.

EBV-transformed BCLs expressing ACE2 were infected with SARS-CoV-2 virus at an MOI of 1 for 120 min at 37 °C. Cells were washed and incubated in R10 at 37 °C. After 24 h, cells were cocultured with T cells at an E:T ratio of 1:2. Degranulation (CD107a expression) and cytokine production of T cells were evaluated by intracellular staining (ICS) as described in **section 2.14**.

2.19 S-Flu virus.

Infection experiments were performed using a pseudotyped infuenza virus that is replication-deficient, known as S-Flu. This virus was developed, produced, and given as a gift from Alain Townsend group. This virus is produced in Madin-Darby Canine Kidney (MDCK) cells. The majority of progeny viral proteins and genes are derived from the Cambridge strain of the PR8 virus, except for the pseudotyped HA protein (S-Flu strain

dependent) and the HA gene – the coding sequence of this gene is replaced by an eGFP gene. Cells infected by S-Flu virus will express eGFP.

2.20 Propagation and titration of SARS-CoV-2 live virus.

SARS-CoV-2 Victoria 01/20 strain (BVIC01) and variants of concern (VoCs) - Alpha (Lineage B.1.1.7, 20I/501Y.V1.HMPP1) and Beta (Lineage B.1.351, 201/501.V2.HV001) were originally from Public Health England and provided by J. McKeating. SARS-CoV-2 Gamma (Lineage P.1) and Omicron (Lineage B.1.1.529) were provided by G. Screaton. The Delta (Lineage B.1.617.2) variant was originally from W. Barclay and T. De Silva (G2P-UK) and provided by G. Screaton.

SARS-CoV-2 and VoCs were propagated with Vero E6/TMPRSS2 (provided by A. Townsend). Vero E6/TMPRSS2 cells were plated overnight and infected with SARS-CoV-2 or VoCs at an MOI of 0.003. Cultures were harvested when visible cytopathic effects were observed 48-72 h later. Virus-containing supernatant was aliquoted and stored at -80 °C. Viral titre was determined by plaque assay with Vero E6/TMPRSS2, and plaque-forming units per ml were used to calculate the MOI.

2.21 Antibody information.

Marker	Fluorophore	Clone	Supplier	Cat number
CD4	APC	SK3	eBioscience	17-0047-42
CD8	BV421	SK1	Biolegend	344748
IFNγ	PE-Cy7	B27	BD Biosciences	557643
TNFα	APC	MAb11	eBioscience	17-7349-82
TNFα	APC-Cy7	MAb11	Biolegend	502944
CD107a	PE	H4A3	BD Biosciences	555801
IL2	BV421	MQ1-17H12	Biolegend	500328
MIP1β	APC-Cy7	D21-1351	BD Biosciences	561280
HLA-ABC	FITC	W6/32	Biolegend	311404
CD11c	PerCP-Cy5.5	3.9	Biolegend	301624
CD14	BV421	63D3	Biolegend	367143
CD16	BV711	3G8	Biolegend	302044
CD54	PE	HA58	Biolegend	353106
CD64	PE-Cy7	10.1	Biolegend	305022
CD206	APC-Cy7	15-2	Biolegend	321120

2.22 Synthetic peptides.

A total of 423 15-18-mer peptides overlapping by ten amino acid residues and spanning the full proteome of SARS-CoV-2 except ORF1 were designed using the software PeptGen: (http://www.hiv.lanl.gov/content/sequence/PEPTGEN/peptgen.html) and synthesized (purity: >75%) by ProImmune.

2.23 Statistical analysis.

We used bioinformatics programs for RNA-Seq analysis. When performing analysis, we plotted gene expression in counts normalised by the DESeq2 program after transformation with a variance stabilising transformation. This transformation is similar to a log2 transformation, and units should be treated as if they are on a log2 scale, rather than as if they are linear. We ran bioinformatics programmes on various platforms. FastQC were run on CBRG bioinformatics servers. R based programmes were run locally.

Quality check was performed with FastQC to get an early profile of the quality of raw sequence files. This program offers a series of quality checks for sequencing data.

Feature counting was performed with featureCounts. We counted aligned sequences using featureCounts version 1.4.5, a part of the Subread package. FeatureCounts is used to obtain count values for gene expression. This programme was used immediately after alignment with STAR to aggregate counted features for all samples in a dataset. For gene counting, we used the genome annotation that pertained to the reference genome used for alignment. We ran featureCounts in paired-end mode. We counted features by exon alignment and aggregated counts by gene id.

Differential gene expression analysis was performed with DESeq2. Heatmap was generated using pheatmap package. We performed standard analysis with DESeq2, usually performing comparisons directly between two factors.

Gene ontology (GO) enrichment analysis was performed with topGO. GO analysis is used to identify generalised trends in gene groups. GOs are annotated groups of genes categorised by the Gene Ontology Consortium. Ontologies are updated with respect to novel biological information, and are generated based on a combination of experimental information, phylogenetic inference, and computational inference. There are over 40,000 ontologies annotated as of 2018. Ontologies are generated based on three concepts: cellular compartment - localisation of gene products; molecular function - molecular activity of gene products; biological process - pathways and interactions between gene products. We used the topGO package to identify enriched genes. This package functions based on statistical tests for enrichment of specific ontologies within a gene set, with comparison to gene incidence expected to occur at random.

Chapter 3

Understanding the impact of IFITM3 on influenza virus and SARS-CoV-2 infection

3.1 Introduction.

IFITM3 plays an important role in immune responses against infections by enveloped RNA viruses[38]. Epithelial cells, antigen-presenting cells and lymphoid cells all require IFITM3 to facilitate their survival and protection from viral infection. Wakim *et al* demonstrated that IFITM3 is selectively maintained in lung tissue-resident memory $CD8^+$ T cells to endow them with enhanced resistance to infection with influenza virus[117]. In addition, Helft *et al* showed that lung migratory dendritic cells expressed high levels of IFITM3, which protected them from influenza virus infection, and thus they were able to cross-present antigens from virally infected cells to virus-specific T cells in the lymph node[118].

The mechanisms of IFITM3-mediated viral restriction are complex. Besides its main function of directly inhibiting the release of viral genome into the cytosol, IFITM3 can also act as a checkpoint regulator of virus-induced cytokine production. Stacey *et al* showed that uncontrolled expression of IL-6 in *Ifitm3*$^{-/-}$ mice triggered the loss of NK cells and impaired control of murine cytomegalovirus (MCMV) replication[119]. Clement *et al* further demonstrated that IFITM3 controlled IL-6 production by promoting the proteasomal degradation of Nogo-B, which is a mediator of TLR-dependent pro-inflammatory cytokine production[63]. In addition, it has also been documented that IFITM3 can incorporate into IAV particles competing with viral hemagglutinin

incorporation, therefore sensitizing the virus to antibody neutralization, and thus having an impact on the infection outcome[120].

Higher levels of IFITM3 mRNA expression were observed in peripheral leukocytes[64] and nasopharyngeal swabs[65] from COVID-19 patients, compared with healthy controls. Upregulated IFITM3 is likely due to the increased IFN signalling during SARS-CoV-2 infection. On the one hand, IFITM3 has been shown to reduce SARS-CoV-2 RNA production in HEK293 cells overexpressing ACE2 by inhibiting Spike-mediated fusion with the plasma membrane[66,67]. On the other hand, IFITM3 has also been reported to facilitate SARS-CoV-2 replication in human epithelial lung cancer cell line Calu-3, cardiomyocytes and gut organoids[66,69]. Therefore, it is still yet clear whether IFITM3 is more of a restrictor or a facilitator for SARS-CoV-2 infection.

The single nucleotide polymorphism, rs12252, resulting in IFITM3-CC protein generation is known to impact antiviral activity of IFITM3, resulting in increased susceptibility to infection and higher disease mortality[52]. Therefore, the association of *IFITM3* rs12252 with COVID-19 disease was of great interest. Ahmadi *et al* investigated an Iranian cohort of 1178 COVID-19 patients and found that the mortality of COVID-19 was significantly higher in patients with *IFITM3* rs12252 CC genotype than in other genotypes[121]. Consistently, a study in a Chinese cohort of 80 COVID-19 patients reported that CC genotype of *IFITM3* rs12252 was connected to greater COVID-19 severity[122]. However, a study of the individuals from Asturias (northern Spain) showed that carriers of rs12252 CC(?) were significantly more frequent in the COVID-19 patients compared to healthy controls but not significantly more common among patients who required ICU[123]. While they do not agree on the contribution of rs12252-CC on disease severity,

all of these studies suggest that *IFITM3* rs12252 is a COVID-19 risk-related genetic factor, highlighting the important role of IFITM3 in the control of SARS-CoV-2 infection.

Previously in our group, whole blood RNA of a large group (n=275) of healthy Chinese donors was obtained and sent for RNA-Seq. Correlation between IFITM3 expression and other genes was investigated. Any gene with a correlation co-efficient of more than 0.6 was considered for further analysis. Interestingly, the gene for transporter associated with antigen processing 1 (TAP1) was among the top 10 IFITM3-correlated genes and its expression was highly correlated to IFITM3 expression (**Figure 3.1 A**). The same correlation between TAP1 and IFITM3 was also observed from RNA-Seq data of a Gambian cohort of healthy babies prior to receiving a live attenuated influenza vaccine (n=112) (**Figure 3.1 B**).

Further correlation analysis of IFITM3 with antigen processing and presentation related genes in the healthy Chinese cohort showed that IFITM3 mRNA expression level was associated with intracellular adhesion molecule-1 (ICAM1), HLA class I and proteasomal subunits (**Table 3.1**). Suggesting that IFITM3 may be linked to the antigen presentation pathway in some way. Additionally, a study published in 2019 showed that HLA-B expression is attenuated in IFN-γ treated IFITM1/IFITM3 double-null cells[124], supporting the hypothesis that IFITM3 can affect antigen processing and presentation. However, considering that many antigen processing and presentation related genes can be stimulated by IFNs, it is hard to tell whether the observed association in our cohorts is IFITM3-dependent, or just a result of enhanced overall IFN signalling. Moreover, no studies have been published on the role of IFITM3 in human antigen-presenting cells.

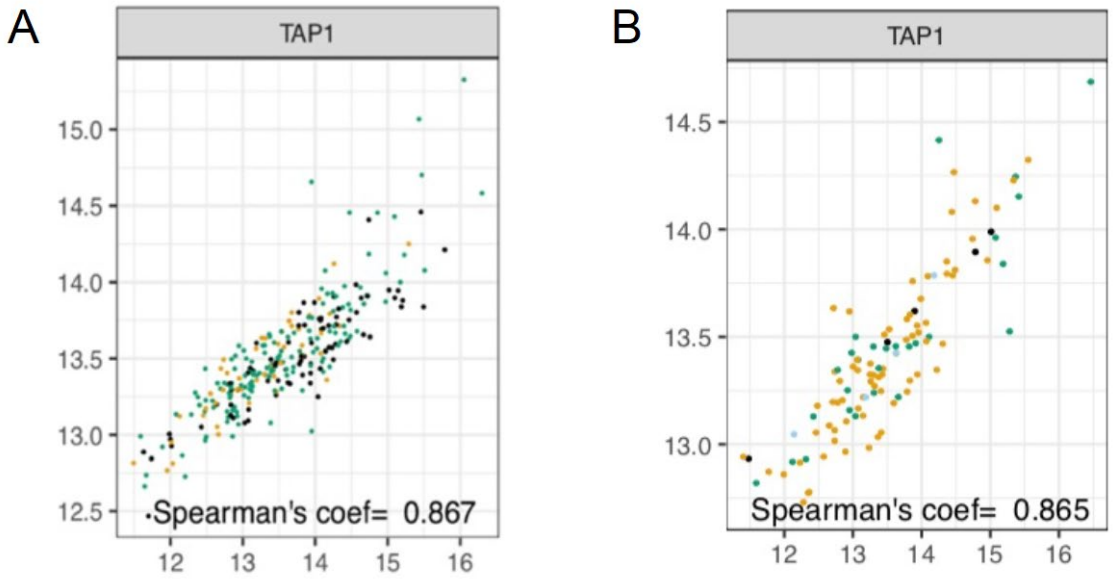


Figure 3.1 Correlation between TAP1 and IFITM3. *(A) Chinese cohort. (B) Gambian cohort.*

Table 3.1 Antigen processing and presentation related genes that correlate with IFITM3.

SYMBOL	GENENAME	Correlation Coefficient
TAP1	Transporter associated with Antigen Processing	0.867
ICAM1 (CD54)	Intercellular Adhesion Molecule-1	0.633
HLA-A	Human Leukocyte Antigen	0.698
HLA-B		0.637
HLA-C		0.59
HLA-E		0.725
PSMB3	Proteasome Subunit Beta type	0.644
PSMB8/LMP7		0.773
PSMB9/LMP2		0.758
PSMB10		0.63
PSME1	Proteasome activator Subunit	0.738

3.2 Aims.

The overall aim of this part of study will be to determine how IFITM3 modulates antiviral processes during IAV and SARS-CoV-2 infection, especially in antigen-presenting cells. Based on preliminary data, the specific aims of this study are to:

- Investigate the correlation of IFITM3 with antigen processing and presentation related genes.
- Search for proteins that interact with IFITM3 during IAV or SARS-CoV-2 infection.

3.3 Hypothesis.

Based on experimental evidence to date, I will probe two hypotheses on how IFITM3 modulates antiviral activities against IAV and SARS-CoV-2:

- IFITM3 facilitates the processing and presentation of viral antigens to strengthen host immune responses against virus-infected cells.
- IFITM3 interacts with other proteins to reduce viral replication during infection.

3.4 Results.

3.4.1 IFITM3 is inducible by type I, II and III interferons in HEK293 cells.

IFITM3 has previously been described to be induced by type I (IFN-α and IFN-β) and type II IFN (IFN-γ). However, it is unclear to what extent that IFITM3 can be induced by different types of IFNs. To investigate this, HEK293 cells were stimulated with 0-10,000 U/ml IFN-α, -β, -γ or -λ for 24 hours with IFITM3 expression measured by western blotting (**Figure 3.2 A**). While increased IFITM3 expression was shown at the highest concentrations with all IFNs, there was a hierarchy of response with type I > type III > type II interferons (**Figure 3.2 B**). IFITM3 can also be mildly pushed to a maximal level following IFN-λ stimulation, while IFITM3 slightly but continuously increases following IFN-γ stimulation without reaching the platform (**Figure 3.2 B**). Considering that 100 U/ml is already higher than the physiological concentration of IFNs, our results suggest that type I IFNs are the key IFNs that are responsible for the high level of IFITM3 during virus infection.

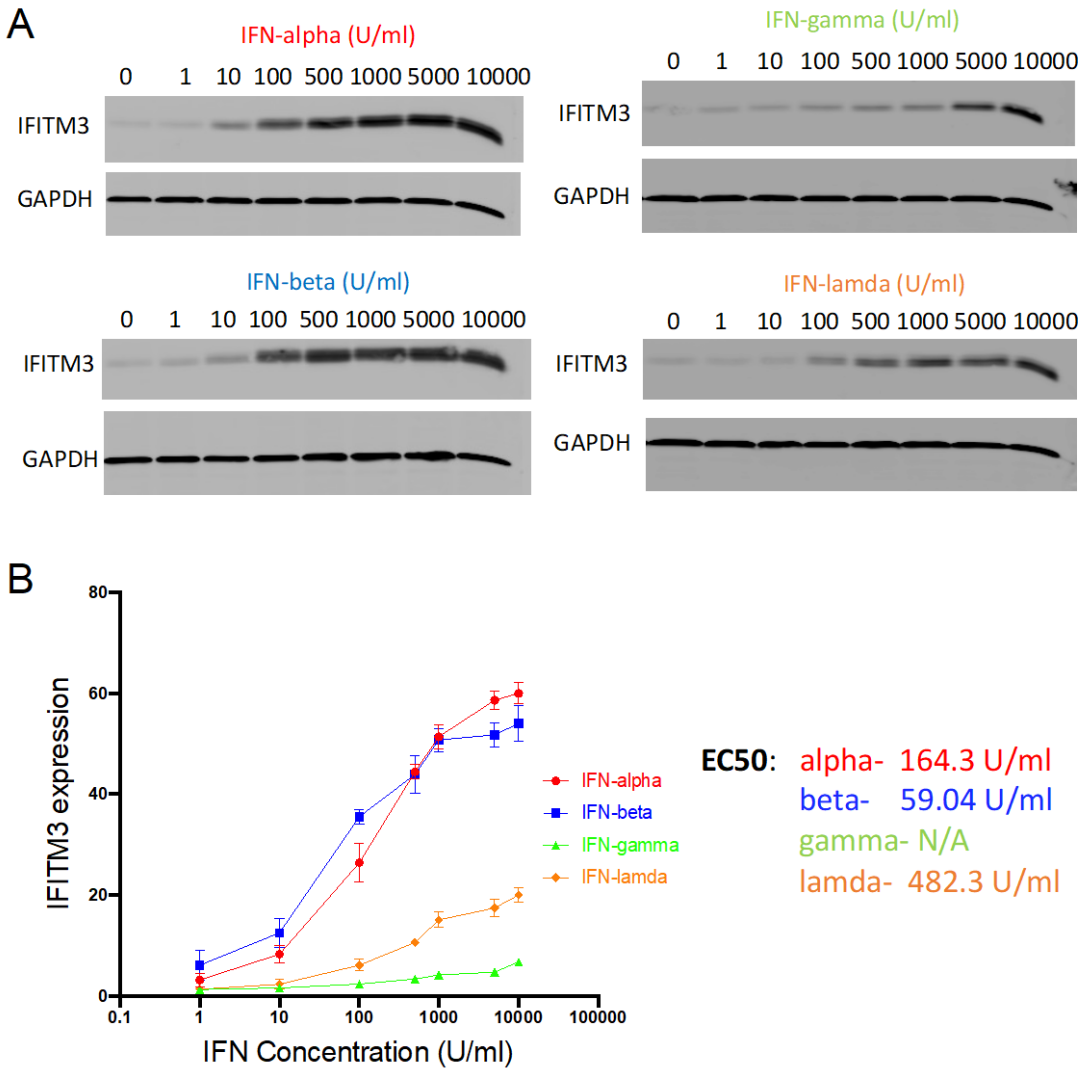


Figure 3.2 Stimulation of IFITM3 by IFNs in HEK293. *HEK293 cells were stimulated by IFN-α, β, γ and λ at the concentration of 1, 10, 100, 500, 1000, 5000 and 10000 U/ml for 24 h. IFITM3 and GAPDH expression was measured by western blotting. (A) Representative western blots of IFITM3 and GAPDH after IFN stimulation. (B) Curves showing IFITM3 responses to stimulation with IFNs. IFITM3 expressions were normalized by GAPDH expression. N=3 for each experiment. Data is expressed as Mean ± SEM. EC50: half maximal effective concentration.*

3.4.2 IFITM3 reduces H1N1 infection rate in HEK293 cells.

To study the impact of IFITM3 on restricting IAV infection, wild type (IFITM3$^{+/+}$) and IFITM3 gene knockout (IFITM3$^{-/-}$, generated by CRISPR-Cas9 technology[125]) HEK293 were used. For these studies we used a modified strain of H1N1, S-Flu PR8. This virus can replicate for a single cycle only and generates green fluorescent protein (GFP)

following replication of the viral genome, but no progeny virions[126]. Infected cells can be easily determined by detection of GFP^+ cells by flow cytometry.

$IFITM3^{+/+}$ and $IFITM3^{-/-}$ HEK293 cells were infected with S-Flu PR8 for 24 hours before determining the percentage of infected cells. It was clear that deletion of IFITM3 in HEK293 cells significantly increased the infection rate, showing an infection rate of ~17.6% in $IFITM3^{+/+}$ cells while ~57.5% in $IFITM3^{-/-}$ cells (**Figure 3.3**). Using IFITM3 knockout cell model, we confirmed IFITM3 as a restriction factor for H1N1 infection. However, it is clear that the presence of IFITM3 within cells cannot fully restrict viral entry into cells.

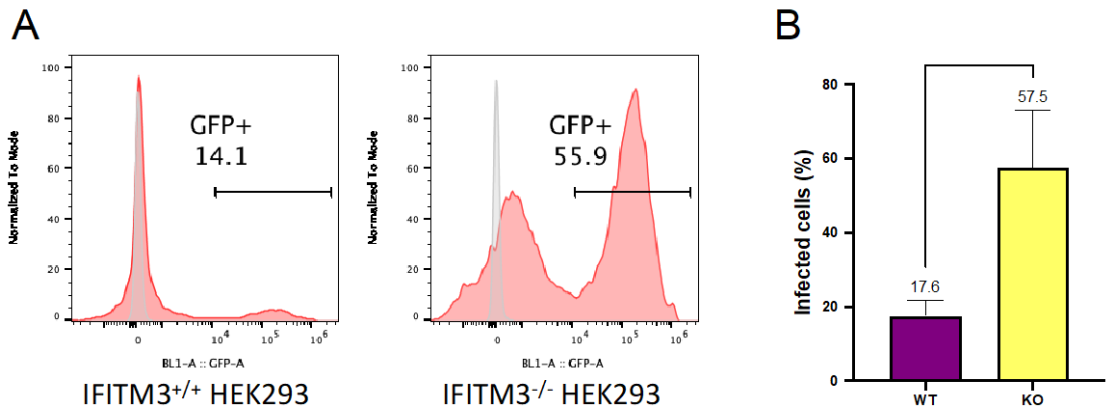


Figure 3.3 S-Flu PR8 (H1N1) infection rate in $IFITM3^{+/+}$ (WT) and $IFITM3^{-/-}$ (KO) HEK293. *HEK293 cells were infected with S-FLU PR8 for 24 h. Infection rates were reflected by the percentage of GFP+ cells measured by flow cytometry. (A) Representative histograms showing GFP expression in $IFITM3^{+/+}$ and $IFITM3^{-/-}$ HEK293 cells following infection. Gray showing uninfected control; red showing infected groups. (B) Percentage of GFP+ cells following infection. *P<0.05 by paired t test. N=3 for each experiment. Data is expressed as Mean ± SEM.*

3.4.3 IFITM3 reduces H1N1, but not H5N1, infection severity in human iPS-derived macrophages.

Based on the preliminary RNA-Seq data showing the potential correlation between IFITM3 and antigen processing and presentation related genes, we were interested to study the role of IFITM3 in antigen-presenting cells.

In collaboration with Dr Jessica Forbester & Prof. Ian Humphreys (Cardiff University), we established IFITM3$^{+/+}$ and IFITM3$^{-/-}$ macrophages derived from human induced pluripotent stem cells (huiPSCs). The protocol for generation of iPS-derived macrophages (iPSDMs), based on the protocol in Wilgenburg *et al*[127], is shown in **Figure 3.4 A**. The first step of this method is to differentiate huiPSCs into embryoid bodies (EBs, comprising ectoderm, mesoderm and endoderm), followed by directed differentiation along the myeloid lineage by stimulation with IL-3 and M-CSF, to produce myeloid precursors. These myeloid precursors can be further differentiated into macrophages with M-CSF only. Generation of EBs expressing myeloid precursors takes ~5-6 weeks but myeloid precursors can then be harvested for up to 6 months.

The resulting macrophages (iPSDMs) are phenotypically and functionally comparable to blood monocyte-derived macrophages. The phenotype of IFITM3$^{+/+}$ and IFITM3$^{-/-}$ iPSDMs was confirmed by the staining of a panel of macrophage-specific markers: CD11c, CD14, CD16, CD54, CD64 and CD206 (**Figure 3.4 B**).

To investigate the impact of IFITM3 on restricting influenza infection in macrophages, IFITM3$^{+/+}$ and IFITM3$^{-/-}$ iPSDMs were infected with S-Flu PR8 for 24 hours and the infection rate was determined by flow cytometry. Infection of these iPSDMs resulted in ~24.6% infected cells in IFITM3$^{+/+}$ cells, compared to ~45.2% in IFITM3$^{-/-}$ cells (**Figure 3.4 C, D**), suggesting that IFITM3 reduced H1N1 infection severity in iPSDMs, although again, IFITM3 is unable to prevent infection. IFITM3 expression was also inducible by either S-Flu PR8 infection or IFN-β stimulation in IFITM3$^{+/+}$ iPSDMs (**Figure 3.4 E, F**).

In our group, we have localised IFITM3 primarily to the late endosomal compartment although expression is also seen on early endosomal and lysosomal

membranes (unpublished observations). The localisation of IFITM3 may be important in regards to IAV infection due to the pH of the compartment. From which compartment IAVs are released depends on optimum pH of HA-mediated membrane fusion[128]. It has been reported that overexpression of IFITM3 in Madin-Darby canine kidney (MDCK) cells inhibits the replication of H1N1, but not H5N1, which requires higher pH for membrane fusion and is released from early endosomes[128].

To investigate the sensitivities of different IAVs to IFITM3 in our cellular system, both IFITM3$^{+/+}$ and IFITM3$^{-/-}$ iPSDMs were also infected with H5N1 PR8 for 24 h and the infection rate was determined by flow cytometry. Infection rate of 100% was observed in both IFITM3$^{+/+}$ and IFITM3$^{-/-}$ iPSDMs, suggesting that IFITM3 can not restrict H5N1 infection (**Figure 3.5**).

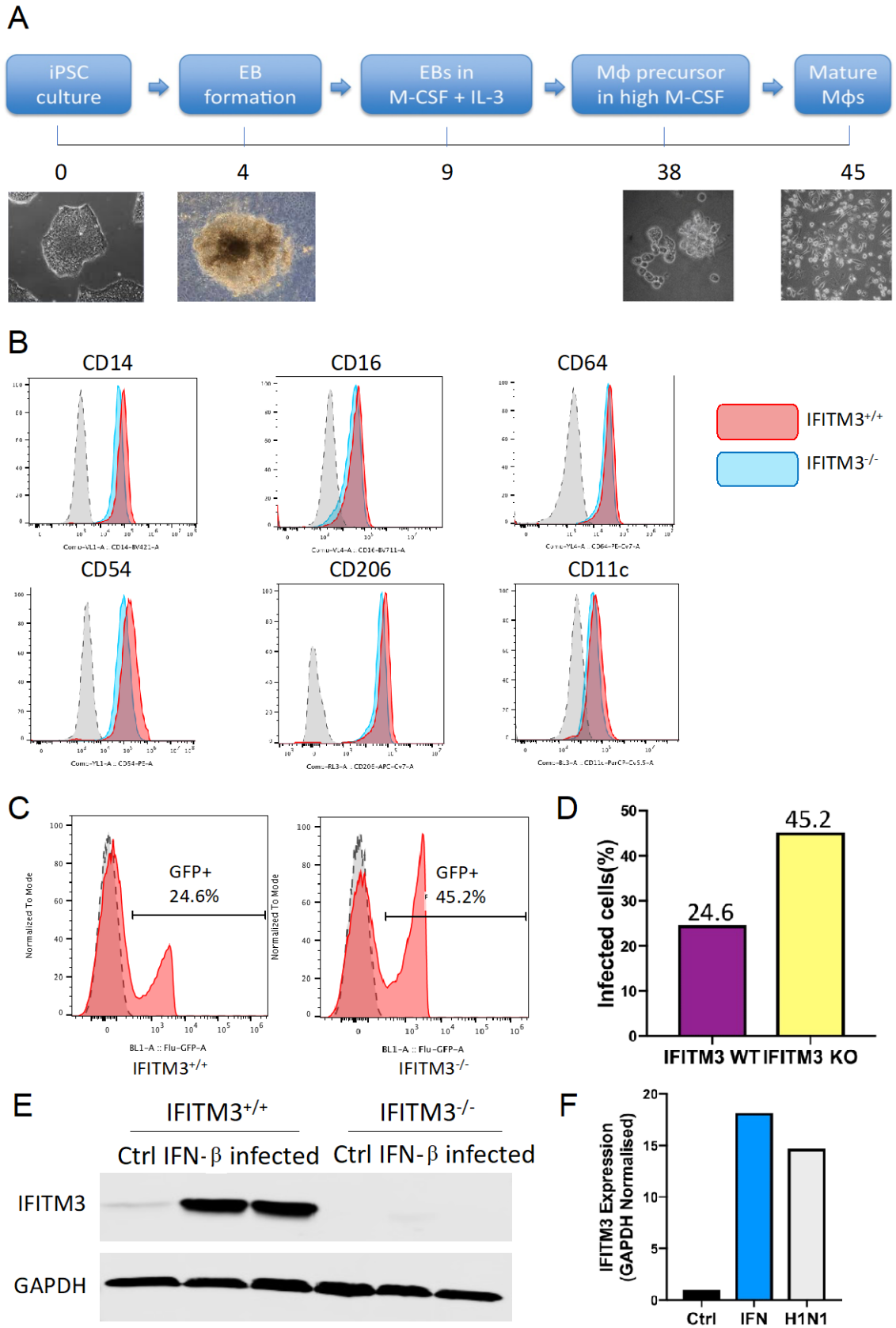


Figure 3.4 S-Flu PR8 (H1N1) infection rate in IFITM3$^{+/+}$ (WT) and IFITM3$^{-/-}$ (KO) iPSDMs. *(A) A schematic diagram showing specific culture conditions required for each differentiation step from iPSCs to macrophages, as well as phase-contrast photomicrographs of differentiation step. Adapted*

from Macrophages Methods and Protocols[129]. (B) Expression of macrophage-specific markers on IFITM3$^{+/+}$ and IFITM3$^{-/-}$ iPSDMs. Gray showing FMO control, red showing IFITM3$^{+/+}$ iPSDMs and blue showing IFITM3$^{-/-}$ iPSDMs. Expressions were measured by flow cytometry. (C) Histograms showing GFP expression in IFITM3$^{+/+}$ and IFITM3$^{-/-}$ iPSDMs following S-Flu PR8 infection. Gray showing uninfected control; red showing infected groups. Columns showing the percentage of GFP+ cells (D). GFP expressions were measured by flow cytometry. (E) IFITM3 and GAPDH expression in IFITM3$^{+/+}$ and IFITM3$^{-/-}$ iPSDMs following 250 U/ml IFN-β stimulation or S-Flu PR8 infection. Columns showing IFITM3 expression normalized by GAPDH expression (F). IFITM3 and GAPDH expression were measured by western blots (E, F).

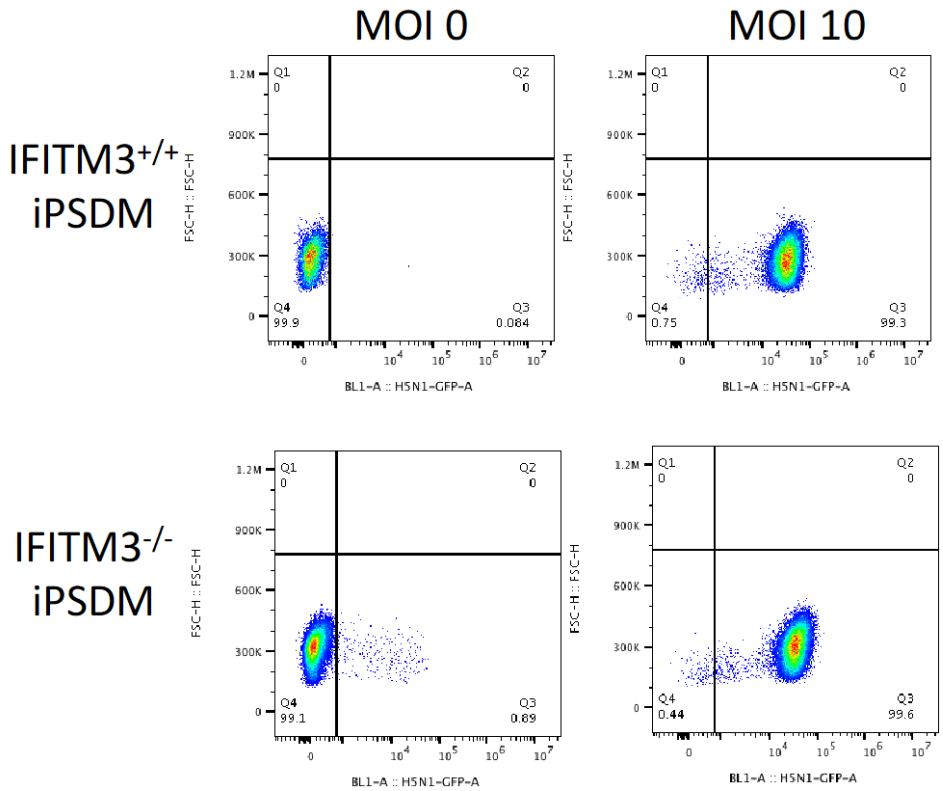


Figure 3.5 H5N1 S-Flu PR8 infection in IFITM3$^{+/+}$ and IFITM3$^{-/-}$ iPSDMs. *IFITM3$^{+/+}$ and IFITM3$^{-/-}$ iPSDMs were infected with H5N1 S-Flu PR8 at MOI 10 for 24 h. Infection rates were reflected by the percentage of GFP+ cells measured by flow cytometry.*

3.4.4 IFITM3 is not correlated with antigen processing and presentation genes in iPSDMs.

Previous RNA-Seq data of the healthy Chinese cohort showed that basal IFITM3 mRNA expression in the whole blood was correlated with TAP1, PSMB8, HLA-ABC and CD54. To investigate the correlation of IFITM3 with antigen processing and presentation, the protein levels of the antigen processing and presentation related genes, listed in **Table 3.1**, were assessed in IFITM3$^{+/+}$ and IFITM3$^{-/-}$ iPSDMs. TAP1 and PSMB8 expression

were measured by western blots as they are both intracellular proteins. HLA-ABC and CD54 expression were measured by flow cytometry as they are expressed on the cell surface.

Basal level of TAP1 protein expression in IFITM3$^{+/+}$ is the same as that in IFITM3$^{-/-}$ iPSDMs. In addition, TAP1 expression can be induced to the same level in IFITM3$^{+/+}$ and IFITM3$^{-/-}$ iPSDMs after IFN-β stimulation (**Figure 3.6 A, B**). This experiment is only done once but we can see from the results that TAP1 is a type I IFN-stimulated gene and the upregulation of TAP1 by IFN-β tends to be compromised in IFITM3$^{-/-}$ iPSDMs.

Basal level of PSMB8 protein expression in IFITM3$^{+/+}$ is also the same as that in IFITM3$^{-/-}$ iPSDMs. However, different from TAP1, PSMB8 protein levels are not affected by IFN-β stimulation (**Figure 3.6 C, D**). Again, this experiment is only done once but there is little evidence of correlation between PSMB8 and IFITM3 at protein levels.

HLA-ABC expression tends to be lower in IFITM3$^{-/-}$ iPSDMs compared to IFITM3$^{+/+}$ iPSDMs, however, this difference is not significant (**Figure 3.6 E, F**). No differences were observed in the CD54 expression levels of IFITM3$^{+/+}$ and IFITM3$^{-/-}$ iPSDMs (**Figure 3.6 G, H**). The absence of IFITM3 doesn't affect the basal protein levels of HLA-ABC or CD54. However, further investigation is needed to understand whether IFITM3 affects the responses of HLA-ABC or CD54, to IFN signalling.

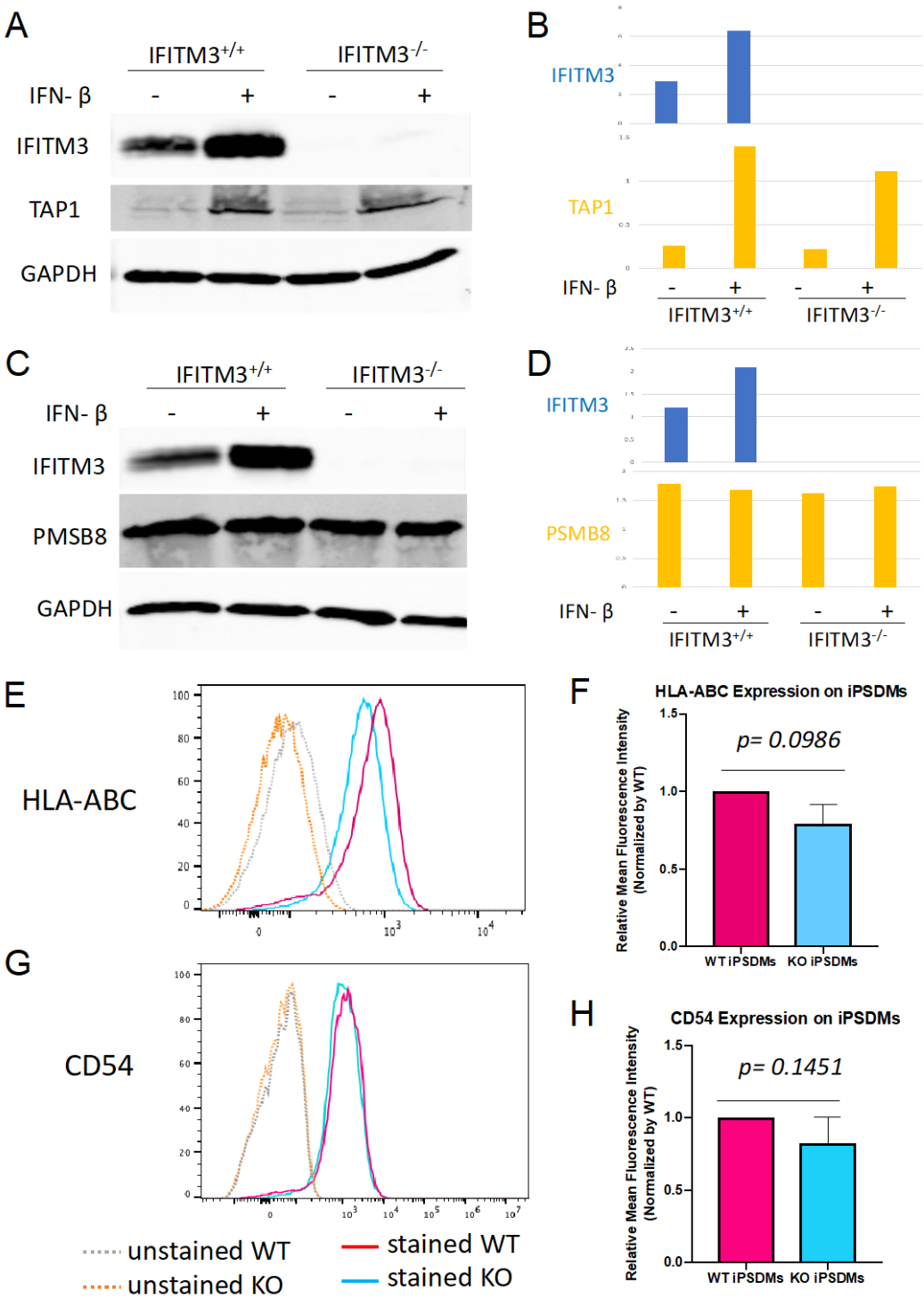


Figure 3.6 Expression of several antigen processing and presentation related proteins in IFITM3$^{+/+}$ (WT) and IFITM3$^{-/-}$ (KO) iPSDMs. *IFITM3$^{+/+}$ and IFITM3$^{-/-}$ iPSDMs were stimulated with 250 U/ml IFN-β for 24 h. TAP1 expression (A, B), or PMSB8 expression (C, D) were measured together with IFITM3 and GAPDH by western blots. (B) Columns showing IFITM3 and TAP1 expression normalized by GAPDH expression. N=1. (D) Columns showing IFITM3 and PMSB8 expression normalized by GAPDH expression. N=1. (E) HLA-ABC expression on IFITM3$^{+/+}$ and IFITM3$^{-/-}$ iPSDMs. (F) Columns showing mean fluorescence intensity (MFI) of HLA-ABC in IFITM3$^{-/-}$ iPSDMs normalized by that in IFITM3$^{+/+}$ iPSDMs. N=4. (G) CD54 expression on IFITM3$^{+/+}$ and IFITM3$^{-/-}$ iPSDMs. (H) Columns showing MFI of CD54 in IFITM3$^{-/-}$ iPSDMs normalized by that in IFITM3$^{+/+}$ iPSDMs. N=4.*

3.4.5 IFITM3 promotes SARS-CoV-2 infection.

To investigate the impact of IFITM3 on the control of SARS-CoV-2 infection in iPSDMs, both IFITM3$^{+/+}$ and IFITM3$^{-/-}$ iPSDMs were infected with live SARS-CoV-2 at MOI 0.1 for 2 hours. Uninfected IFITM3$^{+/+}$ and IFITM3$^{-/-}$ iPSDMs were also set up as control. SARS-CoV-2 virus was then washed off and iPSDMs were replated in fresh medium. The next day, iPSDMs were harvested and RNA was extracted for qPCR. Both cell lines were able to be infected by SARS-CoV-2 but reduced SARS-CoV-2 RNA levels were observed in IFITM3$^{-/-}$ iPSDMs compared to IFITM3$^{+/+}$ iPSDMs (**Figure 3.7 A**), suggesting that IFITM3 promotes SARS-CoV-2 RNA production in iPSDMs.

Next, we were interested in whether the absence of IFITM3 makes any difference to T cell responses against SARS-CoV-2-infected iPSDMs. M24 is a CD4$^+$ epitope from SARS-CoV-2 membrane protein and is restricted by multiple HLAs, including HLA-DRB1*01:01. M24-specific CD4$^+$ T cell clones restricted by HLA-DRB1*01:01-only were established in our lab. ORF3a28 is a CD8$^+$ epitope from SARS-CoV-2 ORF3a protein and is restricted by HLA-A*01:01. ORF3a-specific CD8$^+$ T cell clones were also established in our lab. As HLA-typing of our iPSDMs is both HLA-DRB1*0101 and HLA-A*0101, M24-specific CD4$^+$ T cells and ORF3a28-specific CD8$^+$ T cells were used to evaluate T cell responses to SARS-CoV-2 epitopes presented by iPSDMs.

IFITM3$^{+/+}$ and IFITM3$^{-/-}$ iPSDMs were infected with SARS-CoV-2, as described above. 24 hours later, SARS-CoV-2-specific T cells were co-cultured with infected iPSDMs for 6 hours. T cell responses were then measured by ICS. Strong cytokine production against SARS-CoV-2-infected iPSDMs was observed from M24-specific CD4$^+$ T cells, but not ORF3a28-specific CD8$^+$ T cells (**Figure 3.7 B**). As both CD4$^+$ and CD8$^+$ clones used in this experiment are high avidity ones, the absence of CD8$^+$ responses

reflect the low ORF3a28 antigen load at the cell surface, which may be due to low processing efficiency of ORF3a28 epitope in iPSDMs, or low MHC class I expression at the cell surface of iPSDMs. As for the strength of M24-specific $CD4^+$ responses, no differences were observed between $IFITM3^{+/+}$ and $IFITM3^{-/-}$ iPSDMs (**Figure 3.7 B**).

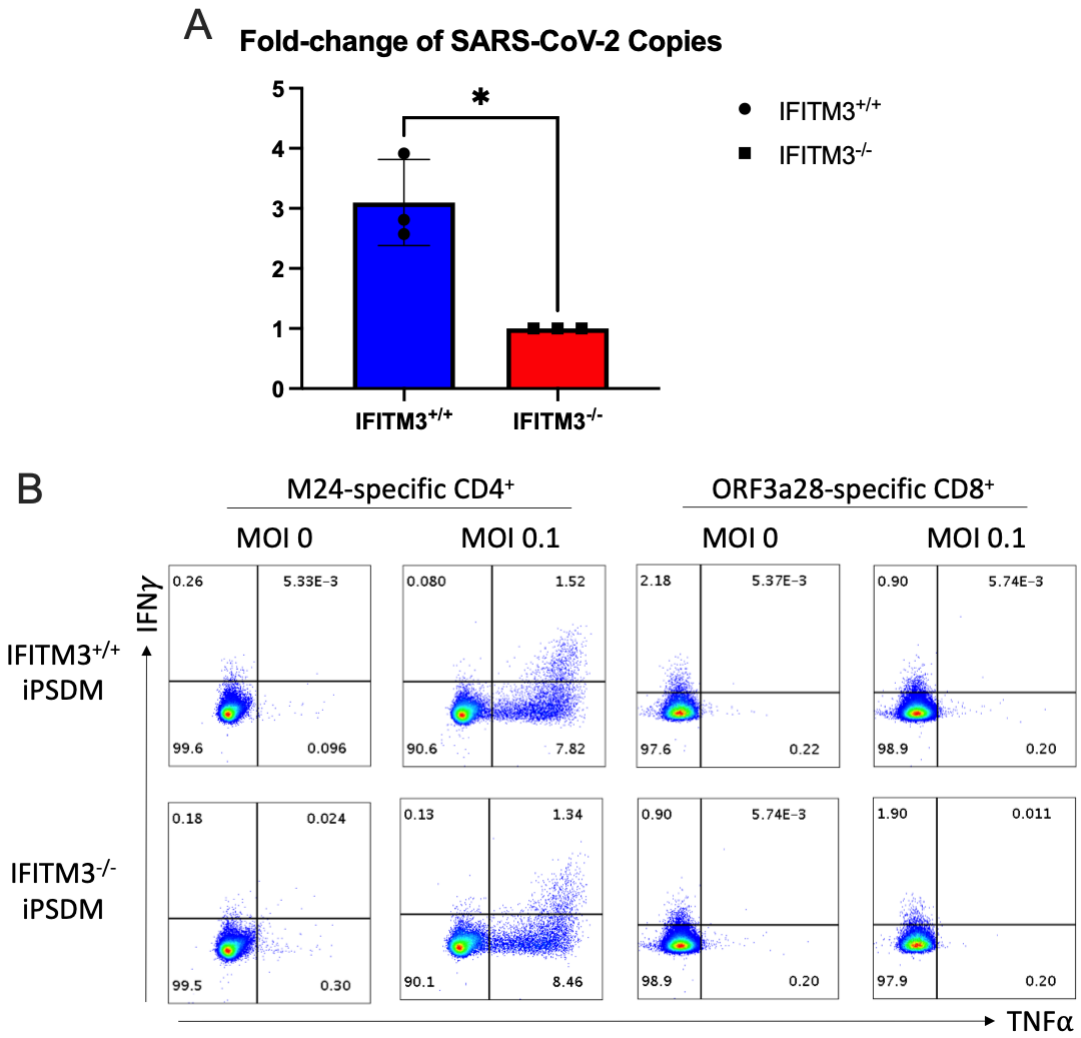


Figure 3.7 SARS-CoV-2 infection in IFITM3$^{+/+}$ and IFITM3$^{-/-}$ iPSDMs and SARS-CoV-2-specific T cell responses against infected iPSDMs. *(A) Fold-change of SARS-CoV-2 copies. Virus copies were measured by qPCR and normalized by the virus copies in IFITM3$^{-/-}$ iPSDMs. *P<0.05 by unpaired t test. N=3. (B) M24-specific $CD4^+$ responses and ORF3a28-specific $CD8^+$ responses to SARS-CoV-2-infected iPSDMs. T cell responses were measured by ICS and flow cytometry.*

3.4.6 RNA sequencing was performed to study IFITM3-dependent gene expression.

Until now, we have been studying the role of IFITM3 in HEK293 cells and iPSDMs. Our data and others so far have suggested that IFITM3 is a restrictor for IAV infection, while

a promoter for SARS-CoV-2 infection. Although we have observed a potential connection between IFITM3 and antigen processing and presentation in previous RNA-Seq analysis of a healthy Chinese cohort, it is still unclear whether this correlation is IFITM3-dependent or just the consequence of upregulated IFN signalling. Therefore, using IFITM3$^{+/+}$ and IFITM3$^{-/-}$ A549 cells, iPSCs and iPSDMs, we designed the following experiments to explore IFITM3-dependent gene expression at transcriptional level during IAV or SARS-CoV-2 infection (**Table 3.2**). RNA was extracted and sent for bulk RNA-Seq. Three biological replicates were completed for each condition.

- To understand whether the depletion of IFITM3 affects fundamental expression of other genes, IFITM3$^{+/+}$ and IFITM3$^{-/-}$ A549, iPSCs and iPSDMs were sent for RNA-Seq to study the impact of IFITM3 in lung epithelial cells, stem cells and macrophages respectively.
- To understand whether the depletion of IFITM3 affects the response of other genes to IFN stimulation, IFITM3$^{+/+}$ and IFITM3$^{-/-}$ iPSDMs were sent for RNA-Seq following 250 U/ml IFN-β treatment. We selected macrophages as our main cellular system because they are not only the targets for IAV or SARS-CoV-2 infection, but also their functions directly affect T cell activation. We chose IFN-β as it was previously shown to induce the greatest increase in IFITM3 expression (**Figure 3.2 B**).
- To understand whether the depletion of IFITM3 affects the response of other genes to virus infection, IFITM3$^{+/+}$ and IFITM3$^{-/-}$ iPSDMs were sent for RNA-Seq following H1N1, H5N1, or SARS-CoV-2 infection. As SARS-CoV-2 is a newly emerged virus and limited studies have been reported on IFITM3 activity during SARS-CoV-2 infection, we collected SARS-CoV-2-infected cells at a series of time

points (0, 6, 12, 24, 48 hours) post infection to study both the short-time and long-time impact of IFITM3 in the control of SARS-CoV-2 infection.

By comparing up-regulated genes in IFITM3$^{-/-}$ iPSDMs after IFN-β stimulation or viral infection with the up-regulated genes in IFITM3$^{+/+}$ iPSDMs, we would be able to find out factors whose expression levels are directly correlated to IFITM3. We are particularly interested in genes that are involved in IFN signalling, antigen processing and presentation, and metabolic pathways. This will provide insights into other factors that may work with IFITM3 to restrict viral replication as well as identifying the mechanisms that compensate when IFITM3 is absent.

Table 3.2 RNA-Seq plan.

	Samples			Repeats	number of samples	Aim to find out
1	IFITM3 WT A549	IFITM3 KO A549		3	6	Fundamental difference between IFITM3 WT and KO A549
2	IFITM3 WT iPSC	IFITM3 KO iPSC (H12)	IFITM3 KO iPSC (F01)	3	9	Fundamental difference between IFITM3 WT and KO iPSC
3	IFITM3 WT iPSDM without IFN	IFITM3 KO iPSDM (H12) without IFN		3	12	IFITM3-dependent IFN-stimulated genes
	IFITM3 WT iPSDM + IFN-beta (250U/ml, 24h)	IFITM3 KO iPSDM (H12) + IFN-beta (250U/ml, 24h)				
4	IFITM3 WT iPSDM without flu	IFITM3 KO iPSDM (H12) without flu		3	12	IFITM3-dependent H1N1-stimulated genes
	IFITM3 WT iPSDM + H1N1 (MOI 10, 24h)	IFITM3 KO iPSDM (H12) + H1N1 (MOI 10, 24h)				
5	IFITM3 WT iPSDM without flu	IFITM3 KO iPSDM (H12) without flu		3	12	IFITM3-dependent H5N1-stimulated genes
	IFITM3 WT iPSDM + H5N1 (MOI 10, 24h)	IFITM3 KO iPSDM (H12) + H5N1 (MOI 10, 24h)				
6	IFITM3 WT iPSDM (KOLF2) without SARS2 (0h)	IFITM3 KO iPSDM (H12) without SARS2 (0h)		3	30	IFITM3-dependent SARS2-stimulated genes
	IFITM3 WT iPSDM (KOLF2) + SARS2 Victoria (MOI 0.1, 6h)	IFITM3 KO iPSDM (H12) + SARS2 Victoria (MOI 0.1, 6h)				
	IFITM3 WT iPSDM (KOLF2) + SARS2 Victoria (MOI 0.1, 12h)	IFITM3 KO iPSDM (H12) + SARS2 Victoria (MOI 0.1, 12h)				
	IFITM3 WT iPSDM (KOLF2) + SARS2 Victoria (MOI 0.1, 24h)	IFITM3 KO iPSDM (H12) + SARS2 Victoria (MOI 0.1, 24h)				
	IFITM3 WT iPSDM (KOLF2) + SARS2 Victoria (MOI 0.1, 48h)	IFITM3 KO iPSDM (H12) + SARS2 Victoria (MOI 0.1, 48h)				

3.4.7 Differentially expressed genes were observed due to IFITM3 depletion.

To investigate if IFITM3 affects the baseline expression of other genes, we first analysed RNA-Seq data from IFITM3$^{+/+}$ and IFITM3$^{-/-}$ iPSCs without any treatment. KO_1 and KO_2 are two IFITM3$^{-/-}$ iPSC clones generated from the same donor as IFITM3$^{+/+}$ iPSCs (WT).

Principal component analysis (PCA) (**Figure 3.8 A**) showed that the major variance (PC1: 42% variance) was caused by IFITM3 depletion as samples of IFITM3$^{+/+}$ iPSCs (WT, blue dots) were separated from IFITM3$^{-/-}$ iPSCs (KO_1 and KO_2, red and green dots, respectively). To find out the differentially expressed genes due to the absence of IFITM3, we compared gene expression in WT with that in KO_1, and in KO_2, respectively. RNA-Seq data was analysed with DESeq2. Significantly upregulated genes (adjusted p-value < 0.05, fold-change > 2) and downregulated genes (adjusted p-value < 0.05, fold-change < 0.5) in both KO_1 and KO_2 were selected and used to generate a heatmap (**Figure 3.8 B**).

12 genes were significantly downregulated, while 15 were significantly upregulated in IFITM3$^{-/-}$ iPSCs. Gene ontology (GO) enrichment analysis was performed on these differentially expressed genes. Three sub-ontologies were included: biological process (BP), molecular function (MF) and cellular component (CC). Enrichment of terms related to DNA-binding transcription activator activity was observed (**Figure 3.8 C**). However, this enrichment finding does not really help us understand the impact of IFITM3 depletion in iPSCs.

We investigated the function of each individual gene that is differentially expressed in IFITM3$^{+/+}$ and IFITM3$^{-/-}$ iPSCs (**Table 3.3**). Among all these genes, serine proteinase inhibitor (serpin) family E member 1 (SERPINE1) caught our attention.

SERPINE1 encodes plasminogen activator inhibitor-1 (PAI-1), which has been reported to inhibit IAV glycoprotein cleavage by targeting extracellular airway proteases, thereby reducing infectivity of progeny viruses[130]. IFITM3 may work collaboratively with SERPINE1 in restricting IAV infection.

From **Table 3.3**, we observed a group of genes encoding membrane proteins, including solute carrier family 16 member 3 (SLC16A3), protocadherin alpha 6 (PCDHA6), cadherin-6 (CDH6), low-density lipoprotein receptor (LDL-R) related protein 2 (LRP2) and cytochrome P450 family 26 subfamily A member 1 (CYP26A1). As IFITM3 is membrane bound, these proteins may interact with IFITM3 within membrane structures.

Another interesting finding is that 7 out of 12 significantly downregulated genes in IFITM3$^{-/-}$ iPSCs have been reported to be associated with tumour growth. Considering that IFITM3 also plays a significant role in the metastasis of many tumours by regulating metastatic mechanisms[131], our data suggested that IFITM3 may regulate tumour metastasis by interacting with the proteins encoded by the 7 genes identified in our experiment. In addition, 7 out of the total 27 differentially expressed genes in IFITM3$^{-/-}$ iPSCs are involved in neuronal development. This implies that IFITM3 may be important in neuronal development as well, which has been poorly studied so far.

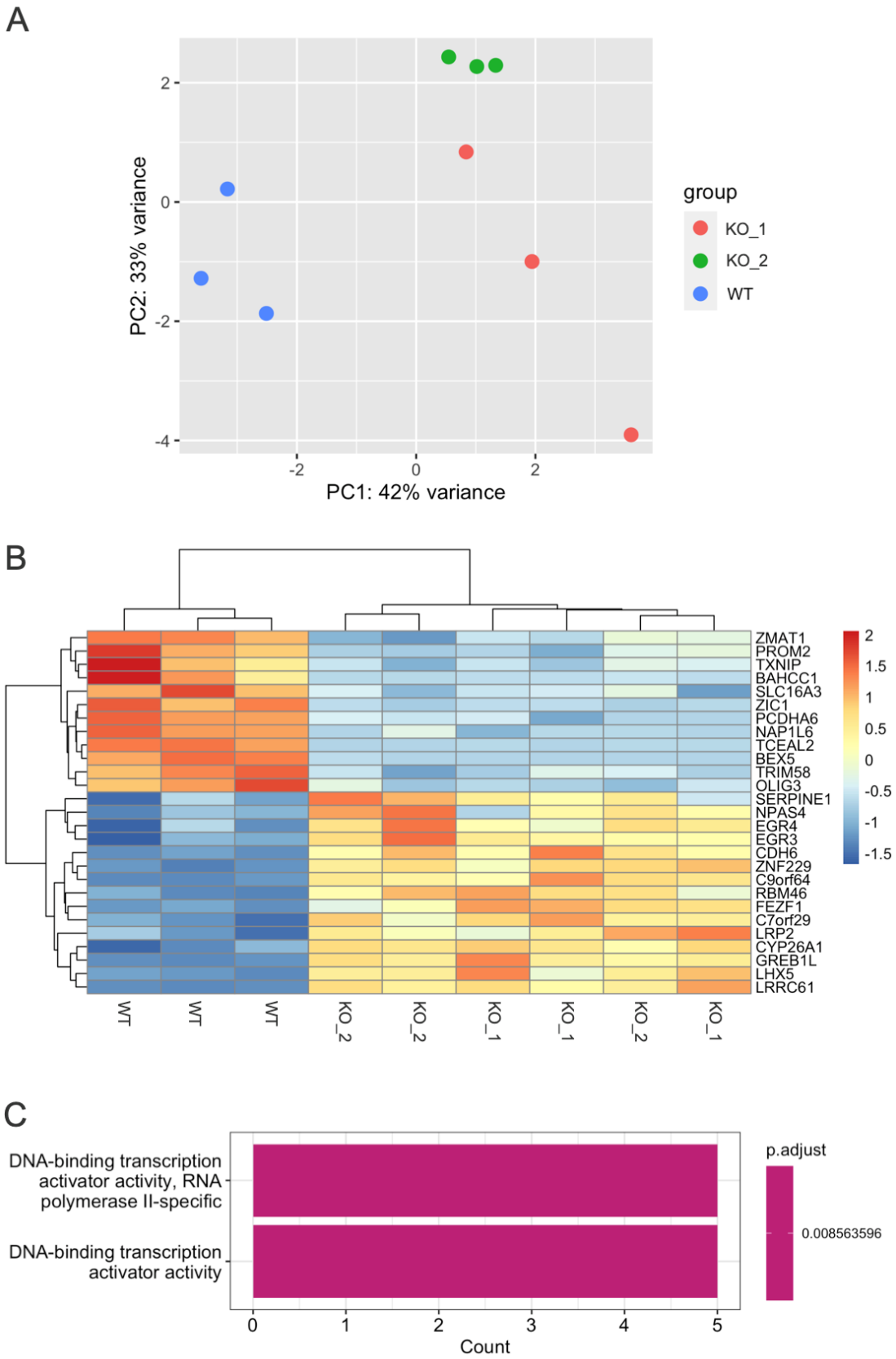


Figure 3.8 The impact of IFITM3 depletion in iPSCs. *(A) PCA plot. Blue dots show IFITM3$^{+/+}$ iPSCs; red and green dots show IFITM3$^{-/-}$ iPSCs. (B) Heatmap of significantly upregulated and downregulated genes in IFITM3$^{-/-}$ iPSCs compared with IFITM3$^{+/+}$ iPSCs. (C) Enriched GO terms.*

Table 3.3 Differentially expressed genes in IFITM3$^{-/-}$ iPSCs compared to IFITM3$^{+/+}$ iPSCs.

Symbol	Name	Description
ZMAT1	Zinc finger matrin type 1	Suppress tumour in pancreatic ductal adenocarcinoma via SIRT3/p53 signalling pathway[132].
PROM2	Prominin 2	Potentially involved in the organization of plasma membrane microdomains in pancreatic cancer[133].
TXNIP	Thioredoxin interacting protein	Promote the accumulation of reactive oxygen species and cellular stress by inhibiting the antioxidative function of thioredoxin[134]; regulate cellular metabolism and ER stress[135]; suppress tumour[136].
BAHCC1	Bromo adjacent homology (BAH) domain and coiled coil containing 1	Potentially enable chromatin binding activity[137].
SLC16A3	Solute carrier family 16 member 3, also known as monocarboxylate transporter 4 (MCT4)	Export lactate across plasma membranes[138].
ZIC1	Zinc finger of the cerebellum (ZIC) family member 1	Transcription factor in neural development[139]; suppress cancer[140-142].
PCDHA6	Protocadherin alpha 6	Plasma membrane proteins in the establishment and function of specific cell-cell connections in the brain[143].
NAP1L6	Nucleosome assembly protein 1 like 6	Long non-coding RNA that promote prostate cancer[144].
TCEAL2	Transcription elongation factor A like 2	Suppress renal cell carcinoma[145].
BEX5	Brain expressed X-linked 5	Potentially involved in signal transduction and be active in cytoplasm[146].
TRIM58	Tripartite motif containing 58	Suppress tumour growth by inactivation of β-catenin signalling via ubiquitination[147]; suppress tumour.
OLIG3	Oligodendrocyte transcription factor 3	Regulate early cerebellar development[148].
SERPINE1	Serine proteinase inhibitor (serpin) family E member 1	Inhibitor of fibrinolysis; reduce IAV infection by inhibiting IAV glycoprotein cleavage[130].
NPAS4	Neuronal Per-Arnt-Sim (PAS) domain protein 4	Transcriptional factor involved in inhibitory synapse development and synaptic plasticity[149].
EGR3	Early growth response 3	Transcriptional factor involved in biological rhythm, muscle development, lymphocyte development, endothelial cell growth and migration, and neuronal development[150].

EGR4	Early growth response 4	Transcriptional factor involved in lymphocyte development[151] and lung cancer cell growth.
CDH6	Cadherin-6	Membrane glycoproteins involved in cell differentiation and morphogenesis, especially kidney development as well as endometrium and placenta formation[152].
ZNF229	Zinc finger protein 229	Potentially enable DNA-binding transcription activator activity.
C9orf64	Chromosome 9 open reading frame 64	Potentially involved in tRNA-guanine transglycosylation.
RBM46	RNA binding motif protein 46	Potentially enable mRNA binding activity and modulate meiotic progression and spermatogenesis[153].
FEZF1	Forebrain embryonic zinc (FEZ) family zinc finger 1	Transcriptional repressor involved in early neural development[154].
C7orf29	Chromosome 7 open reading frame 29	Unknown.
LRP2	Low-density lipoprotein receptor (LDL-R) related protein 2	Multi-ligand endocytic receptor expressed primarily in absorptive epithelial cells and mediate endocytosis of ligands leading to degradation in lysosomes or transcytosis[155].
CYP26A1	Cytochrome P450 family 26 subfamily A member 1	Monooxygenases (ER proteins) that regulates the cellular level of retinoic acid which is involved in regulation of gene expression[156].
GREB1L	Growth regulation by estrogen in breast cancer (GREB) 1 like retinoic acid receptor coactivator	Involved in kidney development and renal agenesis[157].
LHX5	LIM homeobox 5 (LIM is the acronym of LIN-11, Isl-1 and MEC-3)	Transcriptional regulator involved in the control of differentiation and development of the forebrain[158].
LRRC61	Leucine rich repeat containing 61	Predicted to be active in cytosol.

The same PCA and DESeq2 analysis was performed on RNA-Seq data from IFITM3$^{+/+}$ and IFITM3$^{-/-}$ iPSDMs, as well as A549 cells, without any treatment. Like iPSCs, PCA of IFITM3$^{+/+}$ (WT) and IFITM3$^{-/-}$ (KO) iPSDMs showed that the major variance (PC1: 97% variance) was caused by IFITM3 depletion (**Figure 3.9 A**). Significantly upregulated genes (adjusted p-value < 0.05, fold-change > 2) and downregulated genes (adjusted p-value < 0.05, fold-change < 0.5) in KO, compared to WT, were selected, and used to generate a heatmap (**Figure 3.9 B**).

6 genes were significantly downregulated, while 5 were significantly upregulated in KO. Due to the small number of genes identified we did not run GO analysis. Among these 11 genes of interest, serine proteinase inhibitor (serpin) family B member 2 (SERPINB2) caught our attention. SERPINB2 encodes plasminogen activator inhibitor-2 (PAI-2), which is known as a regulator of inflammatory processes with a strong expression in activated macrophages[159]. The observation of downregulated SERPINB2 in IFITM3$^{-/-}$ iPSDMs suggested that in macrophages, IFITM3 may work collaboratively with SERPINB2 during virus infection.

Among these 11 differentially expressed genes in macrophages, again, a group of genes encoding membrane proteins were observed, including solute carrier family 39 member 4 (SLC39A4), protocadherin gamma subfamily A member 3 (PCDHGA3), calcium voltage-gated channel auxiliary subunit alpha 2 delta 4 (CACNA2D4) and ATPase phospholipid transporting 10A (ATP10A). As IFITM3 is a membrane protein and not entering the nucleus, it is unlikely that IFITM3 can directly regulate the gene expression at transcriptional level. However, IFITM3 potentially interacts with other membrane-bound proteins within membrane structure. In addition, genes involved in tumour growth (MAGEA4, TRIM58 and PTCHD3P1) or neuronal development (ELAVL4 and PCDHGA3) were observed, again indicating a role of IFITM3 in these processes.

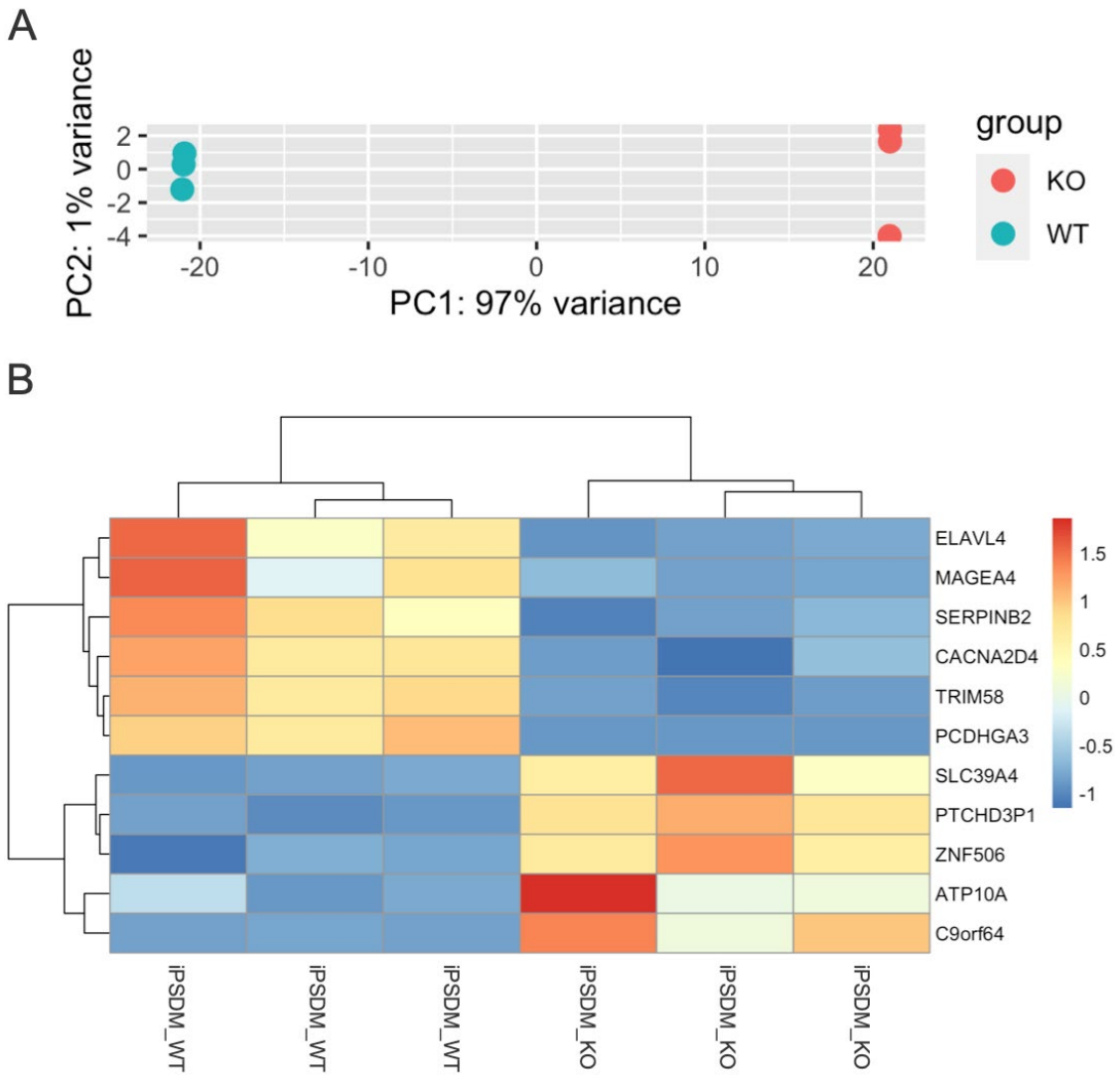
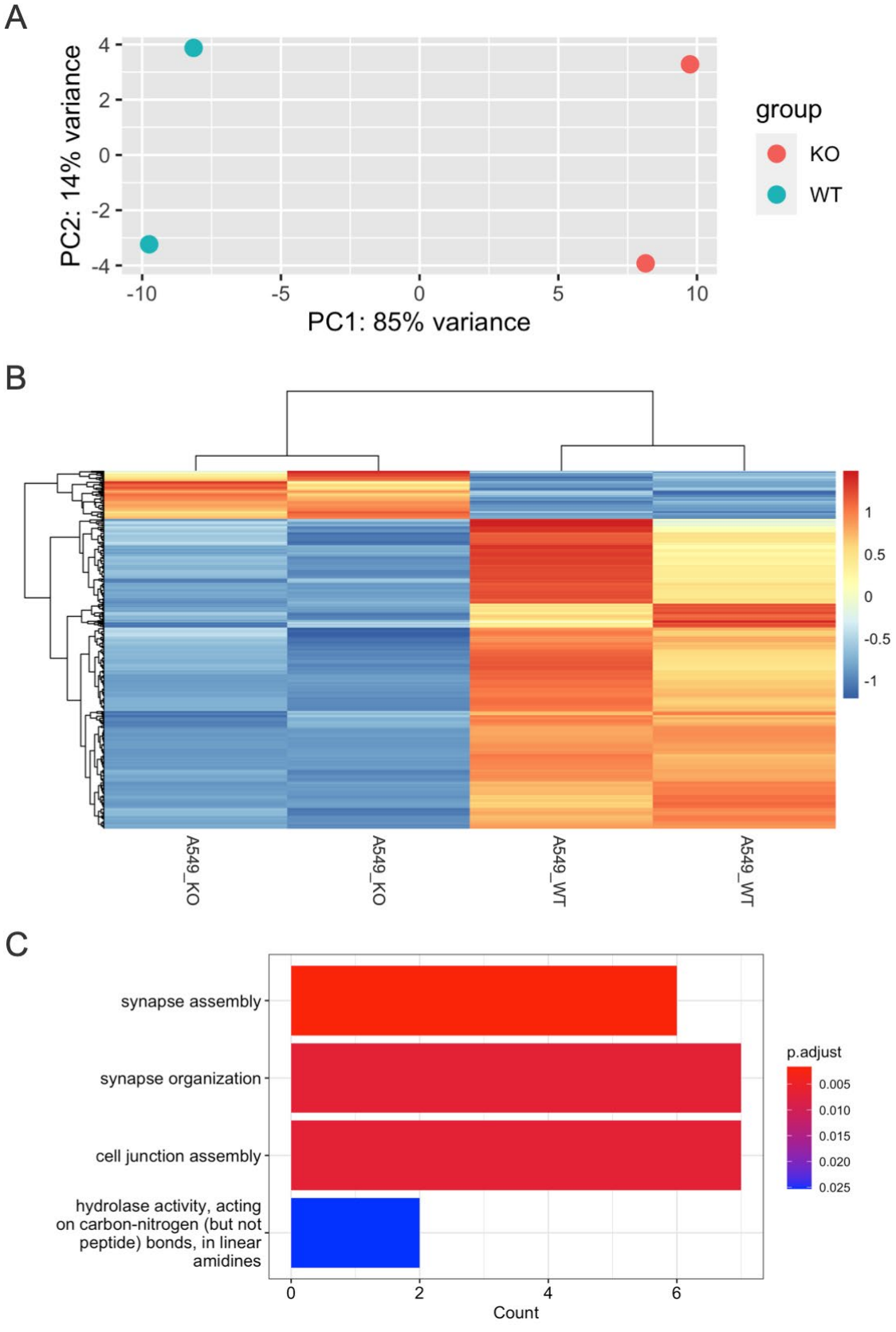


Figure 3.9 The impact of IFITM3 depletion in iPSDMs. *(A) PCA plot. Green dots show IFITM3$^{+/+}$ iPSDMs (WT); red dots show IFITM3$^{-/-}$ iPSDMs (KO). (B) Heatmap of significantly upregulated and downregulated genes in IFITM3$^{-/-}$ iPSDMs compared with IFITM3$^{+/+}$ iPSDMs.*

PCA of IFITM3$^{+/+}$ (WT) and IFITM3$^{-/-}$ (KO) A549 cells showed that the major variance (PC1: 85% variance) was caused by IFITM3 depletion (**Figure 3.10 A**). Three biological replicates were done but one replicate was removed from analysis due to a strong batch effect. Significantly upregulated genes (adjusted p-value < 0.05, fold-change > 2) and downregulated genes (adjusted p-value < 0.05, fold-change < 0.5) in KO, compared to WT, were selected and used to generate a heatmap (**Figure 3.10 B**). Surprisingly, a huge number of genes were affected by IFITM3 depletion in A549. Since

A549 cells are a lung carcinoma epithelial cell line, our data suggest that IFITM3 may have broader influence in lung cells than in stem cells or macrophages. Considering that A549 is a cancer cell line, our findings also suggest that IFITM3 may be cancerous. When examining genes upregulated in IFITM3$^{-/-}$ A549, we observed significant enrichment of GOs related to synapse assembly and organisation, cell junction assembly and hydrolase activity (**Figure 3.10 C**). Most of the downregulated genes in IFITM3$^{-/-}$ A549 are involved in the regulation of hormone levels (**Figure 3.10 D**).


A
PC2: 14% variance
PC1: 85% variance
group
KO
WT
B
A549_KO
A549_KO
A549_WT
A549_WT
C
synapse assembly
synapse organization
cell junction assembly
hydrolase activity, acting on carbon-nitrogen (but not peptide) bonds, in linear amidines
Count
p.adjust

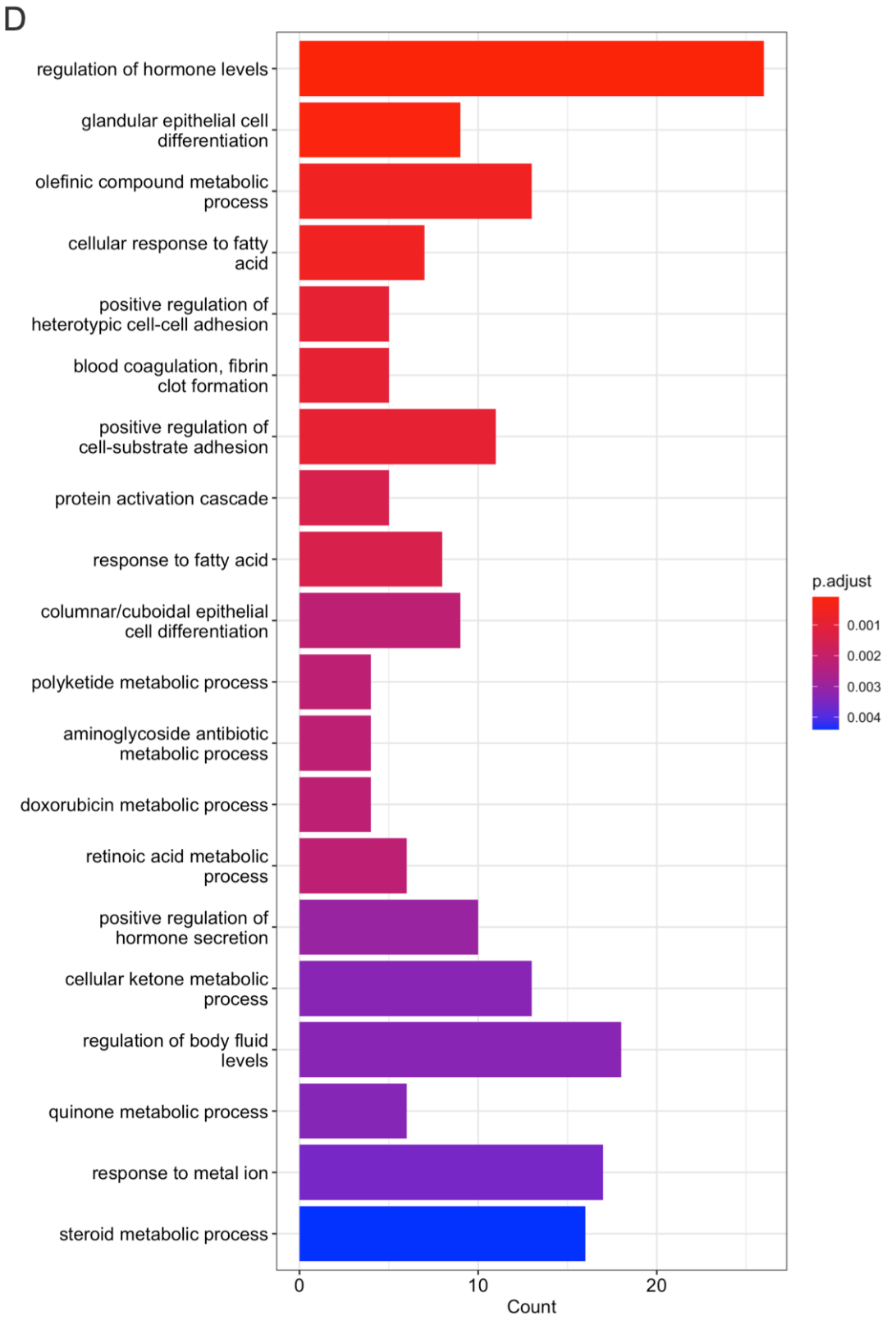


Figure 3.10 The impact of IFITM3 depletion in A549. *(A) PCA plot. Green dots show IFITM3$^{+/+}$ A549 (WT); red dots show IFITM3$^{-/-}$ A549 (KO). (B) Heatmap of significantly upregulated and downregulated genes in IFITM3$^{-/-}$ A549 compared with IFITM3$^{+/+}$ A549. (C) Enriched GO terms of upregulated genes in IFITM3$^{-/-}$ A549. (D) Enriched GO terms of downregulated genes in IFITM3$^{-/-}$ A549.*

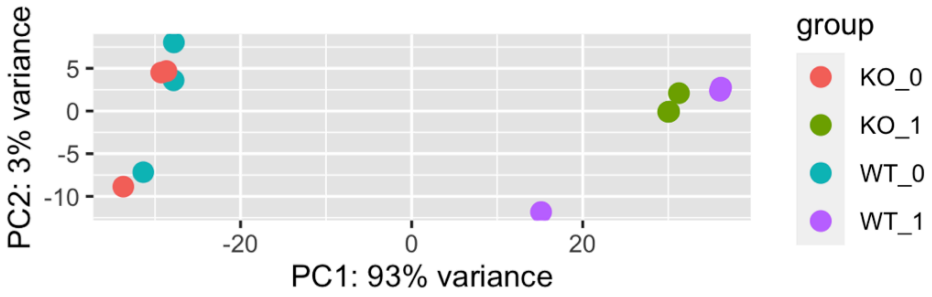
3.4.8 IFITM3 is correlated with antigen processing and presentation in iPSDMs during IFN-β stimulation.

To investigate if IFITM3 affects the response of other genes to IFN stimulation, we analysed RNA-Seq data from IFITM3$^{+/+}$ and IFITM3$^{-/-}$ iPSDMs following 250 U/ml IFN-β stimulation. PCA showed that the major variance (PC1: 93% variance) was caused by IFN-β treatment as samples of IFITM3$^{+/+}$ and IFITM3$^{-/-}$ iPSDMs without IFN-β treatment (WT_0 and KO_0, blue and red dots, respectively) are separated with samples after IFN-β treatment (WT_1 and KO_1, purple and green dots, respectively) on the graph (**Figure 3.11 A**).

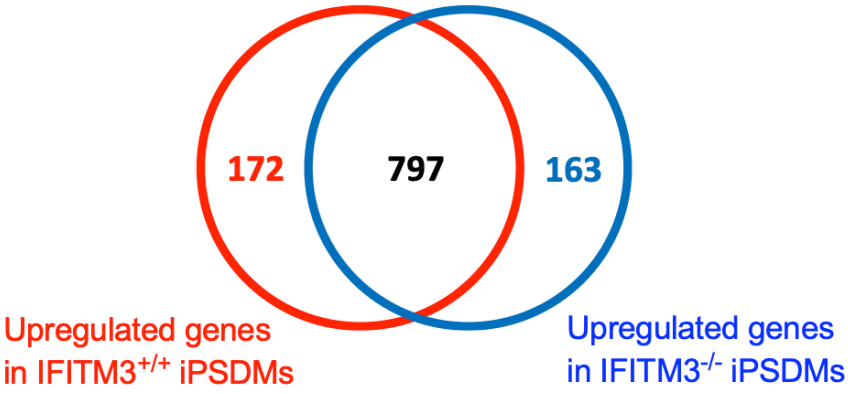
To find out genes that respond differentially to IFN-β stimulation due to the absence of IFITM3, we compared significantly upregulated genes in IFITM3$^{+/+}$ iPSDMs following IFN-β stimulation with those in IFITM3$^{-/-}$ iPSDMs following IFN-β stimulation. Significantly upregulated genes (adjusted p-value < 0.05, fold-change > 2) were obtained by the comparison of gene expression in WT_1 with that in WT_0, and KO_1 with KO_0. RNA-Seq data was analysed with DESeq2. Following IFN-β stimulation, 969 genes were significantly upregulated in IFITM3$^{+/+}$ iPSDMs and 960 were significantly upregulated in IFITM3$^{-/-}$ iPSDMs, with 797 genes overlapped (**Figure 3.11 B**).

We were particularly interested in the 172 genes that only responded to IFN-β stimulation at the presence of IFITM3, however, GO analysis of this group of genes didn't show any enrichment. On the other hand, when examining the 163 genes that only responded to IFN-β in the absence of IFITM3, we observed highly significant enrichment of GOs related to antigen processing and presentation (**Figure 3.11 C**).

A


PC2: 3% variance
5
0
-5
-10
-20
0
20
PC1: 93% variance
group
KO_0
KO_1
WT_0
WT_1

B


172
797
163
Upregulated genes in IFITM3+/+ iPSDMs
Upregulated genes in IFITM3-/- iPSDMs

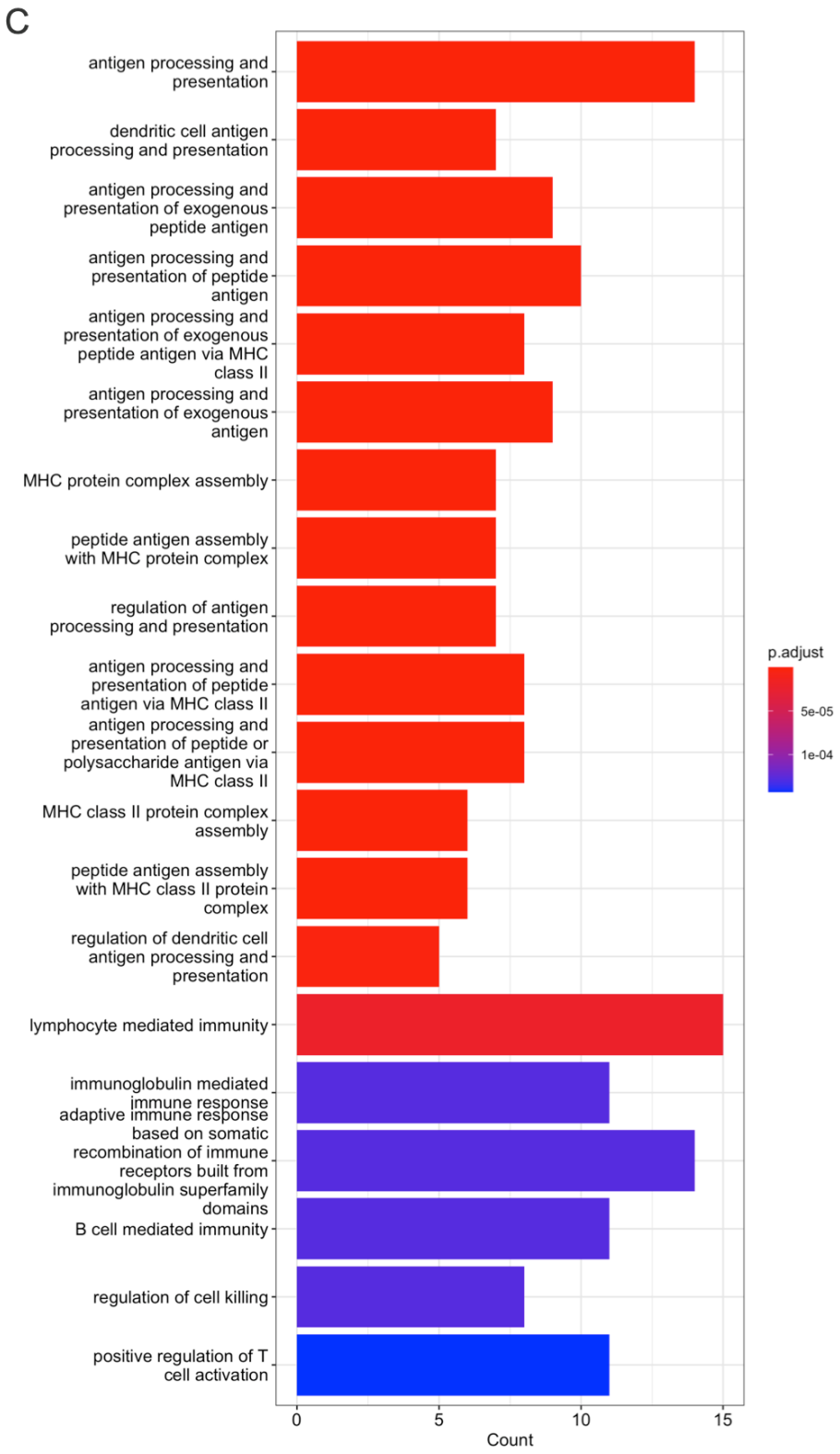


Figure 3.11 The impact of IFITM3 depletion in iPSDMs during IFN-β stimulation. *(A) PCA plot. WT_0: IFITM3$^{+/+}$ iPSDMs without IFN-β; WT_1: IFITM3$^{+/+}$ iPSDMs with IFN-β; KO_0: IFITM3$^{-/-}$ iPSDMs without IFN-β; KO_1: IFITM3$^{-/-}$ iPSDMs with IFN-β. (B) Venn diagram of significantly upregulated genes in IFITM3$^{+/+}$ iPSDMs (red circle) and in IFITM3$^{-/-}$ iPSDMs (blue circle) following IFN-β stimulation. (C) Enriched GO terms of upregulated genes in IFITM3$^{-/-}$ iPSDMs only, but not IFITM3$^{+/+}$ iPSDMs.*

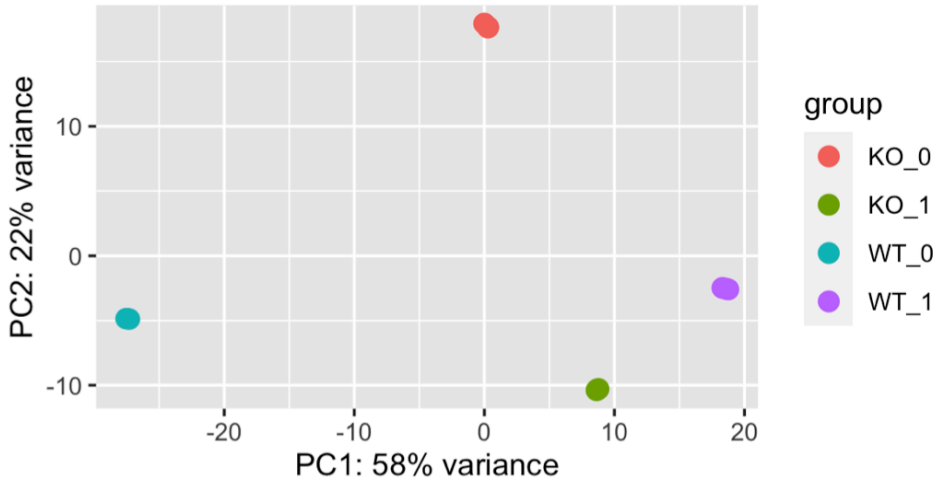
3.4.9 IFITM3 is correlated with response to virus in iPSDMs during H1N1 infection.

To investigate if IFITM3 affects the response of other genes to H1N1 infection, we analysed RNA-Seq data from IFITM3$^{+/+}$ and IFITM3$^{-/-}$ iPSDMs following H1N1 infection.

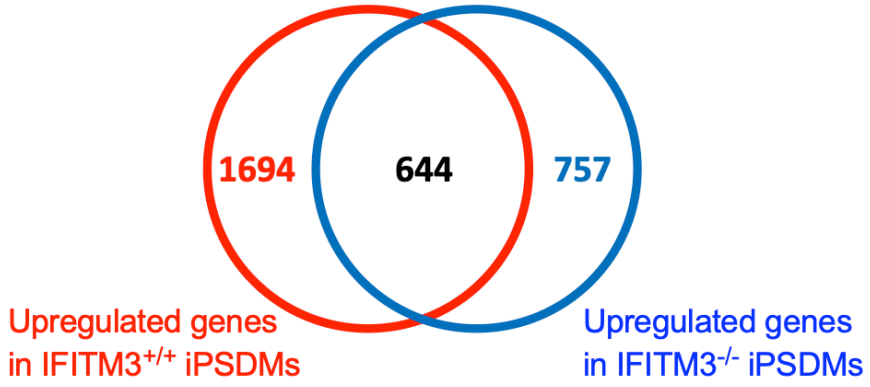
PCA showed that the major variance (PC1: 58% variance) was caused by H1N1 infection as samples of IFITM3$^{+/+}$ and IFITM3$^{-/-}$ iPSDMs without infection (WT_0 and KO_0, blue and red dots, respectively) are separated with samples after infection (WT_1 and KO_1, purple and green dots, respectively) on the graph (**Figure 3.12 A**).

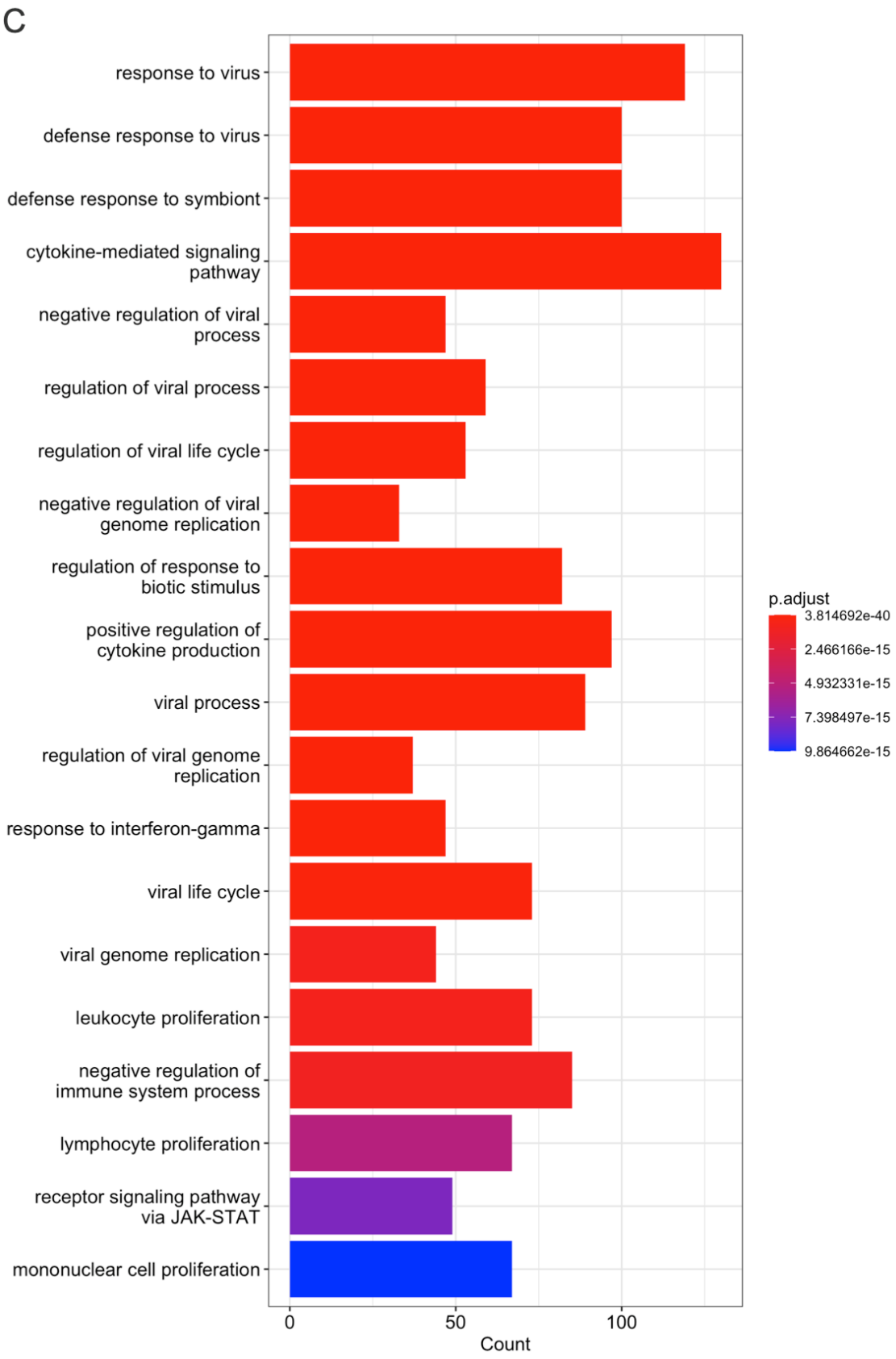
To find out the H1N1-reponding genes affected by IFITM3 depletion, we compared significantly upregulated genes in IFITM3$^{+/+}$ iPSDMs following H1N1 infection with those in IFITM3$^{-/-}$ iPSDMs following H1N1 infection. Significantly upregulated genes (adjusted p-value < 0.05, fold-change > 2) following H1N1 infection were obtained by the comparison of gene expression in WT_1 with that in WT_0, and KO_1 with KO_0. RNA-Seq data was analysed with DESeq2. Following H1N1 infection, 2338 genes were significantly upregulated in IFITM3$^{+/+}$ iPSDMs and 1401 were significantly upregulated in IFITM3$^{-/-}$ iPSDMs, with 644 genes overlapped (**Figure 3.12 B**). Surprisingly, about 72.4% (1694 out of 2338) of H1N1-responding genes cannot be upregulated during H1N1 infection in the absence of IFITM3. GO analysis of this group of genes showed enrichment of terms related to response to virus and regulation of viral process, viral life cycle and viral genome replication (**Figure 3.12 C**), indicating a huge impact of loss of IFITM3 on host defence against H1N1. On the other hand, when examining the 757 genes that were only upregulated in response to H1N1 in the absence of IFITM3, we observed highly significant enrichment of GOs related to mitosis suggesting that the virus is driving replication of the cells (**Figure 3.12 D**).

A


PC2: 22% variance
10
0
-10
-20
-10
0
10
20
PC1: 58% variance
group
KO_0
KO_1
WT_0
WT_1

B


1694
644
757
Upregulated genes in IFITM3+/+ iPSDMs
Upregulated genes in IFITM3-/- iPSDMs


C
response to virus
defense response to virus
defense response to symbiont
cytokine-mediated signaling pathway
negative regulation of viral process
regulation of viral process
regulation of viral life cycle
negative regulation of viral genome replication
regulation of response to biotic stimulus
positive regulation of cytokine production
viral process
regulation of viral genome replication
response to interferon-gamma
viral life cycle
viral genome replication
leukocyte proliferation
negative regulation of immune system process
lymphocyte proliferation
receptor signaling pathway via JAK-STAT
mononuclear cell proliferation
0
50
100
Count
p.adjust
3.814692e-40
2.466166e-15
4.932331e-15
7.398497e-15
9.864662e-15

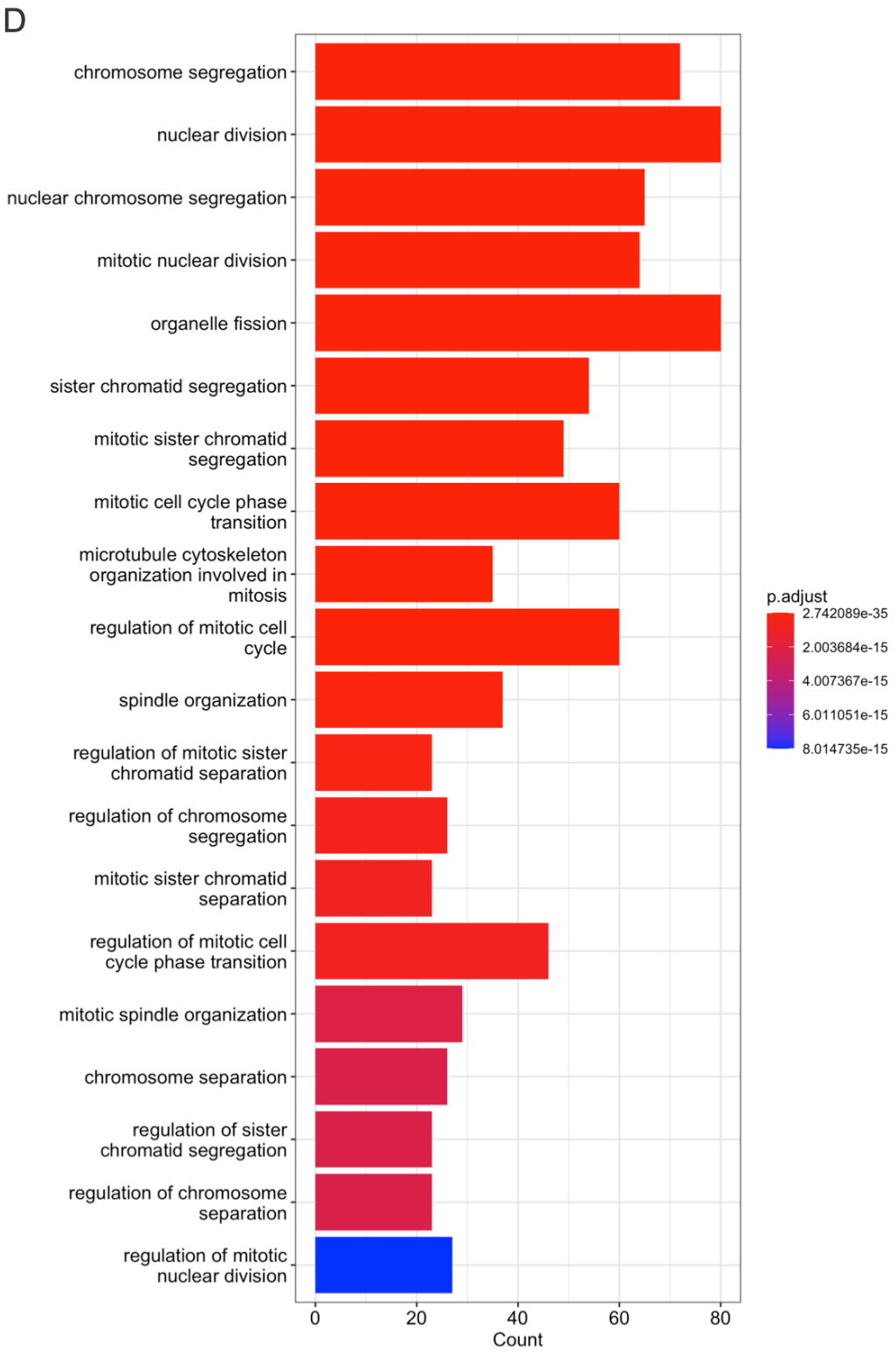


Figure 3.12 The impact of IFITM3 depletion in iPSDMs during H1N1 infection. *(A) PCA plot. WT_0: IFITM3$^{+/+}$ iPSDMs without H1N1; WT_1: IFITM3$^{+/+}$ iPSDMs with H1N1; KO_0: IFITM3$^{-/-}$ iPSDMs without H1N1; KO_1: IFITM3$^{-/-}$ iPSDMs with H1N1. (B) Venn diagram of significantly upregulated genes in IFITM3$^{+/+}$ iPSDMs (red circle) and in IFITM3$^{-/-}$ iPSDMs (blue circle) following H1N1 infection. (C) Enriched GO terms of upregulated genes in IFITM3$^{+/+}$ iPSDMs only, but not IFITM3$^{-/-}$ iPSDMs. (D) Enriched GO terms of upregulated genes in IFITM3$^{-/-}$ iPSDMs only, but not IFITM3$^{+/+}$ iPSDMs.*

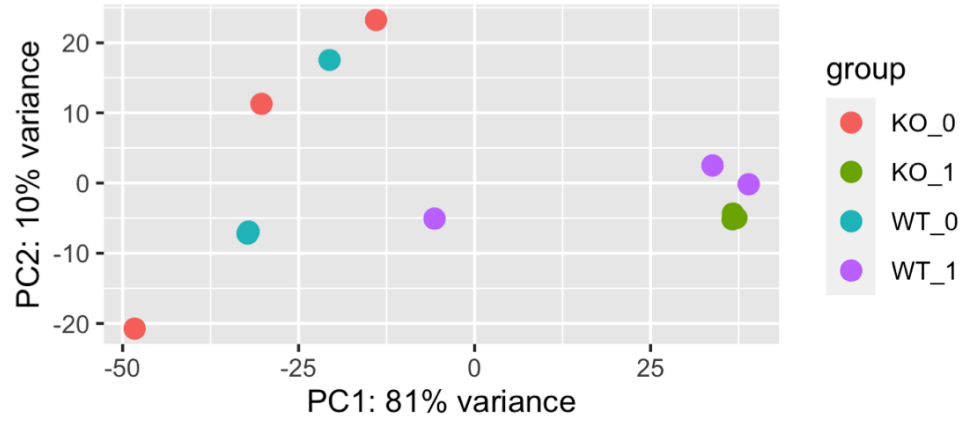
3.4.10 IFITM3 is correlated with receptor signalling pathways in iPSDMs during H5N1 infection.

To investigate if IFITM3 affects the response of other genes to H5N1 infection, we analysed RNA-Seq data from IFITM3$^{+/+}$ and IFITM3$^{-/-}$ iPSDMs following H5N1 infection.

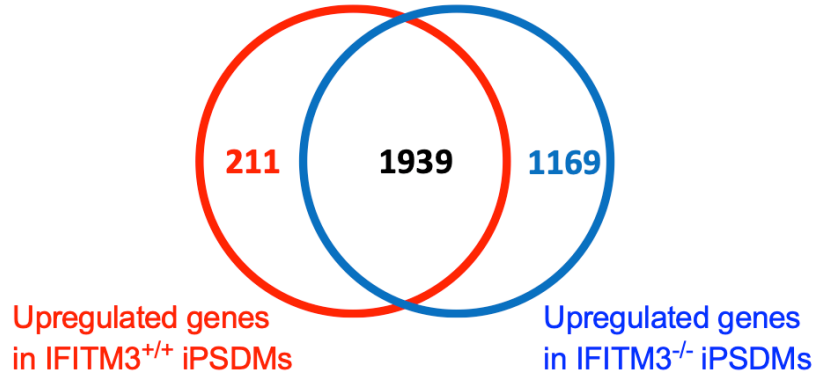
PCA showed that the major variance (PC1: 81% variance) was caused by H5N1 infection as samples of IFITM3$^{+/+}$ and IFITM3$^{-/-}$ iPSDMs without infection (WT_0 and KO_0, blue and red dots, respectively) are separated with samples after infection (WT_1 and KO_1, purple and green dots, respectively) on the graph (**Figure 3.13 A**).

To find out the H5N1-reponding genes affected by IFITM3 depletion, we compared significantly upregulated genes in IFITM3$^{+/+}$ iPSDMs with those in IFITM3$^{-/-}$ iPSDMs following infection. Significantly upregulated genes (adjusted p-value < 0.05, fold-change > 2) following infection were obtained by the comparison of gene expression in WT_1 with that in WT_0, and KO_1 with KO_0. RNA-Seq data was analysed with DESeq2. Following H5N1 infection, 2150 genes were significantly upregulated in IFITM3$^{+/+}$ iPSDMs and 3108 were significantly upregulated in IFITM3$^{-/-}$ iPSDMs, with 1939 genes overlapped (**Figure 3.13 B**). About 9.8% (211 out of 2150) of H5N1-responding genes in IFITM3$^{+/+}$ iPSDMs cannot be upregulated during H5N1 infection due to the absence of IFITM3. GO analysis of this group of genes showed enrichment of terms related to response to virus and receptor signalling pathway via JAK-STAT (**Figure 3.13 C**). On the other hand, when examining the 1169 genes that were only upregulated in response to H5N1 in the absence of IFITM3, we observed enrichment of GOs related to protein catabolic process (**Figure 3.13 D**).

A


PC2: 10% variance
20
10
0
-10
-20
-50
-25
0
25
PC1: 81% variance
group
KO_0
KO_1
WT_0
WT_1

B


211
1939
1169
Upregulated genes in IFITM3+/+ iPSDMs
Upregulated genes in IFITM3-/- iPSDMs

C

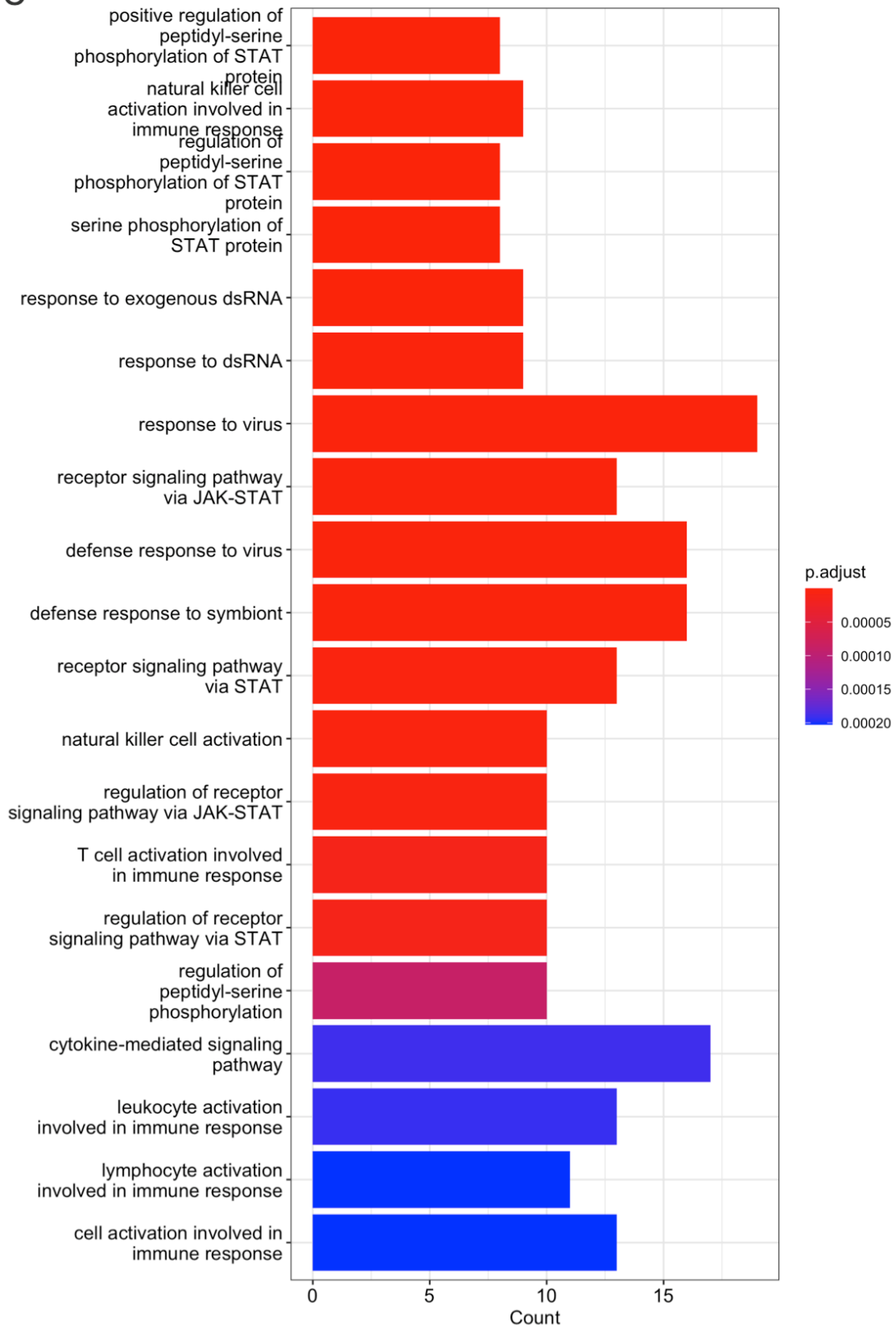

positive regulation of peptidyl-serine phosphorylation of STAT protein
natural killer cell activation involved in immune response
regulation of peptidyl-serine phosphorylation of STAT protein
serine phosphorylation of STAT protein
response to exogenous dsRNA
response to dsRNA
response to virus
receptor signaling pathway via JAK-STAT
defense response to virus
defense response to symbiont
receptor signaling pathway via STAT
natural killer cell activation
regulation of receptor signaling pathway via JAK-STAT
T cell activation involved in immune response
regulation of receptor signaling pathway via STAT
regulation of peptidyl-serine phosphorylation
cytokine-mediated signaling pathway
leukocyte activation involved in immune response
lymphocyte activation involved in immune response
cell activation involved in immune response
0
5
10
15
Count
p.adjust
0.00005
0.00010
0.00015
0.00020



Figure 3.13 The impact of IFITM3 depletion in iPSDMs during H5N1 infection. *(A) PCA plot. WT_0: IFITM3$^{+/+}$ iPSDMs without H5N1; WT_1: IFITM3$^{+/+}$ iPSDMs with H5N1; KO_0: IFITM3$^{-/-}$ iPSDMs without H5N1; KO_1: IFITM3$^{-/-}$ iPSDMs with H5N1. (B) Venn diagram of significantly upregulated genes in IFITM3$^{+/+}$ iPSDMs (red circle) and in IFITM3$^{-/-}$ iPSDMs (blue circle) following H5N1 infection. (C) Enriched GO terms of upregulated genes in IFITM3$^{+/+}$ iPSDMs only, but not IFITM3$^{-/-}$ iPSDMs. (D) Enriched GO terms of upregulated genes in IFITM3$^{-/-}$ iPSDMs only, but not IFITM3$^{+/+}$ iPSDMs.*

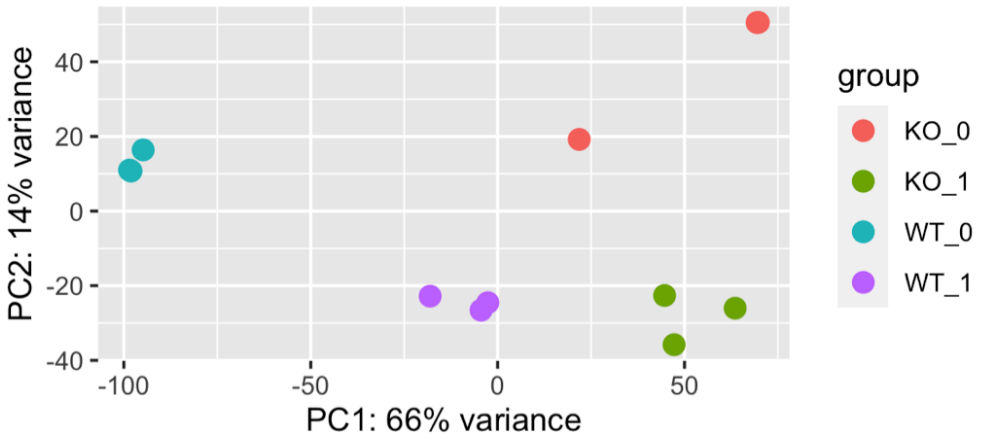
3.4.11 Differentially regulated genes were observed during SARS-CoV-2 infection due to IFITM3 depletion.

To investigate the role of IFITM3 during SARS-CoV-2 infection, we analysed RNA-Seq data from IFITM3$^{+/+}$ and IFITM3$^{-/-}$ iPSDMs following SARS-CoV-2 infection. While data from multiple time points is available, I focus on the results of the 24 hours post infection timepoint, in parallel with H1N1 and H5N1 infection.

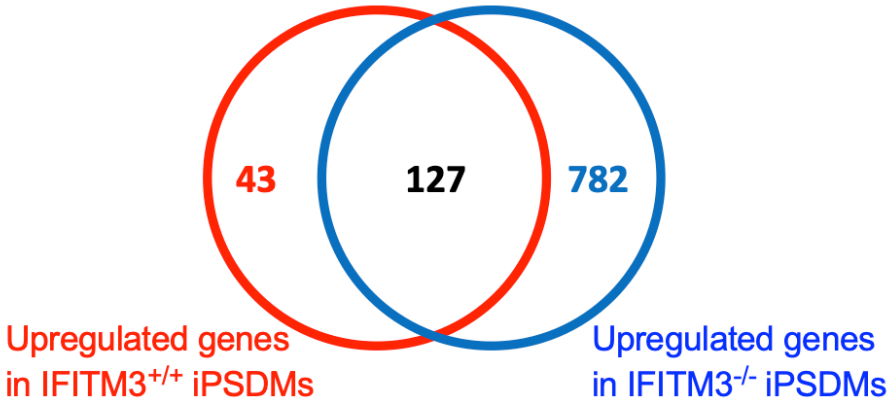
PCA showed that the major variance (PC1: 66% variance) was caused by IFITM3 depletion, while the second major variance (PC2: 14% variance) was caused by SARS-CoV-2 infection (**Figure 3.14 A**).

To find out the SARS-CoV-2-responding genes affected by IFITM3 depletion, we compared significantly upregulated genes in IFITM3$^{+/+}$ iPSDMs with those in IFITM3$^{-/-}$ iPSDMs following infection. Significantly upregulated genes (adjusted p-value < 0.05, fold-change > 2) following infection were obtained by the comparison of gene expression in WT_1 with that in WT_0, and KO_1 with KO_0. RNA-Seq data was analysed with DESeq2. Following SARS-CoV-2 infection, 170 genes were significantly upregulated in IFITM3$^{+/+}$ iPSDMs and 909 were significantly upregulated in IFITM3$^{-/-}$ iPSDMs, with 127 genes overlapped (**Figure 3.14 B**). GO analysis of this group of genes showed enrichment of terms related to cell adhesion (**Figure 3.14 C**). On the other hand, when examining the 782 genes (about 86% of total upregulated genes in IFITM3$^{-/-}$ iPSDMs) that were only upregulated in response to SARS-CoV-2 in the absence of IFITM3, we observed enrichment of a wide range of GOs as shown in **Figure 3.14 D**. Further analysis into this part of RNA-Seq data is needed to understand the role of IFITM3 during SARS-CoV-2 infection.

A


PC2: 14% variance
40
20
0
-20
-40
-100
-50
0
50
PC1: 66% variance
group
KO_0
KO_1
WT_0
WT_1

B


43
127
782
Upregulated genes in IFITM3+/+ iPSDMs
Upregulated genes in IFITM3-/- iPSDMs

C

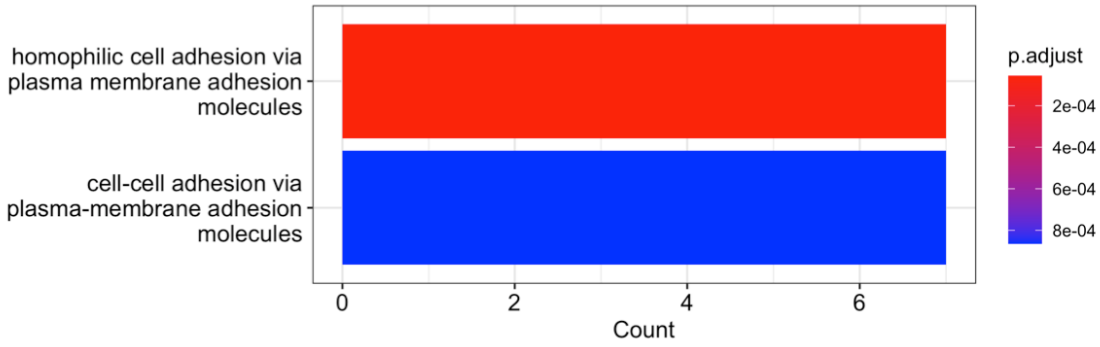

homophilic cell adhesion via plasma membrane adhesion molecules
cell-cell adhesion via plasma-membrane adhesion molecules
0
2
4
6
Count
p.adjust
2e-04
4e-04
6e-04
8e-04



Figure 3.14 The impact of IFITM3 depletion in iPSDMs during SARS-CoV-2 infection. *(A) PCA plot. WT_0: IFITM3$^{+/+}$ iPSDMs without SARS-CoV-2; WT_1: IFITM3$^{+/+}$ iPSDMs with SARS-CoV-2; KO_0: IFITM3$^{-/-}$ iPSDMs without SARS-CoV-2; KO_1: IFITM3$^{-/-}$ iPSDMs with SARS-CoV-2. (B) Venn diagram of significantly upregulated genes in IFITM3$^{+/+}$ iPSDMs (red circle) and in IFITM3$^{-/-}$ iPSDMs (blue circle) following SARS-CoV-2 infection. (C) Enriched GO terms of upregulated genes in IFITM3$^{+/+}$ iPSDMs only, but not IFITM3$^{-/-}$ iPSDMs. (D) Enriched GO terms of upregulated genes in IFITM3$^{-/-}$ iPSDMs only, but not IFITM3$^{+/+}$ iPSDMs.*

3.5 Discussion

It is widely accepted that IFITM3 is a restriction factor for IAV infection. However, the multiple roles of IFITM3 at different stages of IAV infection and in different cell types are not fully understood. In this study, we explored the role of IFITM3 in epithelial cells (HEK293 and A549), macrophages (iPSDMs) and stem cells (iPSCs) using paired IFITM3$^{+/+}$ and IFITM3$^{-/-}$ cell lines established by CRISPR/Cas9 technology. We focused on the impact of IFITM3 during the infection of three acute respiratory viruses: IAV H1N1, IAV H5N1, and the relatively newly emerged SARS-CoV-2. Our data and others demonstrated that IFITM3 is a restrictor for H1N1, while a facilitator for SARS-CoV-2 infection. We also showed a correlation of IFITM3 with antigen processing and presentation and cytokine signalling pathways by RNA-Seq analysis.

In this study, we first investigated the role of IFITM3 as an ISG in HEK293 cells. Our data demonstrated that IFITM3 can be rapidly induced by type I IFNs, while minimally by type II and III IFNs. IFITM3 has previously been reported to be inducible by type I and II IFN in mouse fibroblast cell line NIH/3T3 and in mouse macrophage cell line RAW264.7[160]. The different induction pattern may be due to the different origins of cell lines. In addition, IFITM3 in different cell subsets also respond differently to IFN stimulation. Wellington *et al* showed that there was no significant induction of IFITM3 in total PBMCs after type I, II or III IFN stimulation. However, strong induction of IFITM3 by type I IFN was observed in myeloid cells while no increases were seen in lymphoid cells[161]. To what extent that IFITM3 can be induced is an important concern during viral infection because the expression level of IFITM3 affects the antiviral status. Significant induction of IFITM3 by IFN-β in iPSDMs suggests that iPSDMs is a good cellular system to study IFITM3 functions.

Gene knockout is a vital approach to study the effects and functions of that gene and is useful in studying signalling pathways in all types of cells. Another approach is gene overexpression. However, one limitation of overexpressing genes is that it is difficult to glean meaningful biological insights when genes are expressed at non-physiological levels[162]. Therefore, to study the function of IFITM3, we knocked out IFITM3 gene in HEK293, A549 and iPSCs, and then looked at any changes brought by the disruption of IFITM3.

We did not observe any of the correlations at protein levels in iPSDMs. There are several possible explanations. Firstly, IFITM3 may only affect mRNA levels, but not protein levels, of those antigen processing and presentation related genes. It is worthwhile to measure mRNA levels of those genes in IFITM3$^{+/+}$ and IFITM3$^{-/-}$ iPSDMs by qPCR. Secondly, the correlation of IFITM3 with antigen processing and presentation may be cell type-dependent. It is worthwhile to investigate the impact of IFITM3 on antigen processing and presentation in other cell types.

Our RNA-Seq data suggest that only a small number of genes are affected by IFITM3 depletion in iPSCs and iPSDMs when there is no external stimuli. This is not surprising as IFITM3 is a relatively small protein, only 15kD, and its basal expression is relatively low in the cells. However, when the cells are exposed to IFN or viruses, IFITM3 will be strongly induced[161], thereby exhibit greater influence on the overall response to the stimuli. This is also observed in our study that 17.7% of IFN-stimulated genes failed to respond to IFN and 72.4% of H1N1-stimulated genes failed to respond to H1N1 in IFITM3$^{-/-}$ iPSDMs. Our findings suggest that it is important to study IFITM3 in the context of IFN stimulation or virus infection.

The sensitivity of virus to IFITM3 protein depends on many factors. One study showed that pH optimum of HA-driven membrane fusion of IAVs is one of the factors[128]. They showed that the restriction of H5N1 by IFITM3 was much weaker because H5N1 requires a higher pH for membrane fusion, compared to H1N1. In our study, we observed an infection rate of almost 100% in wild type iPSDMs following H5N1 infection, but we don't know if overexpression of IFITM3 can reduce the infection rate. Our RNA-Seq data show that about 9.8% of H5N1-stimulated genes cannot be upregulated in IFITM3$^{-/-}$ iPSDMs following H5N1 infection, and this group of genes are mainly involved in Janus kinase (JAK)-signal transducer and activator of transcription (STAT) pathway. Normally, sense of H5N1 invasion will induce the production of IFNs, which further activate JAK-STAT pathway. Upon activation, STAT will enter the nucleus and activate the transcription of ISGs including IFITM3. We hypothesize that the continuous activation of JAK-STAT pathway during H5N1 infection relies on IFITM3. In IFITM3$^{-/-}$ iPSDMs, JAK-STAT pathway may still be activated at the beginning of H5N1 infection, however, their activity cannot be maintained due to the lack of IFITM3. Even though JAK-STAT pathway may be turned down at the later stages of infection, the activation of other ISGs may not be affected because of the existence of other signalling pathways that can respond to IFNs.

We investigated whether IFITM3 affects the antigen presenting and presentation ability of iPSDMs. We observed that the expression level of several key antigen processing and presentation related proteins were not affected by IFITM3 either before or after IFN stimulation. However, our RNA-Seq data showed that a group of antigen processing and presentation related genes were upregulated following IFN stimulation only in IFITM3$^{-/-}$ iPSDMs but not in IFITM3$^{+/+}$ iPSDMs. Further investigation into this

group of differentially regulated genes is needed to understand the correlation of IFITM3 with antigen processing and presentation.

3.6 Future directions

As the RNA-Seq data were obtained in July this year, we only got time to do basic analysis comparing gene expression under different treatments. However, there is much more that we can explore from this dataset.

(1) Will IFITM3 affect the induction of other ISGs during H1N1, H5N1, or SARS-CoV-2 infection?

IFITM3 has been reported to interact with ISGs, such as IRF3, during virus infection. Thus, it is worthwhile to investigate the potential interactions of IFITM3 with other ISGs in our iPSDMs following virus infection. We can look into the genes that are only upregulated following virus infection in IFITM3$^{+/+}$ iPSDMs, but not in IFITM3$^{-/-}$ iPSDMs, and see if there are any ISGs involved. IFITM3 may interact with this group of ISGs during virus infection.

(2) What does IFITM3 do at different stages of SARS-CoV-2 infection?

The importance of IFITM3 proteins in viral defence depends on the dynamics of viral entry and the stages of the viral replication at which these mechanisms are evaluated. Influenza studies showed that IFITM3 is critical in the protection against the pathogens during early stages of infection, but not the later stages of virus replication[163]. Our RNA-Seq data include IFITM3$^{+/+}$ and IFITM3$^{-/-}$ iPSDMs collected at different time points (0, 6, 12, 24, and 48 hours) post SARS-CoV-2 infection. It is worthwhile to compare differentially expressed genes due to IFITM3 depletion at

different time points to understand the role of IFITM3 at different stages of SARS-CoV-2 infection.

In addition, current analysis of RNA-Seq data mainly focused on the differentially upregulated genes following IFN stimulation or virus infection. Differentially downregulated genes due to IFITM3 depletion should be considered as well. More importantly, all the findings from RNA-Seq analysis just show the correlation at RNA level. A real impact of IFITM3 needs to be verified at both RNA and protein levels by experiments.

Chapter 4

Mapping and characterizing dominant T cell responses against SARS-CoV-2 in COVID-19 convalescent patients

4.1 Introduction.

Following the emergence of COVID-19, an urgent need arose to understand the role of T cells in controlling disease progression and severity. For the newly emerged SARS-CoV-2 virus, it was unclear at the beginning of the pandemic whether T cells were protective, aiding viral clearance, or harmful, causing tissue damage due to overactivation. Additionally, understanding the immunogenicity of different SARS-CoV-2 antigens for T cell immune responses was also essential for identifying optimal targets for COVID-19 vaccines and treatments.

Identification of dominant SARS-CoV-2 T cell epitopes is crucial for the study of overall T cell responses. T cell immune responses determine how successfully infections can be eliminated, and insufficient or inappropriate responses can result in lack of clearance, immunopathology or autoimmunity[164]. T cell immune responses are elicited from the recognition of peptides presented by MHC molecules. During acute virus infection, only a selection of peptides from viral antigens are able to induce strong T cell responses[165], the strongest of which are referred to as immunodominant T cell epitopes.

Identification of dominant SARS-CoV-2 T cell epitopes will help predict the impact of viral mutations on T cell responses. Mutations within T cell epitopes may affect the binding affinity of that epitope with MHC molecules or TCRs and further affect T cell recognition; mutations in the flanking region of T cell epitopes may affect antigen

processing and presentation, leading to higher or lower antigen load at the cell surface, which potentially will alter T cell responses[166]. However, mutations away from epitope regions will have limited effect.

Identification of dominant T cell epitopes will also facilitate the development of epitope-based vaccines[167]. Epitope-based vaccines are a novel vaccination approach based on multiple B- and T-cell epitopes[168,169]. SARS-CoV-2 T cell epitopes with high immunogenicity should be considered in COVID-19 vaccine design to elicit strong T cell response.

A number of assays exist to evaluate the function of antigen-specific T cells. Enzyme-linked immunosorbent spot (ELISpot) assays, which measure the amount of cytokine, such as IFN-γ and TNF-α, released by activated T cells, is one of the most commonly used methods[170]. ELISpot is quantitative and sensitive allowing us to measure a broad range of magnitudes of T cell responses. More importantly, ELISpot is suitable for high-throughput screening of T cell responses against multiple peptides, serving as a rapid method to measure the breadth of SARS-CoV-2-specific T cell responses.

Intracellular cytokine staining (ICS) combined with flow cytometry assesses T cell immune responses by simultaneously quantifying multiple functional parameters, including cytokines, chemokines and degranulation markers[171]. ICS of stimulated PBMCs also enables the detection of the specific cell subsets like $CD4^+$ and $CD8^+$ T cells by staining of the surface markers[172]. The most common biomarkers for T cell activation used in ICS are IFN-γ, TNF-α, IL-2, MIP-1β and CD107a.

IFN-γ, one of the major effectors of immune response, is secreted predominantly by activated $CD4^+$ T helper type I (Th1) cells and $CD8^+$ cytotoxic T cells[173]. IFN-γ upregulates the expression of MHC molecules[174], as well as the whole antigen processing

and presentation machinery including TAP1/2[175], invariant chain, and the proteasome[176]. TNF-α can be produced by effector $CD4^+$ and $CD8^+$ T cells, leading to the killing of infected cells[177]. The secretion of IL-2 is an early activation marker for $CD4^+$ T cell responses to antigenic stimulation and has often been used as a reliable and early readout of T cell activation[178]. Early availability of IL-2, especially from $CD4^+$ T cells, influences the subsequent expansion and maturation of both $CD4^+$ and $CD8^+$ T cells[179]. Macrophage inflammatory Protein-1β (MIP-1β), which is also known as C-C motif chemokine ligand 4 (CCL4), can chemoattract immune cells such as T cells to sites of infection[180]. The release of MIP-1β is involved in the noncytolytic pathway of $CD8^+$ T cells by preventing viral entry, however, the underlying molecular mechanism is still under investigation[181]. Secretion of MIP-1β by $CD8^+$ T cells has been reported to correlate with soluble noncytolytic suppression of HIV-1[182]. CD107a, also known as lysosomal-associated membrane protein 1 (LAMP1), is a marker of $CD8^+$ T cell degranulation following stimulation, in concert with a release of perforin[183]. The expression of MIP-1β and CD107a are the two strongest responses following antigen stimulation and therefore have been used as indicators for antigen responsiveness[180].

T cell epitopes can be predicted using computational tools based on the properties of peptide sequences and the binding preferences of HLA molecules[184]. In addition, T cell epitopes can also be experimentally defined by high-throughput screening of synthetic peptide libraries. Prediction of T cell epitopes using computational tools is efficient, however, not all of the predicted epitopes are real which may lead to overestimation of the breadth of T cell responses. Therefore, a combination of both computational prediction and experimental verification is the most efficient, as well as accurate, way to define T cell epitopes.

4.2 Aims.

To understand the role of T cell immunity in COVID-19 pathogenesis and long-term protection, I joined the COVID-19 research team in our lab and we used a cohort of 42 UK convalescent patients recovered from COVID-19 to:

- Evaluate overall SARS-CoV-2-specific T cell responses in peripheral blood.
- Map dominant SARS-CoV-2 T cell epitopes.

4.3 Study participants.

The convalescent cohort included 42 individuals recovered from COVID-19. 28 of them were mild cases, while 14 were severe cases. Mild cases had a percentage of oxyhaemoglobin saturation in arterial blood (SaO_2)/fraction of inspired O_2 (FiO_2) ratio over 4.5, while severe cases below 4.5. **Figure 4.1**[185] shows the participant characteristics. No significant differences in age or days post symptom were noted between mild and severe groups (**Figure 4.1 B, C**)[185].

A

	Mild Disease (n=28)		Severe Disease (n=14)	
Overall Median Age (years)	53.8 (47.6—60.9)		60.6 (44.9—74.1)	
Gender	Male (n=17)	Female (n=11)	Male (n=9)	Female (n=5)
Median Age of Male/Female (years)	60.71	43.12	64.28	53.98
Median days post symptom	42.5 (40.2—55.7)		41.5 (40.0—47.5)	

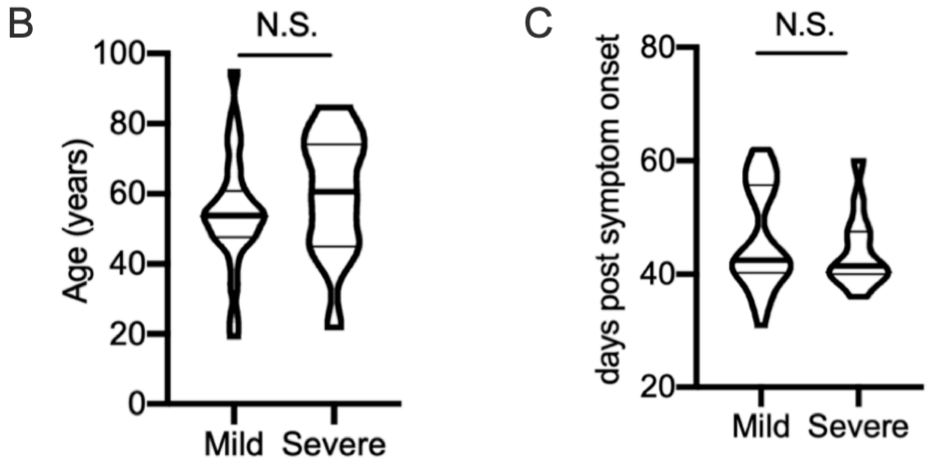


Figure 4.1 Participant characteristics. *(A) Distribution of age, gender and days post symptom when sampling the convalescent patients following SARS-CoV-2 infection. (B, C) Comparison of age (B, p=0.3465) and days post symptom (C, p=0.4075) between mild and severe groups. Unpaired t test with Welch's correction (B) and Mann-Whitney test (C) were used for analysis respectively. Two-tailed p-values were calculated.*

4.4 Results.

4.4.1 Broad and strong memory T cell responses specific to SARS-CoV-2 were observed by ex vivo assessment.

To understand the immunogenicity of different SARS-CoV-2 antigens in terms of cellular immunity, memory T cell responses to different components of SARS-CoV-2 were screened using a synthetic overlapping peptide library spanning SARS-CoV-2 structural and accessory proteins: Spike, Nucleoprotein (NP), Membrane (M), Envelope (Env) and 4 other open reading frames (ORF3a, ORF6, ORF7a, ORF8). 414 SARS-CoV-2 overlapping peptides were grouped into 16 Spike and 13 other pools (comprising 4 NP pools, 2 M pools, 1 Env pool, 3 ORF3a pools, 1 ORF6 pool, 1 ORF7a pool and 1 ORF8 pool). Two-dimensional peptide pools with additional 16 Spike pools and 16 Other pools were designed to identify candidate peptides containing T cell epitopes (**Table 4.1**), which will be discussed in the later part of this chapter.

42 patients recovered from SARS-CoV-2 infection (28 with mild disease and 14 with severe disease, described in **Table 4.1**) were recruited. PBMCs were isolated from patient blood and pulsed with SARS-CoV-2 two-dimensional peptide pools overnight. Any SARS-CoV-2-specific memory T cells that were activated released IFN-γ into the supernatant which was then captured onto the membrane of IFN-γ ELISpot plates. The magnitude of T cell responses to each pool was reflected by the number of dots that appeared in that well. Broad and strong T cell responses to all tested SARS-CoV-2 antigens were observed, with dominant responses focusing on Spike, NP, M and ORF3a (**Figure 4.2**)[185]. The data also showed that severe cases were associated with stronger overall T cell responses compared to mild cases, especially the T cell responses to Spike,

M, ORF3a and ORF8 (**Figure 4.2**)[185], suggesting that strong T cell responses during SARS-CoV-2 infection may contribute to the disease severity.

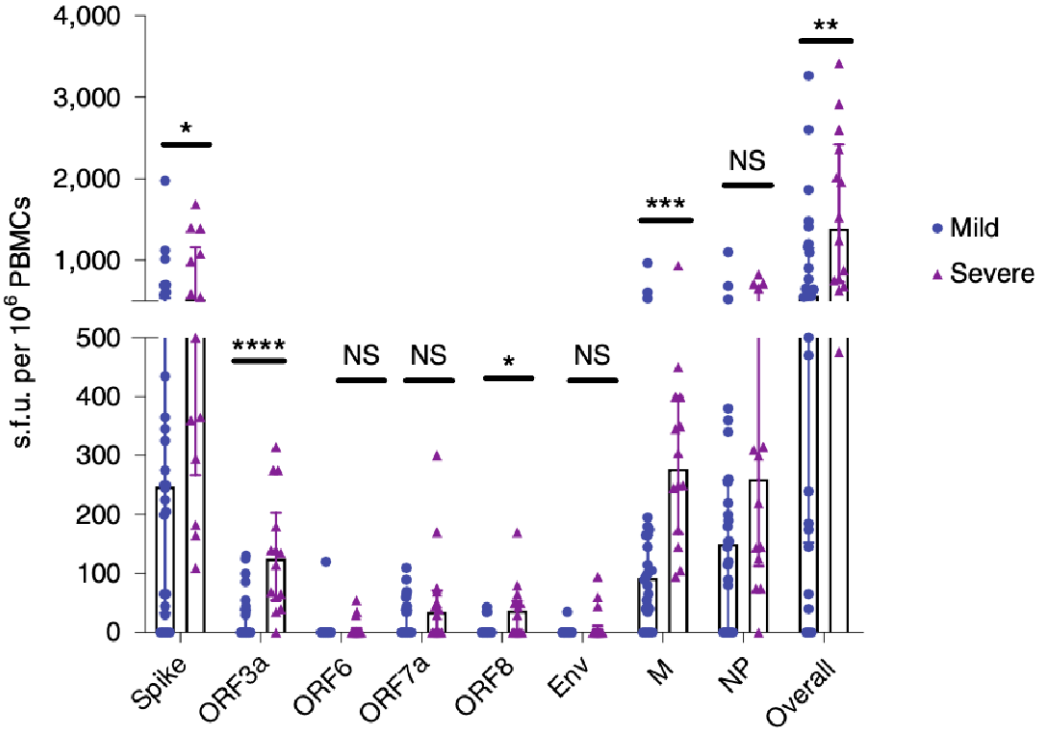


Figure 4.2 Comparison of the magnitude of T cell responses specific to each viral protein between mild (n=28) and severe cases (n=14). *PBMCs were isolated and IFN-γ production was detected by ELISpot after incubation with SARS-CoV-2 peptides. Results were presented as spot-forming units (s.f.u) per 10^6 PBMCs. p-values were as follows: overall: p=0.002; Spike: p=0.021; M: p=0.0003; ORF3a: p<0.0001; ORF8: p=0.011. Data are presented as medians with interquartile ranges. The Mann–Whitney U-test was used for the analysis and two-tailed p-values were calculated. *p<0.05; **p<0.01; ***p<0.001; ****p<0.001. NS, not significant.*

Table 4.1 Two-dimensional peptide pools spanning SARS-CoV-2 Spike, NP, M, Env and ORFs

			Pool-17	Pool-18	Pool-19	Pool-20	Pool-21	Pool-22	Pool-23	Pool-24	Pool-25	Pool-26	Pool-27	Pool-28	Pool-29	Pool-30	Pool-31	Pool-32
Spike pools		Pool-1	S-1	S-2	S-3	S-4	S-5	S-6	S-7	S-8	S-9	S-10	S-11	S-12	S-13	S-14	S-15	S-16
		Pool-2	S-17	S-18	S-19	S-20	S-21	S-22	S-23	S-24	S-25	S-26	S-27	S-28	S-29	S-30	S-31	S-32
		Pool-3	S-33	S-34	S-35	S-36	S-37	S-38	S-39	S-40	S-41	S-42	S-43	S-44	S-45	S-46	S-47	S-48
		Pool-4	S-49	S-50	S-51	S-52	S-53	S-54	S-55	S-56	S-57	S-58	S-59	S-60	S-61	S-62	S-63	S-64
		Pool-5	S-65	S-66	S-67	S-68	S-69	S-70	S-71	S-72	S-73	S-74	S-75	S-76	S-77	S-78	S-79	S-80
		Pool-6	S-81	S-82	S-83	S-84	S-85	S-86	S-87	S-88	S-89	S-90	S-91	S-92	S-93	S-94	S-95	S-96
		Pool-7	S-97	S-98	S-99	S-100	S-101	S-102	S-103	S-104	S-105	S-106	S-107	S-108	S-109	S-110	S-111	S-112
		Pool-8	S-113	S-114	S-115	S-116	S-117	S-118	S-119	S-120	S-121	S-122	S-123	S-124	S-125	S-126	S-127	S-128
		Pool-9	S-129	S-130	S-131	S-132	S-133	S-134	S-135	S-136	S-137	S-138	S-139	S-140	S-141	S-142	S-143	S-144
		Pool-10	S-145	S-146	S-147	S-148	S-149	S-150	S-151	S-152	S-153	S-154	S-155	S-156	S-157	S-158	S-159	S-160
		Pool-11	S-161	S-162	S-163	S-164	S-165	S-166	S-167	S-168	S-169	S-170	S-171	S-172	S-173	S-174	S-175	S-176
		Pool-12	S-177	S-178	S-179	S-180	S-181	S-182	S-183	S-184	S-185	S-186	S-187	S-188	S-189	S-190	S-191	S-192
		Pool-13	S-193	S-194	S-195	S-196	S-197	S-198	S-199	S-200	S-201	S-202	S-203	S-204	S-205	S-206	S-207	S-208
		Pool-14	S-209	S-210	S-211	S-212	S-213	S-214	S-215	S-216	S-217	S-218	S-219	S-220	S-221	S-222	S-223	S-224
		Pool-15	S-225	S-226	S-227	S-228	S-229	S-230	S-231	S-232	S-233	S-234	S-235	S-236	S-237	S-238	S-239	S-240
		Pool-16	S-241	S-242	S-243	S-244	S-245	S-246	S-247	S-248	S-249	S-250	S-251	S-252	S-253			
			Pool-O-14	Pool-O-15	Pool-O-16	Pool-O-17	Pool-O-18	Pool-O-19	Pool-O-20	Pool-O-21	Pool-O-22	Pool-O-23	Pool-O-24	Pool-O-25	Pool-O-26	Pool-O-27	Pool-O-28	Pool-O-29
Other pools	ORF3a	Pool-O-1	ORF3a-1	ORF3a-2	ORF3a-3	ORF3a-4	ORF3a-5	ORF3a-6	ORF3a-7	ORF3a-8	ORF3a-9	ORF3a-10	ORF3a-11	ORF3a-12	ORF3a-13	ORF3a-14	ORF3a-15	ORF3a-16
		Pool-O-2	ORF3a-17	ORF3a-18	ORF3a-19	ORF3a-20	ORF3a-21	ORF3a-22	ORF3a-23	ORF3a-24	ORF3a-25	ORF3a-26	ORF3a-27	ORF3a-28	ORF3a-29	ORF3a-30	ORF3a-31	ORF3a-32
		Pool-O-3	ORF3a-33	ORF3a-34	ORF3a-35													
	ORF6	Pool-O-4	ORF6-1	ORF6-2	ORF6-3	ORF6-4	ORF6-5	ORF6-6	ORF6-7									
	ORF7a	Pool-O-5	ORF7a-1	ORF7a-2	ORF7a-3	ORF7a-4	ORF7a-5	ORF7a-6	ORF7a-7	ORF7a-8	ORF7a-9	ORF7a-10	ORF7a-11	ORF7a-12	ORF7a-13	ORF7a-14	ORF7a-15	
	ORF8	Pool-O-6	ORF8-1	ORF8-2	ORF8-3	ORF8-4	ORF8-5	ORF8-6	ORF8-7	ORF8-8	ORF8-9	ORF8-10	ORF8-11	ORF8-12	ORF8-13	ORF8-14	ORF8-15	ORF8-16
	Env	Pool-O-7	Env-1	Env-2	Env-3	Env-4	Env-5	Env-6	Env-7	Env-8	Env-9							
	M	Pool-O-8	M-1	M-2	M-3	M-4	M-5	M-6	M-7	M-8	M-9	M-10	M-11	M-12	M-13	M-14	M-15	M-16
		Pool-O-9	M-17	M-18	M-19	M-20	M-21	M-22	M-23	M-24	M-25	M-26	M-27	M-28				
	NP	Pool-O-10	NP-1	NP-2	NP-3	NP-4	NP-5	NP-6	NP-7	NP-8	NP-9	NP-10	NP-11	NP-12	NP-13	NP-14	NP-15	NP-16
		Pool-O-11	NP-17	NP-18	NP-19	NP-20	NP-21	NP-22	NP-23	NP-24	NP-25	NP-26	NP-27	NP-28	NP-29	NP-30	NP-31	NP-32
		Pool-O-12	NP-33	NP-34	NP-35	NP-36	NP-37	NP-38	NP-39	NP-40	NP-41	NP-42	NP-43	NP-44	NP-45	NP-46	NP-47	NP-48
		Pool-O-13	NP-49	NP-50	NP-51	NP-52	NP-53	NP-54	NP-55	NP-56	NP-57	NP-58						

4.4.2 SARS-CoV-2-specific $CD8^+$ T cell responses were associated with disease severity.

While the ELISpot assay identified that overall T cell responses to SARS-CoV-2 peptides could be observed, it was unable to distinguish between $CD4^+$ and $CD8^+$ T cell responses. To identify the subset of cells responding to peptide, ICS assays combined with flow cytometry were used to assess T cell responses against positive peptide pools.

PBMCs were stimulated with peptide pools for 1 h prior to the addition of GolgiStop and GolgiPlug (BD Biosciences) to block cytokine secretion. GolgiStop and GolgiPlug work by inhibiting intracellular protein transport processes, resulting in the accumulation of cytokines in the endoplasmic reticulum (ER) (GolgiStop) or in the Golgi complex (GolgiPlug)[171]. PE-anti-CD107a was added at the same time. CD107a must be stained during stimulation of the effector cells as CD107a is only transiently expressed on the membrane due to the constant recycling of granules[183,186]. 5 h later, PBMCs were stained for CD4 and CD8, and the intracellular cytokines, IFN-γ, TNF-α and IL-2.

A greater proportion of overall $CD8^+$ T cell responses was observed in mild cases compared with severe cases (**Figure 4.3**)[185], suggesting that stronger $CD8^+$ T cell responses were protective against SARS-CoV-2 infection and were associated with better clinical outcomes. A larger proportion of $CD8^+$ T cell responses specific to Spike and M/NP, but not ORF/Env, were also observed in mild cases compared to severe cases (**Figure 4.3**)[185]. In this study, we only focused on $CD8^+$ T cell responses as they are one of the major contributors in virus clearance through direct killing of virus-infected cells.

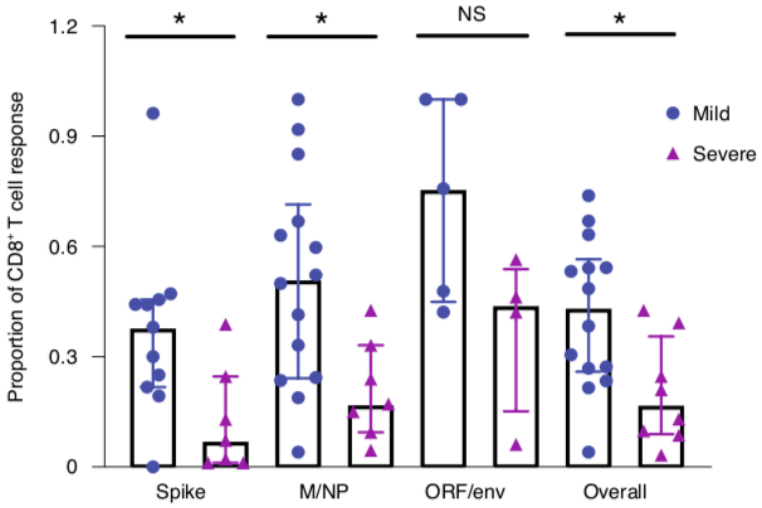


Figure 4.3 Comparison of the relative proportion of SARS-CoV-2 peptide-pool-reactive CD8⁺ T cells between mild and severe cases. *Mild: Spike, n=11; M/NP, n=14; ORF/Env, n=5; Overall, n=14. Severe: Spike, n=7; M/NP, n=7; ORF/Env, n=4; Overall, n=8. p-values were as follows: overall: p=0.0159; Spike: p=0.0268; M/NP: p=0.02. The SARS-CoV-2 peptide-pool-reactive CD8⁺ T cells were identified with at least one of the three cytokines (IFN-γ, TNF-α and IL-2) detected. Data are shown as medians with interquartile ranges. The Mann–Whitney U-test was used for the analysis. Two-tailed p-values were calculated. *p<0.05.*

4.4.3 Identification of one CD8⁺ epitope from SARS-CoV-2 Spike.

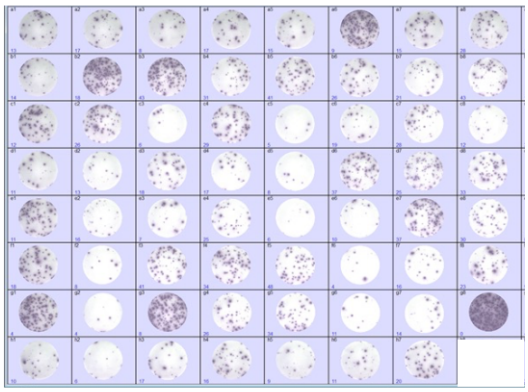
After characterizing the overall T cell responses to SARS-CoV-2, we were interested in the profile of immunodominant T cell epitopes in our cohort. From the results of ELISpot assays using patients' PBMCs pulsed with two-dimensional peptide pools, we were able to find long peptides that contain potential T cell epitopes. To verify the immunogenicity of the potential peptides, IFN-γ ELISpot assays were performed again with each of those peptides individually. T cell responses without peptide stimulation were used as a negative control, and T cell responses to phytohemagglutinin (PHA) served as a positive control. PHA is a lectin that can bind to the sugars on glycosylated surface proteins. Thus, PHA can activate all kinds of T cells by crosslinking TCRs through direct binding with TCRs regardless of their specificities[187].

T cell responses for each of the 42 patients were screened but below only data from patient C-COV19-064 is shown as an example of the process. Strong T cell responses were observed to Spike pool-3, 5, 6, 7, 10, 11 and other pool-2, 9, 12 in the first-dimensional peptide pools (Pool-1 to 16, Pool-O-1 to 16), and to Spike pool-18, 23, 30 and other pool-20, 21 in the second-dimensional peptide pools (Pool-17 to 32, Pool-O-17 to 29) (**Figure 4.4 A, B**). The peptides at the crossings of the first- and second-dimensional peptide pools potentially contain SARS-CoV-2 T cell epitopes.

18 potential peptides containing spike T cell epitopes (highlighted) were identified (**Figure 4.3 C**). At the same time, SARS-CoV-2 spike-specific $CD8^+$ T cell lines (named Spike CD8-064 in the following context), as well as immortalised B cell lines (BCLs), were generated from the PBMCs of the patient C-COV19-064. These cell lines were used for further characterisations of the epitopes due to limited stock of PBMCs and the relatively low number of antigen-specific memory T cells in PBMCs.

To verify T cell responses to each of the 18 candidate peptides, IFN-γ ELISpot assays were performed with individual candidate peptides, as well as Spike peptide pools as a positive control, using Spike CD8-1493. Only the peptide S-98 ($_{486}$FNCYFPLQSYGFQPT$_{500}$) induced spike-specific $CD8^+$ T cell responses and the magnitude of T cell responses to S-98 was equivalent to that to overall Spike peptide pools (**Figure 4.3 D**), suggesting that S98-specific $CD8^+$ T cell response was the dominant spike $CD8^+$ response in the patient C-COV19-064. S98-specific $CD8^+$ T cell (named S98 CD8-064 in the following context) bulk lines and clones were then generated by FACS for IFN-γ- and TNF-α- producing T cells from Spike CD8-1493 after incubation with S-98 pulsed-autologous BCLs.

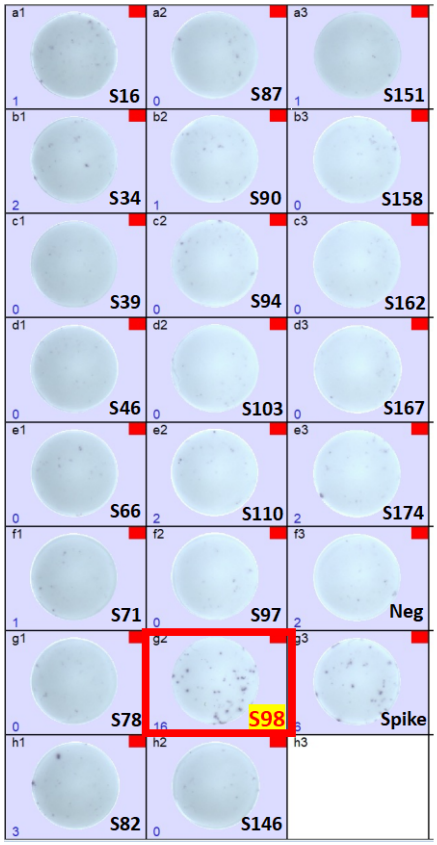
A



B

Spike pools				Other pools			
1st-dimensional		2nd-dimensional		1st-dimensional		2nd-dimensional	
Pool-1	Pool-9	Pool-17	Pool-25	Pool-O-1	Pool-O-9	Pool-O-17	Pool-O-25
Pool-2	Pool-10	Pool-18	Pool-26	Pool-O-2	Pool-O-10	Pool-O-18	Pool-O-26
Pool-3	Pool-11	Pool-19	Pool-27	Pool-O-3	Pool-O-11	Pool-O-19	Pool-O-27
Pool-4	Pool-12	Pool-20	Pool-28	Pool-O-4	Pool-O-12	Pool-O-20	Pool-O-28
Pool-5	Pool-13	Pool-21	Pool-29	Pool-O-5	Pool-O-13	Pool-O-21	Pool-O-29
Pool-6	Pool-14	Pool-22	Pool-30	Pool-O-6	Pool-O-14	Pool-O-22	Neg
Pool-7	Pool-15	Pool-23	Pool-31	Pool-O-7	Pool-O-15	Pool-O-23	PHA
Pool-8	Pool-16	Pool-24	Pool-32	Pool-O-8	Pool-O-16	Pool-O-24	

D



C

		Pool-17	Pool-18	Pool-19	Pool-20	Pool-21	Pool-22	Pool-23	Pool-24	Pool-25	Pool-26	Pool-27	Pool-28	Pool-29	Pool-30	Pool-31	Pool-32
Spike pools	Pool-1	S-1	S-2	S-3	S-4	S-5	S-6	S-7	S-8	S-9	S-10	S-11	S-12	S-13	S-14	S-15	S-16
	Pool-2	S-17	S-18	S-19	S-20	S-21	S-22	S-23	S-24	S-25	S-26	S-27	S-28	S-29	S-30	S-31	S-32
	Pool-3	S-33	S-34	S-35	S-36	S-37	S-38	S-39	S-40	S-41	S-42	S-43	S-44	S-45	S-46	S-47	S-48
	Pool-4	S-49	S-50	S-51	S-52	S-53	S-54	S-55	S-56	S-57	S-58	S-59	S-60	S-61	S-62	S-63	S-64
	Pool-5	S-65	S-66	S-67	S-68	S-69	S-70	S-71	S-72	S-73	S-74	S-75	S-76	S-77	S-78	S-79	S-80
	Pool-6	S-81	S-82	S-83	S-84	S-85	S-86	S-87	S-88	S-89	S-90	S-91	S-92	S-93	S-94	S-95	S-96
	Pool-7	S-97	S-98	S-99	S-100	S-101	S-102	S-103	S-104	S-105	S-106	S-107	S-108	S-109	S-110	S-111	S-112
	Pool-8	S-113	S-114	S-115	S-116	S-117	S-118	S-119	S-120	S-121	S-122	S-123	S-124	S-125	S-126	S-127	S-128
	Pool-9	S-129	S-130	S-131	S-132	S-133	S-134	S-135	S-136	S-137	S-138	S-139	S-140	S-141	S-142	S-143	S-144
	Pool-10	S-145	S-146	S-147	S-148	S-149	S-150	S-151	S-152	S-153	S-154	S-155	S-156	S-157	S-158	S-159	S-160
	Pool-11	S-161	S-162	S-163	S-164	S-165	S-166	S-167	S-168	S-169	S-170	S-171	S-172	S-173	S-174	S-175	S-176
	Pool-12	S-177	S-178	S-179	S-180	S-181	S-182	S-183	S-184	S-185	S-186	S-187	S-188	S-189	S-190	S-191	S-192
	Pool-13	S-193	S-194	S-195	S-196	S-197	S-198	S-199	S-200	S-201	S-202	S-203	S-204	S-205	S-206	S-207	S-208
	Pool-14	S-209	S-210	S-211	S-212	S-213	S-214	S-215	S-216	S-217	S-218	S-219	S-220	S-221	S-222	S-223	S-224
	Pool-15	S-225	S-226	S-227	S-228	S-229	S-230	S-231	S-232	S-233	S-234	S-235	S-236	S-237	S-238	S-239	S-240
	Pool-16	S-241	S-242	S-243	S-244	S-245	S-246	S-247	S-248	S-249	S-250	S-251	S-252	S-253			

Figure 4.4 Mapping of peptides containing SARS-CoV-2 T cell epitopes in the patient C-COV19-064. *(A) Photo of the ELISpot plate. IFN-γ-producing T cells in the PBMCs of the patient C-COV19-064 were detected by ELISpot assay after incubation with SARS-CoV-2 two-dimensional peptide pools. (B) Layout of the two-dimensional peptide pools. Peptide pools that elicited relatively strong T cell responses are highlighted in purple. (C) Potential peptides containing spike CD8$^+$ epitopes were identified by two-dimensional matrix analysis and are highlighted in red. (D) Photo of the ELISpot plate. IFN-γ-producing Spike CD8-1493 were detected by ELISpot assay after incubation with peptide-pulsed BCLs. Individual candidate peptide used for each well is labeled at the right bottom of that well.*

4.4.4 Defining HLA restriction of the S-98 peptide.

Every T cell epitope is presented by a particular allele of HLA at the cell surface. Even though HLAs are quite diverse with over 7000 alleles[188], common HLA alleles can be

grouped by geographic region[189]. For example, a study of a healthy British Caucasian population from Oxfordshire showed that HLA-A*02:01, HLA-B*08:01, HLA-C*07:01 are the most common alleles with allele frequencies of 28.31%, 14.36% and 18.03% respectively[190]. T cell epitopes presented by the common HLAs in a certain population determine the dominant T cell responses in that population. Understanding HLA restriction of SARS-CoV-2 T cell epitopes will help predict the popularity and severity of COVID-19 in certain population. In addition, HLA restriction is the important information in designing epitope-based vaccines.

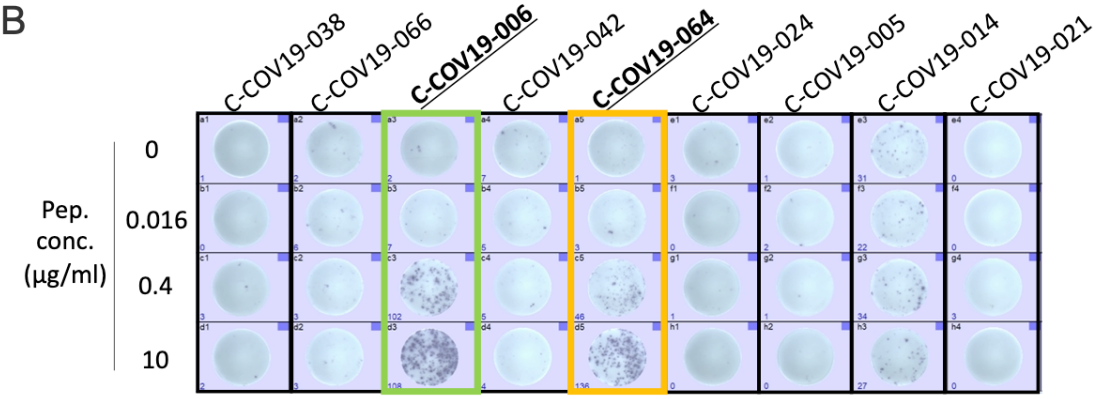
To determine the HLA restriction for S-98 peptide, ELISpot assays were performed using S98-specific T cell lines co-cultured with peptide-loaded HLA-matched and -unmatched BCLs. BCLs generated from the patients that have one or two overlapping HLAs with patient C-COV19-064 were chosen as candidate target cells for S98 CD8-064 bulk T cells. The HLA class I alleles of each BCL are shown in **Figure 4.5 A** with overlapping HLAs highlighted in the same background colour. BCLs were pulsed with S-98 peptide at concentrations of 0, 0.016, 0.4 and 10 μg/ml for 1 h and then co-cultured with S98 CD8-064 bulk T cells overnight on the ELISpot plate.

Among all the BCLs tested, only BCL from patient UKCOV006 and autologous BCL (C-COV19-064) can induce T cell responses after S-98 peptide stimulation (**Figure 4.5 B, C**). The only shared HLA by UKCOV006 and C-COV19-064 is HLA-A*29:02, suggesting that S-98 is restricted by this HLA.

A

	HLA-A1	HLA-A2	HLA-B1	HLA-B2	HLA-C1	HLA-C2
C-COV19-064	24:02	29:02	15:01	44:03	01:02	16:01
C-COV19-038	24:02	02:01	07:02	51:01	04:01	07:02
C-COV19-066	24:03	11:01	13:01	51:06	04:06	12:04
C-COV19-006	01:01/04N	29:02	07:02	45:01	07:01	07:02
C-COV19-042	02:01	24:02	15:01	07:02	03:03	07:02
C-COV19-024	02:01	26:01	08:01	44:03	07:01	07:02
C-COV19-005	01:01/04N	02:01	07:02	27:05	01:02	07:02
C-COV19-014	01:01/04N	01:01/04N	37:01	44:03	06:02	16:01
C-COV19-021	02:01	31:01	40:01	40:01	03:04	03:04

B



C

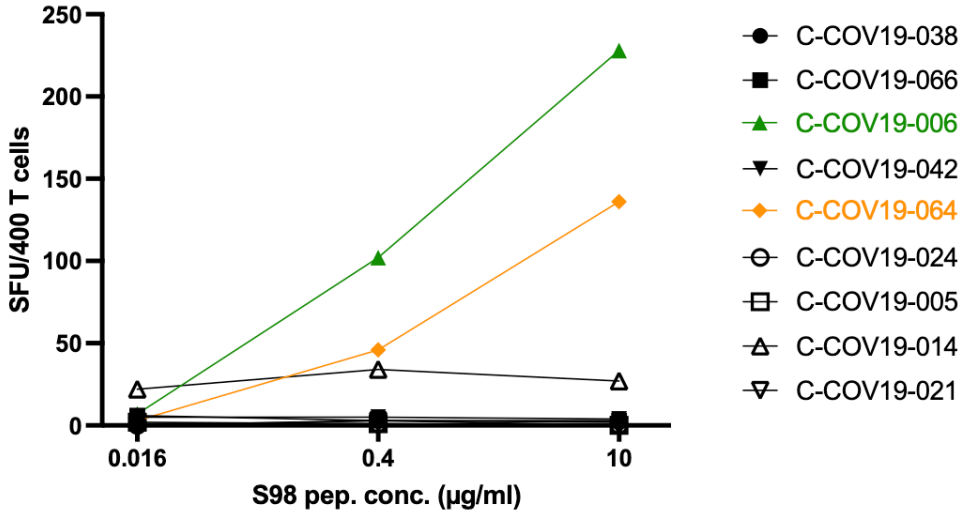


Figure 4.5 Identification of HLA restriction for S-98 CD8 epitope from C-COV19-064*. (A) HLA class I types of HLA-matched and -unmatched BCLs tested as target cells for S98 CD8-064. (B) Photo of ELISpot plate. IFN-γ-producing S98 CD8-064 were detected by ELISpot assay after incubation with S-98 peptide-pulsed HLA-matched and -unmatched BCLs. (C) Curves showing the number of dots on the ELISpot plate.*

4.4.5 Defining epitope sequence within the S-98 peptide.

The peptides used in the two-dimensional peptide pools are 13-18 amino acids, however, when CD8 epitopes are naturally processed and presented at the cell surface, they are usually 8-10 amino acids long due to the size restriction of the peptide binding groove of HLA class I[191]. Extended amino acids at either terminal of the epitopes will affect their binding affinity with HLA molecules and compromise the magnitude of T cell responses. To define the optimal S-98 CD8 epitope sequence within the long peptides, epitope sequences were first predicted using the T cell epitope – MHC binding prediction tools on Immune Epitope Database (IEDB) analysis resource (http://tools.iedb.org/mhci). This tool predicts IC50 values for peptides binding to specific MHC molecules. We put in the sequence of the S-98 peptide $_{486}$FNCYFPLQSYGFQPT$_{500}$ and HLA-A*29:02, and got a list of predicted epitope sequences within S-98 (**Figure 4.6 A** shows the top 5 predicted epitope sequences). This tool gives an output score showing binding affinity of peptide to HLA and a rank showing the percentage of randomly sampled peptides scoring better than the peptide. Predicted peptides of 8-10 amino acids were then synthesized by GenScript.

To verify the optimal epitope sequence within S-98, autologous BCLs from C-COV19-064 were pulsed with three of the predicted peptides (the 1st, 2nd, and 5th on the list as these peptides arrived earlier than the others) separately at a concentration of 0, 0.0032, 0.016, 0.08, 0.4, 2 and 10 µg/ml for 1 h, and then co-cultured with two S98 CD8-064 T cell clones (CL-1 and CL-2) separately overnight on the ELISpot plate. The strongest T cell responses were observed after $_{489}$YFPLQSYGF$_{497}$ stimulation, and weaker responses after $_{488}$CYFPLQSYGF$_{497}$ or full-length S-98 ($_{486}$FNCYFPLQSYGFQPT$_{500}$) stimulation, while no responses against

$_{487}$NCYFPLQSY$_{495}$ were observed (**Figure 4.6 B, C**). This suggests that $_{489}$YFPLQSYGF$_{497}$ is the optimal HLA-A*29:02 epitope sequence within S-98. $_{488}$CYFPLQSYGF$_{497}$ has one amino acid extension at the N-terminus of the epitope, resulting in lower binding affinity with HLA-A*29:02 compared to the optimal epitope confirming that the 9-amino acid peptide is optimal (**Figure 4.6 C**).

Following these results, it seemed unnecessary to test the remaining two peptides as $_{487}$NCYFPLQSY$_{495}$ induced no response, likely due to the lack of phenylalanine (F) at the C-terminus of the peptide. The C-terminus is a key anchor position for peptide binding into the groove of HLA molecules. The remaining two peptides also lacked F at their C-terminus and were an 8- and 10- amino acid version of $_{487}$NCYFPLQSY$_{495}$. The binding affinity of the full-length S-98 ($_{486}$FNCYFPLQSYGFQPT$_{500}$) with HLA-A*29:02 is the lowest (**Figure 4.6 C**) due to three amino acids extension on both terminus of the epitope.

A

Start	End	Length	Peptide sequence	Score	Rank
487	495	9	NCYFPLQSY	0.430781	0.25
489	497	9	YFPLQSYGF	0.383419	0.29
488	495	8	CYFPLQSY	0.320173	0.34
486	495	10	FNCYFPLQSY	0.272628	0.42
488	497	10	CYFPLQSYGF	0.167932	0.66

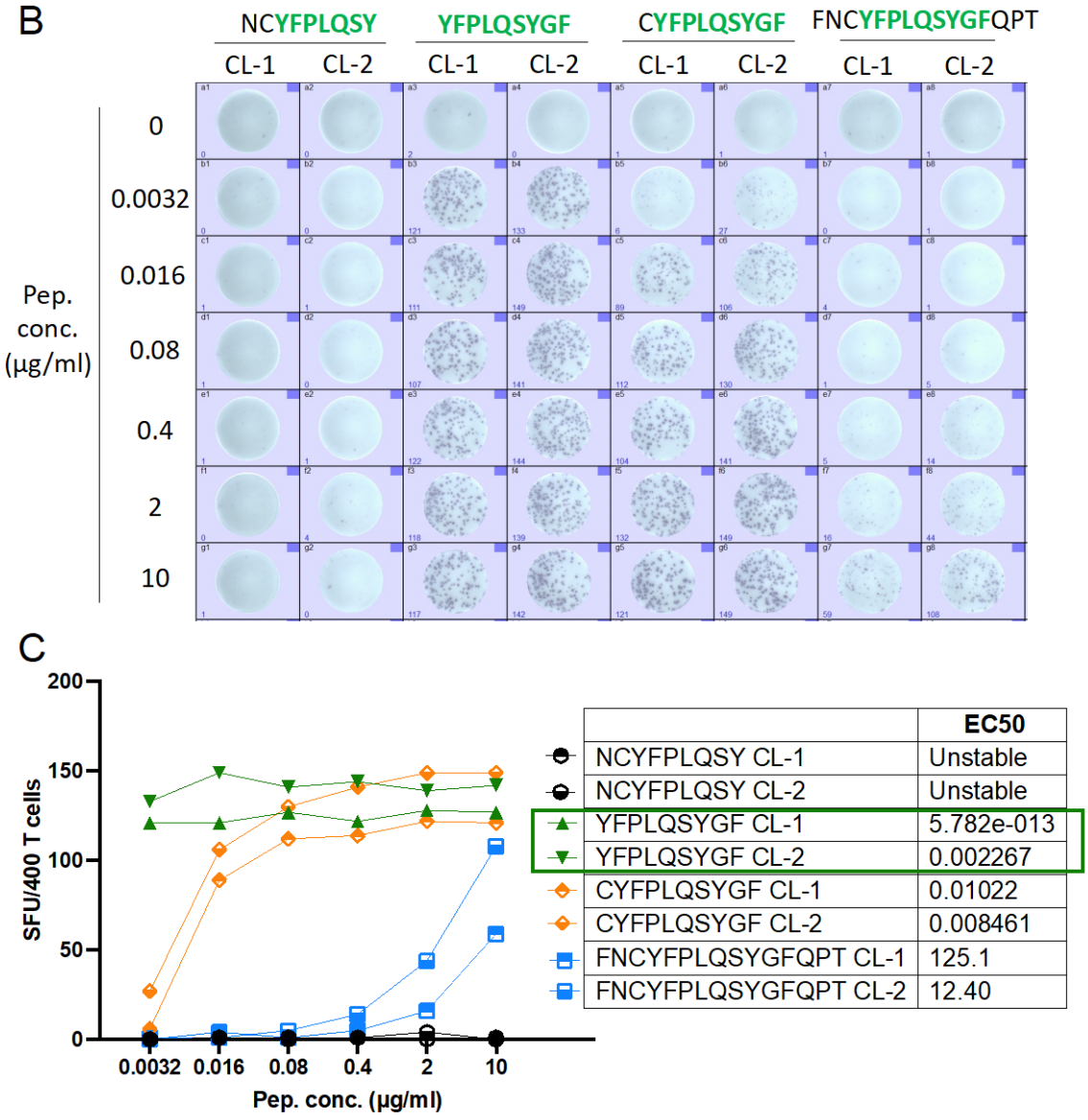


Figure 4.6 Identification of the optimal epitope sequence recognized by S98 CD8-064. *(A) HLA-A*29:02 binding prediction results for S-98 ($_{486}$FNCYFPLQSYGFQPT$_{500}$). Prediction method: NetMHCpan EL 4.1. (B) Photo of ELISpot plate. IFN-γ-producing S98 CD8-064 T cell clones, CL-1 and CL-2, were detected by ELISpot assay after incubation with NCYFPLQSY-, YFPLQSYGF-, CYFPLQSYGF- or FNCYFPLQSYGFQPT-pulsed autologous BCLs. (C) Curves showing the number of dots on the ELISpot plate. "Unstable" means EC50 can not be determined because the top and bottom plateaus can not be defined due to the relatively low response level.*

4.4.6 Identification of SARS-CoV-2 $CD8^+$ epitopes from patient memory responses.

Using the two-dimensional peptide matrix system discussed above, a total of 44 peptides containing SARS-CoV-2 T cell epitope regions were recognized by convalescent patients: 21 from Spike, 10 from NP, 6 from M and 7 from ORF proteins (**Table 4.2**)[185]. S-34, S-151, S-174, NP-16, M-20 and M-24 were recognized by six or more of the participants tested, suggesting that these are the dominant T cell responses in our cohort. ICS assays further confirmed that NP-16 induced strong $CD8^+$ T cell responses while the others induced strong $CD4^+$ responses. NP-1, NP-51 and ORF3a-28 were recognized by three or four of the participants tested and were all confirmed by ICS to induce $CD8^+$ responses only.

Identification of dominant SARS-CoV-2 $CD8^+$ optimal epitopes is crucial in understanding the immunogenicity of SARS-CoV-2 antigens and predicting the impact of viral mutations on $CD8^+$ T cell responses. In addition, NP-47 and NP-51 both contain previously defined SARS-CoV-1 $CD8^+$ epitopes, therefore, we were interested in defining SARS-CoV-2 epitopes within those two peptides to investigate the possibility of cross-reactive T cell immune memory to SARS-CoV-1. S-98 was also of great interest as it is located in the Spike receptor binding domain (RBD) close to two mutation sites found in the Omicron variant of concern.

As described above, using ELISpot assays with B and T cell lines generated from patient PBMCs, in combination with T cell epitope prediction tools, we were able to define the epitope sequence and HLA restriction of seven $CD8^+$ epitopes within the peptides NP-1, NP16, NP-47, NP-51, ORF3a-28 and S-98 (**Table 4.3**)[185].

Table 4.2 Peptides containing SARS-CoV-2 T cell epitopes.

	Peptide ID	Position	Amino acid sequence	Number of participants who responded
Spike (n=21)	S-30	146-160	HKNNKSWMESEFRVY	1
	S-34	166–180	CTFEYVSQPFLMDLE	10
	S-39	191–205	EFVFKNIDGYFKIYS	1
	S-42	206–230	KHTPINLVRDLPQGF	1
	S-43	211–225	NLVRDLPQGFSALEP	1
	S-71	351–365	YAWNRKRISNCVADY	1
	S-75	371-385	SASFSTFKCYGVSPT	1
	S-77	381–395	GVSPTKLNDLCFTNV	1
	S-90	446–460	GGNYNYLYRLFRKSN	1
	S-91	451–465	YLYRLFRKSNLKPFE	1
	S-98	486-500	FNCYFPLQSYGFQPT	1
	S-103	506–520	VVLSFELLHAPATVC	1
	S-106	526–540	GPKKSTNLVKNKCVN	1
	S-145	721–735	SVTTEILPVSMTKTS	1
	S-150	746–760	STECSNLLLQYGSFC	1
	S-151	751–765	NLLLQYGSFCTQLNR	8
	S-161	801–815	NFSQILPDPSKPSKR	2
	S-174	866–880	TDEMIAQYTSALLAG	6
	S-235	1,171–1,185	GINASVVNIQKEIDR	1
	S-240	1,196–1,210	LIDLQELGKYEQYI	1
	S-242	1,206–1,220	YEQYIKWPWYIWLGF	1
NP (n=10)	NP-1	1–17	MSDNGPQNQRNAPRITF	3
	NP-2	8–25	NQRNAPRITFGGPSDSTG	3
	NP-12	82–95	DQIGYYRRATRRIR	1
	NP-15	101–113	MKDLSPRWYFYYL	1
	NP-16	104–121	LSPRWYFYYLGTGPEAGL	12
	NP-46	313–330	AFFGMSRIGMEVTPSGTW	1
	NP-47	321–338	GMEVTPSGTWLTYTGAIK	1
	NP-48	329–346	TWLTYTGAIKLDDKDPNF	2
	NP-50	344–361	PNFKDQVILLNKHIDAYK	1
	NP-51	352–369	LLNKHIDAYKTFPPTEPK	3
M (n=6)	M19	133–150	LLESELVIGAVILRGHLR	3
	M-20	141–158	GAVILRGHLRIAGHHLGR	11
	M-21	149–166	LRIAGHHLGRCDIKDLPK	3
	M-23	165–181	PKEITVATSRTLSYYKL	3
	M-24	172–188	TSRTLSYYKLGASQRVA	16
	M-28	201–218	IGNYKLNTDHSSSSDNIA	1
ORFs (n=7)	ORF3a-20	145–160	YFLCWHTNCYDYCIPY	1
	ORF3a-27	198–215	KDCVVLHSYFTSDYYQLY	3
	ORF3a-28	206–225	YFTSDYYQLYSTQLSTDTGV	4
	ORF3a-30	224–243	GVEHVTFFIYNKIVDEPEEH	1
	ORF7a-2	9–25	LITLATCELYHYQECVR	3
	ORF7a-7	46–63	FHPLADNKFALTCFSTQF	1
	ORF7a-10	69–86	DGVKHVYQLRARSVSPKL	1

Table 4.3 SARS-CoV-2 CD8 optimal epitopes.

	Peptide ID	Epitope position	Epitope sequence	HLA restriction
Spike	S-98	489-497	YFPLQSYGF	A*29:02
NP	NP-1	9–17	QRNAPRITF	B*27:05
	NP-16	105–113	SPRWYFYYL	B*07:02
	NP-47	322–331	MEVTPSGTWL	B*40:01
	NP-51	362–370	KTFPPTEPK	A*03:01
	NP-51	362–370	KTFPPTEPK	A*11:01
ORFs	ORF3a-28	207–215	FTSDYYQLY	A*01:01

4.5 Discussion

In this study, we demonstrated strong and broad memory T cell responses against SARS-CoV-2 Spike, NP, M, Env and ORFs peptides in 42 UK convalescent COVID-19 patients. Furthermore, we identified seven SARS-CoV-2 $CD8^+$ optimal epitopes restricted by HLA-A*01:01, -A*03:01, -A*11:01, -A*29:02, -B*07:02, -B*27:05 and -B*40:01, including the immunodominant epitope $_{105}$SPRWYFYYL$_{113}$-HLA-B*07:02.

Adaptive immune responses, in coordination with innate immune responses, are needed to control and eliminate SARS-CoV-2 infection. There is intense interest in the relative importance of cellular immunity during the infection. Evidence from SARS-CoV-1 and MERS indicates that T cells may be the major mediators of disease control[192].

This collaborative research project demonstrated the association of stronger T cell responses with severe disease. Stronger SARS-CoV-2-specific T cell responses in severe cases may result from higher viral loads[193] compared with mild cases, indicating poorer immune responses, particularly innate immune responses mediated by type I interferons[194], at the early stages of SARS-CoV-2 infection. Indeed, effective clinical control of primary SARS-CoV-2 infection is associated with early and robust interferon and adaptive immune responses, which effectively control viral load. A delayed,

inadequate, and prolonged interferon response is associated with slowed and elevated cellular activation, early inflammation and slow decline in viral load, leading to severe clinical outcomes[195].

Stronger SARS-CoV-2-specific T cell responses in severe cases indicates overactivation of T cell responses, which could be harmful and contribute to disease severity. The overactivation of T cell responses is also reflected by lymphocytopenia, which is widely observed in the blood of many individuals with acute SARS-CoV-2 infection and is correlated with severe clinical outcome[196]. Lymphocytopenia is also seen in several other acute respiratory virus infections such as influenza virus[197], however, it seems to be more rapid, profound, and long-lasting in the setting of COVID-19.

On the other hand, the observation that a greater proportion of $CD8^+$ T cell responses was demonstrated to associate with mild cases, indicates a potential protective role of SARS-CoV-2-specific $CD8^+$ T cells during COVID-19 progression. Our study provided evidence that $CD8^+$ T cells can generate a functional memory pool, which is essential in convalescent COVID-19 infection. At the same time, there were also many studies looking into acute COVID-19 infection and those studies indicated that functional $CD8^+$ T cells played a role in the early immune response to SARS-CoV-2. Notarbartolo *et al* demonstrated that early development of a cytotoxic $CD8^+$ T cell response, typically observed within 7 days of symptoms and peaking at 14 days, was correlated with effective viral clearance[198], and was in line with similar kinetics for humoral responses[199]. In addition, Su *et al* reported that high expression levels of effector molecules by $CD8^+$ T cells in acute COVID-19 were associated with improved clinical outcome[200]. Effective SARS-CoV-2 viral control was also reported to be associated with type 1 $CD4^+$ T cells, however, type 2 $CD4^+$ T cells were often seen in severe cases[198]. Altogether, our study

and others suggested that the functional capacity of $CD8^+$ cell response is a key determinant of clinical outcome.

This study focused on memory T cell responses isolated from peripheral blood. Other studies focused on tissue-resident memory T cells (T_{RM}) positioned within the respiratory tract and lung, which probably provide the most protection at the early stages of virus infection. Grau-Exposito *et al*[201] found that lung-T_{RM} were frequently detected in convalescent patients even 10 months after initial infection, indicating that persisting T_{RM} cells were important for future protection against SARS-CoV-2 infection. Poon *et al*[202] reported that memory T cells and B cells against SARS-CoV-2 were present in bone marrow, spleen, lung and multiple lymph nodes (LNs) for up to 6 months after infection. They also showed that the lungs and lung-associated LNs were the most prevalent sites for SARS-CoV-2-specific memory T and B cells with significant correlations between circulating and tissue-resident memory T and B cells in all sites. These findings indicate the important role of site-specific protection against future SARS-CoV-2 challenges.

T cell responses against SARS-CoV-2 were identified rapidly following release of SARS-CoV-2 sequence. The use of peptide pools covering the entire viral proteome allowed rapid identification of T cell responses against almost all proteins. Dominant SARS-CoV-2-specific T cell responses were observed against Spike, NP, M and ORF3a in this study. This observation may be due to viral protein size, abundance or turnover rates but further investigation is required to understand this in detail. Using a suite of ribosome-profiling techniques, Finkel *et al* quantified the expression of canonical SARS-CoV-2 ORFs in Vero E6 cells following SARS-CoV-2 infection and revealed a map of SARS-CoV-2 coding capacity[203]. Their work showed that NP was the most efficiently translated SARS-CoV-2 viral protein. M and ORF3a were also among the top 7 efficiently

translated viral proteins[203]. High translation levels of NP, M and ORF3a could be one of the factors that contributes to the immunodominance of those proteins. Although Spike was less efficiently translated, the size of Spike protein is the largest, which could contribute to its immunodominance.

This study demonstrates the advantages of a two-dimensional peptide matrix system to characterize overall memory T cell responses and to map T cell epitopes. IFN-γ ELISpot and ICS are the two main assays used in this system. Both are well-established methods for functional evaluation of antigen-specific T cells in virus infections and vaccine studies[204-206]. Another recently developed assay is the activation induced marker (AIM) assay, capable of detecting early responding T cells, which is independent of cytokine production[207]. AIM assays have been widely used in COVID-19 T cell studies[208,209], assessing the expression of T cell activation markers such as CD137, OX40 and CD69. All these three assays are valid, but ICS is less sensitive than the other two.

Using our two-dimensional peptide matrix system, we have identified 7 $CD8^+$ optimal epitopes. NP-16 restricted by HLA-B*07:02 was considered the most dominant one. Peng *et al*[210] found that strong responses to NP16 was associated with mild disease. They further demonstrated a beneficial association of NP16-specific T cells with expansion of T cell precursors, high functional avidity and antiviral efficacy, pointing to inclusion for future vaccine design.

M-24 was recognized by 16 out of 34 participants tested in our cohort (**Table 4.2**). Yao *et al* in our lab took over the project to investigate the multiple HLA restrictions of this dominant M-24. Three dominant Spike peptides, S-34, S-151 and S-174, were recognized by 10, 8, 6 out of 34 participants respectively (**Table 4.2**) and induced strong $CD4^+$ T cell responses. As Spike is the key component in COVID vaccines, it is of great

importance to characterize dominant Spike T cell responses. Liu *et al* in our lab continued to study those three $CD4^+$ T cell specificities focusing on their use of distinct signalling and cytotoxic pathways.

We were the first group to report the characteristics of memory T cell responses against SARS-CoV-2 in UK convalescent individuals. There were several similar COVID studies on memory T cell responses at the same time but in different cohorts such as USA[209] and Singapore[211]. We and others were also different in the way of evaluating T cell functions: we used ICS while others used AIM assays. No matter what methods were used, robust T cell responses were observed in all the cohorts studied. There were also lots of studies on the immunodominant T cell epitopes at the same time[212,213]. Most of the T cell epitope papers predicted SARS-CoV-2 T cell epitopes using computational tools and usually provided with a result of hundreds of T cell epitopes. Prediction of T cell epitopes by computational analysis is fast but not all the epitopes predicted are real. Different from those studies, all the epitopes in our study were defined by the experiments, which are more accurate and solid, but took longer time.

T cell recognition relies on peptides presented by MHC molecules, therefore, SARS-CoV-2 mutations within T cell epitopes may alter cellular immune responses. One of the $CD8^+$ T cell epitopes identified in our study, NP-1 ($_9$QRNAPRITF$_{17}$) restricted by HLA-B*27:05, has been reported to carry one mutation site P13L in SARS-CoV-2 Omicron strain, and this mutation completely abolished recognition by NP-1-specific T cells[214]. Mutations located in the flanking regions of SARS-CoV-2 T cell epitopes can also alter memory T cell responses due to enhanced or compromised antigen processing and presentation. Wellington *et al* in our lab have looked into the impact of flanking region mutations in two most dominant $CD8^+$ epitopes from SARS-CoV-2 NP, NP-1 and

NP-16, on T cell activation using a SARS-CoV-2 NP transduction system. They also looked into the impact of the mutations on antigen processing efficiency using an *in vitro* proteasomal digestion system.

Since the emergence of SARS-CoV-2 VoCs, it is of great importance to know whether memory T cell responses established against original SARS-CoV-2 strain are still able to recognize those variants. Considering the breadth of T cell responses within individual donors, which have been estimated against approximately 19 $CD4^+$ epitopes and 17 $CD8^+$ epitopes in most people[215], the majority of T cell responses are likely to be maintained when a convalescent or vaccinated individual is exposed to the variants. Indeed, many studies have reported that SARS-CoV-2-specific memory T cells are able to cross-recognize variants[216]. However, current studies so far have all been based on the stimulation with high concentration peptides, which might underestimate the impact of mutations on T cells. In addition, exogenously synthetic peptides might be different from those that are naturally processed and presented by the host cells. To address the impact of viral mutations on T cell recognition in a scenario closer to real infection, we established an *ex vivo* system to evaluate SARS-CoV-2-specific T cell responses to naturally processed antigens, which will be discussed in the next chapter.

4.6 Future directions

Although multiple studies have indicated that T cells play a role in the early immune response to SARS-CoV-2 and can generate and can generate a functional memory pool, there are still multiple unanswered questions in this field in relation to disease severity, memory formation and vaccination:

1) The impact of clinical and virological factors including sex, age and chronic diseases on the strength and efficacy of the early antiviral T cell responses. During acute COVID-19 infection, there is a broad clinical spectrum including asymptomatic, mild, severe and fatal outcomes. And after recovery, some individuals still experience other symptoms for an extended period, known as long COVID, despite viral clearance. Many studies have shown that worse clinical outcomes are associated with compromised cellular responses against SARS-CoV-2, however, how the clinical and virological factors affect the development and function of T cell responses need further investigation.
2) The impact of immunological factors on the generation of SARS-CoV-2-specific T cells. The ability of the host to generate efficient T cell responses after exposure to SARS-CoV-2 depends on the target epitopes, antigen abundance, pre-existing cross-reactive T cells, and host genetic factors such as HLA types and TCR repertoires. Furthermore, the level of inflammation and the amount of proinflammatory cytokines are likely to be associated with T cell activation, exhaustion and subsequent memory formation.
3) The link between vaccine-induced T cell immunity and vaccination outcome. Whether cellular responses will be equally induced in all age groups by vaccine and how long these responses will persist in blood and draining lymph nodes need further investigation.

Chapter 5

Evaluating T cell responses against naturally processed spike antigens of SARS-CoV-2 and variants of concern

5.1 Introduction.

Following the outbreak of COVID-19, multiple vaccines were developed against SARS-CoV-2. Vaccines do their job by activating both antibody and T cell immune responses. Antibodies clear the SARS-CoV-2 virus by neutralization, while T cells suppress the replication of SARS-CoV-2 virus by coordinating immune responses and killing virus-infected cells directly. Although the vaccines are proving highly efficacious against SARS-CoV-2, lots of concerns remain, such as the durability of the immunity elicited by these vaccines and the extent to which they can protect against the variants of SARS-CoV-2 spreading rapidly around the world. In addition, since infection with COVID-19 also prompt the body to produce antibodies and T cells targeting SARS-CoV-2, it has been of great interest to compare the immune responses induced by infection or vaccination. People were asking whether they still need vaccines if they have had COVID-19 before. To answer these questions, it is rather important to understand how infection and vaccination influence the immune defence they elicit, and whether they protect against variants.

T cells play a key role in preventing severe COVID-19, as discussed in the previous chapter. Since COVID-19 vaccines started to be distributed worldwide, an urgent need arose to understand the vaccination-induced T cell immune responses against SARS-CoV-2 Spike. The durability and functions of SARS-CoV-2-specific T cells after

vaccination are one of the most important indicators of vaccine efficacy, especially in protection against serious illness[217].

The emergence of rapidly spreading SARS-CoV-2 variants in multiple parts of the world, including Alpha, Beta, Gamma[218], and the highly transmissible Delta and Omicron[219], induced great concern about the cross-reactivity of immune responses against novel strains. The survival advantages of the variants come from higher virulence and potential immune evasion. While antibodies against the original SARS-CoV-2 elicited by either infection or vaccination generally remain protective against Alpha, their activity against Beta, Gamma, Delta and Omicron is compromised[220-226]. Despite the lower cross-reactivity of neutralizing antibodies, T cell immunity seems to be less prone to evasion by the variants due to the highly conserved T cell epitope regions. Among 280 $CD4^+$ and 523 $CD8^+$ T cell epitopes from the original SARS-CoV-2 strain, an average of 91.5% (for $CD4^+$) and 98.1% (for $CD8^+$) are mapped to the unmutated regions of Alpha, Beta and Gamma[217]. Focusing on just the Spike sequence, 89.7% of the $CD4^+$ epitopes and 96.4% of the $CD8^+$ epitopes are conserved[227]. However, considering the number of immunodominant T cell epitopes for one individual, which has been estimated to be approximately 19 $CD4^+$ epitopes and 17 $CD8^+$ epitopes in most people[215], small changes in the sequences of T cell epitopes can have unneglectable impact on T cell responses in that individual.

The ChAdOx1 nCoV-19 vaccine (Oxford-AstraZeneca; Cambridge, UK) consists of the replication-deficient adenovirus vector ChAdOx1 encoding the full-length SARS-CoV-2 Spike protein[228]. In an analysis of more than 130 SARS-CoV-2-infected health care workers in India, reduced ChAdOx1 vaccine effectiveness was observed against Delta compared to the ancestral, Alpha and Beta strain[225]. Another analysis of 60 health

care workers after immunization with ChAdOx1, consistent cross-neutralization of the Beta and Delta variants was observed, but neutralization of Omicron was significantly lower[229]. However, studies on the cross-recognition of the variants, including Omicron particularly, by ChAdOx1-induced SARS-CoV-2 Spike-specific T cells are limited.

Current COVID T cell studies on the cross-recognition of SARS-CoV-2 variants are using exogenously synthetic peptide pools. Stimulation of T cells with peptide pools spanning the entire spike sequences of different variants is an efficient way of high-throughput screening of T cell responses to the variants. However, in a real infection scenario, not all the peptides from SARS-CoV-2 are efficiently generated in the host cells and delivered at the cell surface[165]. Therefore, the synthetic peptide pools cannot accurately reflect the antigen pools present at the cell surface, and neither can the concentration of peptides used reflect the antigen load at the cell surface. For mutations that happen in T cell epitope regions, their impact on T cell responses can be well studied using synthetic peptides. However, for mutations that happened in the flanking region of T cell epitopes, especially those that affect antigen processing and presentation, their impact on T cell responses will be neglected if using synthetic peptides. Therefore, to study the impact of SARS-CoV-2 mutations in a more comprehensive way, it is necessary to develop a method to evaluate T cell responses against naturally processed SARS-CoV-2 antigens.

Vaccinia virus (VACV) is well known as the first vaccine in human history and it successfully eradicated smallpox[230]. VACV can infect almost all kinds of mammalian cells[231]. To enter host cells, VACV can induce transient micropinocytosis followed by endocytic internalization and penetration through the limiting membrane of pinosomes by membrane fusion[232]. Moreover, continued research demonstrated the ability of the

VACV genome to accommodate additional genetic materials. With the relative ease of generating recombinant VACVs to express heterologous genes, widespread attention has been given to the idea of using VACVs as a vehicle for antigen delivery[231,233]. Therefore, infection of EBV-transformed BCLs with recombinant VACVs expressing spike from SARS-CoV-2 will be a good system to deliver naturally processed Spike antigens to T cells.

5.2 Aims.

We used both a convalescent cohort (9 people recovered from COVID-19) and a vaccinated cohort (9 people immunized with first dose of ChAdOx1) to:

- Evaluate the cross-reactivity of natural infection- or vaccination-induced T cells against Delta and Omicron live virus.
- Evaluate the cross-reactivity of natural infection- or vaccination-induced T cells against vaccinia virus expressing Delta or Omicron Spike.
- Discover mutation sites in SARS-CoV-2 spike that affect T cell recognition.

5.3 Hypotheses.

- Vaccination will generate comparable immunity against SARS-CoV-2 spike as natural infection.
- Both natural infection- and vaccination-induced T cells can cross-recognized SARS-CoV-2 variants.

5.4 Study participants.

To assess T cell responses following ChAdOx1 vaccination or natural infection, we isolated PBMCs from N=9 vaccinated participants 3 weeks after the first dose of ChAdOx1 and N=9 convalescent patients 1-3 months post-infection. PBMCs were stimulated with SARS-CoV-2 spike peptide pools and cultured for 14 days. Spike-specific $CD4^+$ and $CD8^+$ T cell lines were then isolated and expanded by FACS sorting of IFNγ and/or TNFα and/or IL2-secreting T cells after stimulation of spike peptides. Meanwhile, autologous B cell lines (BCLs) were established from PBMCs by EBV transformation.

5.5 Results.

The best option for studying T cell responses to naturally processed antigens is to use a live virus system. The epitopes presented by SARS-CoV-2-infected cells are naturally processed SARS-CoV-2 antigens and can reflect antigen pools, as well as antigen loads, in a real infection scenario. To achieve this, cell lines meeting the following two requirements are needed. Firstly, they express ACE2, the host cell receptor for SARS-CoV-2, so that they can be infected by SARS-CoV-2 virus[234]. Secondly, they can provide multiple HLA options so that they can present most of the T cell epitopes. Indefinitely proliferating B cell lines (BCLs) are easily accessible from PBMCs by Epstein-Barr virus (EBV) transformation[235]. Establishment of BCLs from each study participant will provide multiple HLA options. However, BCLs don't normally express ACE2. Therefore, transduction of ACE2 into BCLs will make them the perfect target cells that can be infected by live SARS-CoV-2 virus, and then process and present SARS-CoV-2 antigens to T cells, which is a more natural way to stimulate T cells compared to exogenously peptide pulsing.

5.5.1 ACE2 lentivirus transduction of B cell lines.

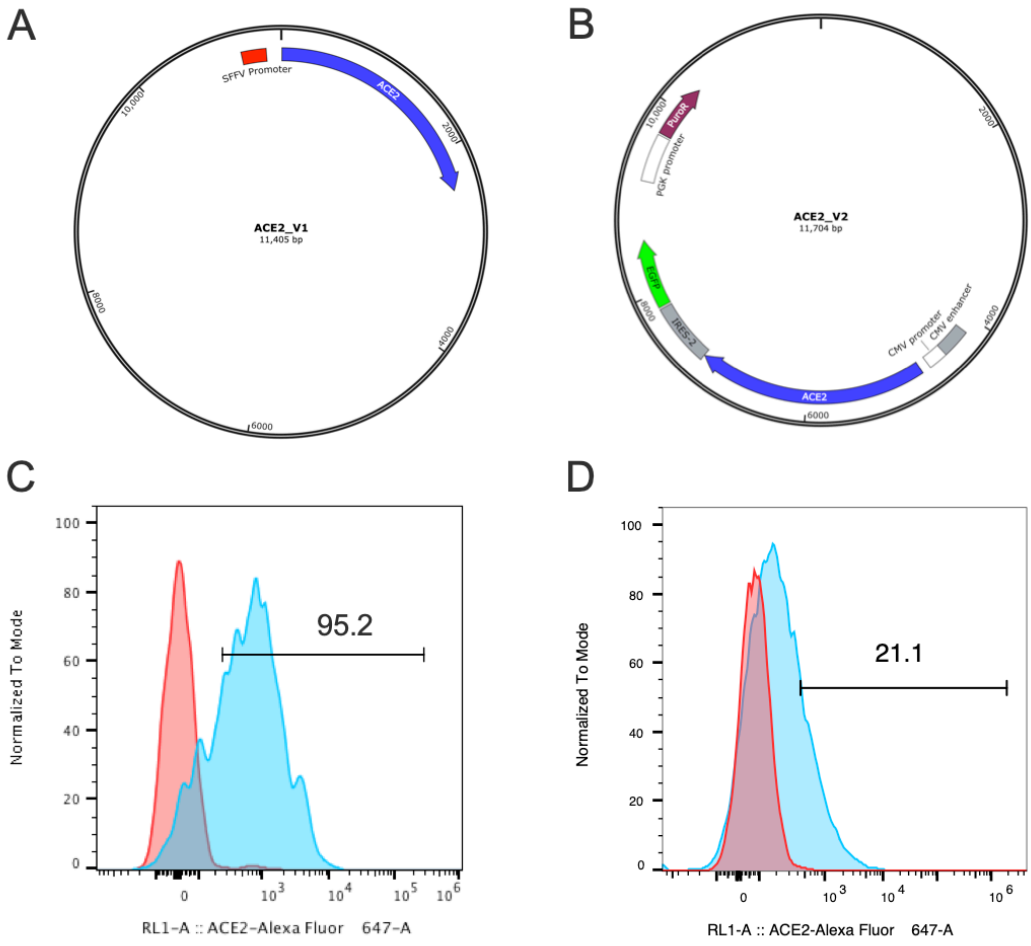
We decided to transduce ACE2 into BCLs using lentivirus as lentiviral transduction is an efficient method for the delivery of transgenes to mammalian cells[236]. Lentivirus will transport the DNA encoding ACE2 directly into the nucleus of BCLs and make the BCLs stably express ACE2. Several ACE2 constructs were tried to establish stable BCL-ACE2. ACE2_V1, as shown in **Figure 5.1 A**, used the spleen focus-forming virus (SFFV) promoter. ACE2 was shown to be stably transduced into HEK293 cells using ACE2_V1 for another study and the ACE2 expression is above 95% (**Figure 5.1 C**). Three BCLs

were transduced with lentivirus made from ACE2_V1, however, for the three BCLs, only 20% of cells were expressing ACE2 (**Figure 5.1 D**) and ACE2 levels dropped overtime. Constant sorting of $ACE2^+$ BCLs was needed to maintain ACE2 expression, which was not ideal for future infection experiments.

With the help of Philip Hublitz (WIMM Genome Engineering Facility), we designed another construct, ACE2_V2, as shown in **Figure 5.1 B**, which uses the cytomegalovirus (CMV) promoter and also included GFP as a reporter gene and a puromycin resistance gene as a selection marker. BCLs were then transduced with lentivirus made from ACE2_V2 followed by the sorting of $ACE2^+$ BCLs 10±3 days after transduction. BCLs were cultured with 0.5 μg/ml puromycin to maintain ACE2 expression. Unfortunately, transduction of all 18 B cell lines for our cohort with ACE_V2 only yielded 5 stable ACE2-expressing cell lines when they were cultured with puromycin and ACE2 expression levels were 39%-69% (**Figure 5.1 E, Table 5.1**) . For the other BCLs, they were growing very well with puromycin but their ACE2 expression levels were all below 10%, indicating that the puromycin resistance gene was successfully inserted into host genome but not the ACE2 gene.

Following these results, we tried several other strategies to improve ACE2 expression in our B cells. Firstly, as the CMV promoter has been shown to be silenced in lymphoid cells we tried adding 0.1% DMSO to our cell cultures[237] to prevent the gene silencing. However, it only worked in the first few days and ACE2 still dropped after that. Secondly, we completely changed from the CMV to the elongation factor-1 alpha (EF1α) promoter, which was known to drive strong gene expression in mammalian cells including lymphoid cells[238]. However, ACE2 levels still decreased overtime even with puromycin selection. We then started to think that it was ACE2 itself that was not

compatible with BCLs. One hypothesis was that ACE2 as a transmembrane protein was not favourably expressed on the cell membrane of BCLs. Again, with the help of Philip Hublitz, we designed a chimeric ACE2 construct with its original transmembrane domain replaced by HLA-B transmembrane domain. Unfortunately, the expression of the chimeric ACE2 was unstable. Another hypothesis was that ACE2 as an enzyme was too active to stably stay in BCLs. It was reported that in ACE2, Arg273 was a critical amino acid for substrate binding and His345 acted as the hydrogen bond donor/ acceptor in the formation of the tetrahedral peptide intermediate[239]. Therefore, we mutated these two residues to abolish ACE2 enzymatic activity. Still, the mutation didn't improve the stability of BCLs.



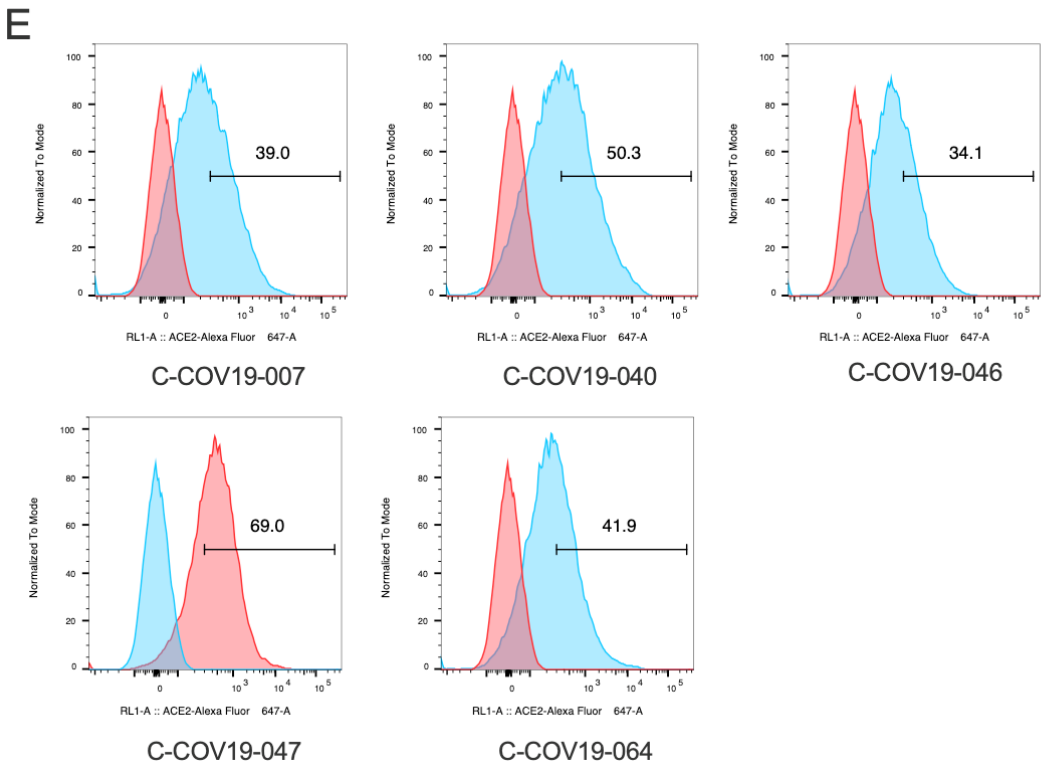


***Figure 5.1 Transduction of ACE2 into BCLs**. (A) Schematic illustrating ACE2 construct, ACE2_V1. (B) Schematic illustrating ACE2 construct, ACE2_V2. (C, D) ACE2 expression in HEK293 cells (C) and BCLs-ACE2 (D) transduced with lentivirus made from ACE2_V1. (E) ACE2 expression in different BCL-ACE2. BCLs were transduced with lentivirus made from ACE2_V2.*

Table 5.1 HLA-typing of BCL-ACE2

	A1	A2	B1	B2	Cw1	Cw2	DRB1-1	DRB1-2	DRB345-1	DRB345-2	DQB1-1	DQB1-2	DPB-1	DPB-2
UKCOV-007	01:01/04N	01:01/04N	07:02	07:02	07:02	07:02	11:02	15:01	DRB3	DRB5	03:01	06:02	04:01:01	16:01:01
RTH08-1180	01:04N	03:01	27:05	57:01	01:02	06:02	01:01	07:01	DRB4	NF	03:03	05	03:01:01	11:01:01
RTH08-1201	02:01	03:01	07:02	44:02	05:01/03	07:02	04:01	15:01	DRB4	DRB5	03:01	06:02	04:01:01	04:01:01
RTH08-1344	24:02	24:02	27:05	27:05	01:02	02:02	08:01	15:01	DRB5	NF	04	06:02	04:01:01	04:01:01
RTH08-1493	24:02	29:02	15:01	44:03	01:02	16:01	07:01	15:01	DRB4	DRB5	02	06:02	02:01:02	11:01:01

5.5.2 Live SARS-CoV-2 infection system was established to evaluate antiviral T cell immune responses.

To confirm that BCL-ACE2 cells can be infected by SARS-CoV-2 and to determine the optimal MOI for SARS-CoV-2 infection, BCL-ACE2 were inoculated with SARS-CoV-2 virus at MOI 0.1 and 1 for 2 hours. Virus was then washed off and BCL-ACE2 were replated in fresh culture medium. 24 hours later, BCL-ACE2 were harvested and lysed for RNA extraction. qPCR was run with SARS-CoV-2 N1 probe to determine the virus

load in the cells. Virus load of MOI 1 was twice that of MOI 0.1 (**Figure 5.2 A**), therefore MOI 1 was used for future infection experiments.

ICS and suppression assays were the two methods used to evaluate antiviral activity of T cells. ICS evaluates cytokine secretion of IFN-γ, TNF-α, IL-2 and the expression of CD107a by T cells. Suppression evaluates the inhibition effect of T cells on virus growth. For ICS assays, BCL-ACE2 were first inoculated with SARS-CoV-2 virus for 2 hours. 24 hours later, during which period virus can replicate in the host cells, infected BCL-ACE2 were co-cultured with SARS-CoV-2 spike-specific $CD4^+$ or $CD8^+$ T cells for 6 hours. GolgiStop, GolgiPlug and CD107a-PE were added at the same time with T cells. After co-culture, $CD4^+$ T cell responses were measured using IFN- , TNF- , IL-2 and CD107a, while $CD8^+$ responses were measured using IFN- , TNF- , MIP1β and CD107a. Strong cytokine responses of both $CD4^+$ and $CD8^+$ T cells were observed against SARS-CoV-2- infected BCL-ACE2 (**Figure 5.2 B**), confirming the role of BCL-ACE2 as a target cells for ICS assays.

Suppression assays were performed in parallel with ICS. BCL-ACE2 were infected with SARS-CoV-2 virus for 2 hours. Virus was then washed off, and SARS-CoV-2 Spike-specific $CD4^+$ or $CD8^+$ T cells were added immediately to infected BCL-ACE2 at E:T ratio of 4:1, which meant the number of T cell was 4 times that of infected BCL-ACE2. After 48-hour co-culture, the mixture of BCL-ACE2 and T cells were harvested and lysed for RNA extraction. qPCR was performed with probe that targets N1 regions of SARS-CoV-2 NP to determine the virus load in the cells. Suppression data will be discussed in the later result parts.

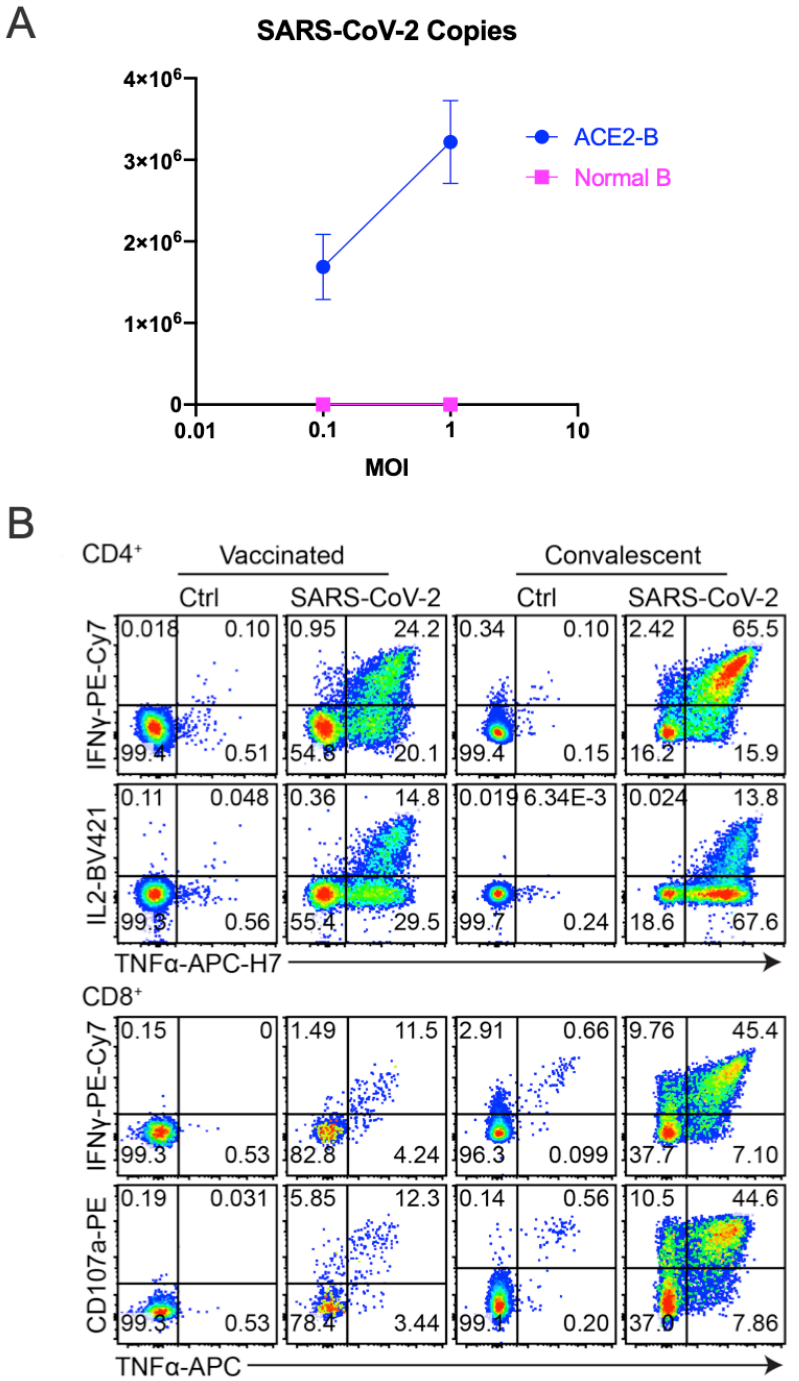


Figure 5.2 Establishment of live SARS-CoV-2 infection system. *(A) SARS-CoV-2 copies in BCLs and BCL-ACE2 24 hours post infection. Virus copies were measured by qPCR. N=3 for each MOI. (B) FACS plots showing both spike CD4⁺ and CD8⁺ responses to SARS-CoV-2-infected BCL-ACE2 in one vaccinated donor and one convalescent patient.*

5.5.3 Non-autologous BCLs were screened for target cells.

As we only managed to transduce ACE2 into 5 of the BCLs, for the other donors who didn't have autologous BCLs transduced with ACE2, we tried to select non-autologous but HLA matched BCL-ACE2 as their target cells. According to their HLA-typing (**Table 5.2**), we made a plan of target cell screening for spike-specific $CD8^+$ T cells (**Table 5.3**) and $CD4^+$ T cells (**Table 5.4**). Here, target cell screening for Spike CD4-J267 is shown as an example. C-COV19-007, -040, -046 and -047 all have overlapping HLA class II with J267. Therefore, BCLs from C-COV19-007, -040, -046, -047 and J267 were pulsed with spike peptide pools at the concentration of 0, 0.016 and 2 ng/μl for 1 hour and then were co-cultured with Spike CD4-J267 for 6 hours. Cytokine responses were detected by ICS. C-COV19-046 BCLs induced T cell responses of similar level as autologous J267 BCLs did following peptide stimulation (**Figure 5.3 A**), suggesting that the HLA class II of C-COV19-046 can present most of the $CD4^+$ epitopes as J267 and C-COV19-046 are the most matched BCLs that can be used as target cells for Spike CD4-J267.

To confirm that C-COV19-046 BCL-ACE2 can present epitopes to Spike CD4-J267 during a real infection, ICS was performed after SARS-CoV-2 infection of C-COV19-046 BCL-ACE2. Strong cytokine responses were observed (**Figure 5.3 B**), suggesting that C-COV19-046 BCL-ACE2 can be used as target cells for Spike CD4-J267 in the future infection experiments.

After target cell screening, we decided the target cells for both spike-specific $CD4^+$ and $CD8^+$ T cells of all the individuals from vaccinated and convalescent cohorts (**Table 5.5**).

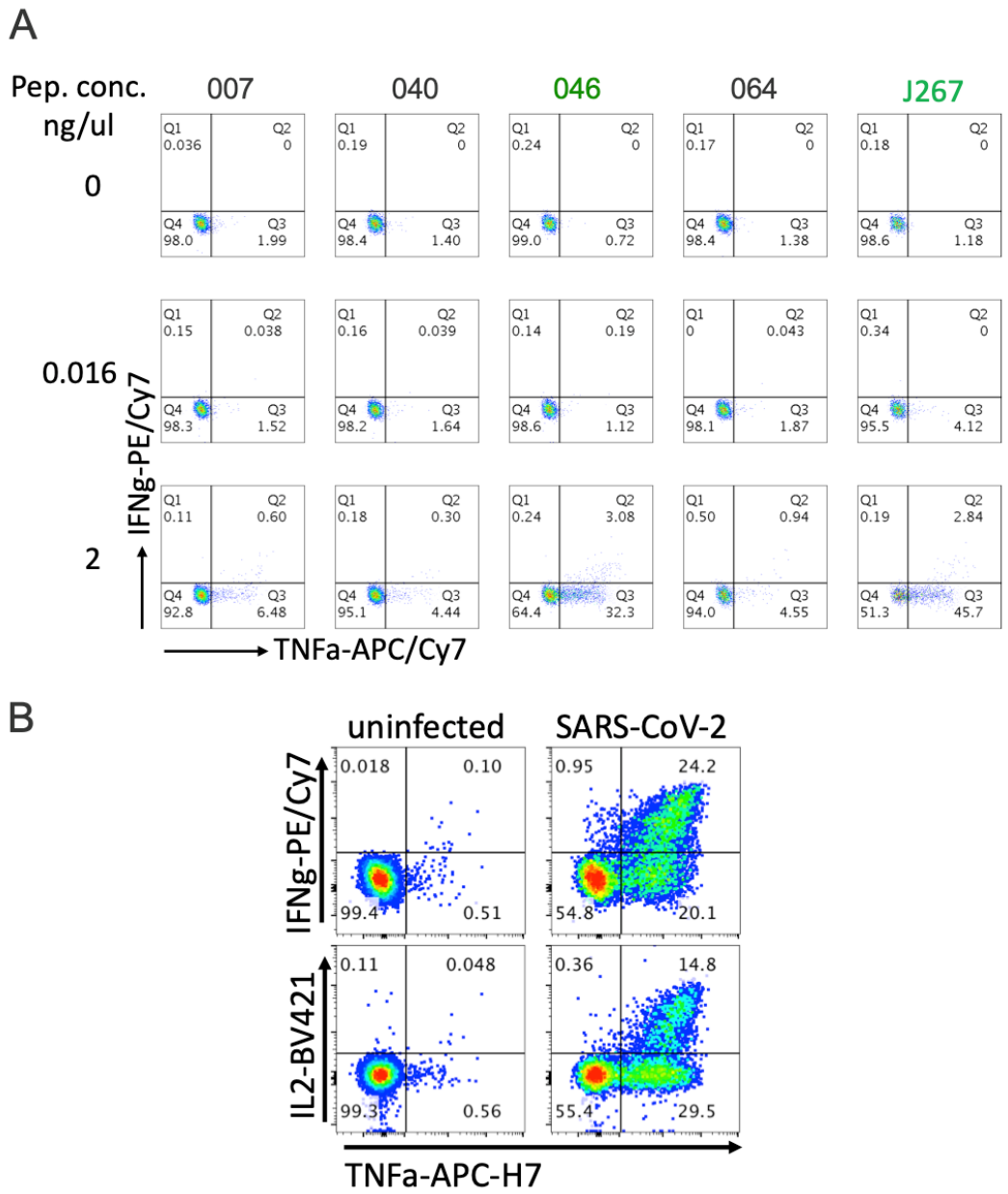


Figure 5.3 Identification of non-autologous BCLs as target cells. *(A) Screening of non-autologous BCLs for Spike CD4-J267 using Spike peptide pools. (B) FACS plots showing Spike CD4-J267 responses to SARS-CoV-2-infected 1201 BCL-ACE2.*

Table 5.2 HLA-typing of donors that don't have autologous BCL-ACE2.

	A1	A2	B1	B2	Cw1	Cw2	DRB1.1	DRB1.2	DRB345.1	DRB345.2	DQB1.1	DQB1.2	DPB.1	DPB.2
J006	*03:01:01	*24:02:01	*07:02:01	*56:01:01	*01:02:01	*07:02:01	*04:01:01	*15:01:01	DRB4	DRB5	*03:01	*06:02:01	*01:01:01	*04:01:01
J033	*24:02:01	*69:01:01	*13:02:01	*58:01:01	*03:02:02	*06:02:01	*07:01:01	*13:02:01	DRB3	DRB4	*02:02	*06:09:01	*02:01:02	*17:01:01
J167	*02:01:01	*11:01:01	*08:01:01	*51:01:01	*07:01:01	*07:02	*04:01:01	*14:54:01	DRB3	DRB4	*03:02	*05:03:01	*03:01:01	*13:01
J234	*03:01:01	*26:01:01	*15:01:01	*49:01:01	*03:03:01	*07:01:01	*04:05:01	*13:01:01	DRB3	DRB4	*03:02	*06:03:01	*02:01:02	*04:01:01
J267	*01:01:01	*02:01:01	*08:01:01	*44:02:01	*05:01:01	*07:01:01	*03:01:01	*04:01:01	DRB3	DRB4	*02:01	*03:01	*03:01:01	*16:01:01
RTH08-1105	*01:01/04N	*03:01	*07:02	*52:01	*07:02	*12:02	*15:01	*15:01	DRB5	DRB5	*06:01/06	*06:02	*04:01:01	*04:01:01

Table 5.3 Plan of target cell screening for CD8⁺ T cell lines

		A1	A2	B1	B2	Cw1	Cw2
CD8 T	J167	*02:01:01	*11:01:01	*08:01:01	*51:01:01	*07:01:01	*07:02
BCL	RTH08-1201	**02:01**	03:01	07:02	44:02	05:01/03	**07:02**
BCL	RTH08-1062	**11:01**	**11:01**	07:02	07:05/06	03:04	**07:02**
CD8 T	J234	*03:01:01	*26:01:01	*15:01:01	*49:01:01	*03:03:01	*07:01:01
BCL	RTH08-1180	01:04N	**03:01**	27:05	57:01	01:02	06:02
BCL	RTH08-1493	24:02	29:02	**15:01**	44:03	01:02	16:01
CD8 T	J267	*01:01:01	*02:01:01	*08:01:01	*44:02:01	*05:01:01	*07:01:01
BCL	RTH08-1201	**02:01**	03:01	07:02	**44:02**	**05:01/03**	07:02
BCL	RTH08-1493	24:02	29:02	15:01	**44:03**	01:02	16:01
BCL	UKCOV007	**01:01/04N**	**01:01/04N**	07:02	07:02	07:02	07:02
CD8 T	RTH08-1105	01:01/04N	03:01	07:02	52:01	07:02	12:02
BCL	UKCOV007	**01:01/04N**	**01:01/04N**	**07:02**	**07:02**	**07:02**	**07:02**
BCL	RTH08-1180	**01:04N**	**03:01**	27:05	57:01	01:02	06:02
BCL	RTH08-1201	02:01	**03:01**	**07:02**	44:02	05:01/03	**07:02**

Table 5.4 Plan of target cell screening for CD4⁺ T cell lines

		DRB1-1	DRB1-2	DRB345-1	DRB345-2	DQB1-1	DQB1-2	DPB-1	DPB-2
CD4 T	J006	*04:01:01	*15:01:01	DRB4	DRB5	*03:01/276N	*06:02:01	*01:01:01	*04:01:01
BCL	RTH08-1201	**04:01**	**15:01**	**DRB4**	**DRB5**	**03:01**	**06:02**	**04:01:01**	**04:01:01**
BCL	RTH08-1493	07:01	**15:01**	**DRB4**	**DRB5**	02	**06:02**	02:01:02	11:01:01
CD4 T	J033	*07:01:01	*13:02:01	DRB3	DRB4	*02:02	*06:09:01	*02:01:02	*17:01:01
BCL	RTH08-1493	**07:01/05-08**	15:01	**DRB4**	DRB5	**02**	06:02	**02:01:02**	11:01:01
CD4 T	J167	*04:01:01	*14:54:01	DRB3	DRB4	*03:02	*05:03:01	*03:01:01	*13:01
BCL	RTH08-1180	01:01	07:01	**DRB4**	NF	**03:03**	**05**	**03:01:01**	11:01:01
BCL	RTH08-1201	**04:01**	15:01	**DRB4**	DRB5	**03:01**	06:02	04:01:01	04:01:01
BCL	UKCOV007	11:02	15:01	**DRB3**	DRB5	**03:01**	06:02	04:01:01	**16:01:01**
CD4 T	J234	*04:05:01	*13:01:01	DRB3	DRB4	*03:02:02	*06:03:01	*02:01:02	*04:01:01
BCL	RTH08-1493	07:01/05-08	15:01	**DRB4**	DRB5	02	/10/11/13-16/	**02:01:02**	11:01:01
BCL	RTH08-1201	**04:01**	15:01	**DRB4**	DRB5	**03:01**	/10/11/13-16/	**04:01:01**	**04:01:01**
BCL	UKCOV007	11:02	15:01	**DRB3**	DRB5	**03:01**	/10/11/13-16/	**04:01:01**	**16:01:01**
CD4 T	J267	*03:01:01	*04:01:01	DRB3	DRB4	*02:01	*03:01	*03:01:01	*16:01:01
BCL	UKCOV007	11:02/21/36	15:01	**DRB3**	DRB5	**03:01**	06:02	04:01:01	**16:01:01**
BCL	RTH08-1493	07:01/05-08	15:01	**DRB4**	DRB5	**02**	06:02	02:01:02	**11:01:01**
BCL	RTH08-1201	**04:01**	15:01	**DRB4**	DRB5	**03:01**	06:02	04:01:01	04:01:01
BCL	RTH08-1180	01:01	07:01	**DRB4**	NF	**03:03**	05	**03:01:01**	11:01:01
CD4 T	RTH08-1105	15:01:00	15:01:00	DRB5	DRB5	06:01/06	06:02:00	04:01:01	04:01:01
BCL	UKCOV007	11:02	**15:01**	DRB3	**DRB5**	03:01	**06:02**	**04:01:01**	16:01:01
BCL	RTH08-1201	04:01	**15:01**	DRB4	**DRB5**	03:01	**06:02**	**04:01:01**	**04:01:01**
BCL	RTH08-1493	07:01	**15:01**	DRB4	**DRB5**	02	**06:02**	02:01:02	11:01:01

Table 5.5 Summary of target cells for each T cell line

	CD4 Target	CD8 Target
J006	C-COV19-046	C-COV19-064
J033	C-COV19-064	C-COV19-064
J167	C-COV19-040	C-COV19-046
J234	C-COV19-007, 046, 064	C-COV19-064
J267	C-COV19-046	C-COV19-064
C-COV19-036	C-COV19-064	C-COV19-040
C-COV19-040	C-COV19-040	C-COV19-040
C-COV19-046	C-COV19-046	C-COV19-046
C-COV19-047	C-COV19-047	C-COV19-047
C-COV19-064	C-COV19-064	C-COV19-064

5.5.4 Robust T cell responses was observed against original SARS-CoV-2 virus in both vaccinated and convalescent cohorts.

To evaluate SARS-CoV-2 spike-specific $CD4^+$ and $CD8^+$ responses against the original strain in both vaccinated and convalescent cohorts, target BCL-ACE2 identified above were infected with SARS-CoV-2, and then ICS and suppression were performed at the same time with matched T cell lines. $CD4^+$ T cell responses to the original SARS-CoV-2 strain were observed for 11 subjects (6 are convalescent and 5 are vaccinated), and $CD8^+$ T cell responses were observed for 9 subjects (4 are convalescent and 5 are vaccinated).

For ICS, functional $CD4^+$ T cells were measured using IFN-γ, TNF-α, IL-2 and CD107a, while $CD8^+$ T cells were IFN-γ, TNF-α, MIP1β and CD107a. Both $CD4^+$ and $CD8^+$ showed strong responses against SARS-CoV-2 live virus with expression of multiple effector molecules including multiple cytokines and degranulation markers of CD107a (**Figure 5.4 A**). No difference in $CD4^+$ or $CD8^+$ T cell functionality was observed between convalescent and vaccinated cohorts.

A strong suppression of SARS-CoV-2 replication was observed in the presence of $CD4^+$ T cells generated from both vaccinated donors and convalescent individuals (**Figure 5.4 B**), while suppression by $CD8^+$ T cells showed great variation (**Figure 5.4 C**). However, the suppression of virus replication by both spike-specific $CD4^+$ and $CD8^+$ T cells strongly correlated to the proportion of IFNγ (**Figure 5.4 D**) and TNFα (**Figure 5.4 E**) producing cells when encountering with virus-infected targets.

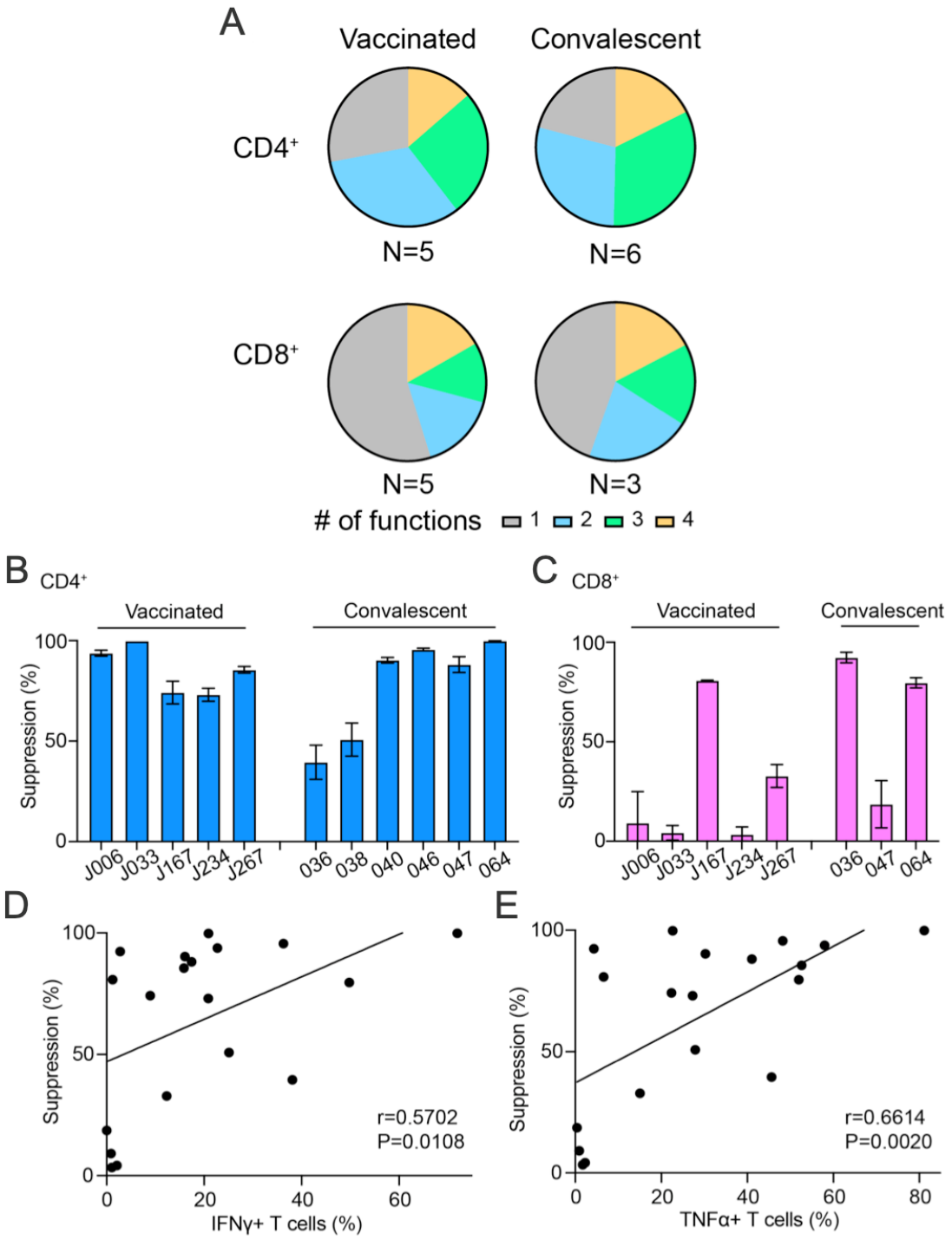


Figure 5.4 Functional evaluation of T cell responses against original SARS-CoV-2 virus in vaccinated and convalescent cohorts*. ICS and suppression were performed with SARS-CoV-2-infected BCL-ACE2 and matched T cell lines at the same time. (A) The functionality of Spike-specific CD4⁺ and CD8⁺ T cells is defined by the different combination of IFN-γ, TNF-α, CD107a and IL-2/MIP1β. (B, C) SARS-CoV-2 suppression by spike-specific CD4⁺ (B) and CD8⁺ (C) T cells. (D, E) Correlation of SARS-CoV-2 suppression with proportion of T cells producing IFN-γ (D) and TNF-α (E).*

5.5.5 Recombinant vaccinia virus system was established to evaluate antiviral T cell immune responses.

This live SARS-CoV-2 infection system is able to evaluate anti-viral efficacy of SARS-CoV-2 spike-specific T cell responses. However, this system has limitations. First of all, ACE2 transduction is challenging. Only about 1 in 5 BCLs can be stably transduced with ACE2, which limits the application of this system in a larger cohort with more people involved. Secondly, $CD8^+$ epitope loads are generally quite low in SARS-CoV-2-infected BCLs, therefore, it is hard to detect the change of $CD8^+$ response level due to the mutation. In addition, all the infection work, as well as T cell function assays, have to be done in CL3 lab, which is not available in all departments.

To overcome the weaknesses in our live virus system, another system using recombinant vaccinia virus (**Figure 5.5 A**), which also takes into account the natural processing of viral antigens, was developed by Dr. Jili Chen in our lab in collaboration with Yongxu Lu from Geoffrey L Smith's lab in Cambridge University. Spike sequences of ancestral SARS-CoV-2 were recombined into the thymidine kinase locus of the lister strain of vaccinia virus (named VV_SARS2), which is a replication competent strain that can infect almost all kinds of mammalian cells including B cells. Vaccinia virus carrying the membrane gene from Zika virus (named VV_Zika) was used as negative control. It is unlikely that any of the donors from our cohorts would have been previously exposed to Zika virus due to their county of residence being the UK and therefore T cells we tested in this study would not respond to the vaccinia virus carrying this viral antigen. In addition, experiments with vaccinia virus can be done in CL2 lab.

Both VV_SARS2 and VV_Zika showed a similar infection rate in the target BCLs (**Figure 5.5 B**). Similar to live virus system, cytokine secretion of SARS-CoV-2 spike-

specific $CD4^+$ or $CD8^+$ T cell lines was assessed by ICS after co-culturing with autologous BCLs infected with VV_SARS2 or VV_Zika. As shown in **Figure 5.5 C** and **D**, strong $CD4^+$ and $CD8^+$ T cell responses against WT spike were observed, with both $CD4^+$ and $CD8^+$ T cells displaying poly-functionality by expressing functional effector molecules including IFN-γ, TNF-α, IL-2, MIP1β and CD107a. Consistent with our live virus infection results, no differences in functionality were observed between $CD4^+$ or $CD8^+$ T cells elicited by vaccination and infection. However, the proportion of activated $CD8^+$ T cells was much greater in the vaccinia virus system compared to the live virus infection system (**Figure 3 E**), suggesting that the antigen load of spike epitopes was greatly increased.

Taken together, this data suggests that recombinant vaccinia virus can be used as alternative as live SARS-CoV-2 virus for rapid and high-throughput evaluation of T cell responses to naturally processed spike antigens.

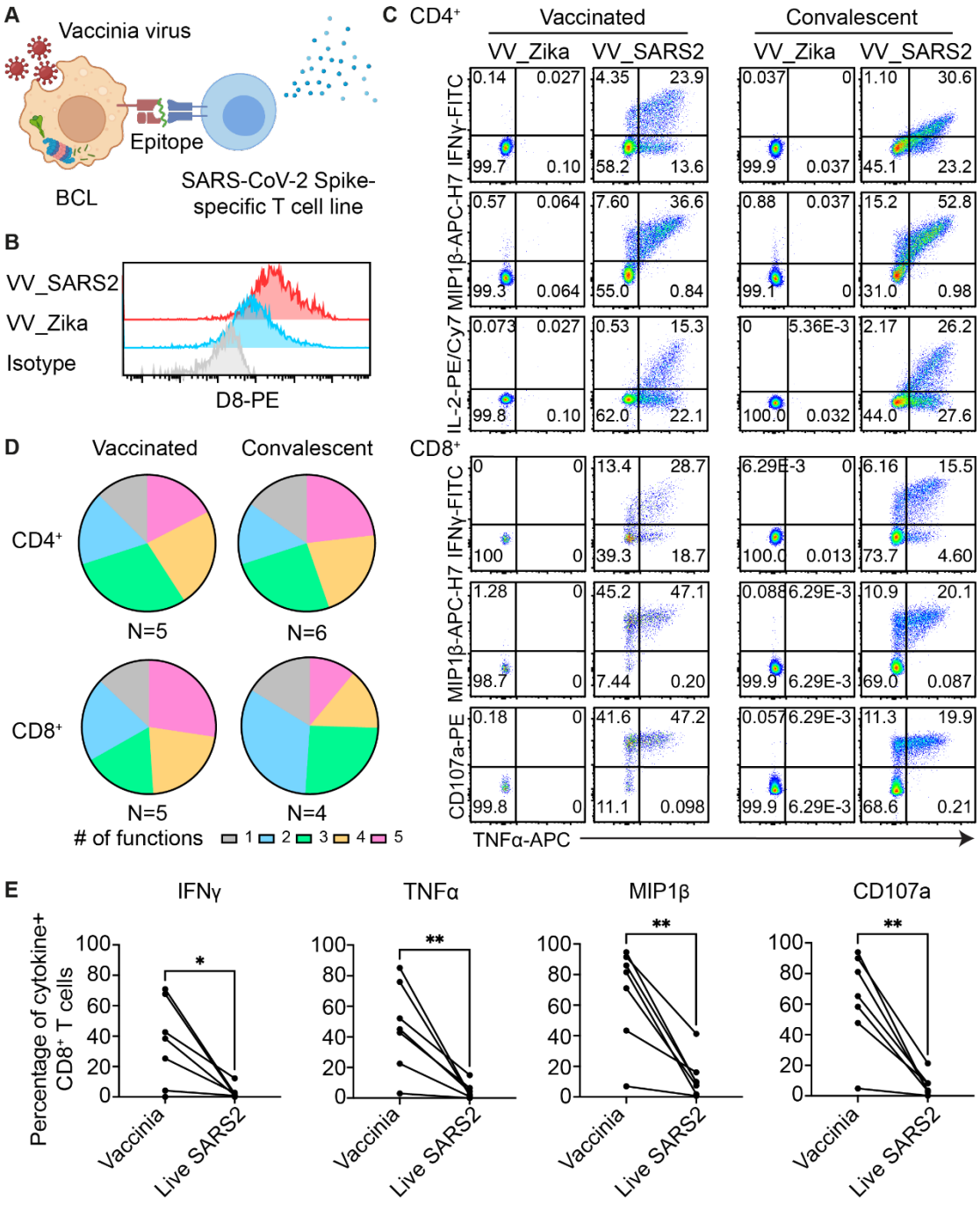


Figure 5.5 Evaluation of spike-specific CD4⁺ and CD8⁺ T cell responses to BCLs infected with VV_SARS2 or VV_Zika. *(A) Diagram of the recombinant vaccinia virus system (created with BioRender). (B) Expression of recombinant vaccinia virus in BCLs following infection. Infection rate was assessed by intracellular staining of D8 protein. Isotype: unstained control. (C) Representative cytokine responses of CD4⁺ and CD8⁺ T cells of a vaccinated participant and a convalescent patient to BCLs infected with VV_SARS2 or VV_Zika. (D) Proportion of T cells expressing 1, 2, 3, 4 or all 5 of the following functional markers: IFN-γ, TNF-α, IL-2, MIP1β and CD107a. (E) Proportion of T cells expressing IFN–γ, TNF-α, IL-2, MIP1β and CD107a following VV_SARS2 or live SARS-CoV-2 infection.*

5.5.6 Evaluation of cross-reactivity of spike-specific T cells against SARS-CoV-2 variants using both systems.

We next engaged this recombinant vaccinia virus infection system to investigate the impact of SARS-CoV-2 viral mutations on T cell recognition. Vaccinia viruses carrying spike genes of ancestral SARS-CoV-2, Alpha, Beta, Gamma, Delta and Omicron (named VV_WT, VV_Alpha, VV_Beta, VV_Gamma, VV_Delta and VV_Omicron respectively in the following context) were made. As before, T cells were co-cultured with recombinant vaccinia virus-infected autologous BCLs and their responses to the spike antigen were subsequently assessed by ICS. Strong $CD4^+$ and $CD8^+$ T cell responses against vaccinia virus carrying WT or mutant spikes were observed (**Figure 5.6 A**). For each donor, we calculated the fold-change in both $CD4^+$ T cell response (IFNγ- or IL-2-producing cells, **Figure 5.6 B**) and $CD8^+$ T cell response (IFNγ- or CD107a-expressing cells, **Figure 5.6 C**) against spike protein of VoCs compared to that seen to the WT spike. We found that most of donors showed minimal variance in T cell responses to each variant of concern spike protein with a fold change threshold of 2 (in a range between 0.6 and 2.1 as indicated by the dotted lines). This suggests that most of memory $CD4^+$ and $CD8^+$ spike T cell responses elicited by vaccination and natural infection are cross-reactive to SARS-CoV-2 VoCs. However, reduced T cell responses were also observed in some individuals against Delta or Omicron, indicating potential immune escape due to the mutation in these variants. In-depth mapping of this escape is shown in the section **5.5.7**.

In parallel with vaccinia virus system, we also assessed the recognition of T cells to live viruses including Victoria, Delta and Omicron by coculturing the T cells with BCLs infected with individual viral strains. T cell responses were evaluated by ICS. As

in vaccinia virus system, we calculated the fold-change in both $CD4^+$ T cell response (IFNγ- or IL-2-producing cells) and $CD8^+$ T cell response (IFNγ- or CD107a-expressing cells) against SARS-CoV-2 variants compared to that seen to the ancestral strain. As shown in **Figure 5.6 D** and **E**, a strong correlation of the fold change in IFNγ producing-cells and TNFα producing-cells between these two systems was observed, suggesting that recombinant vaccinia virus can be used as alternative as live SARS-CoV-2 virus for rapid and high-throughput evaluation of cross-reactivity of T cells to emerging viral variants.

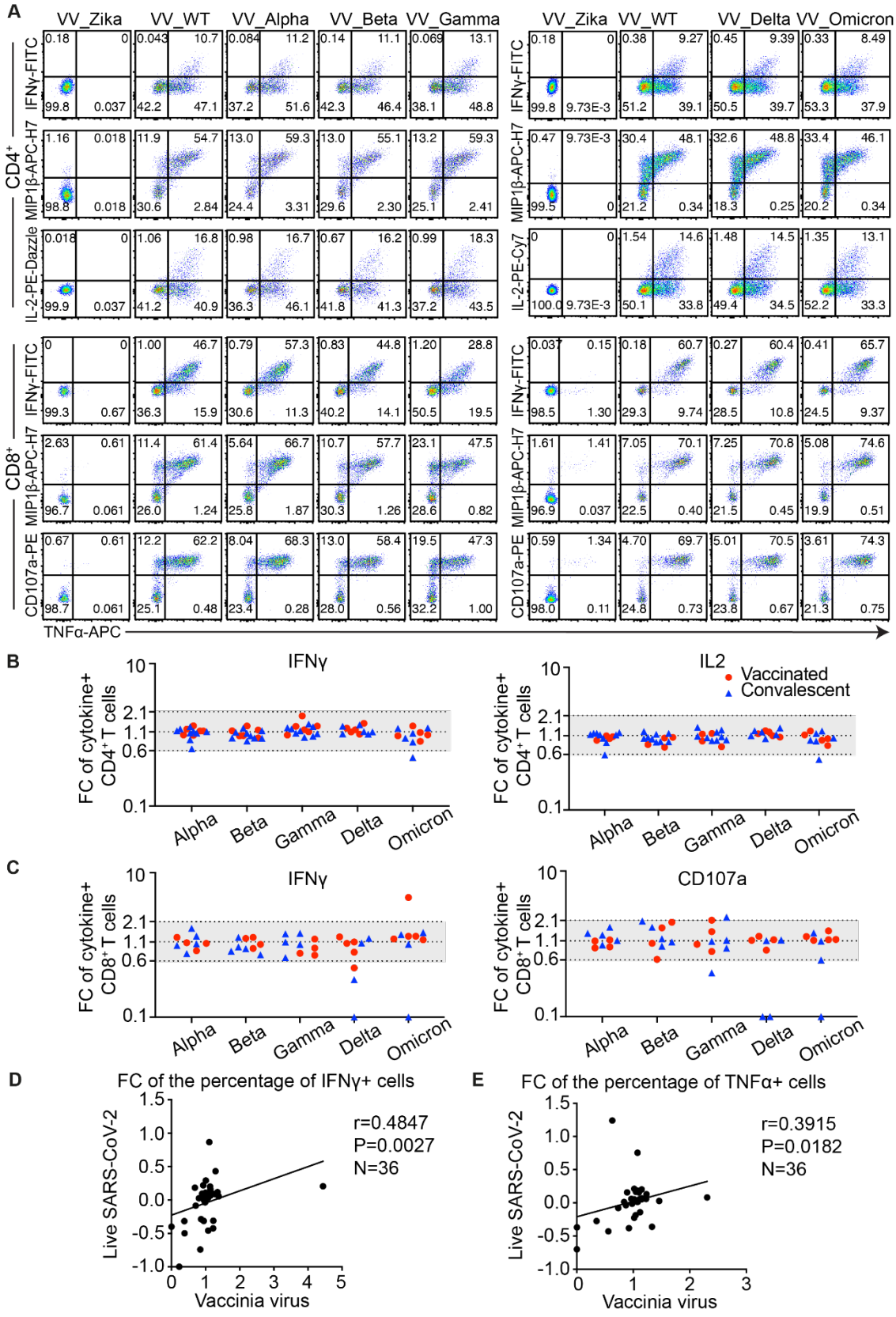


Figure 5.6 Evaluation of spike-specific CD4⁺ and CD8⁺ T cell responses to SARS-CoV-2 VoCs using recombinant vaccinia virus system and live SARS-CoV-2 infection system. *(A) Representative cytokine responses of CD4⁺ and CD8⁺ T cells of a participant to BCLs following vaccinia virus*

infection. (B) Fold-changes of the percentage of IFN + or IL2+ $CD4^+$ T cells in response to various spikes were calculated relative to that in response to WT spike. Pseudocounts 0.1 was added to each fold-change value. For Alpha, Beta and Gamma, N=13 (4 vaccinated in red and 9 convalescent in blue; for Delta and Omicron, N=11 (5 vaccinated in red and 6 convalescent in blue). (C) Fold-changes of the percentage of IFN + or CD107a+ $CD8^+$ T cells in response to spike variants were calculated relative to that in response to WT spike. Pseudocounts 0.1 was added to each fold-change value. For Alpha, Beta and Gamma, N=9 (4 vaccinated in red and 5 convalescent in blue); for Delta and Omicron, N=9 (5 vaccinated in red and 4 convalescent in blue). (D, E) Correlation of fold-change of the percentage of IFN + (D) or TNF + (E) $CD4^+$ or $CD8^+$ T cells evaluated using live SARS-CoV-2 virus and recombinant vaccinia virus. Correlation analysis was performed using Spearman's rank correlation coefficient and the two-tailed P value was calculated. The final y values plotted on graph (D, E) were derived from fold-changes, FC, evaluated using live SARS-CoV-2 infection system, following treatment with the equation $y = log_{10}(FC + 0.1)$ *. N=36 was 18 individuals responding to two strains (Delta and Omicron).*

5.5.7 T cell escape mutants were identified by vaccinia virus system and confirmed by live virus system.

Convalescent patients (36-64 days post infection) were recruited before the end of May 2020, therefore, all these patients were infected with original SARS-CoV-2 strain. While the majority of responses fell within the threshold of fold-change we set to show variance in T cell response, several outliers were also observed (**Figure 5.6 B, C**). Especially for C-COV19-040 and -047, Delta completely escaped $CD8^+$ T cell recognition. A summary of individuals whose T cell responses were reduced against VoCs is shown in **Table 5.6**. To understand how mutations in spikes of VoCs impaired T cell recognition, dominant epitopes in these individuals were then mapped and defined. If any of the dominant epitopes has known mutation sites of the SARS-CoV-2 variants, T cell lines specific to the original epitope will then be generated, and T cell responses against original or mutant epitopes will be assessed using vaccinia virus and peptides, and further confirmed by live virus. Below, identification of escape from a $CD8^+$ epitope in donor C-COV19-064 is shown as an example. Using this method we were able to identify one $CD4^+$ and three $CD8^+$ SARS-CoV-2 Spike epitopes that contain escape mutations within our small cohort.

$CD8^+$ T cell responses against VV_Omicron infected BCLs were compromised in C-COV19-064 (**Figure 5.7 A**). Since we have already known from Chapter 4 that the

dominant spike $CD8^+$ epitope in C-COV19-064 is S98, $_{489}$YFPLQSYGF$_{497}$, and it contains two mutation sites in Omicron, Q493R and G496, it is highly likely that these mutations lead to escape from T cell recognition of the S98 epitope. S98 CD8-064 T cell responses to VV_WT-, VV_Delta- and VV_Omicron-infected BCLs were then assessed by ICS. Abolished T cell responses to Omicron were again observed (**Figure 5.7 B**), suggesting that mutations in S98 escaped T cell recognition.

To further determine which mutation site contributed to the immune escape, $_{489}$YFPLRSYGF$_{497}$ (Q493R), $_{489}$YFPLQSYSF$_{497}$ (G493S) and $_{489}$YFPLRSYSF$_{497}$ (Q493R G496S) peptides were ordered from GenScript and used to test S98 CD8-064 T cell responses against original or mutant peptides-pulsed BCLs. T cell responses were observed against G496S, but not Q493R or the double mutated (**Figure 5.7 C**), suggesting that Q493R, but not G496S, in Omicron led to escape from $CD8^+$ T cell recognition.

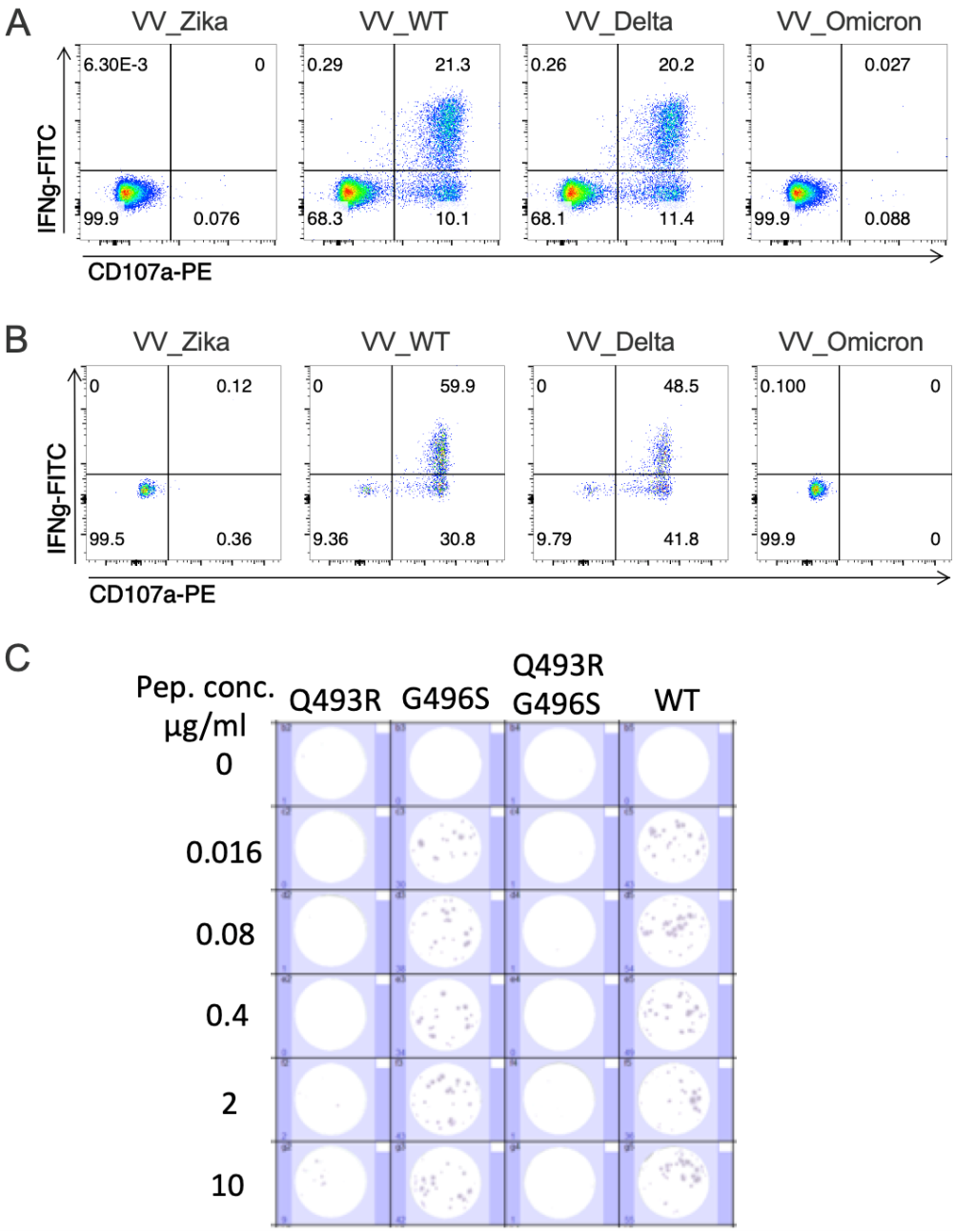


Figure 5.7 Confirmation of single escape mutation in Omicron. *Spike CD8-1493 (A), and S98 CD8-064 (B) T cell responses were assessed with VV_Zika, VV_WT, VV_Delta or VV_Omicron-infected BCLs by ICS of IFN-γ, TNF-α, IL-2, CD107a and MIP1β. (C) S98 CD8-064 T cell responses against* $_{489}$*YFPLRSYGF*$_{497}$ *(Q493R)-,* $_{489}$*YFPLQSYSF*$_{497}$ *(G493S)-,* $_{489}$*YFPLRSYSF*$_{497}$ *(Q493R G496S)- or* $_{489}$*YFPLQSYGF*$_{497}$ *(WT)-pulsed BCLs were assessed by ELISpot.*

Table 5.6 Potential T cell immune escape observed by vaccinia virus system.

	Patient ID	Alpha escape	Delta escape	Omicron escape
CD4	C-COV19-064	✓		✓
CD8	C-COV19-064			✓
	C-COV19-047		✓	
	C-COV19-040		✓	
	J033		✓	

Table 5.7 T cell epitopes that contain immune escape mutations.

Epitope ID	Epitope sequence	CD4/CD8	HLA restriction	Escaped variant	Mutation sites	Donors
S75	SASFSTFKCYGVSPT	CD4	HLA-DRB1 15:01	Omicron	N/A	C-COV19-064
S30	HKNNKSWMESEFRVY	CD8	N/A	Delta	N/A	C-COV19-040
S90	NYNYLYRLF	CD8	A*24:02	Delta	L452R	J033, C-COV19-047
S98	YFPLQSYGF	CD8	A*29:02	Omicron	G496S	C-COV19-064

5.6 Discussion

A lot has been learnt about T cell responses since the start of the SARS-CoV-2 pandemic through peptide-based and predictive assays that, while invaluable for the rapid collection of information and determination of T cell responses, do not take into account the processing of the antigens that occurs naturally. Here we have established both a live SARS-CoV-2 virus infection system and a recombinant vaccinia virus system to evaluate T cell responses to naturally processed spike antigens. Using these two systems, we evaluated SARS-CoV-2 spike-specific T cell responses from 9 people after the first dose of ChAdOx1 and 9 people recovered from COVID-19. Our data showed that SARS-CoV-2 spike-specific T cells can cross-recognize SARS-CoV-2 variants in both cohorts. T cell immune escape was also observed in one donor from the vaccinated cohort and three donors from the convalescent cohort. Mutations in one $CD4^+$ and three $CD8^+$ T cell epitopes were identified and confirmed to escape T cell recognition.

Peptide-based assays may overestimate the levels of cross reactivity between seasonal coronaviruses and SARS-CoV-2 as, although the epitope sequences are similar or identical, the flanking region of epitope sequences often differ. These differences in

the flanking regions are likely to have a major impact on antigen processing and presentation and will in turn affect cell surface epitope expression. These two systems allow us to evaluate the overall contribution to T cell escape through the entire antigen processing and presentation pathway with newly emerging viral variants. Using the vaccinia system in particular, we are able to assess T cell responses to new variants in a rapid, high-throughput manner.

Using these systems, we were able to assess the differences in vaccine- and infection-induced immunity. In our small cohort, which was limited by the proportion of BCLs successfully transduced with ACE2, we encouragingly saw relatively little difference in the activation or functionality of the memory T cells.

To transduce ACE2 into BCLs, we did lots of optimisation on promoters. One study evaluated the levels of transgene expression with lentiviral vectors containing SFFV, CMV or EF1α promoter, and showed that SFFV promoter was much stronger in driving transgene expression in Raji cells and EBV-transformed BCLs[240]. Another study demonstrated that CMV promoter gave 4- to 6-fold higher gene expression than did EF1α promoter in primary human B lymphocytes[241]. In our study, we tried three different promoters, including SFFV, CMV and EF1α. All of the promoters can induce high level of ACE2 expression in over 80% BCLs within about 7 days after transduction. However, none of these promoters can keep high expression of ACE2 longer than 14 days after transduction.

Another fact is that SARS-CoV-2 NP can be easily and stably transduced into almost all the BCLs using CMV promoter and the percentage of NP+ BCLs is normally over 90%, suggesting that CMV promoter has no problem driving transgene expression in BCLs. Similar to ACE2, transduction of SARS-CoV-2 Spike and M protein is also

difficult. We can only get around 20% of BCLs stably expressing M protein after transduction, while no BCLs can be successfully transduced with Spike. The difficulties in ACE2, Spike and M transduction indicate that membrane proteins are associated with low transduction efficiency for some reason, the cause of which requires further investigation. In addition, the success of ACE2 transduction in certain BCLs, but not all BCLs, indicates that transduction efficiency is associated with the heterogenicity of BCLs.

Nonviral methods for gene transfer into human BCLs are worth consideration. Clustered regularly interspaced short palindromic repeats (CRISPR) and CRISPR-associated protein 9 (Cas9) technology has been widely used in genome editing of primary human BCLs, especially for gene therapy[242-248]. ACE2 gene can be inserted into specific location in the host genome as designed using CRISPR/Cas9 system, while the insertion of ACE2 using lentivirus is relatively random. Therefore, CRISPR/Cas9 will potentially enhance the opportunity of stable insertion. However, CRISPR/Cas9 is unlikely to improve the stability of the expression of exogenously expressed transmembrane protein in the BCLs.

In our study, SARS-CoV-2 spike-specific $CD4^+$ and $CD8^+$ T cell lines were generated from PBMCs and expanded in vitro, while other studies used PBMCs to evaluate T cell responses to Spike antigens[216]. One of the reasons to use PBMCs is that the magnitude of T cell responses observed in PBMCs can reflect the magnitude of T cell responses in that individual, while the responses of T cell lines will change every time after expansion. However, due to the quite small percentage of SARS-CoV-2 spike-specific T cells in the whole PBMCs, it is hard to detect cytokine secretion, even after stimulation with high concentration peptides, and the percentage of cytokine+ T cells is usually below 1%[216]. Therefore, studies with PBMCs normally use AIM assays to assess

the expression of T cell activation markers, which are more sensitive than cytokine secretion. However, the cytokine secretion of IFN-γ, TNF-α and IL-2 is more direct reflection of T cell functions compared to the expression of T cell activation markers. To understand the cytokine profile of T cell responses, as well as to identify T cell immune escape, SARS-CoV-2 spike-specific T cells need to be enriched to make the cytokine responses detectable and comparable. Therefore, in this study, we chose T cell lines to investigate T cell cytokine responses following natural infection or vaccination.

Currently, there are mainly four ways to present SARS-CoV-2 spike antigens to T cells: spike peptide pools-pulsed BCLs, vaccinia virus-infected BCLs, SARS-CoV-2 protein transduced BCLs and live SARS-CoV-2-infected BCL-ACE2. Each method has their own strength and weakness (**Table 5.8**).

(1) Antigen origin, antigen processing, antigen load and antiviral efficacy. Peptides are exogenously synthesized while the other three systems are presenting T cell epitopes that are naturally processed in BCLs. Among all the four systems, antigens from live SARS-CoV-2 are the most representative of the epitopes present at the cell surface in real infection, in terms of epitope pools and epitope load. Both vaccinia virus system and SARS-CoV-2 protein transduction system only express Spike antigen, which overlooks the impact of other SARS-CoV-2 components on Spike antigen processing, as well as the impact of modification of Spike protein, such as glycosylation[249-252], on Spike antigen processing. In addition, the expression levels of Spike are usually much higher in vaccinia virus-infected BCLs and SARS-CoV-2 protein-transduced BCLs compared to live SARS-CoV-2-infected BCL-ACE2. Taken together, live SARS-CoV-2 infection system can best evaluate the true antiviral activity of SARS-CoV-2-specific T cells.

(2) Expression stability, high-throughput, overall escape and epitope escape. Although live SARS-CoV-2 infection is the ideal way to evaluate antiviral activities of T cells, it is not suitable for high-throughput screening of T cell responses in large cohorts due to the low efficiency in establishing BCL-ACE2. It is neither suitable for identification of $CD8^+$ T cell immune escape since $CD8^+$ epitope loads are generally very low at the surface of SARS-CoV-2-infected BCLs. Peptides are the traditional, as well as high-throughput, way of screening T cell responses. Peptides are also able to identify mutations within epitope regions that alter T cell responses. However, using peptides to evaluate overall T cell immune responses may overlook the impact of mutations in the flanking regions of the epitopes, which may compromise epitope generation and further reduce T cell responses. Besides peptides, vaccinia virus and protein transduction systems are also practical for high-throughput screening of T cell responses. One advantage of SARS-CoV-2 protein-transduced BCLs is that they constantly express SARS-CoV-2 epitopes at the cell surface so there is no need do peptide pulsing or virus infection before co-culture with T cells, which saves lots of time.

Table 5.8 Comparison of current methods for T cell functional evaluation.

	Peptides	Vaccinia virus infection	SARS2 protein transduction	Live SARS-CoV-2 infection
Antigen origin	Synthetic	Naturally processed	Naturally processed	Naturally processed
Antigen processing	-	++	++	+++
Antigen load	+++	++	++	+
Expression stability	+	+	+++	+
High-throughput	+++	++	++	-
Antiviral efficacy	+	+	+	+++
Overall escape	+	+++	+++	++
Epitope escape	+++	++	++	++

5.7 Future directions

In this study, we identified mutation sites that alter T cell responses. However, it is still not yet known whether the mutations in the epitope affect the binding with MHC molecules so that they cannot be presented at the cell surface, or affect the binding with TCR so that they cannot be recognized by T cells but are still available at the cell surface. To answer this question, binding affinity of mutant epitopes with MHC or TCR need further investigation. The structure of MHC-peptide-TCR complex will also help explain the impact of mutations on T cell immune responses.

BCLs were used as target cells in this study and low abundance of $CD8^+$ epitopes were observed in live SARS-CoV-2-infected BCL-ACE2. Considering that the antigen processing and presentation may be different in other antigen-presenting cells such as dendritic cells and macrophages, or epithelial cells such as lung alveolar cells, it is worthwhile testing T cell responses against other cell types following live SARS-CoV-2. Dendritic cells and macrophages can endocytose SARS-CoV-2, and lung alveolar cells have intrinsic ACE2 expression so all these three kinds of cells can be easily infected by SARS-CoV-2 without trouble of ACE2 transduction. Characterisation of T cell epitopes in various cell types will help understand T cell responses elicited at different stage of infection, as well as different sites.

We put lots of efforts in establishing a live SARS-CoV-2 infection system at the beginning of this study, however, the intrinsic incompatibility of BCLs with ACE2 limits the wide application of this method. On the other hand, vaccinia virus system was demonstrated to be a robust method to evaluate T cell responses against naturally processed antigens and suitable for high-throughput screening. In this study, vaccinia virus system was used to investigate the cross-reactivity of SARS-CoV-2 Spike-specific

T cells elicited by ChAdOx1 immunization or natural infection, and to identify potential immune escape. Besides, vaccinia virus can have wider applications not only in presenting viral antigens but also tumour antigens. Vaccinia virus expressing tumour antigens can be used for high-throughput screening of dominant T cell epitopes from that antigen.

Chapter 6

Summary and Final Discussion

The strength and efficiency of host immune responses to viral infection determine the clinical disease severity. In this study, we explored host defence against acute respiratory viruses (H1N1, H5N1 and SARS-CoV-2) from two aspects: antiviral activities of an innate immune effector, IFITM3, and dominant T cell responses against SARS-CoV-2.

In Chapter 3, by analysing RNA profiles of IFITM3$^{+/+}$ and IFITM3$^{-/-}$ A549, iPSCs and iPSDMs, we showed that the impact of IFITM3 on baseline expression of other genes was cell type-dependent. In human stem cells (iPSCs) and macrophages (iPSDMs), IFITM3 depletion only affects a small group of genes encoding membrane proteins and genes involved in tumour growth. However, in lung cells (A549), IFITM3 depletion affects a much larger group of genes involved in synapse assembly and organization, cell junction assembly, hydrolase activity, and regulation of hormone levels. Abortive infection of macrophages serves as a "dead end" for viral infection and contributes to effective host defence. Therefore, we further investigated the role of IFITM3 during virus infection in iPSDMs.

We demonstrated that IFITM3 restricted H1N1 infection in iPSDMs. Currently, IFITM3 restriction of IAV replication in macrophages has only been reported in mouse models[253]. Our data showed evidence for the first time of IFITM3-mediated H1N1 restriction in human macrophages. We analysed RNA profiles in IFITM3$^{+/+}$ and IFITM3$^{-/-}$ iPSDMs following H1N1 infection and found that lack of IFITM3 was associated with impaired upregulation of genes involved in response to virus and regulation of viral

process, viral life cycle and viral genome replication. Our findings indicate that IFITM3 is necessary in human macrophages for high anti-viral status against H1N1. Further investigations into differentially regulated genes due to IFITM3 depletion are needed to understand the underlying molecular mechanisms of IFITM3-mediated restriction.

Conversely to IAV infection, we demonstrated that endogenous IFITM3 expression was required for efficient infection of SARS-CoV-2 in iPSDMs. Similar results have been reported in human lung cells in other studies with the evidence that SARS-CoV-2 spike interacts with IFITM3 and hijacks it for efficient viral infection[66,67]. Our results suggest this may also be the case in iPSDMs. Co-immunoprecipitation assay with SARS-CoV-2-infected iPSDMs would be a good way to determine their interactions, perhaps confirming that the spike protein and IFITM3 directly interact. Moreover, live cell imaging of SARS-CoV-2-infected iPSDMs would also allow us to visualize spike and IFITM3 expression dynamically.

On the other hand, it has been reported that overexpression of IFITM3 protein in HEK293T cells prevents the entry of SARS-CoV-2[66]. It is not yet fully understood why overexpressed and endogenous IFITM3 have opposite effects on SARS-CoV-2 infection. It is possible that artificial overexpression may change the topology, localization and endocytic activity of IFITM3[254], thus further converting IFITM3 from an enhancer to an inhibitor of SARS-CoV-2 infection. While preliminary analysis of the RNA-Seq data of $IFITM3^{+/+}$ and $IFITM3^{-/-}$ iPSDMs following SARS-CoV-2 infection have been completed, further analysis and follow up experiments are needed to fully understand the role of IFITM3 during SARS-CoV-2 infection.

In Chapter 4, we demonstrated the presence of robust memory T cell responses specific for SARS-CoV-2 in the blood of donors who have recovered from COVID-19.

Broader and stronger SARS-CoV-2-specific T cell responses were observed in severe cases, compared to mild cases, which may be the result of higher viral loads and may reflect a poorly functioning innate immunity or early T cell response that failed to control the virus. Moreover, a greater proportion of overall $CD8^+$ T cell responses was observed in mild cases, compared to severe cases, suggesting a potential protective role of $CD8^+$ T cell responses in mild disease, or a pathogenic role of $CD4^+$ T cell responses in severe disease, which merits further investigation.

We identified 41 peptides containing T cell epitopes from SARS-CoV-2. The majority of $CD4^+$ epitopes derive from the spike protein, while most of the $CD8^+$ epitopes are from NP. This finding is consistent with others showing that $CD8^+$ T cells predominantly target SARS-CoV-2 NP[255]. This is very similar to influenza virus infection, where viral surface hemagglutinin elicited mostly $CD4^+$ T cell responses, whereas the majority of $CD8^+$ T cell responses were specific to viral internal proteins[205]. The immunodominant epitope regions and peptides containing T cell epitopes identified in this study will contribute to the understanding of SARS-CoV-2-specific T cells in protection and immune pathology. The identification of non-spike dominant $CD8^+$ T cell epitopes suggests the potential importance of including NP in future vaccine design.

In Chapter 5, we established both a live SARS-CoV-2 infection system and a recombinant vaccinia virus system to evaluate T cell responses to naturally processed and presented SARS-CoV-2 spike antigens. Using these two systems, we demonstrated that SARS-CoV-2 spike-specific T cells could cross-recognize VoCs in majority of the individuals after the first dose of ChAdOx1 as well as in individuals recovered from COVID-19. Additionally, we identified mutations in one $CD4^+$ epitope and three $CD8^+$ epitopes in SARS-CoV-2 spike. Our findings are consistent with others showing overall

preserved T cell responses against VoCs but scattered observations of immune escape[216,256-259]. However, these additional studies characterizing natural infection- or vaccination-induced T cell responses used peptide-based assays, which overlook the impact of mutations on antigen processing and presentation. In contrast, the two systems in our study allow us to evaluate the overall contribution to T cell escape through the entire antigen processing and presentation pathway with newly emerging viral variants. Using the vaccinia virus system, we can assess T cell responses to new variants in a rapid, high-throughput manner.

Our study of T cell immunity against SARS-CoV-2 has great implications for future vaccine design. We demonstrated the protective role of T cells in COVID-19 and the conservation of T cell epitopes in SARS-CoV-2 VoCs, highlighting the importance and necessity of inducing effective T cell responses in vaccine strategies. Vaccines designed should be able to induce $CD4^+$ and/or $CD8^+$ T cells with effector functions that directly contribute to viral clearance via cell-mediated effector mechanisms, rather than only $CD4^+$ T cell help for B cells leading to protective antibody responses.

Vaccine formulation is one of the key factors that affect the level of induced T cell responses[260]. Significant advances in cutting edge vaccine technologies over the past decade have resulted in a great variety of COVID-19 vaccine formulations, including live attenuated vaccines, inactivated vaccines, protein subunit vaccines, DNA vaccines, replication-deficient viral vectored vaccines and mRNA vaccines. Inactivated vaccines and protein subunit vaccines are known to produce poor $CD8^+$ T cell responses because they can not positively infect cells or encode antigens within the cells. DNA vaccines were at one time thought to be the ideal way of inducing T cell responses. After injection, they express the encoded antigen inside the host cells resulting in both the cellular and

humoral immunity. Unfortunately, the early successes of DNA vaccines in pre-clinical studies did not translate into clinical trials, with induction of only very low magnitude T cell responses in humans[261]. Although efforts have been made to find an adjuvant to increase the immunogenicity of DNA vaccines in humans, success has so far been modest[262]. Currently, at least eight DNA vaccine candidates are in clinical trials for COVID-19 but their abilities to induce T cell responses have not been reported yet.

Replication-deficient viral vectored vaccines now lead the field in inducing strong and broad T cell responses. Of all the replication-deficient viral vectors available, adenovirus is the most potent in priming T cell responses to the recombinant antigen. The ChAdOx1 nCoV-19 vaccine (AZD1222) investigated in this study is a replication-deficient simian adenovirus vectored vaccine[228]. We and others demonstrated that ChAdOx1 immunization could induce robust $CD4^+$ and $CD8^+$ T cell responses with multi-functionality[258]. Recombinant replication-deficient poxviruses have also been used with considerable success, and when used to boost an existing response rather than prime a novel one, the response becomes focused on the recombinant antigen rather than inducing significant anti-vector immunity[263]. Using a recombinant replication-deficient poxvirus to boost T cell responses to conserved internal influenza antigens (nucleoprotein and matrix protein 1) has shown a large expansion in circulating influenza-specific T cells after a single vaccination. However, the clinical trials were stopped after one season for futility[264].

mRNA vaccines are also able to elicit strong and broad T cell responses, owing to the efficient presentation of endogenously produced antigens on MHC class I molecules, in addition to potent $CD4^+$ T cell responses. Two mRNA vaccines, Pfizer/BioNTech and Moderna, were approved for use early in the pandemic. Strong and

long-lasting T cell immune responses have been reported following vaccination with either of the two mRNA vaccines[216].

Antigens involved in the vaccine is another key factor that will affect the level of induced T cell responses. The choice of antigens is determined by whether T cell responses against the antigen have been found to be protective, and the degree of polymorphism found between different isolates, with highly conserved antigens clearly favoured. T cell epitopes within the antigens may be identified either by bioinformatics prediction and experimental confirmation, or by taking an empirical approach using peptide library spanning the complete antigen sequence. It is possible to combine conserved regions from more than one protein to produce a synthetic vaccine antigen[265,266]. It is preferable to induce more than one antigen in the vaccine to reduce the likelihood of immune escape. Our study identified SARS-CoV-2 NP as an immunogenic antigen for $CD8^+$ T cell recognition. In addition, NP are highly conserved in VoCs and so far few mutations are near epitope regions. Highlighting the potential of including NP within future COVID-19 vaccine designs.

In conclusion, our whole study provides insights into host immune responses against acute viral respiratory infection. These include the role of IFITM3 during viral infection, and T cell immune responses against the novel pathogen, SARS-CoV-2. Our findings contribute to the understanding of host defence against respiratory viruses, which is essential in developing therapeutic interventions and vaccine strategies to better control influenza, COVID-19 and potentially future respiratory diseases caused by a viral agent.

References

1. van Doorn HR, Yu H. Viral Respiratory Infections. Hunter's Tropical Medicine and Emerging Infectious Disease. 2013;269-274. doi:10.1016/B978-1-4160-4390-4.00029-1

2. Denny FW Jr. The clinical impact of human respiratory virus infections. Am J Respir Crit Care Med. 1995 Oct;152(4 Pt 2):S4-12. doi: 10.1164/ajrccm/152.4_Pt_2.S4. PMID: 7551411..

3. Piret J, Boivin G. Pandemics Throughout History. *Front Microbiol*. 2020;11:631736. doi:10.3389/fmicb.2020.631736

4. Leung NHL. Transmissibility and transmission of respiratory viruses. *Nat Rev Microbiol*. Aug 2021;19(8):528-545. doi:10.1038/s41579-021-00535-6

5. Arbeitskreis Blut U. Influenza Virus. *Transfus Med Hemother*. 2009;36(1):32-39. doi:10.1159/000197314

6. Chen X, Liu S, Goraya MU, Maarouf M, Huang S, Chen JL. Host Immune Response to Influenza A Virus Infection. *Front Immunol*. 2018;9:320. doi:10.3389/fimmu.2018.00320

7. Sparrow E, Wood JG, Chadwick C, et al. Global production capacity of seasonal and pandemic influenza vaccines in 2019. *Vaccine*. Jan 15 2021;39(3):512-520. doi:10.1016/j.vaccine.2020.12.018

8. Okoli GN, Racovitan F, Abdulwahid T, Righolt CH, Mahmud SM. Variable seasonal influenza vaccine effectiveness across geographical regions, age groups and levels of vaccine antigenic similarity with circulating virus strains: A systematic review and meta-analysis of the evidence from test-negative design studies after the 2009/10 influenza pandemic. *Vaccine*. Feb 22 2021;39(8):1225-1240. doi:10.1016/j.vaccine.2021.01.032

9. Nauta J. Vaccine Effectiveness Studies. In: Nauta J, ed. *Statistics in Clinical and Observational Vaccine Studies*. Springer International Publishing; 2020:129-150.

10. Cevik M, Kuppalli K, Kindrachuk J, Peiris M. Virology, transmission, and pathogenesis of SARS-CoV-2. *BMJ*. Oct 23 2020;371:m3862. doi:10.1136/bmj.m3862

11. Corman VM, Muth D, Niemeyer D, Drosten C. Hosts and Sources of Endemic Human Coronaviruses. *Adv Virus Res*. 2018;100:163-188. doi:10.1016/bs.aivir.2018.01.001

12. Kahn JS, McIntosh K. History and recent advances in coronavirus discovery. *Pediatr Infect Dis J*. Nov 2005;24(11 Suppl):S223-7, discussion S226. doi:10.1097/01.inf.0000188166.17324.60

13. V'Kovski P, Kratzel A, Steiner S, Stalder H, Thiel V. Coronavirus biology and replication: implications for SARS-CoV-2. *Nat Rev Microbiol*. Mar 2021;19(3):155-170. doi:10.1038/s41579-020-00468-6

14. Jamison DA, Jr., Anand Narayanan S, Trovao NS, et al. A comprehensive SARS-CoV-2 and COVID-19 review, Part 1: Intracellular overdrive for SARS-CoV-2 infection. *Eur J Hum Genet*. Aug 2022;30(8):889-898. doi:10.1038/s41431-022-01108-8

15. Grellet E, L'Hote I, Goulet A, Imbert I. Replication of the coronavirus genome: A paradox among positive-strand RNA viruses. *J Biol Chem*. May 2022;298(5):101923. doi:10.1016/j.jbc.2022.101923

16. Shrotri M, Swinnen T, Kampmann B, Parker EPK. An interactive website tracking COVID-19 vaccine development. *The Lancet Global Health*. 2021;9(5):e590-e592. doi:10.1016/s2214-109x(21)00043-7

17. Lou F, Li M, Pang Z, et al. Understanding the Secret of SARS-CoV-2 Variants of Concern/Interest and Immune Escape. *Front Immunol*. 2021;12:744242. doi:10.3389/fimmu.2021.744242

18. Li M, Lou F, Fan H. SARS-CoV-2 variants: a new challenge to convalescent serum and mRNA vaccine neutralization efficiency. *Signal Transduct Target Ther*. Apr 10 2021;6(1):151. doi:10.1038/s41392-021-00592-6

19. Pilishvili T, Gierke R, Fleming-Dutra KE, et al. Effectiveness of mRNA Covid-19 Vaccine among U.S. Health Care Personnel. *N Engl J Med*. Dec 16 2021;385(25):e90. doi:10.1056/NEJMoa2106599

20. Jensen S, Thomsen AR. Sensing of RNA viruses: a review of innate immune receptors involved in recognizing RNA virus invasion. *J Virol*. Mar 2012;86(6):2900-10. doi:10.1128/JVI.05738-11

21. Akira S, Uematsu S, Takeuchi O. Pathogen recognition and innate immunity. *Cell*. Feb 24 2006;124(4):783-801. doi:10.1016/j.cell.2006.02.015

22. Akira S, Takeda K. Toll-like receptor signalling. *Nat Rev Immunol*. Jul 2004;4(7):499-511. doi:10.1038/nri1391

23. O'Neill LA. How Toll-like receptors signal: what we know and what we don't know. *Curr Opin Immunol*. Feb 2006;18(1):3-9. doi:10.1016/j.coi.2005.11.012

24. Yoneyama M, Kikuchi M, Natsukawa T, et al. The RNA helicase RIG-I has an essential function in double-stranded RNA-induced innate antiviral responses. *Nat Immunol*. Jul 2004;5(7):730-7. doi:10.1038/ni1087

25. Kang DC, Gopalkrishnan RV, Lin L, et al. Expression analysis and genomic characterization of human melanoma differentiation associated gene-5, mda-5: a novel type I interferon-responsive apoptosis-inducing gene. *Oncogene*. Mar 4 2004;23(9):1789-800. doi:10.1038/sj.onc.1207300

26. Yoneyama M, Kikuchi M, Matsumoto K, et al. Shared and unique functions of the DExD/H-box helicases RIG-I, MDA5, and LGP2 in antiviral innate immunity. *J Immunol*. Sep 1 2005;175(5):2851-8. doi:10.4049/jimmunol.175.5.2851

27. Kanneganti TD, Lamkanfi M, Nunez G. Intracellular NOD-like receptors in host defense and disease. *Immunity*. Oct 2007;27(4):549-59. doi:10.1016/j.immuni.2007.10.002

28. Petrilli V, Dostert C, Muruve DA, Tschopp J. The inflammasome: a danger sensing complex triggering innate immunity. *Curr Opin Immunol*. Dec 2007;19(6):615-22. doi:10.1016/j.coi.2007.09.002

29. Takeuchi O, Akira S. Innate immunity to virus infection. *Immunol Rev*. Jan 2009;227(1):75-86. doi:10.1111/j.1600-065X.2008.00737.x

30. Honda K, Takaoka A, Taniguchi T. Type I interferon [corrected] gene induction by the interferon regulatory factor family of transcription factors. *Immunity*. Sep 2006;25(3):349-60. doi:10.1016/j.immuni.2006.08.009

31. Platanias LC. Mechanisms of type-I- and type-II-interferon-mediated signalling. *Nat Rev Immunol*. May 2005;5(5):375-86. doi:10.1038/nri1604

32. Stark GR, Darnell JE, Jr. The JAK-STAT pathway at twenty. *Immunity*. Apr 20 2012;36(4):503-14. doi:10.1016/j.immuni.2012.03.013

33. Schneider WM, Chevillotte MD, Rice CM. Interferon-stimulated genes: a complex web of host defenses. *Annu Rev Immunol*. 2014;32:513-45. doi:10.1146/annurev-immunol-032713-120231

34. Wang F, Ma Y, Barrett JW, et al. Disruption of Erk-dependent type I interferon induction breaks the myxoma virus species barrier. *Nat Immunol*. Dec 2004;5(12):1266-74. doi:10.1038/ni1132

35. Saleiro D, Platanias LC. Intersection of mTOR and STAT signaling in immunity. *Trends Immunol*. Jan 2015;36(1):21-9. doi:10.1016/j.it.2014.10.006

36. Schreiber G. The molecular basis for differential type I interferon signaling. *J Biol Chem*. May 5 2017;292(18):7285-7294. doi:10.1074/jbc.R116.774562

37. Jiang D, Weidner JM, Qing M, et al. Identification of five interferon-induced cellular proteins that inhibit west nile virus and dengue virus infections. *J Virol*. Aug 2010;84(16):8332-41. doi:10.1128/JVI.02199-09

38. Brass AL, Huang IC, Benita Y, et al. The IFITM proteins mediate cellular resistance to influenza A H1N1 virus, West Nile virus, and dengue virus. *Cell*. Dec 24 2009;139(7):1243-54. doi:10.1016/j.cell.2009.12.017

39. Zhang Y, Burke CW, Ryman KD, Klimstra WB. Identification and characterization of interferon-induced proteins that inhibit alphavirus replication. *J Virol*. Oct 2007;81(20):11246-55. doi:10.1128/JVI.01282-07

40. Schoggins JW, Wilson SJ, Panis M, et al. A diverse range of gene products are effectors of the type I interferon antiviral response. *Nature*. Apr 28 2011;472(7344):481-5. doi:10.1038/nature09907

41. Neil S, Bieniasz P. Human immunodeficiency virus, restriction factors, and interferon. *J Interferon Cytokine Res*. Sep 2009;29(9):569-80. doi:10.1089/jir.2009.0077

42. Wang X, Hinson ER, Cresswell P. The interferon-inducible protein viperin inhibits influenza virus release by perturbing lipid rafts. *Cell Host Microbe*. Aug 16 2007;2(2):96-105. doi:10.1016/j.chom.2007.06.009

43. Der SD, Zhou A, Williams BR, Silverman RH. Identification of genes differentially regulated by interferon alpha, beta, or gamma using oligonucleotide arrays. Proc Natl Acad Sci U S A. 1998 Dec 22;95(26):15623-8. doi: 10.1073/pnas.95.26.15623. PMID: 9861020; PMCID: PMC28094..

44. Lanford RE, Guerra B, Lee H, Chavez D, Brasky KM, Bigger CB. Genomic response to interferon-alpha in chimpanzees: implications of rapid downregulation for hepatitis C kinetics. *Hepatology*. May 2006;43(5):961-72. doi:10.1002/hep.21167

45. Zhao X, Li J, Winkler CA, An P, Guo JT. IFITM Genes, Variants, and Their Roles in the Control and Pathogenesis of Viral Infections. *Front Microbiol*. 2018;9:3228. doi:10.3389/fmicb.2018.03228

46. Liao Y, Goraya MU, Yuan X, Zhang B, Chiu SH, Chen JL. Functional Involvement of Interferon-Inducible Transmembrane Proteins in Antiviral Immunity. *Front Microbiol*. 2019;10:1097. doi:10.3389/fmicb.2019.01097

47. Bailey CC, Zhong G, Huang IC, Farzan M. IFITM-Family Proteins: The Cell's First Line of Antiviral Defense. *Annu Rev Virol*. Nov 1 2014;1:261-283. doi:10.1146/annurev-virology-031413-085537

48. Lozach PY, Huotari J, Helenius A. Late-penetrating viruses. *Curr Opin Virol*. Jul 2011;1(1):35-43. doi:10.1016/j.coviro.2011.05.004

49. Perreira JM, Chin CR, Feeley EM, Brass AL. IFITMs restrict the replication of multiple pathogenic viruses. *J Mol Biol*. Dec 13 2013;425(24):4937-55. doi:10.1016/j.jmb.2013.09.024

50. Mudhasani R, Tran JP, Retterer C, et al. IFITM-2 and IFITM-3 but not IFITM-1 restrict Rift Valley fever virus. *J Virol*. Aug 2013;87(15):8451-64. doi:10.1128/JVI.03382-12

51. Karlas A, Machuy N, Shin Y, et al. Genome-wide RNAi screen identifies human host factors crucial for influenza virus replication. *Nature*. Feb 11 2010;463(7282):818-22. doi:10.1038/nature08760

52. Everitt AR, Clare S, Pertel T, et al. IFITM3 restricts the morbidity and mortality associated with influenza. *Nature*. Mar 25 2012;484(7395):519-23. doi:10.1038/nature10921

53. Zhang YH, Zhao Y, Li N, et al. Interferon-induced transmembrane protein-3 genetic variant rs12252-C is associated with severe influenza in Chinese individuals. *Nat Commun*. 2013;4:1418. doi:10.1038/ncomms2433

54. Huang IC, Bailey CC, Weyer JL, et al. Distinct patterns of IFITM-mediated restriction of filoviruses, SARS coronavirus, and influenza A virus. *PLoS Pathog*. Jan 6 2011;7(1):e1001258. doi:10.1371/journal.ppat.1001258

55. Ling S, Zhang C, Wang W, et al. Combined approaches of EPR and NMR illustrate only one transmembrane helix in the human IFITM3. *Sci Rep*. Apr 5 2016;6:24029. doi:10.1038/srep24029

56. Dou D, Revol R, Ostbye H, Wang H, Daniels R. Influenza A Virus Cell Entry, Replication, Virion Assembly and Movement. *Front Immunol*. 2018;9:1581. doi:10.3389/fimmu.2018.01581

57. Li K, Markosyan RM, Zheng YM, et al. IFITM proteins restrict viral membrane hemifusion. *PLoS Pathog*. Jan 2013;9(1):e1003124. doi:10.1371/journal.ppat.1003124

58. Desai TM, Marin M, Chin CR, Savidis G, Brass AL, Melikyan GB. IFITM3 restricts influenza A virus entry by blocking the formation of fusion pores following virus-endosome hemifusion. *PLoS Pathog*. Apr 2014;10(4):e1004048. doi:10.1371/journal.ppat.1004048

59. Spence JS, He R, Hoffmann HH, et al. IFITM3 directly engages and shuttles incoming virus particles to lysosomes. *Nat Chem Biol*. Mar 2019;15(3):259-268. doi:10.1038/s41589-018-0213-2

60. Wee YS, Roundy KM, Weis JJ, Weis JH. Interferon-inducible transmembrane proteins of the innate immune response act as membrane organizers by influencing clathrin and v-ATPase localization and function. *Innate Immun*. Dec 2012;18(6):834-45. doi:10.1177/1753425912443392

61. Fu B, Wang L, Li S, Dorf ME. ZMPSTE24 defends against influenza and other pathogenic viruses. *J Exp Med*. Apr 3 2017;214(4):919-929. doi:10.1084/jem.20161270

62. Jiang LQ, Xia T, Hu YH, et al. IFITM3 inhibits virus-triggered induction of type I interferon by mediating autophagosome-dependent degradation of IRF3. *Cell Mol Immunol*. Sep 2018;15(9):858-867. doi:10.1038/cmi.2017.15

63. Clement M, Forbester JL, Marsden M, et al. IFITM3 restricts virus-induced inflammatory cytokine production by limiting Nogo-B mediated TLR responses. *Nat Commun*. Sep 8 2022;13(1):5294. doi:10.1038/s41467-022-32587-4

64. Regino-Zamarripa NE, Ramirez-Martinez G, Jimenez-Alvarez LA, et al. Differential Leukocyte Expression of IFITM1 and IFITM3 in Patients with Severe Pandemic Influenza A(H1N1) and COVID-19. *J Interferon Cytokine Res*. Jun 14 2022;doi:10.1089/jir.2022.0036

65. Gilbert C, Lefeuvre C, Preisser L, et al. Age-Related Expression of IFN-lambda1 Versus IFN-I and Beta-Defensins in the Nasopharynx of SARS-CoV-2-Infected Individuals. *Front Immunol*. 2021;12:750279. doi:10.3389/fimmu.2021.750279

66. Prelli Bozzo C, Nchioua R, Volcic M, et al. IFITM proteins promote SARS-CoV-2 infection and are targets for virus inhibition in vitro. *Nat Commun*. Jul 28 2021;12(1):4584. doi:10.1038/s41467-021-24817-y

67. Shi G, Kenney AD, Kudryashova E, et al. Opposing activities of IFITM proteins in SARS-CoV-2 infection. *EMBO J*. Feb 1 2021;40(3):e106501. doi:10.15252/embj.2020106501

68. Buchrieser J, Dufloo J, Hubert M, et al. Syncytia formation by SARS-CoV-2-infected cells. *EMBO J*. Dec 1 2020;39(23):e106267. doi:10.15252/embj.2020106267

69. <IFITMs promote VoC infection.pdf>.

70. Westphalen K, Gusarova GA, Islam MN, et al. Sessile alveolar macrophages communicate with alveolar epithelium to modulate immunity. *Nature*. Feb 27 2014;506(7489):503-6. doi:10.1038/nature12902

71. Tumpey TM, Garcia-Sastre A, Taubenberger JK, et al. Pathogenicity of influenza viruses with genes from the 1918 pandemic virus: functional roles of alveolar macrophages and neutrophils in limiting virus replication and mortality in mice. *J Virol*. Dec 2005;79(23):14933-44. doi:10.1128/JVI.79.23.14933-14944.2005

72. Murphy EA, Davis JM, McClellan JL, Carmichael MD, Rooijen NV, Gangemi JD. Susceptibility to infection and inflammatory response following influenza virus (H1N1, A/PR/8/34) challenge: role of macrophages. *J Interferon Cytokine Res*. Jun 2011;31(6):501-8. doi:10.1089/jir.2010.0143

73. Guilliams M, Lambrecht BN, Hammad H. Division of labor between lung dendritic cells and macrophages in the defense against pulmonary infections. *Mucosal Immunol*. May 2013;6(3):464-73. doi:10.1038/mi.2013.14

74. Hargadon KM, Zhou H, Albrecht RA, Dodd HA, Garcia-Sastre A, Braciale TJ. Major histocompatibility complex class II expression and hemagglutinin subtype influence the infectivity of type A influenza virus for respiratory dendritic cells. *J Virol*. Nov 2011;85(22):11955-63. doi:10.1128/JVI.05830-11

75. Ichinohe T, Pang IK, Kumamoto Y, et al. Microbiota regulates immune defense against respiratory tract influenza A virus infection. *Proc Natl Acad Sci U S A*. Mar 29 2011;108(13):5354-9. doi:10.1073/pnas.1019378108

76. Desch AN, Randolph GJ, Murphy K, et al. CD103+ pulmonary dendritic cells preferentially acquire and present apoptotic cell-associated antigen. *J Exp Med*. Aug 29 2011;208(9):1789-97. doi:10.1084/jem.20110538

77. Baumeister W, Walz J, Zühl F, Seemüller E. The proteasome: paradigm of a self-compartmentalizing protease. Cell. 1998 Feb 6;92(3):367-80. doi: 10.1016/s0092-8674(00)80929-0. PMID: 9476896.

78. Uebel S, Tampé R. Specificity of the proteasome and the TAP transporter. Curr Opin Immunol. 1999 Apr;11(2):203-8. doi: 10.1016/s0952-7915(99)80034-x. PMID: 10322157.

79. Abele R, Tampé R. Function of the transport complex TAP in cellular immune recognition. Biochim Biophys Acta. 1999 Dec 6;1461(2):405-19. doi: 10.1016/s0005-2736(99)00171-6. PMID: 10581370.

80. The ABCs of Immunology: Structure and Function of TAP, the Transporter Associated with Antigen Processing Rupert Abele and Robert Tampé Physiology 2004 19:4, 216-224

81. Tanaka K. The proteasome: overview of structure and functions. Proc Jpn Acad Ser B Phys Biol Sci. 2009;85(1):12-36. doi:10.2183/pjab.85.12

82. Murata S, Takahama Y, Kasahara M, Tanaka K. The immunoproteasome and thymoproteasome: functions, evolution and human disease. *Nat Immunol*. Sep 2018;19(9):923-931. doi:10.1038/s41590-018-0186-z

83. Reits E, Neijssen J, Herberts C, Benckhuijsen W, Janssen L, Drijfhout JW, Neefjes J. A major role for TPPII in trimming proteasomal degradation products for MHC class I antigen presentation. Immunity. 2004 Apr;20(4):495-506. doi: 10.1016/s1074-7613(04)00074-3. PMID: 15084277.

84. Beninga J, Rock KL, Goldberg AL. Interferon-gamma can stimulate post-proteasomal trimming of the N terminus of an antigenic peptide by inducing leucine aminopeptidase. *J Biol Chem*. Jul 24 1998;273(30):18734-42. doi:10.1074/jbc.273.30.18734

85. Kessler JH, Khan S, Seifert U, et al. Antigen processing by nardilysin and thimet oligopeptidase generates cytotoxic T cell epitopes. *Nat Immunol*. Jan 2011;12(1):45-53. doi:10.1038/ni.1974

86. Stoltze L, Schirle M, Schwarz G, Schröter C, Thompson MW, Hersh LB, Kalbacher H, Stevanovic S, Rammensee HG, Schild H. Two new proteases in the MHC class I processing pathway. Nat Immunol. 2000 Nov;1(5):413-8. doi: 10.1038/80852. PMID: 11062501.

87. Lopez de Castro JA. How ERAP1 and ERAP2 Shape the Peptidomes of Disease-Associated MHC-I Proteins. *Front Immunol*. 2018;9:2463. doi:10.3389/fimmu.2018.02463

88. Hammer GE, Gonzalez F, James E, Nolla H, Shastri N. In the absence of aminopeptidase ERAAP, MHC class I molecules present many unstable and highly immunogenic peptides. *Nat Immunol*. Jan 2007;8(1):101-8. doi:10.1038/ni1409

89. Neumann L, Tampé R. Kinetic analysis of peptide binding to the TAP transport complex: evidence for structural rearrangements induced by substrate binding. J Mol Biol. 1999 Dec 17;294(5):1203-13. doi: 10.1006/jmbi.1999.3329. PMID: 10600378.

90. Grandea AG 3rd, Van Kaer L. Tapasin: an ER chaperone that controls MHC class I assembly with peptide. Trends Immunol. 2001 Apr;22(4):194-9. doi: 10.1016/s1471-4906(01)01861-0. PMID: 11274924.

91. Cresswell P, Bangia N, Dick T, Diedrich G. The nature of the MHC class I peptide loading complex. Immunol Rev. 1999 Dec;172:21-8. doi: 10.1111/j.1600-065x.1999.tb01353.x. PMID: 10631934.

92. Sharipo A, Imreh M, Leonchiks A, Imreh S, Masucci MG. A minimal glycine-alanine repeat prevents the interaction of ubiquitinated I kappaB alpha with the proteasome: a new mechanism for selective inhibition of proteolysis. Nat Med. 1998 Aug;4(8):939-44. doi: 10.1038/nm0898-939. PMID: 9701247.

93. Shen L, Sigal LJ, Boes M, Rock KL. Important role of cathepsin S in generating peptides for TAP-independent MHC class I crosspresentation in vivo. *Immunity*. Aug 2004;21(2):155-65. doi:10.1016/j.immuni.2004.07.004

94. Kovacsovics-Bankowski M, Rock KL. A phagosome-to-cytosol pathway for exogenous antigens presented on MHC class I molecules. Science. 1995 Jan 13;267(5195):243-6. doi: 10.1126/science.7809629. PMID: 7809629.

95. Smed-Sorensen A, Chalouni C, Chatterjee B, et al. Influenza A virus infection of human primary dendritic cells impairs their ability to cross-present antigen to CD8 T cells. *PLoS Pathog*. 2012;8(3):e1002572. doi:10.1371/journal.ppat.1002572

96. Bender BS, Croghan T, Zhang L, Small PA Jr. Transgenic mice lacking class I major histocompatibility complex-restricted T cells have delayed viral clearance and increased mortality after influenza virus challenge. J Exp Med. 1992 Apr 1;175(4):1143-5. doi: 10.1084/jem.175.4.1143. PMID: 1552285; PMCID: PMC2119177.

97. Bromley SK, Mempel TR, Luster AD. Orchestrating the orchestrators: chemokines in control of T cell traffic. *Nat Immunol*. Sep 2008;9(9):970-80. doi:10.1038/ni.f.213

98. Osinska I, Popko K, Demkow U. Perforin: an important player in immune response. *Cent Eur J Immunol*. 2014;39(1):109-15. doi:10.5114/ceji.2014.42135

99. <apoptosis by death factor.pdf>.

100. Hu X, Ivashkiv LB. Cross-regulation of signaling pathways by interferon-gamma: implications for immune responses and autoimmune diseases. *Immunity*. Oct 16 2009;31(4):539-50. doi:10.1016/j.immuni.2009.09.002

101. Ziegler HK, Unanue ER. Decrease in macrophage antigen catabolism caused by ammonia and chloroquine is associated with inhibition of antigen presentation to T cells. Proc Natl Acad Sci U S A. 1982 Jan;79(1):175-8. doi: 10.1073/pnas.79.1.175. PMID: 6798568; PMCID: PMC345685.

102. Cell, Vol. 84, 505–507, February 23, 1996,

103. Immunity, Vol. 10, 197–206, February, 1999,

104. Mellins ED, Stern LJ. HLA-DM and HLA-DO, key regulators of MHC-II processing and presentation. *Curr Opin Immunol*. Feb 2014;26:115-22. doi:10.1016/j.coi.2013.11.005

105. Boyden AW, Legge KL, Waldschmidt TJ. Pulmonary infection with influenza A virus induces site-specific germinal center and T follicular helper cell responses. *PLoS One*. 2012;7(7):e40733. doi:10.1371/journal.pone.0040733

106. Fuse S, Tsai CY, Molloy MJ, et al. Recall responses by helpless memory CD8+ T cells are restricted by the up-regulation of PD-1. *J Immunol*. Apr 1 2009;182(7):4244-54. doi:10.4049/jimmunol.0802041

107. Ann Rheum Dis 2002;61(Suppl II):ii54–ii58.

108. Aberdein JD, Cole J, Bewley MA, Marriott HM, Dockrell DH. Alveolar macrophages in pulmonary host defence the unrecognized role of apoptosis as a

mechanism of intracellular bacterial killing. *Clin Exp Immunol*. Nov 2013;174(2):193-202. doi:10.1111/cei.12170

109. Belz GT, Wodarz D, Diaz G, Nowak MA, Doherty PC. Compromised influenza virus-specific CD8(+)-T-cell memory in CD4(+)-T-cell-deficient mice. *J Virol*. Dec 2002;76(23):12388-93. doi:10.1128/jvi.76.23.12388-12393.2002

110. Knaut H, Werz C, Geisler R, Nusslein-Volhard C, Tubingen Screen C. A zebrafish homologue of the chemokine receptor Cxcr4 is a germ-cell guidance receptor. *Nature*. Jan 16 2003;421(6920):279-82. doi:10.1038/nature01338

111. NATURE | VOL 393 | 4 JUNE 1998.

112. Zhang S, Zhang H, Zhao J. The role of CD4 T cell help for CD8 CTL activation. *Biochem Biophys Res Commun*. Jul 10 2009;384(4):405-8. doi:10.1016/j.bbrc.2009.04.134

113. Crotty S. A brief history of T cell help to B cells. *Nat Rev Immunol*. Mar 2015;15(3):185-9. doi:10.1038/nri3803

114. J Immunol 1982; 128:233-238;

115. Aghbash PS, Hemmat N, Nahand JS, et al. The role of Th17 cells in viral infections. *Int Immunopharmacol*. Feb 2021;91:107331. doi:10.1016/j.intimp.2020.107331

116. Antunes I, Kassiotis G. Suppression of innate immune pathology by regulatory T cells during Influenza A virus infection of immunodeficient mice. *J Virol*. Dec 2010;84(24):12564-75. doi:10.1128/JVI.01559-10

117. Wakim LM, Gupta N, Mintern JD, Villadangos JA. Enhanced survival of lung tissue-resident memory CD8(+) T cells during infection with influenza virus due to selective expression of IFITM3. *Nat Immunol*. Mar 2013;14(3):238-45. doi:10.1038/ni.2525

118. Helft J, Manicassamy B, Guermonprez P, et al. Cross-presenting CD103+ dendritic cells are protected from influenza virus infection. *J Clin Invest*. Nov 2012;122(11):4037-47. doi:10.1172/JCI60659

119. Stacey MA, Clare S, Clement M, et al. The antiviral restriction factor IFN-induced transmembrane protein 3 prevents cytokine-driven CMV pathogenesis. *J Clin Invest*. Apr 3 2017;127(4):1463-1474. doi:10.1172/JCI84889

120. Lanz C, Schotsaert M, Magnus C, et al. IFITM3 incorporation sensitizes influenza A virus to antibody-mediated neutralization. *J Exp Med*. Jun 7 2021;218(6)doi:10.1084/jem.20200303

121. Ahmadi I, Afifipour A, Sakhaee F, et al. Impact of interferon-induced transmembrane protein 3 gene rs12252 polymorphism on COVID-19 mortality. *Cytokine*. Sep 2022;157:155957. doi:10.1016/j.cyto.2022.155957

122. Zhang Y, Qin L, Zhao Y, et al. Interferon-Induced Transmembrane Protein 3 Genetic Variant rs12252-C Associated With Disease Severity in Coronavirus Disease 2019. *J Infect Dis*. Jun 16 2020;222(1):34-37. doi:10.1093/infdis/jiaa224

123. Gomez J, Albaiceta GM, Cuesta-Llavona E, et al. The Interferon-induced transmembrane protein 3 gene (IFITM3) rs12252 C variant is associated with COVID-19. *Cytokine*. Jan 2021;137:155354. doi:10.1016/j.cyto.2020.155354

124. Gomez-Herranz M, Nekulova M, Faktor J, et al. The effects of IFITM1 and IFITM3 gene deletion on IFNgamma stimulated protein synthesis. *Cell Signal*. Aug 2019;60:39-56. doi:10.1016/j.cellsig.2019.03.024

125. Makvandi-Nejad S, Laurenson-Schafer H, Wang L, et al. Lack of Truncated IFITM3 Transcripts in Cells Homozygous for the rs12252-C Variant That is Associated With Severe Influenza Infection. *J Infect Dis*. Jan 4 2018;217(2):257-262. doi:10.1093/infdis/jix512

126. Powell TJ, Silk JD, Sharps J, Fodor E, Townsend AR. Pseudotyped influenza A virus as a vaccine for the induction of heterotypic immunity. *J Virol*. Dec 2012;86(24):13397-406. doi:10.1128/JVI.01820-12

127. van Wilgenburg B, Browne C, Vowles J, Cowley SA. Efficient, long term production of monocyte-derived macrophages from human pluripotent stem cells under partly-defined and fully-defined conditions. *PLoS One*. 2013;8(8):e71098. doi:10.1371/journal.pone.0071098

128. June 2017 Volume 91 Issue 11 e00246-17

129. <iPSDM protocols.pdf>.

130. Dittmann M, Hoffmann HH, Scull MA, et al. A serpin shapes the extracellular environment to prevent influenza A virus maturation. *Cell*. Feb 12 2015;160(4):631-643. doi:10.1016/j.cell.2015.01.040

131. Rajapaksa US, Jin C, Dong T. Malignancy and IFITM3: Friend or Foe? *Front Oncol*. 2020;10:593245. doi:10.3389/fonc.2020.593245

132. Ma Z, Li Z, Wang S, et al. ZMAT1 acts as a tumor suppressor in pancreatic ductal adenocarcinoma by inducing SIRT3/p53 signaling pathway. *J Exp Clin Cancer Res*. Apr 7 2022;41(1):130. doi:10.1186/s13046-022-02310-8

133. Fargeas CA, Florek M, Huttner WB, Corbeil D. Characterization of prominin-2, a new member of the prominin family of pentaspan membrane glycoproteins. *J Biol Chem*. Mar 7 2003;278(10):8586-96. doi:10.1074/jbc.M210640200

134. Yang Q, Cai W, Jin H, Shen T, Yu J. Downregulation of Inflammatory Response via Nrf2/Trx1/TXNIP Axis in Oxidative Stress-Induced ARPE-19 Cells and Mouse Model of AMD. *Oxid Med Cell Longev*. 2022;2022:1497813. doi:10.1155/2022/1497813

135. Pan M, Zhang F, Qu K, Liu C, Zhang J. TXNIP: A Double-Edged Sword in Disease and Therapeutic Outlook. *Oxid Med Cell Longev*. 2022;2022:7805115. doi:10.1155/2022/7805115

136. Hu J, Feng L, Ren M, et al. Colorectal Cancer Cell Differentiation Is Dependent on the Repression of Aerobic Glycolysis by NDRG2-TXNIP Axis. *Dig Dis Sci*. Aug 2022;67(8):3763-3772. doi:10.1007/s10620-021-07188-8

137. Fan H, Lu J, Guo Y, et al. BAHCC1 binds H3K27me3 via a conserved BAH module to mediate gene silencing and oncogenesis. *Nat Genet*. Dec 2020;52(12):1384-1396. doi:10.1038/s41588-020-00729-3

138. Contreras-Baeza Y, Sandoval PY, Alarcon R, et al. Monocarboxylate transporter 4 (MCT4) is a high affinity transporter capable of exporting lactate in high-lactate microenvironments. *J Biol Chem*. Dec 27 2019;294(52):20135-20147. doi:10.1074/jbc.RA119.009093

139. Aruga J, Millen KJ. ZIC1 Function in Normal Cerebellar Development and Human Developmental Pathology. In: Aruga J, ed. *Zic family: Evolution, Development and Disease*. Springer Singapore; 2018:249-268.

140. Ge Q, Hu Y, He J, et al. Zic1 suppresses gastric cancer metastasis by regulating Wnt/beta-catenin signaling and epithelial-mesenchymal transition. *FASEB J*. Feb 2020;34(2):2161-2172. doi:10.1096/fj.201901372RR

141. Hou Y, Chen K, Liao R, Li Y, Yang H, Gong J. LINC01419-mediated epigenetic silencing of ZIC1 promotes metastasis in hepatocellular carcinoma through the PI3K/Akt

signaling pathway. *Lab Invest*. May 2021;101(5):570-587. doi:10.1038/s41374-021-00539-z

142. Zhang YW, Ma J, Shi CT, et al. Roles and correlation of FOXA1 and ZIC1 in breast cancer. *Curr Probl Cancer*. Oct 2020;44(5):100559. doi:10.1016/j.currproblcancer.2020.100559

143. Yagi T, Takeichi M. Cadherin superfamily genes: functions, genomic organization, and neurologic diversity. *Genes & Development*. 2000;14(10):1169-1180.

144. Zheng Y, Gao Y, Li X, et al. Long non-coding RNA NAP1L6 promotes tumor progression and predicts poor prognosis in prostate cancer by targeting Inhibin-beta A. *Onco Targets Ther*. 2018;11:4965-4977. doi:10.2147/OTT.S163680

145. Zhou Y, Zhang Y, Li W, et al. TCEAL2 as a Tumor Suppressor in Renal Cell Carcinoma is Associated with the Good Prognosis of Patients. *Cancer Manag Res*. 2020;12:9589-9597. doi:10.2147/CMAR.S271647

146. Alvarez E, Zhou W, Witta SE, Freed CR. Characterization of the Bex gene family in humans, mice, and rats. *Gene*. Aug 29 2005;357(1):18-28. doi:10.1016/j.gene.2005.05.012

147. Liu X, Long Z, Cai H, Yu S, Wu J. TRIM58 suppresses the tumor growth in gastric cancer by inactivation of beta-catenin signaling via ubiquitination. *Cancer Biol Ther*. 2020;21(3):203-212. doi:10.1080/15384047.2019.1679554

148. Lowenstein ED, Rusanova A, Stelzer J, et al. Olig3 regulates early cerebellar development. *Elife*. Feb 16 2021;10doi:10.7554/eLife.64684

149. Spiegel I, Mardinly AR, Gabel HW, et al. Npas4 regulates excitatory-inhibitory balance within neural circuits through cell-type-specific gene programs. *Cell*. May 22 2014;157(5):1216-29. doi:10.1016/j.cell.2014.03.058

150. Zhang S, Xia C, Xu C, et al. Early growth response 3 inhibits growth of hepatocellular carcinoma cells via upregulation of Fas ligand. *Int J Oncol*. Mar 2017;50(3):805-814. doi:10.3892/ijo.2017.3855

151. Mookerjee-Basu J, Hooper R, Gross S, et al. Suppression of Ca(2+) signals by EGR4 controls Th1 differentiation and anti-cancer immunity in vivo. *EMBO Rep*. May 6 2020;21(5):e48904. doi:10.15252/embr.201948904

152. AJRl1998; 39:96-107

153. Qian et al., Sci. Adv. 8, eabq2945 (2022) 24 August 2022

154. Liu X, Su P, Lu L, Feng Z, Wang H, Zhou J. Function of FEZF1 during early neural differentiation of human embryonic stem cells. *Sci China Life Sci*. Jan 2018;61(1):35-45. doi:10.1007/s11427-017-9155-4

155. Spuch C, Ortolano S, Navarro C. LRP-1 and LRP-2 receptors function in the membrane neuron. Trafficking mechanisms and proteolytic processing in Alzheimer's disease. *Front Physiol*. 2012;3:269. doi:10.3389/fphys.2012.00269

156. Abu-Abed S, Dolle P, Metzger D, Beckett B, Chambon P, Petkovich M. The retinoic acid-metabolizing enzyme, CYP26A1, is essential for normal hindbrain patterning, vertebral identity, and development of posterior structures. *Genes Dev*. Jan 15 2001;15(2):226-40. doi:10.1101/gad.855001

157. Brophy PD, Rasmussen M, Parida M, et al. A Gene Implicated in Activation of Retinoic Acid Receptor Targets Is a Novel Renal Agenesis Gene in Humans. *Genetics*. Sep 2017;207(1):215-228. doi:10.1534/genetics.117.1125

158. Yin Y, Morgunova E, Jolma A, et al. Impact of cytosine methylation on DNA binding specificities of human transcription factors. *Science*. May 5 2017;356(6337)doi:10.1126/science.aaj2239

159. Schroder WA, Major L, Suhrbier A. The Role of SerpinB2 in Immunity. 2011-03-10 2011;31(1):15-30. doi:10.1615/CritRevImmunol.v31.i1.20

160. Bailey CC, Huang IC, Kam C, Farzan M. Ifitm3 limits the severity of acute influenza in mice. *PLoS Pathog*. Sep 2012;8(9):e1002909. doi:10.1371/journal.ppat.1002909

161. Wellington D, Yin Z, Abdel-Haq A, et al. IFITM3-specific antibody reveals IFN preferences and slow IFN induction of the antiviral factor IFITM3 in humans. *Eur J Immunol*. Mar 2021;51(3):742-745. doi:10.1002/eji.202048706

162. Prelich G. Gene overexpression: uses, mechanisms, and interpretation. *Genetics*. Mar 2012;190(3):841-54. doi:10.1534/genetics.111.136911

163. October 2021 Volume 95 Issue 20 e00837-21 doi:10.1128/JVI

164. Stone JD, Demkowicz WE, Jr., Stern LJ. HLA-restricted epitope identification and detection of functional T cell responses by using MHC-peptide and costimulatory microarrays. *Proc Natl Acad Sci U S A*. Mar 8 2005;102(10):3744-9. doi:10.1073/pnas.0407019102

165. Wellington D, Yin Z, Kessler BM, Dong T. Immunodominance complexity: lessons yet to be learned from dominant T cell responses to SARS-COV-2. *Curr Opin Virol*. Oct 2021;50:183-191. doi:10.1016/j.coviro.2021.08.009

166. Ranasinghe SR, Kramer HB, Wright C, et al. The antiviral efficacy of HIV-specific CD8(+) T-cells to a conserved epitope is heavily dependent on the infecting HIV-1 isolate. *PLoS Pathog*. May 2011;7(5):e1001341. doi:10.1371/journal.ppat.1001341

167. Tahir Ul Qamar M, Saleem S, Ashfaq UA, Bari A, Anwar F, Alqahtani S. Epitope-based peptide vaccine design and target site depiction against Middle East Respiratory Syndrome Coronavirus: an immune-informatics study. *J Transl Med*. Nov 8 2019;17(1):362. doi:10.1186/s12967-019-2116-8

168. Oyarzun P, Kobe B. Recombinant and epitope-based vaccines on the road to the market and implications for vaccine design and production. *Hum Vaccin Immunother*. Mar 3 2016;12(3):763-7. doi:10.1080/21645515.2015.1094595

169. Parvizpour S, Pourseif MM, Razmara J, Rafi MA, Omidi Y. Epitope-based vaccine design: a comprehensive overview of bioinformatics approaches. *Drug Discov Today*. Jun 2020;25(6):1034-1042. doi:10.1016/j.drudis.2020.03.006

170. Slota M, Lim JB, Dang Y, Disis ML. ELISpot for measuring human immune responses to vaccines. *Expert Rev Vaccines*. Mar 2011;10(3):299-306. doi:10.1586/erv.10.169

171. Smith SG, Smits K, Joosten SA, et al. Intracellular Cytokine Staining and Flow Cytometry: Considerations for Application in Clinical Trials of Novel Tuberculosis Vaccines. *PLoS One*. 2015;10(9):e0138042. doi:10.1371/journal.pone.0138042

172. Maecker HT, Rinfret A, D'Souza P, et al. Standardization of cytokine flow cytometry assays. *BMC Immunol*. Jun 24 2005;6:13. doi:10.1186/1471-2172-6-13

173. Castro F, Cardoso AP, Goncalves RM, Serre K, Oliveira MJ. Interferon-Gamma at the Crossroads of Tumor Immune Surveillance or Evasion. *Front Immunol*. 2018;9:847. doi:10.3389/fimmu.2018.00847

174. Proc. Natl. Acad. Sci. USA Vol. 87, pp. 5183-5187, July 1990

175. Cramer LA, Nelson SL, Klemsz MJ. Synergistic induction of the Tap-1 gene by IFN-gamma and lipopolysaccharide in macrophages is regulated by STAT1. *J Immunol*. Sep 15 2000;165(6):3190-7. doi:10.4049/jimmunol.165.6.3190

176. FEBS Letters 363 (1995) 85-89

177. Mehta AK, Gracias DT, Croft M. TNF activity and T cells. *Cytokine*. Jan 2018;101:14-18. doi:10.1016/j.cyto.2016.08.003

178. Sojka DK, Bruniquel D, Schwartz RH, Singh NJ. IL-2 secretion by CD4+ T cells in vivo is rapid, transient, and influenced by TCR-specific competition. *J Immunol*. May 15 2004;172(10):6136-43. doi:10.4049/jimmunol.172.10.6136

179. Schluns KS, Lefrancois L. Cytokine control of memory T-cell development and survival. *Nat Rev Immunol*. Apr 2003;3(4):269-79. doi:10.1038/nri1052

180. Kiniry BE, Hunt PW, Hecht FM, Somsouk M, Deeks SG, Shacklett BL. Differential Expression of CD8(+) T Cell Cytotoxic Effector Molecules in Blood and Gastrointestinal Mucosa in HIV-1 Infection. *J Immunol*. Mar 1 2018;200(5):1876-1888. doi:10.4049/jimmunol.1701532

181. NATURE | VOL 391 | 26 FEBRUARY 1998.

182. Saunders KO, Ward-Caviness C, Schutte RJ, et al. Secretion of MIP-1beta and MIP-1alpha by CD8(+) T-lymphocytes correlates with HIV-1 inhibition independent of coreceptor usage. *Cell Immunol*. 2011;266(2):154-64. doi:10.1016/j.cellimm.2010.09.011

183. Betts MR, Brenchley JM, Price DA, et al. Sensitive and viable identification of antigen-specific CD8+ T cells by a flow cytometric assay for degranulation. *Journal of Immunological Methods*. 2003;281(1-2):65-78. doi:10.1016/s0022-1759(03)00265-5

184. Schaap-Johansen AL, Vujovic M, Borch A, Hadrup SR, Marcatili P. T Cell Epitope Prediction and Its Application to Immunotherapy. *Front Immunol*. 2021;12:712488. doi:10.3389/fimmu.2021.712488

185. Peng Y, Mentzer AJ, Liu G, et al. Broad and strong memory CD4(+) and CD8(+) T cells induced by SARS-CoV-2 in UK convalescent individuals following COVID-19. *Nat Immunol*. Nov 2020;21(11):1336-1345. doi:10.1038/s41590-020-0782-6

186. Chan KS, Kaur A. Flow cytometric detection of degranulation reveals phenotypic heterogeneity of degranulating CMV-specific CD8+ T lymphocytes in rhesus macaques. *J Immunol Methods*. Aug 31 2007;325(1-2):20-34. doi:10.1016/j.jim.2007.05.011

187. J Immunol 1988; 141:3868-3874

188. Markov PV, Pybus OG. Evolution and Diversity of the Human Leukocyte Antigen(HLA). *Evol Med Public Health*. Jan 10 2015;2015(1):1. doi:10.1093/emph/eou033

189. Pillai NE, Okada Y, Saw WY, et al. Predicting HLA alleles from high-resolution SNP data in three Southeast Asian populations. *Hum Mol Genet*. Aug 15 2014;23(16):4443-51. doi:10.1093/hmg/ddu149

190. Neville MJ, Lee W, Humburg P, et al. High resolution HLA haplotyping by imputation for a British population bioresource. *Hum Immunol*. Mar 2017;78(3):242-251. doi:10.1016/j.humimm.2017.01.006

191. Wieczorek M, Abualrous ET, Sticht J, et al. Major Histocompatibility Complex (MHC) Class I and MHC Class II Proteins: Conformational Plasticity in Antigen Presentation. *Front Immunol*. 2017;8:292. doi:10.3389/fimmu.2017.00292

192. Zhao et al., Sci. Immunol. 2, eaan5393 (2017) 4 August 2017 SCIENCE IMMUNOLOGY

193. Pujadas E, Ibeh N, Hernandez MM, et al. Comparison of SARS-CoV-2 detection from nasopharyngeal swab samples by the Roche cobas 6800 SARS-CoV-2 test and a laboratory-developed real-time RT-PCR test. *J Med Virol*. Sep 2020;92(9):1695-1698. doi:10.1002/jmv.25988

194. Hadjadj et al., Science 369, 718–724 (2020) 7 August 2020.

195. Lucas C, Wong P, Klein J, et al. Longitudinal analyses reveal immunological misfiring in severe COVID-19. *Nature*. Aug 2020;584(7821):463-469. doi:10.1038/s41586-020-2588-y

196. Chen G, Wu D, Guo W, et al. Clinical and immunological features of severe and moderate coronavirus disease 2019. *J Clin Invest*. May 1 2020;130(5):2620-2629. doi:10.1172/JCI137244

197. Fox A, Le NM, Horby P, et al. Severe pandemic H1N1 2009 infection is associated with transient NK and T deficiency and aberrant CD8 responses. *PLoS One*. 2012;7(2):e31535. doi:10.1371/journal.pone.0031535

198. Notarbartolo et al., Sci. Immunol. 6, eabg5021 (2021) 10 August 2021

199. Lucas C, Klein J, Sundaram ME, et al. Delayed production of neutralizing antibodies correlates with fatal COVID-19. *Nat Med*. Jul 2021;27(7):1178-1186. doi:10.1038/s41591-021-01355-0

200. Su Y, Chen D, Yuan D, et al. Multi-Omics Resolves a Sharp Disease-State Shift between Mild and Moderate COVID-19. *Cell*. Dec 10 2020;183(6):1479-1495.e20. doi:10.1016/j.cell.2020.10.037

201. Grau-Exposito J, Sanchez-Gaona N, Massana N, et al. Peripheral and lung resident memory T cell responses against SARS-CoV-2. *Nat Commun*. May 21 2021;12(1):3010. doi:10.1038/s41467-021-23333-3

202. Poon et al., Sci. Immunol. 6, eabl9105 (2021) 19 November 2021

203. Finkel Y, Mizrahi O, Nachshon A, et al. The coding capacity of SARS-CoV-2. *Nature*. Jan 2021;589(7840):125-130. doi:10.1038/s41586-020-2739-1

204. <assay discussion-1.pdf>.

205. Lee LY, Ha do LA, Simmons C, et al. Memory T cells established by seasonal human influenza A infection cross-react with avian influenza A (H5N1) in healthy individuals. *J Clin Invest*. Oct 2008;118(10):3478-90. doi:10.1172/JCI32460

206. Powell TJ, Fox A, Peng Y, et al. Identification of H5N1-specific T-cell responses in a high-risk cohort in vietnam indicates the existence of potential asymptomatic infections. *J Infect Dis*. Jan 1 2012;205(1):20-7. doi:10.1093/infdis/jir689

207. Reiss S, Baxter AE, Cirelli KM, et al. Comparative analysis of activation induced marker (AIM) assays for sensitive identification of antigen-specific CD4 T cells. *PLoS One*. 2017;12(10):e0186998. doi:10.1371/journal.pone.0186998

208. Rydyznski Moderbacher C, Ramirez SI, Dan JM, et al. Antigen-Specific Adaptive Immunity to SARS-CoV-2 in Acute COVID-19 and Associations with Age and Disease Severity. *Cell*. Nov 12 2020;183(4):996-1012 e19. doi:10.1016/j.cell.2020.09.038

209. Grifoni A, Weiskopf D, Ramirez SI, et al. Targets of T Cell Responses to SARS-CoV-2 Coronavirus in Humans with COVID-19 Disease and Unexposed Individuals. *Cell*. Jun 25 2020;181(7):1489-1501 e15. doi:10.1016/j.cell.2020.05.015

210. Peng Y, Felce SL, Dong D, et al. An immunodominant NP105-113-B*07:02 cytotoxic T cell response controls viral replication and is associated with less severe COVID-19 disease. *Nat Immunol*. Jan 2022;23(1):50-61. doi:10.1038/s41590-021-01084-z

211. Le Bert N, Tan AT, Kunasegaran K, et al. SARS-CoV-2-specific T cell immunity in cases of COVID-19 and SARS, and uninfected controls. *Nature*. Aug 2020;584(7821):457-462. doi:10.1038/s41586-020-2550-z

212. Grifoni A, Sidney J, Vita R, et al. SARS-CoV-2 human T cell epitopes: Adaptive immune response against COVID-19. *Cell Host Microbe*. Jul 14 2021;29(7):1076-1092. doi:10.1016/j.chom.2021.05.010

213. Nelde A, Bilich T, Heitmann JS, et al. SARS-CoV-2-derived peptides define heterologous and COVID-19-induced T cell recognition. *Nat Immunol*. Jan 2021;22(1):74-85. doi:10.1038/s41590-020-00808-x

214. de Silva TI, Liu G, Lindsey BB, et al. The impact of viral mutations on recognition by SARS-CoV-2 specific T cells. *iScience*. Nov 19 2021;24(11):103353. doi:10.1016/j.isci.2021.103353

215. Tarke A, Sidney J, Kidd CK, et al. Comprehensive analysis of T cell immunodominance and immunoprevalence of SARS-CoV-2 epitopes in COVID-19 cases. *Cell Rep Med*. Feb 16 2021;2(2):100204. doi:10.1016/j.xcrm.2021.100204

216. Tarke A, Coelho CH, Zhang Z, et al. SARS-CoV-2 vaccination induces immunological T cell memory able to cross-recognize variants from Alpha to Omicron. *Cell*. Mar 3 2022;185(5):847-859 e11. doi:10.1016/j.cell.2022.01.015

217. Neidleman J, Luo X, McGregor M, et al. mRNA vaccine-induced T cells respond identically to SARS-CoV-2 variants of concern but differ in longevity and homing properties depending on prior infection status. *Elife*. Oct 12 2021;10doi:10.7554/eLife.72619

218. Plante JA, Mitchell BM, Plante KS, Debbink K, Weaver SC, Menachery VD. The variant gambit: COVID-19's next move. *Cell Host Microbe*. Apr 14 2021;29(4):508-515. doi:10.1016/j.chom.2021.02.020

219. Kumar S, Thambiraja TS, Karuppanan K, Subramaniam G. Omicron and Delta variant of SARS-CoV-2: A comparative computational study of spike protein. *J Med Virol*. Apr 2022;94(4):1641-1649. doi:10.1002/jmv.27526

220. Wang P, Nair MS, Liu L, et al. Antibody resistance of SARS-CoV-2 variants B.1.351 and B.1.1.7. *Nature*. May 2021;593(7857):130-135. doi:10.1038/s41586-021-03398-2

221. Volz E, Mishra S, Chand M, et al. 2021;doi:10.1101/2020.12.30.20249034

222. Hoffmann M, Arora P, Gross R, et al. SARS-CoV-2 variants B.1.351 and P.1 escape from neutralizing antibodies. *Cell*. Apr 29 2021;184(9):2384-2393 e12. doi:10.1016/j.cell.2021.03.036

223. Kuzmina A, Khalaila Y, Voloshin O, et al. SARS-CoV-2 spike variants exhibit differential infectivity and neutralization resistance to convalescent or post-vaccination

sera. *Cell Host Microbe*. Apr 14 2021;29(4):522-528 e2. doi:10.1016/j.chom.2021.03.008

224. Edara VV, Norwood C, Floyd K, et al. Infection- and vaccine-induced antibody binding and neutralization of the B.1.351 SARS-CoV-2 variant. *Cell Host Microbe*. Apr 14 2021;29(4):516-521 e3. doi:10.1016/j.chom.2021.03.009

225. Mlcochova P, Kemp SA, Dhar MS, et al. SARS-CoV-2 B.1.617.2 Delta variant replication and immune evasion. *Nature*. Nov 2021;599(7883):114-119. doi:10.1038/s41586-021-03944-y

226. Mohsin M, Mahmud S. Omicron SARS-CoV-2 variant of concern: A review on its transmissibility, immune evasion, reinfection, and severity. *Medicine (Baltimore)*. May 13 2022;101(19):e29165. doi:10.1097/MD.0000000000029165

227. Tarke A, Sidney J, Methot N, et al. Impact of SARS-CoV-2 variants on the total CD4(+) and CD8(+) T cell reactivity in infected or vaccinated individuals. *Cell Rep Med*. Jul 20 2021;2(7):100355. doi:10.1016/j.xcrm.2021.100355

228. Folegatti PM, Ewer KJ, Aley PK, et al. Safety and immunogenicity of the ChAdOx1 nCoV-19 vaccine against SARS-CoV-2: a preliminary report of a phase 1/2, single-blind, randomised controlled trial. *The Lancet*. 2020;396(10249):467-478. doi:10.1016/s0140-6736(20)31604-4

229. GeurtsvanKessel et al., Sci. Immunol. 7, eabo2202 (2022) 25 March 2022

230. Jacobs BL, Langland JO, Kibler KV, et al. Vaccinia virus vaccines: past, present and future. *Antiviral Res*. Oct 2009;84(1):1-13. doi:10.1016/j.antiviral.2009.06.006

231. <vaccinia virus-1.pdf>.

232. Mercer J, Knebel S, Schmidt FI, Crouse J, Burkard C, Helenius A. Vaccinia virus strains use distinct forms of macropinocytosis for host-cell entry. *Proc Natl Acad Sci U S A*. May 18 2010;107(20):9346-51. doi:10.1073/pnas.1004618107

233. Proc. Natl. Acad. Sci. USA Vol. 93, pp. 11341-11348, October 1996

234. Yan et al., Science 367, 1444–1448 (2020) 27 March 2020

235. <EBV transformation.pdf>.

236. Elegheert J, Behiels E, Bishop B, et al. Lentiviral transduction of mammalian cells for fast, scalable and high-level production of soluble and membrane proteins. *Nat Protoc*. Dec 2018;13(12):2991-3017. doi:10.1038/s41596-018-0075-9

237. Verheijen M, Lienhard M, Schrooders Y, et al. DMSO induces drastic changes in human cellular processes and epigenetic landscape in vitro. *Sci Rep*. Mar 15 2019;9(1):4641. doi:10.1038/s41598-019-40660-0

238. Wang X, Xu Z, Tian Z, et al. The EF-1alpha promoter maintains high-level transgene expression from episomal vectors in transfected CHO-K1 cells. *J Cell Mol Med*. Nov 2017;21(11):3044-3054. doi:10.1111/jcmm.13216

239. Guy JL, Jackson RM, Jensen HA, Hooper NM, Turner AJ. Identification of critical active-site residues in angiotensin-converting enzyme-2 (ACE2) by site-directed mutagenesis. *FEBS J*. Jul 2005;272(14):3512-20. doi:10.1111/j.1742-4658.2005.04756.x

240. Winiarska M, Nowis D, Firczuk M, et al. Selection of an optimal promoter for gene transfer in normal B cells. *Mol Med Rep*. Sep 2017;16(3):3041-3048. doi:10.3892/mmr.2017.6974

241. Bovia F, Salmon P, Matthes T, et al. Efficient transduction of primary human B lymphocytes and nondividing myeloma B cells with HIV-1-derived lentiviral vectors. *Blood*. Mar 1 2003;101(5):1727-33. doi:10.1182/blood-2001-12-0249

242. Johnson MJ, Laoharawee K, Lahr WS, Webber BR, Moriarity BS. Engineering of Primary Human B cells with CRISPR/Cas9 Targeted Nuclease. *Sci Rep*. Aug 14 2018;8(1):12144. doi:10.1038/s41598-018-30358-0

243. Akidil E, Albanese M, Buschle A, et al. Highly efficient CRISPR-Cas9-mediated gene knockout in primary human B cells for functional genetic studies of Epstein-Barr virus infection. *PLoS Pathog*. Apr 2021;17(4):e1009117. doi:10.1371/journal.ppat.1009117

244. Wang X, Ray R, Kratochvil S, et al. Multiplexed CRISPR/CAS9-mediated engineering of pre-clinical mouse models bearing native human B cell receptors. *EMBO J*. Jan 15 2021;40(2):e105926. doi:10.15252/embj.2020105926

245. <CRISPR BCL-4.pdf>.

246. Wu CM, Roth TL, Baglaenko Y, et al. Genetic engineering in primary human B cells with CRISPR-Cas9 ribonucleoproteins. *J Immunol Methods*. Jun 2018;457:33-40. doi:10.1016/j.jim.2018.03.009

247. Hartweger H, McGuire AT, Horning M, et al. HIV-specific humoral immune responses by CRISPR/Cas9-edited B cells. *Journal of Experimental Medicine*. 2019;216(6):1301-1310. doi:10.1084/jem.20190287

248. Kleinboehl E, Laoharawee K, Moriarity BS. Primary B cell engineering for therapeutic research. *Trends in Molecular Medicine*. 2022;28(6):528-529. doi:10.1016/j.molmed.2022.03.007

249. Zhao X, Chen H, Wang H. Glycans of SARS-CoV-2 Spike Protein in Virus Infection and Antibody Production. *Front Mol Biosci*. 2021;8:629873. doi:10.3389/fmolb.2021.629873

250. Sanda M, Morrison L, Goldman R. N- and O-Glycosylation of the SARS-CoV-2 Spike Protein. *Anal Chem*. Feb 2 2021;93(4):2003-2009. doi:10.1021/acs.analchem.0c03173

251. Watanabe et al., Science 369, 330–333 (2020) 17 July 2020

252. Gong Y, Qin S, Dai L, Tian Z. The glycosylation in SARS-CoV-2 and its receptor ACE2. *Signal Transduct Target Ther*. Nov 15 2021;6(1):396. doi:10.1038/s41392-021-00809-8

253. Londrigan SL, Wakim LM, Smith J, Haverkate AJ, Brooks AG, Reading PC. IFITM3 and type I interferons are important for the control of influenza A virus replication in murine macrophages. *Virology*. Jan 15 2020;540:17-22. doi:10.1016/j.virol.2019.11.003

254. Zhao X, Sehgal M, Hou Z, et al. Identification of Residues Controlling Restriction versus Enhancing Activities of IFITM Proteins on Entry of Human Coronaviruses. *J Virol*. Mar 15 2018;92(6)doi:10.1128/JVI.01535-17

255. Taus E, Hofmann C, Ibarrondo FJ, et al. Dominant CD8(+) T Cell Nucleocapsid Targeting in SARS-CoV-2 Infection and Broad Spike Targeting From Vaccination. *Front Immunol*. 2022;13:835830. doi:10.3389/fimmu.2022.835830

256. Liu J, Chandrashekar A, Sellers D, et al. Vaccines elicit highly conserved cellular immunity to SARS-CoV-2 Omicron. *Nature*. Mar 2022;603(7901):493-496. doi:10.1038/s41586-022-04465-y

257. De Marco L, D'Orso S, Pirronello M, et al. Assessment of T-cell Reactivity to the SARS-CoV-2 Omicron Variant by Immunized Individuals. *JAMA Netw Open*. Apr 1 2022;5(4):e2210871. doi:10.1001/jamanetworkopen.2022.10871

258. GeurtsvanKessel et al., Sci. Immunol. 7, eabo2202 (2022) 25 March 2022

259. Keeton R, Tincho MB, Ngomti A, et al. T cell responses to SARS-CoV-2 spike cross-recognize Omicron. *Nature*. Mar 2022;603(7901):488-492. doi:10.1038/s41586-022-04460-3

260. Gilbert SC. T-cell-inducing vaccines - what's the future. *Immunology*. Jan 2012;135(1):19-26. doi:10.1111/j.1365-2567.2011.03517.x

261. NATURE MEDICINE VOLUME 9 | NUMBER 6 | JUNE 2003

262. Baden LR, Blattner WA, Morgan C, et al. Timing of plasmid cytokine (IL-2/Ig) administration affects HIV-1 vaccine immunogenicity in HIV-seronegative subjects. *J Infect Dis*. Nov 15 2011;204(10):1541-9. doi:10.1093/infdis/jir615

263. Sheehy SH, Duncan CJ, Elias SC, et al. Phase Ia clinical evaluation of the Plasmodium falciparum blood-stage antigen MSP1 in ChAd63 and MVA vaccine vectors. *Mol Ther*. Dec 2011;19(12):2269-76. doi:10.1038/mt.2011.176

264. Evans TG, Bussey L, Eagling-Vose E, et al. Efficacy and safety of a universal influenza A vaccine (MVA-NP+M1) in adults when given after seasonal quadrivalent influenza vaccine immunisation (FLU009): a phase 2b, randomised, double-blind trial. *The Lancet Infectious Diseases*. 2022;22(6):857-866. doi:10.1016/s1473-3099(21)00702-7

265. Goodman AL, Epp C, Moss D, et al. New candidate vaccines against blood-stage Plasmodium falciparum malaria: prime-boost immunization regimens incorporating human and simian adenoviral vectors and poxviral vectors expressing an optimized antigen based on merozoite surface protein 1. *Infect Immun*. Nov 2010;78(11):4601-12. doi:10.1128/IAI.00315-10

266. Letourneau S, Im EJ, Mashishi T, et al. Design and pre-clinical evaluation of a universal HIV-1 vaccine. *PLoS One*. Oct 3 2007;2(10):e984. doi:10.1371/journal.pone.0000984